

Springer Theses

Recognizing Outstanding Ph.D. Research

Huizhong Shen

Polycyclic Aromatic Hydrocarbons

Their Global Atmospheric Emissions,
Transport, and Lung Cancer Risk



Springer

Springer Theses

Recognizing Outstanding Ph.D. Research

Aims and Scope

The series “Springer Theses” brings together a selection of the very best Ph.D. theses from around the world and across the physical sciences. Nominated and endorsed by two recognized specialists, each published volume has been selected for its scientific excellence and the high impact of its contents for the pertinent field of research. For greater accessibility to non-specialists, the published versions include an extended introduction, as well as a foreword by the student’s supervisor explaining the special relevance of the work for the field. As a whole, the series will provide a valuable resource both for newcomers to the research fields described, and for other scientists seeking detailed background information on special questions. Finally, it provides an accredited documentation of the valuable contributions made by today’s younger generation of scientists.

Theses are accepted into the series by invited nomination only and must fulfill all of the following criteria

- They must be written in good English.
- The topic should fall within the confines of Chemistry, Physics, Earth Sciences, Engineering and related interdisciplinary fields such as Materials, Nanoscience, Chemical Engineering, Complex Systems and Biophysics.
- The work reported in the thesis must represent a significant scientific advance.
- If the thesis includes previously published material, permission to reproduce this must be gained from the respective copyright holder.
- They must have been examined and passed during the 12 months prior to nomination.
- Each thesis should include a foreword by the supervisor outlining the significance of its content.
- The theses should have a clearly defined structure including an introduction accessible to scientists not expert in that particular field.

More information about this series at <http://www.springer.com/series/8790>

Huizhong Shen

Polycyclic Aromatic Hydrocarbons

Their Global Atmospheric Emissions,
Transport, and Lung Cancer Risk

Doctoral Thesis accepted by
College of Urban and Environmental Sciences,
Peking University, Beijing, China

 Springer

Author

Dr. Huizhong Shen
Laboratory for Earth Surface Processes,
College of Urban and Environmental
Sciences
Peking University
Beijing
China

Supervisor

Prof. Shu Tao
Laboratory for Earth Surface Processes,
College of Urban and Environmental
Sciences
Peking University
Beijing
China

ISSN 2190-5053

Springer Theses

ISBN 978-3-662-49678-7

DOI 10.1007/978-3-662-49680-0

ISSN 2190-5061 (electronic)

ISBN 978-3-662-49680-0 (eBook)

Library of Congress Control Number: 2016934444

© Springer-Verlag Berlin Heidelberg 2016

This work is subject to copyright. All rights are reserved by the Publisher, whether the whole or part of the material is concerned, specifically the rights of translation, reprinting, reuse of illustrations, recitation, broadcasting, reproduction on microfilms or in any other physical way, and transmission or information storage and retrieval, electronic adaptation, computer software, or by similar or dissimilar methodology now known or hereafter developed.

The use of general descriptive names, registered names, trademarks, service marks, etc. in this publication does not imply, even in the absence of a specific statement, that such names are exempt from the relevant protective laws and regulations and therefore free for general use.

The publisher, the authors and the editors are safe to assume that the advice and information in this book are believed to be true and accurate at the date of publication. Neither the publisher nor the authors or the editors give a warranty, express or implied, with respect to the material contained herein or for any errors or omissions that may have been made.

Printed on acid-free paper

This Springer imprint is published by Springer Nature
The registered company is Springer-Verlag GmbH Berlin Heidelberg

Parts of this thesis have been published in the following journal articles:

Shen, H. Z., Huang, Y., Wang, R., Zhu, D., Li, W., Shen, G., et al. (2013). Global atmospheric emissions of polycyclic aromatic hydrocarbons from 1960 to 2008 and future predictions. *Environmental Science & Technology*, *47*, 6415–6424. (REUSE WITH PERMISSION)

Shen, H. Z., Tao, S., Liu, J., Huang, Y., Chen, H., Li, W., et al. (2014). Global lung cancer risk from PAH exposure highly depends on emission sources and individual susceptibility. *Scientific Reports*, DOI: 10.1038/srep06561. (REUSE WITH PERMISSION)

Shen, H. Z., Tao, S., Wang, R., Wang, B., Shen, G. F., Li, W., et al. (2011). Global time trends in PAH emissions from motor vehicles. *Atmospheric Environment*, *45*, 2067–2073. (REUSE WITH PERMISSION)

Supervisor's Foreword

As a group of widely spread contaminants with potential impact on human health, polycyclic aromatic hydrocarbons (PAHs) are among the top priority pollutants in many countries especially developing ones where solid fuels are extensively used in industrial and residential sectors. Moreover, pollution of PAHs is a global issue not only because they are emitted everywhere, but also because they can travel among countries or even continents due to strong long-range transport potential. To this stage, quantitative information on sources, fate, and health impact of PAHs on a global scale is not available, resulting in difficulty for policy-makers to formulate abatement strategies. In this thesis, Dr. Huizhong Shen has provided an integrated analysis on emissions, transport, inhalation exposure (ambient air), and subsequently lung cancer risks of PAHs on a global scale. The transport modeling and the exposure risk assessment were conducted using benzo[*a*]pyrene (BaP) as an indicator for PAHs. The emission inventory features in high spatial and temporal resolutions as well as detailed source information, based on a lately compiled fuel consumption data product (PKU-FUEL, which can be freely downloaded together with a series of emission inventories at inventory.pku.edu.cn). By using subnational, instead of national fuel data, the spatial bias caused by conventional spatial disaggregation assuming even per person fuel consumptions within countries was able to be reduced. Meantime, the detailed source information enables the author to distinguish relative contributions of various sectors on the PAH exposure induced lung cancer morbidity. The simulated near-surface air concentrations of BaP were satisfactorily validated after the calculated concentrations were spatially down-scaled to match the grid resolution with the observation sites. It was estimated that the PAH exposure induced incremental lifetime lung cancer risk in 2007 was 3.1×10^{-5} globally, with hot spots in South and East Asia. One of the important findings is that the overall risk would be underestimated by approximately 50 % (1.4×10^{-5}) if individual (mostly genetic) susceptibility was not taken into consideration. Moreover, the susceptibility leads to significant increases in the size of both high and low vulnerable populations. Among various emission sources,

combustion of solid fuels including coal, wood, and crop residues in residential sector contributed more than half of the overall risk. Although PAHs can travel long distance globally, majority of PAH exposure induced lung cancer morbidity was due to local emissions.

Beijing
January 2016

Prof. Shu Tao

Abstract

Environmental polycyclic aromatic hydrocarbons (PAHs) are mainly emitted from incomplete combustion of fuels, waste burning, open biomass burning, and gas leaking in industrial processes. PAHs are of great concern because of their adverse health effects on human. This study estimated global atmospheric emissions of 16 PAH compounds from 69 emission source types during the period from 1960 to 2030. Using regression analysis and technology split method, country- and time-specific emission factors were derived. Based on high-resolution fuel combustion inventory, historical energy data, and six IPCC SRES scenarios, high-resolution PAHs emission inventory at a resolution of $0.1^\circ \times 0.1^\circ$ and time trend of historical emissions at a country level were developed separately. Using this inventory and the Model for Ozone and Related Chemical Tracers (MOZART-4), global transport of benzo[*a*]pyrene (BaP), one of the high molecular weight PAH compounds, was performed and evaluated with observations. Global near-surface concentrations of BaP were generated following a spatial downscaling method. This concentration distribution was used to evaluate lung cancer risk of global population being induced by inhalation exposure to ambient PAHs. Influence of individual susceptibility, contributions of various emission sources, and trans-boundary pollution were also quantified.

It is estimated that the global total annual atmospheric emission of 16 PAHs in 2007 was 655 Gg (521–816 Gg, as interquartile range), with residential/commercial biomass burning (52.4 %), petroleum consumption by on-road motor vehicles (16.5 %), and open-field biomass burning (agricultural waste burning, deforestation, and wildfire, 12.5 %) as the major sources. South, East, and Southeast Asia were the regions with the highest PAH emission densities, contributing half of the global total PAH emissions. Among the global total PAH emissions, 7.7 % of the emissions were in the form of high molecular weight carcinogenic compounds and the percentage of the carcinogenic PAHs was higher in developing countries (8.0 %) than in developed countries (6.4 %), due to the differences in energy structures and the disparities of technology. The potential health impact of the PAH emissions was greatest in the parts of the world with high

anthropogenic PAH emissions, because of the overlap of the high emissions and high population densities.

Global total PAH emissions peaked at 869 Gg in 1978 and declined gradually to 624 Gg in 2008. Total PAH emissions from developed countries peaked at 261 Gg in the early 1970s and decreased to 51 Gg in 2008. Emissions from developing countries peaked at 663 Gg in the early 1990s and decreased to 558 Gg in 2008. Simulation of PAH emissions from 2009 to 2030 revealed that PAH emissions in developed and developing countries would decrease by 46–71 % and 48–64 %, respectively, based on the six IPCC SRES scenarios.

Based on the inventory, global chemical transport of BaP was performed, distribution of global BaP concentrations was derived with downscaling method, and lung cancer risk being induced by PAHs exposure was evaluated using BaP as an indicator. The results indicate that global lung cancer risk represented as Incremental Lifetime Lung Cancer Risk (*ILCR*) was 3.1×10^{-5} , individual susceptibility strongly influenced the outcomes of quantitative risk assessment. If the individual susceptibility was not taken into consideration, the risk would be underestimated by 55 %, and the fraction of the most vulnerable population ($ILCR > 3.1 \times 10^{-5}$) would be underestimated by more than 90 %. Further analysis revealed a significantly positive correlation ($p < 0.1$) between the country-specific *ILCR*s and lung cancer incidences. Contributions of individual sources to the overall risk depend not only on the emission strengths but also on the proximities to people.

Globally, biomass fuel burning in residential/commercial sector contributes 40 % of the total *ILCR*, followed by residential/commercial fossil fuel combustion (14 %), coke production (13 %), primary aluminium production (12 %), and motor vehicles (9 %). *ILCR*s also vary dramatically among populations at different risk levels. A small fraction (1.7 %) of the population facing high risk ($ILCR > 3 \times 10^{-4}$) is largely because of exposure to emissions from coke and aluminium productions. Emissions from residential solid fuel combustion contribute mainly to the population at risk levels between 3×10^{-8} and 1×10^{-4} . These results provide a sound scientific basis for abatement strategy formulation. Globally, residential biomass burning causes the largest overall lung cancer risk and should be the top priority in the emission abatement. On the other hand, control of emissions from motor vehicles and residential coal combustion with the highest *SILCR* is the most effective way of reducing risk. If the objective is to protect the most vulnerable people, emissions from coke and aluminium production should be addressed first. However, the specific strategies should be different among countries, depending on local emission and risk. For example, the overall risk in Russia is dominated by primary aluminium production, while motor vehicles are responsible for the risk of vulnerable populations in Indonesia. Of course, abatement costs should also be taken into account before the action plan is formulated.

It appears that interregional transport within the Eurasian continent is active. As a result of the westerly wind movement and lower air loss rate in high-latitude area, the transport of BaP from Western/Eastern Europe to the Former Soviet Union region represents the largest *ILCR* flow, leading to a 4.5×10^{-7} increase to local *ILCR* of the latter. The second largest movement occurs from East Asia to Southeast

Asia owing to the extraordinary emission intensity in the source region. The net exported risk (NER), defined as the difference between the exported and imported *ILCR* multiplied by regional population, is calculated for each region. Western/Eastern Europe (NER = 145), South Asia (NER = 57), and East Asia (NER = 42) are the main export regions of risk, with positive values of exported risk, while Southeast Asia (NER = -126), the former Soviet Union (NER = -92), and the Middle East (NER = -19) are risk passive recipients. Still, even with the active interregional transport, regional risks are predominantly caused by local emissions. The highest external contribution to local *ILCR* is merely 2.6 % (Southeast Asia).

Keywords Polycyclic aromatic hydrocarbons · Emission inventory · Global chemical transport modeling · Inhalation exposure · Lung cancer risk

Acknowledgments

During my 9-year study in Peking University, I would like to express my hearty gratitude to many people. The first one is Prof. Shu Tao who is my supervisor in both my undergraduate and graduate research study and who is a tireless teacher with infectious enthusiasm of learning and challenging. He is also a good army chess friend. He places himself third in chess in the laboratory (I am the first by the way). His nature of curiosity and character of doing things inspire me and influence my research career deeply. Second, I would like to thank Prof. Junfeng Liu who gave the detailed instruction in model development and performance. No one but he could bear me with continuous interruption four times (or even more) every day. Without his patient instruction and expert guidance, this thesis would not be completed satisfactorily.

I would like to thank Dr. Yanxu Zhang. I learned a lot from him at the beginning of my academic research. To a certain degree, my research on emission development and transport modeling, not as brilliant as his though, are achieved based on his research. He is always an ideal example of young scientists in my mind.

Also, I would like to thank all the colleagues and professors in the laboratory. Thank my roommate Wei Li, my teammate Rong Wang and Ye Huang, and others including Guofeng Shen (Da S), Bin Wang, Yanyan Zhang, Yuanchen Chen, Han Chen, Nan Lin, Shu Su, Prof. Bengang Li, Prof. Xuejun Wang, Prof. Xiqing Li, Prof. Xilong Wang, Prof. Yu Liu, Prof. Bingjun Meng.

At last, I would like to express my gratitude to my family for their continuous support and encouragement, especially to my beloved wife, my parents, and my great-aunt. Without them, there would not be so much gratification.

The research carried out in the thesis was funded by the National Natural Science Foundation of China (Grant 40730737, 41001343, 40503018, 41130754, and 41390240), Ministry of Environmental Protection (201209018), Beijing Municipal Government (YB20101000101), and NIEHS (P42 ES016465).

Huizhong Shen

Contents

1	Introduction	1
1.1	Background	1
1.2	Main Objectives	3
1.3	Thesis Structure	3
	References	4
2	Research Background	7
2.1	Introduction of Polycyclic Aromatic Hydrocarbons	7
2.2	Emissions of Polycyclic Aromatic Hydrocarbons	8
2.3	Global Transport Modeling of Polycyclic Aromatic Hydrocarbons	13
2.4	Toxicity of Polycyclic Aromatic Hydrocarbons	15
2.5	Inhalation Exposure and Risk Assessment of Polycyclic Aromatic Hydrocarbons	17
	References	18
3	Methodology	23
3.1	Development of Global Emission Inventory	23
3.1.1	Activity Data	24
3.1.2	Emission Factor Analysis	29
3.1.3	Uncertainty Analysis	44
3.2	Atmospheric Transport Modeling	53
3.2.1	Mozart-4	53
3.2.2	Incorporation of PAH Module	53
3.2.3	Model Validation and Downscaling	58
3.3	Lung Cancer Risk Assessment	59
3.3.1	Incremental Lifetime Cancer Risk	59
3.3.2	Quantification of Distributions of Individual Differences	61
3.3.3	Evaluation of Source-Specific Health Risks	75

3.3.4	Evaluation of Transboundary Pollution.	75
3.3.5	The Uncertainty and the Distribution of Risks.	76
References	77
4	Global Atmospheric Emissions of PAH Compounds	85
4.1	Global High-Resolution Fuel Combustion Inventory.	85
4.2	Global Time Trend of Emissions from Motor Vehicles.	86
4.2.1	Variations in EF_{PAH} for Motor Vehicles.	86
4.2.2	Factors Affecting EF_{PAH} for Motor Vehicles.	89
4.2.3	Prediction of EF_{PAH} for Motor Vehicles.	91
4.2.4	Model Comparison	94
4.2.5	Difference in EF_{PAH} Among PAH Compounds	97
4.2.6	Time Trends of PAH Emission from Motor Vehicles in the World.	97
4.3	Global Emissions of Atmospheric PAHs from All Sources	99
4.3.1	Total Emission and Source Profile.	100
4.3.2	Composition Profile.	103
4.3.3	Geographic Distribution	106
4.3.4	Historical Time Trends.	110
4.3.5	Future Time Trends.	114
4.4	Summary	115
References	116
5	Global Atmospheric Transport Modeling of benzo[<i>a</i>]pyrene.	121
5.1	Model Validation.	121
5.1.1	Validation at Background Sites	122
5.1.2	Validation at Non-background Sites.	123
5.2	Spatial Distribution	131
5.3	Summary	135
References	136
6	Global Lung Cancer Risks Induced by Inhalation Exposure to PAHs	139
6.1	Risk Assessment and Influence of Individual Susceptibility	140
6.2	Source Contributions	144
6.3	Transport Across Continents	147
6.4	Summary	152
References	153
7	Conclusions	155
Appendix	157

Chapter 1

Introduction

1.1 Background

Polycyclic aromatic hydrocarbons (PAHs) are a class of organic chemicals, which include carbon and hydrogen with a fused ring structure containing at least 2 benzene rings (Baek et al. 1991; Ravindra et al. 2008). Exposure to PAHs through various routes is associated with cancer (USEPA 2014; Boffetta et al. 1997; Chen and Liao 2006). Increased lung cancer risks from both occupational and environmental exposure to PAHs were observed and well documented by previous studies (Boffetta et al. 1997; IARC 2014; Armstrong et al. 2004). As molecular weight increase, the carcinogenicity of PAHs also tends to increase (Ravindra et al. 2008). Benzo[*a*]pyrene (BaP), one of the high molecular weight PAHs, is probably the first chemical carcinogen to be discovered, and now has been classified into the group of most carcinogenic agents by the International Agency for Research on Cancer (Ravindra et al. 2008).

Atmospheric PAHs are mostly emitted from incomplete combustion (USEPA 1998), including both anthropogenic activities and natural sources, such as indoor solid fuel burning, waste burning, exhaust of motor vehicles, coke production, industrial boilers, and deforestation and wildfires (Ravindra et al. 2008). Focusing on evaluation of source contributions of atmospheric PAH emissions, several studies have developed emission inventories on regional scales, including well-established inventories in the United States, the United Nation, the former Soviet Union, China, and European countries (USEPA 2011; NAEI 2011; EMEP 2011; van der Gon et al. 2007; Galarneau et al. 2007; Xu et al. 2006; Zhang and Tao 2009). Some inventories are spatially resolved and can be used for atmospheric transport modelling and exposure risk assessment (UNECE 2012; Zhang et al. 2011; Zhang et al. 2009; Lang et al. 2008). However, on a global scale, only country-level emission data can be obtained (Zhang and Tao 2009). Considering the large spatial variation of PAH emissions within individual countries, establishment

of an integrated global PAH emission inventory with spatial information is needed to evaluate their health impacts on a global scale.

In top-down emission inventories, even larger uncertainty can be induced from the variation in emission factors (EF_{PAHs} , the mass of PAHs emitted per unit mass of fuel burned) (Zhang and Tao 2009). For a given PAH compound, EFs from a particular combustion source often vary over several orders of magnitude, depending on the country, facility, operation method, emission control device, environmental setting, measuring time and procedure, and other factors (Ravindra et al. 2008). For example, EFs of benzo[*a*]pyrene for light-duty gasoline vehicles vary over 4 orders of magnitude from 0.204 to 1910 ng/kg. These sources of uncertainty should be taken into consideration in the development of a global PAH emission inventory.

Widespread PAH emissions and potential for long-range transport lead to the fact that PAHs can be detected all around the world, including in polar regions (Lunde and Björseth 1977). Using global chemical transport models, the fates of PAHs have been quantitatively characterized (Lammel et al. 2009; Zhang et al. 2011; Friedman and Selin 2013). However, the spatial resolutions of these models are usually as large as 1–5° longitude and latitude limited by computing load and meteorological information, which means that models can only provide averaged values within grids of ten thousand to several hundred thousand square kilometers. Concentrations calculated at such coarse resolutions are not suitable for risk assessments because population densities vary at a much finer spatial resolution. This scale mismatch will hinder the true values when evaluating the health impacts. Additional procedures should be carried out to transform modeled concentration field to a finer resolution. Additionally, different PAH emission sources contribute to human exposure to PAHs to different extents because of their different emission strengths, compound profiles, and proximities to people (Shen et al. 2013). The quantification of source–receptor relationships is essential for assessing the health risks associated with different sources and for developing cost-effective abatement strategies.

Evidence from molecular epidemiologic studies has indicated that individual susceptibility plays an important role in cancer development in humans under environmental stress (Perera 1997). However, the influences of susceptibility on cancer risks in populations grouped by gender, age, and genetic heritage are difficult to characterize quantitatively. It is a challenge to distinguish the relative contributions of the exposure dose and individual susceptibility to the risks associated with PAHs (Perera 1997). Based on the result of an epidemical study conducted in Xuanwei, China (Mumford et al. 1995), and relationship between DNA adduct level and number of at-risk alleles, an attempt has been made in a study in which the risks of PAH exposure inducing lung cancer were assessed with consideration of susceptibility associated with individual genetic polymorphisms in the Chinese population (Zhang et al. 2009). Similar analysis must be considered in global assessment to address the effects of individual susceptibility on the overall health outcomes.

1.2 Main Objectives

- (1) Establishing a database of PAHs emission factors based on a thorough literature review;
- (2) Addressing the key factors influencing emission factor values, predicting country- and time-specified emission variations;
- (3) Developing a global PAH emission inventory, the inventory include three components: spatial high resolution emission inventory; historical emission time trends be country; future emission projection based on IPCC sceneries;
- (4) Global transport modeling of PAHs based on emission inventory;
- (5) Assessing lung cancer risk being induced by inhalation exposure to PAHs;
- (6) Evaluating influences of individual susceptibility, source contributions, and trans-boundary pollutions.

1.3 Thesis Structure

Chapter 1. Introduction. A brief introduction of the background, the research objectives and structure of the thesis.

Chapter 2. Research Background. In this section, a detailed review on the physical and chemical property, emission inventory development, transport modelling, and health impacts of polycyclic aromatic hydrocarbons is provided.

Chapter 3. Methodology. Detailed methodology is described including the collection of emission factors and processing methods used to predict country- and time-specified EF values, emission inventory development, global transport modelling, and lung cancer risk assessment.

Chapter 4. Global atmospheric emissions of PAH compounds. In this section, the results of the global emission estimation are illustrated and discussed, including the total amount, temporal trends, source contribution, and compound profiles. Spatial distribution of emissions are shown together with region-specified source contributions. Potential health impacts are discussed directly based on the distributions of emissions and population.

Chapter 5. Global atmospheric transport modeling of benzo[*a*]pyrene. This section shows the model validation of the transport modeling of benzo[*a*]pyrene based on a global chemical transport model. Global distribution of the near-surface BaP concentrations is illustrated.

Chapter 6. Global lung cancer risks induced by inhalation exposure to PAHs. In this section, using BaP as an indicator, lung cancer risk being induced by inhalation exposure to PAHs is evaluated with consideration of individual susceptibility. The source contributions and trans-boundary pollution are also discussed.

Chapter 7. Conclusions. In this section, the main conclusion of this thesis is summarized.

References

- Armstrong, B., Hutchinson, E., Unwin, J., & Fletcher, T. (2004). Lung cancer risk after exposure to polycyclic aromatic hydrocarbons: a review and meta-analysis. *Environmental Health Perspectives*, *112*, 970–978.
- Baek, S. O., Field, R. A., Goldstone, M. E., Kirk, P. W., Lester, J. N., & Perry, R. (1991). A review of atmospheric polycyclic aromatic-hydrocarbons-sources, fate and behavior. *Water, Air, and Soil Pollution*, *60*(3–4), 279–300.
- Boffetta, P., Jourenkova, N., & Gustavsson, P. (1997). Cancer risk from occupational and environmental exposure to polycyclic aromatic hydrocarbons. *Cancer Causes and Control*, *8*, 444–472.
- Chen, S. C., & Liao, C. M. (2006). Health risk assessment on human exposed to environmental polycyclic aromatic hydrocarbons pollution sources. *Science of the Total Environment*, *366*, 112–123.
- European Monitoring and Evaluation Programme (EMEP) (2011). *Centre on emission inventories and projections*. Retrieved from <http://www.ceip.at>
- Friedman, C. L., & Selin, N. E. (2013). Long-range atmospheric transport of polycyclic aromatic hydrocarbons: a global 3-D model analysis including evaluation of arctic sources. *Environmental Science and Technology*, *46*, 9501–9510.
- Galarneau, E., Makar, P. A., Sassi, M., & Diamond, M. L. (2007). Estimation of atmospheric emissions of six semivolatile polycyclic aromatic hydrocarbons in southern Canada and the United States by use of an emissions processing system. *Environmental Science and Technology*, *41*(12), 4205–4213.
- International Agency for Research on Cancer (2014). *Agents classified by the IARC monographs, Vols 1–109*. Retrieved from <http://monographs.iarc.fr/ENG/Classification/index.php>
- Lammel, G., Sehili, A. M., Bond, T. C., Feichter, J., & Grassl, H. (2009). Gas/particle partitioning and global distribution of polycyclic aromatic hydrocarbons—a modelling approach. *Chemosphere*, *76*, 98–106.
- Lang, C., Tao, S., Liu, W. X., Zhang, Y. X., & Simonich, S. (2008). Atmospheric transport and outflow of polycyclic aromatic Hydrocarbons from China. *Environmental Science and Technology*, *42*, 5196–5201.
- Lunde, G., & Björseth, A. (1977). Polycyclic aromatic hydrocarbons in long-range transported aerosols. *Nature*, *268*, 518–519.
- Mumford, J. L., Li, X., Hu, F., Lu, X. B., & Chuang, J. C. (1995). Human exposure and dosimetry of polycyclic aromatic hydrocarbons in urine from Xuan Wei, China with high lung cancer mortality associated with exposure to unvented coal smoke. *Carcinogenesis*, *16*, 3031–3036.
- National Atmospheric Emissions Inventory (NAEI) (2011). Retrieved from http://naei.defra.gov.uk/data_warehouse.php
- Perera, F. P. (1997). Environment and cancer: who are susceptible? *Science*, *278*, 1068–1073.
- Ravindra, K., Sokhi, R., & Van Grieken, R. (2008). Atmospheric polycyclic aromatic hydrocarbons: Source attribution, emission factors and regulation. *Atmospheric Environment*, *42*(13), 2895–2921.
- Shen, H. Z., Huang, Y., Wang, R., Zhu, D., Li, W., Shen, G., et al. (2013). Global atmospheric emissions of polycyclic aromatic hydrocarbons from 1960 to 2008 and future predictions. *Environmental Science and Technology*, *47*, 6415–6424.
- United Nations Economic Commission for Europe (UNECE) (2012). *Convention on long-range transboundary air pollution*. Retrieved from <http://www.unece.org/env/lrtap>
- United States Environmental Protection Agency (USEPA) (1998). *Locating and estimating air emission from sources of polycyclic organic matter*. Retrieved from EPA-454/R-98-014. <http://www.epa.gov/ttn/chief>
- United States Environmental Protection Agency (USEPA) (2011). *Clearinghouse for inventories & emissions factors*. Retrieved from <http://www.epa.gov/ttn/chief/index.html>

- United States Environmental Protection Agency (USEPA) (2014). *Provisional guidance for quantitative risk assessment of polycyclic aromatic hydrocarbons*. Retrieved from <http://cfpub.epa.gov/ncea/cfm/recorddisplay.cfm?deid=49732>
- van der Gon, H. D., van het Bolscher, M., Visschedijk, A., & Zandveld, P. (2007). Emissions of persistent organic pollutants and eight candidate POPs from UNECE-Europe in 2000, 2010 and 2020 and the emission reduction resulting from the implementation of the UNECE POP protocol. *Atmospheric Environment*, *41*(40), 9245–9261.
- Xu, S. S., Liu, W. X., & Tao, S. (2006). Emission of polycyclic aromatic hydrocarbons in China. *Environmental Science and Technology*, *40*(3), 702–708.
- Zhang, Y. X., & Tao, S. (2009). Global atmospheric emission inventory of polycyclic aromatic hydrocarbons (PAHs) for 2004. *Atmospheric Environment*, *43*(4), 812–819.
- Zhang, Y. X., Tao, S., Shen, H. Z., & Ma, J. M. (2009). Inhalation exposure to ambient polycyclic aromatic hydrocarbons and lung cancer risk of Chinese population. *Proceedings of the National Academy of Sciences of the United States of America*, *106*(50), 21063–21067.
- Zhang, Y., Tao, S., Ma, J., & Simonich, S. (2011). Transpacific transport of benzo[a]pyrene emitted from Asia. *Atmospheric Chemistry and Physics*, *11*(23), 11993–12006.

Chapter 2

Research Background

2.1 Introduction of Polycyclic Aromatic Hydrocarbons

Polycyclic aromatic hydrocarbons (PAHs) are a class of organic chemicals, which include carbon and hydrogen with a fused ring structure containing at least 2 benzene rings (Baek et al. 1991; Ravindra et al. 2008). Due to their persistency and long-range transport capacity, PAHs are ubiquitous in ambient air (Lunde and Björseth 1977; Wang et al. 2010). PAHs are of great concerns as these compounds were one of the first atmospheric pollutants that were identified as being carcinogenic (Boffetta et al. 1997; Armstrong et al. 2004). Recently, benzo[*a*]pyrene (BaP), one of the high molecular weight PAHs, has been classified into the group of most carcinogenic agents by the International Agency for Research on Cancer (IACR 2014). Atmospheric PAHs are mostly emitted by incomplete combustion of carbonaceous materials, including both anthropogenic activities and natural sources, such as indoor solid fuel burning, waste burning, vehicle exhausts, coke production, industrial boilers, and deforestation and wildfires (Ravindra et al. 2008).

Because of their low vapor pressure, some PAHs are present in both gas and particle phases (adsorbed on particles) in air. The lower molecular weight PAHs, such as naphthalene, acenaphthene, and phenanthrene, are found almost in gas phase, while the higher molecular weight PAHs, such as benzo[*a*]pyrene, are almost exclusively in particle phase. The molecular structures and physiochemical properties of sixteen parent-PAH compounds are listed in Fig. 2.1 and Table 2.1.

In the environment, PAHs are usually present as mixtures with relatively higher melting and boiling points. Because of their distinguished structures, different PAH compounds have different physiochemical properties. Compounds with similar molecular weights and rings exhibit similar physiochemical properties and environmental behaviors. Generally, as rings and molecular weights increase, their solubility, saturation vapor pressure, and Henry's constants decrease leading to the decrease of volatility and water solubility, whereas octanol–water partition coefficient and lipophilicity increase (Smith et al. 1999).

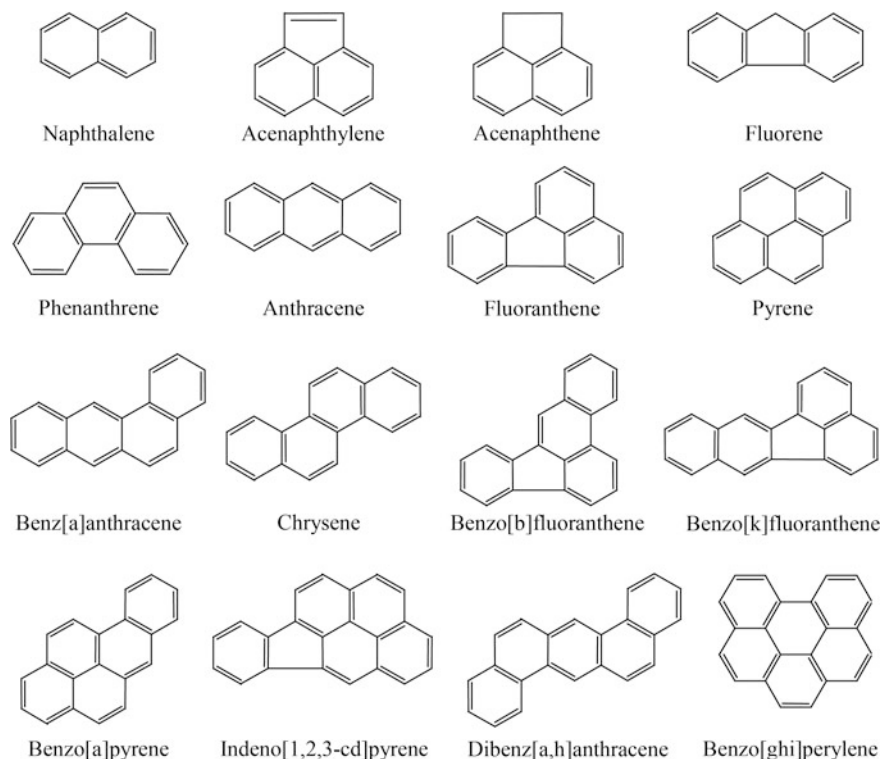


Fig. 2.1 The molecular structures of sixteen priority-listed PAHs

2.2 Emissions of Polycyclic Aromatic Hydrocarbons

Major PAH emission sources have been identified thanks to numerous studies on PAH emission characteristics. Incomplete combustion of carbonaceous materials such as biomass burning in residential stoves can lead to the release of high levels of PAHs. Other processes such as pyrolytic conditions in coking plants and oxidation reduction reactions in primary aluminum production are also conducive to PAH formation (Ravindra et al. 2008). Although natural sources contribute a part of atmospheric PAH emissions, anthropogenic activities contribute the majority. Not only residential and industrial sources but also motor vehicles, ships, and agricultural sources are responsible for PAH contamination. Although there were many factor affecting emission factor values of different sources, most of them can be classified into two categories: combustion efficiency and emission control device. Lower combustion efficiency leads to much more rapid PAH formation during combustion, and emission control devices with lower PM remove efficiency also release more particle-phase PAHs.

Table 2.1 The physicochemical properties of sixteen priority-listed PAHs

Compound	SN	Rings	MW	BP	MP	S	V_p	H	$\lg K_{ow}$
Naphthalene	NAP	2	128.18	209	80	31.5	1.1×10^1	43.0	3.37
Acenaphthylene	ACY	2	152.20	290	124	3.93	8.9×10^{-1}	11.55	4.00
Acenaphthene	ACE	2	154.20	252	108	3.93	2.9×10^{-1}	24.0	3.92
Fluorene	FLO	2	166.23	276	119	1.98	8.0×10^{-2}	8.50	4.18
Phenanthrene	PHE	3	178.24	326	136	1.15	2.5×10^{-2}	4.0	4.57
Anthracene	ANT	3	178.24	326	136	0.075	1.1×10^{-3}	6.0	4.54
Fluoranthene	FLA	3	202.26	369	166	0.206	1.1×10^{-3}	0.659	5.22
Pyrene	PYR	4	202.26	369	166	0.132	5.5×10^{-4}	1.10	5.18
Benz(a)anthracene	BaA	4	228.30	400	177	0.009	1.5×10^{-5}	0.102	5.91
Chrysene	CHR	4	228.30	400	177	0.002	6.1×10^{-7}	0.106	5.86
Benzo(b)fluoranthene	BbF	4	252.32	461	209	0.002	2.1×10^{-5}	0.054	5.80
Benzo(k)fluoranthene	BkF	4	252.32	430	194	0.0008	1.3×10^{-7}	0.111	6.00
Benzo(a)pyrene	BaP	5	252.32	461	209	0.004	7.5×10^{-7}	0.009	6.04
Indeno(1,2,3-cd)pyrene	IcdP	5	276.34	498	233	0.0005	1.0×10^{-10}	N/A	6.50
Dibenz(a,h)anthracene	DahA	5	278.36	487	218	0.0006	4.3×10^{-10}	0.007	6.75
Benzo(g,h,i)perylene	BghiP	6	276.34	467	218	0.0003	1.4×10^{-8}	0.001	6.50

Note SN short name; MW molecular weight; BP boiling point (°C); MP melting point (°C); S water solubility at 25 °C (mg/L); V_p saturation vapor pressure at 25 °C (Pa); H Henry's constant (Pa·m³/mol)

Residential sources. Residential sources including residential burning of firewood, straw, coal, garbage, or other organic substances within fireplace, woodstoves, and other devices for heating, cooking, and lighting contribute the largest part of PAH emissions. Generally, these devices are lack of exhaust control treatment, and stove design, fuel types and characteristics, and operational practice determine the combustion efficiency and consequently PAH emission rates. Modification of air flow control, thermal control and heat storage, and usage of combustion catalysts can lead to reduced PAH formation and release (Mead et al. 1986; Kelly 1983). In terms of fuel types, coal, oil, and gas are all associated with PAH emissions, but burning of gas shows a much lower emission level. Residential biomass burning represents the highest PAH emission rates among all combustion sources and fuel types. In developing countries, solid biomass including wood, straw, and dung cakes is widely used for cooking and heating because they are cheaper and much easier to access. About 3 billion residents are using solid fuels for daily cooking globally, and among them a large fraction use solid biomass. Therefore, residential biomass burning is of great concerns in terms of PAH exposure and human health (WHO 2002).

Transportation sources. Transportation sources include exhaust emissions from on-road motor vehicles, ships, and aircrafts, among which on-road motor vehicles are the most important sources in terms of either emission amount or proximity to people. In urban areas, a great deal of PAH contaminations are associated with vehicle emissions which include emissions from both oil burning in internal-combustion engines and leaking of unburned fuels and lubricant (USEPA 1998). Emission factor levels of motor vehicles depend on engine type, load, fuel type and quality, driving mode (such as cold or warm start), and exhaust control device. Emission factors of different vehicle types are quite different. Generally, heavy duty vehicles have higher emission factor values than light duty ones, and emission factors of diesel vehicles tend to be higher than those of gasoline ones (Riddle et al. 2007). Driving mode is also an importing factor influencing PAH emissions. Compared to driving with constant speed, congested traffic conditions with vehicles only traveling short journeys enhance PAH emissions significantly (Kado et al. 2005). Additionally, emission factors measured using different methods could be very different. For example, it was reported that emission factors derived from real-world test were significantly higher than those from dynamometer tests (Kristensson et al. 2004), and emission factors observed in a tunnel test were considerably higher than those measured in a roadside test (Wingfors et al. 2001). Other factors including age, load, and lubricant oil also lead to differences of emission factors of motor vehicles. Although factors affecting vehicle emissions are complicated, it is the implementation of emission standards that actually drives the descending tendency of emission factors over time. For instance, from 1992 to 2014, six emission standards (Euro I to Euro VI) have been carried out among European Union (Timilsina and Dulal 2009), while in the USA, an important step toward vehicle emission control was taken in 1970 when the Congress passed the Clean Air Act, which was further amended in 1977 and 1990 (Timilsina and Dulal 2009). Development of most new emission control technologies was primarily driven by these regulations. The first-generation catalytic converter introduced in the mid-1970s helped to cut car emission substantially (USEPA 1999). After the three-way catalysts with on-board computer and oxygen sensor hit the market in the 1980s, more evident reduction in car emission was achieved (USEPA 1999). Although PAH emission was not regulated directly, the new technologies aiming at other pollutants including particulates and nitrogen oxide helped to trim down PAH emission “unintentionally.” Except for exhaust control devices, emission standards lead to technical improvement of vehicle engines at the same time. The increase of combustion efficiency directly limits PAH formation and further reduces PAH release in the exhaust. For the same reason, vehicle emission was also gradually reduced in developing countries over years, although the progress was hysteretic (ADB 2003). For example, China V emission standard, which is similar to Euro V, already went into effect in China in 2015.

Industrial sources. Industrial sources include emissions from power plants and industrial boilers, leaking from coke and primary aluminum production processes, iron and steel industry, and petroleum industry. Given that industrial boilers are often equipped with emission control devices, factors determining PAH emissions

from these boilers involve both boiler combustion efficiency and types of control devices. Control devices with higher PM remove efficiency can remove PAHs more effectively, especially those compounds with high molecular weights (USEPA 1998). Generally, the bag dust removal has the highest remove efficiency following the electrostatic precipitation, wet dust removal, and cyclone dust removal. In developed countries, bag dust removal has been widely applied to the assistance of one or several other devices, while in developing countries electrostatic precipitation is still the most popular control device for industrial boilers. Despite all this, given the much higher combustion efficiency and remove efficiency, industrial boilers contribute only small fractions of total atmospheric PAH emissions both in developed countries and in developing countries (Zhang and Tao 2009). Coking industry can be divided into mechanical coking and beehive coking with regard to PAH emissions. Emissions from coke production are mainly due to leak from coke oven plants in which the pyrolytic process that facilitates PAH formation occurs. Beehive coking which has been seldom seen in developed countries is found to be associated with high levels of PAH emissions because of the poor design of coke ovens and lack of control devices. Beehive coking had spread without restriction in China in the 1990s, especially in Shanxi and Guizhou provinces (Zhang et al. 2007). The coal law promoted in the late 1990s prohibited beehive coking on a national scale (Law of the People's Republic of China 1996). However, since this coking activity is quite difficult to be found out, beehive coking has never been eradicated thoroughly in China. Although better than beehive coking in terms of PAH release, mechanical coking also represents higher emission factors. Since gas in the coke ovens contains high levels of PAH, leaking around the ovens is associated with severe release of PAHs into ambient air. The processes that can induce emission include leaking from charging, pushing, quenching, doors and topside, as well as combustion-related emissions from battery stacks (USEPA 2011). Control devices have been applied to these leaking points, which can significantly reduce emissions. However, leaks cannot be entirely avoided, and as a result, coking industry is responsible for a large fraction of PAH emissions. Regarding the type of reduction cell used, primary aluminum production can be divided into prebaked and Soderberg (USEPA 2011). Prebaked technology came out later than Soderberg. It is expected that PAHs have already been released during anodes prebaking process, when the emissions can be easily controlled; the emission from reduction of prebaked technology are much less than those from Soderberg cells (USEPA 2011). Addressing different technology and control devices associated with different industry activities is crucial for reducing uncertainty of PAH emission estimation.

Agricultural and natural sources. Agricultural and natural sources mainly include emissions from agricultural machinery, open burning of agricultural waste, deforestation, savanna, forest, and peat fires (Ravindra et al. 2008; Zhang and Tao 2009). PAHs are emitted from fossil fuel combustion in internal engines of agricultural machinery. The emissions are similar to those of on-road motor vehicles. Agricultural waste open burning and deforestation are common methods for residue disposal and land preparation. These activities involve burning of organic matters under suboptimum combustion conditions and thus lead to a large amount of PAH

emissions (Ravindra et al. 2008). Similar combustion conditions can be found during savanna, forest, and peat fires. Studies reveal that vegetation fires contribute more than 10 % to total PAH exposure in sub-Saharan Africa (Lammel et al. 2013). High contributions from these sources can be also expected in South America and Southeast Asia where vegetation and peat fires are widespread.

Development of PAH emission inventory is essential to source appointment, transport modeling, and exposure and health risk assessment of these compounds. Many studies have been carried out to address PAH emissions on regional to global scales. Emission inventories have been established for countries such as the USA, the United Kingdom, the former Soviet Union, China, and regions such as North America, Europe, Asia, as well as the globe (USEPA 2011; NAEI 2011; EMEP 2011; van der Gon et al. 2007; Galarneau et al. 2007; Xu et al. 2006; Zhang et al. 2009). Estimates from some of these studies are listed in Table 2.2. Emissions from transportation sources often contribute a significant fraction in developed countries, while in developing countries biomass in residential sector is commonly dominant. In a previous study, global emissions of 16 PAH compounds were estimated to be 520 Gg in 2004. The contributions of residential biomass burning and wildfires are 56.7 and 17.0 %, respectively. China (114 Gg), India (90 Gg), and the USA (32 Gg) are three countries with the highest total emissions (Zhang et al. 2009). This is the only study that addressed PAH emissions on a global scale. However, being limited by activity data and emission factors, only 1-year country-level emissions were reported without spatial information. Hence, establishment of spatially resolved and temporally informed emission inventory is expected for transport modeling and health risk assessment.

Methods to estimate emissions of other compounds are instructional for PAH emission estimation. For instance, in a previous study, a technology split method

Table 2.2 Comparison of PAH emission estimations from various emission inventories

Region	Period	Compound	Emission, Gg/y	Reference
Former Soviet Union	1990–1997	6 PAHs	1.02	Tsibulsky et al. (2001)
Europe	1970–1995	BaP	0.59	Pacyna et al. (2003)
Europe	1990	6 PAHs	12.5	Berdowski et al. (1997)
Europe	1990	4 PAHs	2.4	EMEP (2011)
U.K.	1970–2008	16 PAHs	1.56	NAEI (2011)
U.K.	1995	16 PAHs	3.8	Wenborn et al. (1999)
Great Lakes	2002	BaP	0.0268	Great Lakes Comm. (2007)
U.S.A	1990	16 PAHs	26.5	USEPA (2011)
North America	2002	6 PAHs	18.2	Galarneau et al. (2007)
China	1980–2003	16 PAHs	25.3	Xu et al. (2006)
Globe	1966–1969	BaP	5	Suess (1976)
Globe	2004	16 PAHs	520 Gg	Zhang et al. (2009)

has been applied to estimate global emission of black carbon (Bond et al. 2004). This method employs Gauss curve to simulate temporal trends of technology diffusion such as the application of new engine designs, new industrial processes, or highly efficient control devices. This method is also suitable for PAHs and should significantly reduce uncertainty in emission estimation.

2.3 Global Transport Modeling of Polycyclic Aromatic Hydrocarbons

As early as 1960s, the long-range transport potential of PAHs had become a major concern as an environmental issue (Björseth 1979) when PAHs were first detected in the air and sediment of the North Polar Region (Lunde and Björseth 1977). The atmospheric long-range transport was suggested as a possible pathway of the occurrence of these compounds far from their sources. Recently, as the development of numerical simulation with computers, their long-range transport can be performed quantitatively.

Several critical processes are undergoing during their long-range transport. For instance, researches have shown that the reactions of NO_2 and OH radicals with PAHs are major processes for PAH degradation in the air (Brubaker and Hites 1998; Lammel et al. 2009). Further study revealed that the reactivity of PAHs in the gas phase is significantly larger than that in the particulate phase, and compared to NO_2 , reaction with OH radicals will be the dominant loss process of PAHs (Esteve et al. 2006). Through the comparison of four different gas-particle partitioning schemes, researchers came to the conclusion that a dual black carbon adsorption and organic matter absorption scheme could best describe PAH distributions and thus was suggested as an optimal scheme for long-range transport modeling (Lohmann and Lammel 2004). The suitability of the dual sorption scheme was further proven by model experiments conducted by Sehili and Lammel (2007) when the long-range transport of PAH emissions from Europe and Russia was studied. They also found that the soil compartment contributes a large fraction of the total environmental burden of PAHs. In their following study, the global atmospheric distribution and long-range transport of three PAH compounds were simulated using a global emission inventory (Lammel et al. 2009). This study indicated that gas-particle partitioning drastically influences the atmospheric cycling of PAHs, and that the degradation in the particulate phase must be slower than that in the gas phase. They found that the dual sorption scheme agrees best with the observations at remote sites and suggested that PAHs adsorbed in the particulate matter is shielded from the gas phase.

With consideration of major environmental behaviors such as gas-particle partitioning, OH degradation in the air, and surface-air exchange, Zhang et al. (2011) studied the trans-Pacific transport of PAHs emitted from Asia. It was found that the trans-Pacific transport flux was 1.6 times higher in the winter than in the summer, near ground concentration of BaP induced by Asia Sources in North America varied

between 1 and 20 pg/m^3 . The study also indicated a positive correlation between the interannual variability of transport and the Southern Oscillation Index. Based on a global emission inventory and the GEOS-Chem model, Friedman and Selin (2012) simulated long-range transport of three PAH compounds. Their model considered the dual sorption scheme of gas-particle partitioning with temperature-dependency and incorporated snow/ice scavenging and on-particle oxidation. The model provided a good agreement with observations at remote sites including sites in the high Arctic. Their next study evaluated impacts of climate change and emissions on the atmospheric PAH transport to the Arctic (Friedman et al. 2014) and revealed that emissions have a greater impact on multitude concentrations than climate does. The model also indicated a future “climate penalty” for volatile PAHs as a result of increasing temperature and corresponding surface-to-air fluxes of previously deposited PAHs and a “climate benefit” for particle-bound PAHs as a result of increasing deposition.

From the study on a single environmental process to numerical simulation of global transport, an integrated framework for PAH transport modelling has been gradually formulated (see, Fig. 2.2). Although many details remain to be explored, the framework can largely provide PAH transport simulation and environmental distributions with reasonable uncertainty. To achieve the simulation, a spatially resolved emission inventory is required. For global transport models, the spatial resolutions of emissions normally range from 1 to 5° latitude and longitude. Additionally, the critical environmental processes including photochemical degradation, wet/dry deposition, gas-particle partition should be considered. The reaction between gas phase PAHs and OH radicals is the major photochemical degradation process. The wet/dry deposition of particle-bound PAHs can follow the same scheme as black carbon and organic carbon, and the gas-particle partitioning scheme can follow the dual sorption scheme as mentioned above. Finally, the surface-air exchange should be included with consideration of the fates of PAHs in soil and seawater.

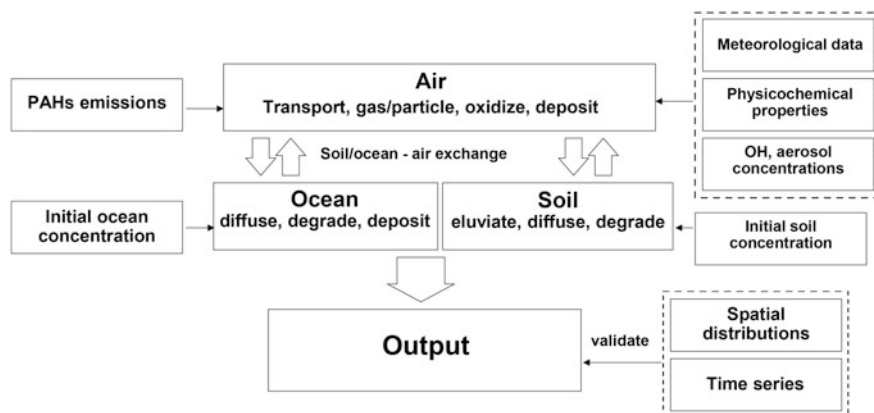


Fig. 2.2 Major environmental processes and modeling framework for PAH compounds

Although most global chemical transport models haven't involved PAH compounds in their original simulation, the simulation of these compounds can be achieved by adding emissions and necessary processes into the models, given that most of their environmental behaviors have been well studied and parameterized. Observations at remote sites are commonly chosen to evaluate model performance on the long-range transport capacity of PAHs, since comparisons at these sites partly avoid the influence of possible spatial bias induced by emission inventory. The available remote sites include the Alert site in the high Arctic, several sites monitored under the European Monitoring and Evaluation Program, and the measurements around the Great Lakes in the North America (EMEP 2012; Wang et al. 2010; Friedman and Selin 2012).

2.4 Toxicity of Polycyclic Aromatic Hydrocarbons

The greatest toxic concern of PAH compounds came from the observations that some of these compounds may cause tumors in humans (Boström et al. 2002). The first relevant event was reported in 1775 when scrotal cancer in chimney sweeps was observed and considered to originate from occupational exposure to soot (Pott 1775). One century later, elevated incidences of skin cancers were confirmed in workers in the coal tar industry (von Volkman 1875). In the early 1900s, soot, coal tar, and pitch were widely recognized to be carcinogenic to humans (Dipple 1985). In the following several decades, many epidemiologic studies and animal experiments have shown the carcinogenicity of these materials are associated with the fraction of PAH contents (Boström et al. 2002; Armstrong et al. 2004). Being evaluated by the International Agency for Research on Cancer, the carcinogenicity of PAHs in humans seems to be beyond dispute (IARC 1984a, b, 1985, 1987, 1989), and one of the high molecular weight PAHs, benzo[*a*]pyrene, has been recently classified into the group of the most carcinogenic agents (IARC 2014).

Among all the exposure routes, inhalation exposure to ambient PAHs and the related lung cancer risks are the most concerned aspect. Armstrong et al. (2004) conducted a review and meta-analysis of published reports of thirty-nine occupational epidemiologic studies. Their study showed the average estimated unit relative risk at 100 $\mu\text{g}/\text{m}^3$ years benzo[*a*]pyrene to be 1.20 (1.11–1.29 as 95 % confidence interval). Several studies have shown that benzo[*a*]pyrene can be regarded as a good indicator for risk assessment of inhalation exposure to PAH mixtures in the air (Boström et al. 2002; Muller 1997).

Carcinogenesis is believed to be a multistep, multimechanism process involving mutagenic events, epigenetic events, and altered cell survival (Boström et al. 2002; Hanahan and Weinberg 2000), and the carcinogenic process is often divided into three steps, including initiation, promotion, and progression (Pitot and Dragan 1996). PAH compounds may act at different steps in the carcinogenic process and may exert both mutagenic and epigenetic actions (Boström et al. 2002). One of the

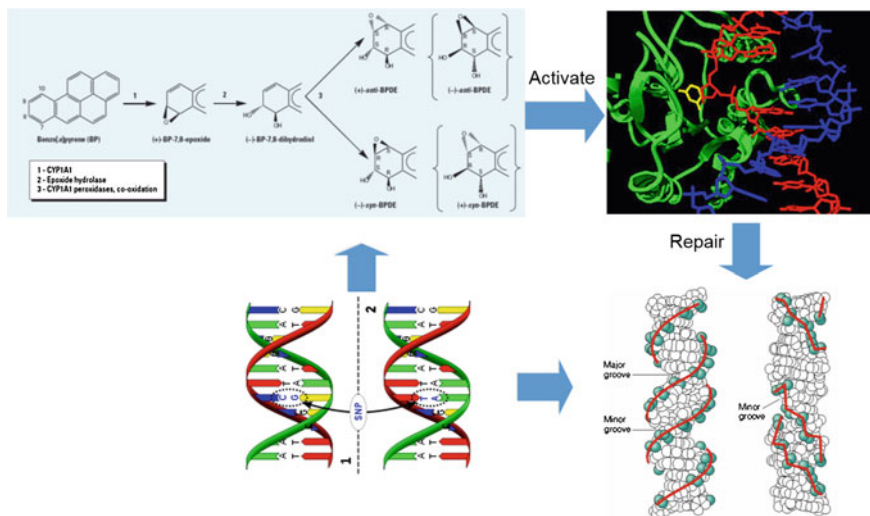


Fig. 2.3 A potential carcinogenic process. Through metabolic activation, PAHs can be converted into reactive electrophilic intermediates. The intermediates can then form adducts with DNA which influence transcription and protein synthesis. The adducts can be repaired by DNA repair enzyme

most important properties of PAHs is their metabolic conversion to reactive electrophilic intermediates (Boström et al. 2002). These intermediates can not only form adducts with DNA which induce mutations and eventually tumors, but also react with other cellular targets and interfere with transcription, DNA replication, and protein synthesis (Boström et al. 2002; Sims and Grover 1974; Thakker et al. 1985) (Fig. 2.3). Other properties of PAHs that are associated with routes of action include the high affinity to the cytosolic aryl hydrocarbon and the inhibitory effect on gap junctional intercellular communication (Boström et al. 2002).

However, researches on animal experiments and occupational environments may hinder the underlying mechanisms in ambient environments, since ambient PAH levels are often much lower. Evidences from animal experiments illustrate a non-linear dose–response relationship that show a significant increase of response in high exposure levels (Ehrenberg and Scalia-Tomba 1991), but this relationship may not be suitable for ambient exposure. The reason may rely on the two steps in the carcinogenic process at which PAHs can act. In the first step, namely the initiation, the dose–response relationship is regarded as a linear relation, while in the second step as the promotion, the relationship is nonlinear. In the ambient environment, the PAH action may not penetrate to the promotion step, and thus, a linear dose–response function can better describe the relationship.

2.5 Inhalation Exposure and Risk Assessment of Polycyclic Aromatic Hydrocarbons

PAH exposure routes that are associated with health effects involve oral exposure, inhalation exposure, and dermal exposure. Inhalation exposure is tightly linked with ambient atmospheric PAH contamination. As mentioned above, a linear function can represent the dose–response relationship in the ambient environment.

Two different methods can be applied to assess health risk of PAHs due to inhalation exposure in the ambient air. The first one is to sum up the risks from individual PAH compounds based on the dose–response relationship determined from animal experiments. Generally, a nonlinear function for a selected compound can be obtained between exposure dose and response in the experiments. A cancer slope factor of the compound is then calculated as the slope of the reduced linear risk function in the ambient level of exposure dose. The cancer risk of the specific compound can be addressed using the cancer slope factor and exposure dose. Additionally, toxic equivalency factors (TEFs) can be generated from the comparison of different compounds (see, Table 2.3). TEFs describe the relative toxicity of different compounds under the same exposure dose. Hence, given the risk of a single compounds and a compound profile in the mixture, risks of every individual compounds can be calculated directly using the TEF values, and the risk of the mixture is evaluated by summing-up risks of individual compounds.

The other approach is to use BaP as an indicator of the whole PAH mixture and assess the risk based on the dose–response relationship from epidemiologic studies. Unit Risk is often used to achieve risk assessment. The cancer risk from exposure to

Table 2.3 Toxic equivalency factors of sixteen PAHs

Compound	TEF
NAP	0.001
ACY	0.001
ACE	0.001
FLO	0.001
PHE	0.001
ANT	0.01
FLA	0.001
PYR	0.001
BaA	0.1
CHR	0.01
BbF	0.1
BkF	0.1
BaP	1
IcdP	0.1
DahA	1
BghiP	0.01

ambient PAH mixture can be calculated as the product of the Unite Risk and the long-term average BaP concentration. Since most epidemiologic studies that focused on health impacts of PAHs took places in occupational environments such as coking plants and aluminum smelter workplaces, application of this approach has to assume first the similarity of compound profiles in the ambient air and in workplaces where the epidemiologic studies were carried out (Boström et al. 2002). This assumption considerably introduces uncertainty into risk assessment. However, this approach has still been chosen by the World Health Organization for risk assessment in the Air Quality Guidelines for Europe (WHO 2000). Because compared to this approach (using BaP as an indicator), the first approach (the summing-up approach) underestimates the risk by about two orders of magnitude (Muller 1997). In fact, only a handful of PAH compounds can be taken into consideration for summing up, which leads to significant underestimate.

Evidence from molecular epidemiologic studies has indicated that individual susceptibility plays an important role in cancer development in humans under environmental stress (Perera 1997). However, it is a challenge to distinguish the relative contributions of the exposure dose and individual susceptibility to the risks associated with PAHs (Perera 1997). A previous attempt has been made in a study in which the risks of PAH exposure inducing lung cancer were assessed with consideration of susceptibility associated with individual genetic polymorphisms in the Chinese population (Zhang et al. 2009). The results showed that the lung cancer susceptibility of half of the Chinese population varied from 35 to 280 % of the average, and the risk of 5 % of the most susceptible Chinese population is at least 10 times higher than that of the average population. The differences in individual susceptibility can be caused by gender, age, genetic heritage, etc. Their influences on risk assessment of PAH exposure will be discussed in this thesis. Consideration of these factors can reduce the uncertainty in risk assessment and provide more information for policy making.

References

- Armstrong, B., Hutchinson, E., Unwin, J., & Fletcher, T. (2004). Lung cancer risk after exposure to polycyclic aromatic hydrocarbons: A review and meta-analysis. *Environmental Health Perspectives*, 112, 970–978.
- Asian Development Bank (ADB). (2003). *Reducing vehicle emissions in Asia* (pp. 14–22). Philippines: Manila.
- Baek, S. O., Field, R. A., Goldstone, M. E., Kirk, P. W., Lester, J. N., & Perry, R. (1991). A review of atmospheric polycyclic aromatic-hydrocarbons-sources, fate and behavior. *Water, Air, and Soil Pollution*, 60(3–4), 279–300.
- Berdowski J. J. M., Baas J., Bloos J. P. J., Visschedijk A. J. H., & Zandveld P. Y. J. (1997). *The European Emission Inventory of Heavy Metals and Persistent Organic Pollutants for 1990*. TNO Institute of Environmental Sciences, Energy Research and Process Innovation.
- Björseth, A., Lunde, G., & Lindskog, A. (1979). Long-range transport of polycyclic aromatic-hydrocarbons. *Atmospheric Environment*, 13(1), 45–53.

- Boffetta, P., Jourenkova, N., & Gustavsson, P. (1997). Cancer risk from occupational and environmental exposure to polycyclic aromatic hydrocarbons. *Cancer Causes and Control*, 8, 444–472.
- Bond, T. C., Streets, D. G., Yarber, K. F., Nelson, S. M., Woo, J. H., & Klimont, Z. (2004). A technology-based global inventory of black and organic carbon emissions from combustion. *Journal of Geophysical Research-Atmospheres*, 109(D14).
- Boström, C. E., Gerde, P., Hanberg, A., Jernstrom, B., Johansson, C., Kyrklund, T., et al. (2002). Cancer risk assessment, indicators, and guidelines for polycyclic aromatic hydrocarbons in the ambient air. *Environmental Health Perspectives*, 110, 451–488.
- Brubaker, W. W., & Hites, R. A. (1998). OH reaction kinetics of polycyclic aromatic hydrocarbons and polychlorinated dibenzo-p-dioxins and dibenzofurans. *Journal of Physical Chemistry*, 102, 915–921.
- Dipple, A. (1985). Polycyclic aromatic hydrocarbon carcinogenesis: An introduction. In R. G. Harvey (Ed.), *Polycyclic Hydrocarbons and Carcinogenesis* (pp. 1–17). Washington, DC: American Chemical Society.
- Ehrenberg L., & Scalia-Tomba G. (1991). Mathematical models for the initiating and promotive action of carcinogens. In L. Hothorn (Ed.), *Statistical Methods in Toxicology (Lecture Notes in Medical Informatics)* (pp. 65–78). Berlin: Springer.
- Esteve, W., Budzinski, H., & Villenave, E. (2006). Relative rate constants for the heterogeneous reactions of NO₂ and OH radicals with polycyclic aromatic hydrocarbons adsorbed on carbonaceous particles. Part 2: PAHs adsorbed on diesel particulate exhaust SRM 1650a. *Atmospheric Environment*, 40(2), 201–211.
- European Monitoring and Evaluation Programme (EMEP). (2011). *Centre on emission inventories and projections*. Retrieved from <http://www.ceip.at>.
- European Monitoring and Evaluation Programme (EMEP). (2012). *EMEP POP data*. Retrieved from <http://www.nilu.no/projects/ccc/emepdata.html>.
- Friedman, C. L., & Selin, N. E. (2012). Long-range atmospheric transport of polycyclic aromatic hydrocarbons: A global 3-D model analysis including evaluation of Arctic sources. *Environmental Science and Technology*, 46(17), 9501–9510.
- Friedman, C. L., Zhang, Y., & Selin, N. E. (2014). Climate change and emissions impacts on atmospheric PAH transport to the Arctic. *Environmental Science and Technology*, 48(1), 429–437.
- Galarnau, E., Makar, P. A., Sassi, M., & Diamond, M. L. (2007). Estimation of atmospheric emissions of six semivolatile polycyclic aromatic hydrocarbons in southern Canada and the United States by use of an emissions processing system. *Environmental Science and Technology*, 41(12), 4205–4213.
- Great Lakes Comm. (2007). *Assessment of Benzo[a]pyrene Air Emissions in the Great Lakes Region*. Great Lakes Regional Toxic Air Emissions Inventory Steering Committee.
- Hanahan, D., & Weinberg, R. A. (2000). The hallmarks of cancer. *Cell*, 100(1), 57–70.
- International Agency for Research on Cancer (IARC). (1984a). *Polynuclear Aromatic Compounds. Part 2. Carbon Blacks, Mineral Oils and Some Nitroarenes*. IARC Monographs on the Evaluation of Carcinogenic Risks to Humans 33. Lyon, France.
- International Agency for Research on Cancer (IARC). (1984b). *Polynuclear Aromatic Compounds, Part 3, Industrial Exposures in Aluminium Production, Coal Gasification, Coke Production, and Iron and Steel Founding*. IARC Monographs on the Evaluation of Carcinogenic Risks to Humans 34. Lyon, France.
- International Agency for Research on Cancer (IARC). (1985). *Polynuclear Aromatic Compounds. Part 4. Bitumens, Coal-tars and Derived Products, Shale-oils and Soots*. IARC Monographs on the Evaluation of Carcinogenic Risks to Humans 35. Lyon, France.
- International Agency for Research on Cancer (IARC). (1987). *Tobacco Smoking*. IARC Monographs on the Evaluation of Carcinogenic Risks to Humans 38. Lyon, France.

- International Agency for Research on Cancer (IARC). (1989). *Occupational Exposures in Petroleum Refining; Crude Oil and Major Petroleum Fuels*. IARC Monographs on the Evaluation of Carcinogenic Risks to Humans 45. Lyon, France.
- International Agency for Research on Cancer (IARC). (2014). *Agents classified by the IARC monographs, volumes 1–109*. Retrieved from <http://monographs.iarc.fr/ENG/Classification/index.php>.
- Kado, N. Y., Okamoto, R. A., Kuzmicky, P. A., Kobayashi, R., Ayala, A., Gebel, M. E., et al. (2005). Emissions of toxic pollutants from compressed natural gas and low sulfur diesel-fueled heavy-duty transit buses tested over multiple driving cycles. *Environmental Science and Technology*, 39(19), 7638–7649.
- Kelly, M. E. (1983). Sources and Emissions of Polycyclic Organic Matter. U.S. Environmental Protection Agency, Research Triangle Park, North Carolina (pp. 5-9–5-44). EPA Report No. 450/5-83-010b.
- Kristensson, A., Johansson, C., Westerholm, R., Swietlicki, E., Gidhagen, L., Wideqvist, U., et al. (2004). Real-world traffic emission factors of gases and particles measured in a road tunnel in Stockholm. Sweden. *Atmospheric Environment*, 38(5), 657–673.
- Lammel, G., Sehili, A. M., Bond, T. C., Feichter, J., & Grassl, H. (2009). Gas/particle partitioning and global distribution of polycyclic aromatic hydrocarbons – a modelling approach. *Chemosphere*, 76, 98–106.
- Lammel, G., Heil, A., Stemmler, I., Dvorska, A., & Klanova, J. (2013). On the contribution of biomass burning to POPs (PAHs and PCDDs) in air in Africa. *Environmental Science and Technology*, 47(20), 11616–11624.
- Law of the People’s Republic of China on the Coal Industry. (1996). *Order of the President of the People’s Republic of China*, No. 75.
- Lohmann, R., & Lammel, G. (2004). Adsorptive and absorptive contributions to the gas-particle partitioning of polycyclic aromatic hydrocarbons: State of knowledge and recommended parametrization for modeling. *Environmental Science and Technology*, 38(14), 3793–3803.
- Lunde, G., & Björseth, A. (1977). Polycyclic aromatic hydrocarbons in long-range transported aerosols. *Nature*, 268, 518–519.
- Mead, R. C., Brooks, G. W., & Post, B. K. (1986). Summary of Trace Emissions from and Recommendations of Risk Assessment Methodologies for Coal and Oil Combustion Sources. Prepared for U.S. Environmental Protection Agency, Pollutant Assessment Branch, Research Triangle Park, North Carolina. EPA Contract No. 68-02-3889, Work Assignment 41.
- Muller, P. (1997). *Scientific Criteria Document for Multimedia Standards Development Polycyclic Aromatic Hydrocarbons (PAH)*. Part 1: Hazard Identification and Dose-Response Assessment. Ontario, CN: Standard Development Branch, Ontario Ministry of Environment and Energy.
- National Atmospheric Emissions Inventory (NAEI). (2011). Retrieved from http://naei.defra.gov.uk/data_warehouse.php.
- Pacyna, J. M., Breivik, K., Munch, J., & Fudala, J. (2003). European atmospheric emissions of selected persistent organic pollutants, 1970–1995. *Atmospheric Environment*, 37, S119–S131.
- Perera, F. P. (1997). Environment and cancer: Who are susceptible? *Science*, 278, 1068–1073.
- Pitot, H. C., & Dragan, Y. P. (1996). *Chemical carcinogenesis*. In C. D. Klaassen (Ed.) *Casarett and Doull’s Toxicology* (pp. 201–267). New York: McGraw-Hill.
- Pott, P. (1775). Chirurgical observations. Reproduced in: *National Cancer Institute Monograph 1963*, 7–13. Research on Cancer.
- Ravindra, K., Sokhi, R., & Van Grieken, R. (2008). Atmospheric polycyclic aromatic hydrocarbons: Source attribution, emission factors and regulation. *Atmospheric Environment*, 42(13), 2895–2921.
- Riddle, S. G., Robert, M. A., Jakober, C. A., Hannigan, M. P., & Kleeman, M. J. (2007). Size distribution of trace organic species emitted from heavy-duty diesel vehicles. *Environmental Science and Technology*, 41(6), 1962–1969.
- Sehili, A. M., & Lammel, G. (2007). Global fate and distribution of polycyclic aromatic hydrocarbons emitted from Europe and Russia. *Atmospheric Environment*, 41(37), 8301–8315.

- Sims, P., & Grover, P. L. (1974). Epoxides in polycyclic aromatic hydrocarbon metabolism and carcinogenesis. *Advance Cancer Research*, 20, 165–275.
- Smith, J. R., Egbe, M. E., & Lyman, W. L. (1999). Bioremediation of polychlorinated biphenyls and polycyclic aromatic hydrocarbons. In D. C. Adriano, J. -M. Bollag, W. T. Frankenberger Jr., & Sims R. C. (Eds.). *Bioremediation of Contaminated Soil*, (No. 37, pp. 665–713). Madison, WI: American Society of Agronomy.
- Suess, M. J. (1976). The environmental load and cycle of polycyclic aromatic hydrocarbons. *Science of the Total Environment*, 6(3), 239–250.
- Thakker, D. R., Yagi, H., Levin, W., Wood, A. W., Conney, A. H., & Jerina, D. M. (1985). Polycyclic aromatic hydrocarbons: metabolic activation to ultimate carcinogens. In M. W. Anders (Ed.), *Bioactivation of Foreign Compounds* (pp. 177–242). New York: Academic Press.
- Timilsina, G. R., & Dulal, H. B. (2009). A Review of Regulatory Instruments to Control Environmental Externalities from the Transport Sector. *The World Bank*. WPS4867.
- Tsibulsky, V., Sokolovsky, V., & Dutchak, S. (2001). *MSC-E contribution to the HM and POP emission inventories*. Technical Note 7/2001. Retrieved from <http://www.msceast.org/publications.html>.
- United States Environmental Protection Agency (USEPA). (1998). *Locating and Estimating Air Emission From Sources of Polycyclic Organic Matter*. EPA-454/R-98-014. Retrieved from <http://www.epa.gov/ttn/chief>.
- United States Environmental Protection Agency (USEPA). (1999). *The History of Reducing Tailpipe Emissions*. EPA420-F-99-017.
- United States Environmental Protection Agency (USEPA). (2011). *Clearinghouse for Inventories & Emissions factors*. Retrieved from <http://www.epa.gov/ttn/chief/index.html>.
- van der Gon, H. D., van het Bolscher, M., Visschedijk, A., & Zandveld, P. (2007). Emissions of persistent organic pollutants and eight candidate POPs from UNECE-Europe in 2000, 2010 and 2020 and the emission reduction resulting from the implementation of the UNECE POP protocol. *Atmospheric Environment*, 41(40), 9245–9261.
- von Volkman, R. (1875). *Beiträge zur Chirurgie* [in German]. Leipzig, Germany.
- Wang, R., Tao, S., Wang, B., Yang, Y., Lang, C., Zhang, Y. X., et al. (2010). Sources and pathways of polycyclic aromatic hydrocarbons transported to Alert, the Canadian High Arctic. *Environmental Science and Technology*, 44, 1017–1022.
- Wenborn, M., Coleman, P., Passant, N., Lymberidi, E., Sully, J., Weir, R. (1999). *Speciated PAH inventory for the UK*. Department of the Environment TatR.
- Wingfors, H., Sjodin, A., Haglund, P., & Brorstrom-Lunden, E. (2001). Characterisation and determination of profiles of polycyclic aromatic hydrocarbons in a traffic tunnel in Gothenburg, Sweden. *Atmospheric Environment*, 35(36), 6361–6369.
- World Health organization (WHO). (2000). *Air Quality Guidelines for Europe* (2nd ed.). WHO Regional Publications, European Series No. 91. World Health Organization: Copenhagen.
- World Health organization (WHO). (2002). *World Health Report 2002: Reducing Risks, Promoting Life*. Retrieved from <http://www.who.int/whr/en/S>.
- Xu, S. S., Liu, W. X., & Tao, S. (2006). Emission of polycyclic aromatic hydrocarbons in China. *Environmental Science and Technology*, 40(3), 702–708.
- Zhang, Y. X., & Tao, S. (2009). Global atmospheric emission inventory of polycyclic aromatic hydrocarbons (PAHs) for 2004. *Atmospheric Environment*, 43(4), 812–819.
- Zhang, Y. X., Tao, S., Cao, J., & Coveney, R. M. (2007). Emission of polycyclic aromatic hydrocarbons in China by county. *Environmental Science and Technology*, 41(3), 683–687.
- Zhang, Y. X., Tao, S., Shen, H. Z., & Ma, J. M. (2009). Inhalation exposure to ambient polycyclic aromatic hydrocarbons and lung cancer risk of Chinese population. *Proceedings of the National Academy of Sciences of the United States of America*, 106(50), 21063–21067.
- Zhang, Y., Tao, S., Ma, J., & Simonich, S. (2011). Transpacific transport of benzo[a]pyrene emitted from Asia. *Atmospheric Chemistry and Physics*, 11(23), 11993–12006.

Chapter 3

Methodology

3.1 Development of Global Emission Inventory

The emission inventory was developed using a bottom-up approach based on activity intensity and emission factor as follows:

$$E = A \times EF,$$

where E is the estimated emission amount of a specified compound from a specified emission source; A is the activity data of the source—that is, for industrial sector, the amount of fuel combusted or the industrial production levels, for transportation, the distances traveled or the oil consumed, for wildfire, the dry matter burned, etc.; EF is the emission factor—emission per unit activity, which depends significantly on the compound and the source category. This work contains two types of sector-informed emission inventory: one describing temporal trends by country from 1960 to 2007 with future predictions and another for 2007 with detailed spatial information. Development of the inventories require a collection of country-level historical activity data, a spatially resolved activity database, and a dynamic database of EF s which can reflect EF disparity caused by technical differences among countries and development over years.

The 16 PAHs included in the inventory are as follows: naphthalene (NAP), acenaphthylene (ACY), acenaphthene (ACE), fluorene (FLO), phenanthrene (PHE), anthracene (ANT), fluoranthene (FLA), pyrene (PYR), benz(a)anthracene (BaA), chrysene (CHR), benzo[*b*]fluoranthene (BbF), benzo[*k*]fluoranthene (BkF), benzo[*a*]pyrene (BaP), dibenz(a,h)anthracene (DahA), indeno(1,2,3-*cd*)pyrene (IcdP), and benzo(g,h,i)perylene (BghiP). The term “total PAHs” means the sum of these 16 PAHs.

3.1.1 Activity Data

Historical Activity Data. Since PAHs are mainly emitted from incomplete combustion, most emission sources are related with fuel consumption activity. In this work, country-level sector-informed fuel consumption data were obtained from World Energy Statistics Database reported by the International Energy Agency (IEA 2011). Other emission sources and relevant data including primary aluminum production (USGS 2012a, b), deforestation/wildfire (van der Werf et al. 2010), brick kiln (UNIDO 2008), gas flaring (NOAA 2012), petroleum cracking (USEIA 2012), agriculture waste burning (FAO 2012), firewood/crop residue ratios (FAO 2012), non-organized waste burning (UNSD 2011), shipping (global total) (Endresen et al. 2007), and 5 processes in iron-steel industry (WSA 2012) were derived from the United States Geological Survey (USGS 2012a, b), Global Fire Emissions Database (van der Werf et al. 2010), United Nations Industrial Development Organization (UNIDO 2008), National Oceanic and Atmospheric Administration (NOAA 2012), Food and Agriculture Organization of the United Nations (FAO 2012), United Nations Statistics Division (UNSD 2011), and other reports/studies (USEIA 2012; WSA 2012; Endresen et al. 2007). A total of 222 countries/territories and 69 sources were taken into consideration. The detailed information on source category and data source is listed in Table 3.1. Sources were divided into 6 socioeconomic sectors (energy production, industry, transportation, commercial/residential sources, agriculture, and natural sources, see “Sector” column) or 6 categories (as 5 combustion sectors of coal, petroleum, natural gas, solid wastes, and biomass, and an industrial process sector, see “Category” column). The “No.” column included in Tables 3.1, 3.3, 3.6, 3.7, 3.8, and 3.9 were uniform source index in order to make source information easier to retrieve. For the future predictions, the fuels were classified into coal, oil, gas, biomass, other renewable fuels, crop residue, and biomass burned in deforestation/wildfire. The utilization rates of these fuels in the future were derived from the six IPCC SRES scenarios (A1, A2, B1, B2, A1G, and A1T) (Nakićenović et al. 2000).

Spatially Resolved Activity Data. The emission inventory with spatial information for 2007 was built upon a high-resolution fuel combustion inventory, PKU-FUEL-2007 (Wang et al. 2013). PKU-FUEL-2007 was established based on subnational data so that the spatial disaggregation bias caused by unequal per-capita fuel consumptions within individual countries could be substantially reduced. This fuel inventory with 64 source layers was spatially allocated at 0.1×0.1 resolution using different proxies for individual source layers (Wang et al. 2013). The main constraints of PKU-FUEL-2007 include the lack of subnational data for some large countries such as Indonesia and Argentina, inaccuracy of geolocations of power plants from the Carbon Monitoring for Action (CARMA) database version 2.0 (Carbon Monitoring for Action 2013), and relatively high disaggregation uncertainty for aviation, dung cake, and cement production (Wang et al. 2013). Nonetheless, considering that the subnational fuel consumption data of PKU-FUEL-2007 covered approximately 70 % of the overall global fuel consumption, the spatial accuracy of

Table 3.1 Detailed information on 69 PKU-PAH sources

Sector	No.	Category	Activity	Activity density index	Data source ^a	
					Spatial	Temporal
Energy production	1	Coal	Anthracite consumed	Fuel consumption	PKU-FUEL	IEA
	2	Coal	Bituminous coal consumed	Fuel consumption	PKU-FUEL	IEA
	3	Coal	Lignite consumed	Fuel consumption	PKU-FUEL	IEA
	4	Coal	Coking coal consumed	Fuel consumption	PKU-FUEL	IEA
	5	Coal	PEAT consumed	Fuel consumption	PKU-FUEL	IEA
	6	Oil	Gas/diesel consumed	Fuel consumption	PKU-FUEL	IEA
	7	Oil	Residue fuel oil consumed	Fuel consumption	PKU-FUEL	IEA
	8	Biomass	Solid biomass consumed	Fuel consumption	PKU-FUEL	IEA
	9	Biomass	Biogas consumed	Fuel consumption	PKU-FUEL	IEA
	10	Waste	Municipal waste consumed	Fuel consumption	PKU-FUEL	IEA
	11	Waste	Industrial waste consumed	Fuel consumption	PKU-FUEL	IEA
	12	Gas	Dry natural gas consumed	Fuel consumption	PKU-FUEL	IEA
	13	Oil	Natural gas liquid consumed	Fuel consumption	PKU-FUEL	IEA
Industry	14	Process	Petroleum catalytic cracking	Catalytic cracking capacity	USEIA ^b	USEIA
	15	Process	Coke production	Coke production	PKU-FUEL	IEA
	16	Process	Brick production	Brick production	PKU-FUEL	UNIDO
	17	Process	Primary Al production	Primary Al production	PKU-FUEL	USGS
	18	Gas	Gas flaring	Gas flaring mass	PKU-FUEL	NOAA
	19	Process	Iron sintering	Pig iron production	WSA ^c	WSA
	20	Process	Electric arc furnace	Crude steel production	WSA ^c	WSA
	21	Process	Open hearth furnace	Crude steel production	WSA ^c	WSA

(continued)

Table 3.1 (continued)

Sector	No.	Category	Activity	Activity density index	Data source ^a	
					Spatial	Temporal
	22	Process	Oxygen blown converter	Crude steel production	WSA ^c	WSA
	23	Process	Hot rolling	Hot rolled steel production	WSA ^c	WSA
	24	Oil	Gas/diesel consumed	Fuel consumption	PKU-FUEL	IEA
	25	Coal	Anthracite consumed	Fuel consumption	PKU-FUEL	IEA
	26	Coal	Coking coal consumed	Fuel consumption	PKU-FUEL	IEA
	27	Coal	Bituminous coal consumed	Fuel consumption	PKU-FUEL	IEA
	28	Coal	Lignite consumed	Fuel consumption	PKU-FUEL	IEA
	29	Coal	Peat consumed	Fuel consumption	PKU-FUEL	IEA
	30	Oil	Residue fuel oil consumed	fuel consumption	PKU-FUEL	IEA
	31	Biomass	Solid biomass consumed	Fuel consumption	PKU-FUEL	IEA
	32	Biomass	Biogas consumed	Fuel consumption	PKU-FUEL	IEA
	33	Waste	Municipal waste consumed	Fuel consumption	PKU-FUEL	IEA
	34	Waste	Industrial waste consumed	Fuel consumption	PKU-FUEL	IEA
	35	Gas	Dry natural gas consumed	Fuel consumption	PKU-FUEL	IEA
	36	Oil	Natural gas liquid consumed	Fuel consumption	PKU-FUEL	IEA
Residential and commercial	37	Waste	Non-organized waste burning	Waste burned	PKU-FUEL	UNSD
	38	Coal	Anthracite consumed	Fuel consumption	PKU-FUEL	IEA
	39	Coal	Coking coal consumed	Fuel consumption	PKU-FUEL	IEA
	40	Coal	Bituminous coal consumed	Fuel consumption	PKU-FUEL	IEA
	41	Coal	Lignite consumed	Fuel consumption	PKU-FUEL	IEA
	42	Coal	Peat consumed	FUEL consumption	PKU-FUEL	IEA

(continued)

Table 3.1 (continued)

Sector	No.	Category	Activity	Activity density index	Data source ^a		
					Spatial	Temporal	
	43	Gas	Liquid petroleum gas consumed	Fuel consumption	PKU-FUEL	IEA	
	44	Gas	Dry natural gas consumed	Fuel consumption	PKU-FUEL	IEA	
	45	Oil	Natural gas liquid consumed	Fuel consumption	PKU-FUEL	IEA	
	46	Oil	Kerosene consumed	Fuel consumption	PKU-FUEL	IEA	
	47	Gas	Biogas consumed	Fuel consumption	PKU-FUEL	IEA	
	48	Biomass	Indoor firewood burning	Fuel consumption	PKU-FUEL	IEA, FAO	
	49	Biomass	Indoor crop residue burning	Fuel consumption	PKU-FUEL	IEA, FAO	
	50	Biomass	Indoor dung cake burning	Fuel consumption	PKU-FUEL	TERI	
	Transportation	51	Oil	Vehicle gasoline	Fuel consumption	PKU-FUEL	IEA
		52	Oil	Vehicle diesel	Fuel consumption	PKU-FUEL	IEA
53		Biomass	Vehicle liquid biofuels	Fuel consumption	PKU-FUEL	IEA	
54		Oil	Aviation gasoline	Fuel consumption	PKU-FUEL	IEA	
55		Oil	Jet kerosene	Fuel consumption	PKU-FUEL	IEA	
56		Oil	Ocean tanker	Fuel consumption	PKU-FUEL	Endresen	
57		Oil	Ocean container	Fuel consumption	PKU-FUEL	Endresen	
58		Oil	Ocean bulk and combined carries	Fuel consumption	PKU-FUEL	Endresen	
59		Oil	General-cargo vessels	Fuel consumption	PKU-FUEL	Endresen	
60		Oil	Non-cargo vessels	Fuel consumption	PKU-FUEL	Endresen	
61		Oil	Auxiliary engines	Fuel consumption	PKU-FUEL	Endresen	
62		Oil	Military vessels	Fuel consumption	PKU-FUEL	Endresen	

(continued)

Table 3.1 (continued)

Sector	No.	Category	Activity	Activity density index	Data source ^a	
					Spatial	Temporal
Agriculture	63	Waste	Agriculture waste burning	Crop residue burned	PKU-FUEL	FAO
	64	Oil	Gas/diesel	Fuel consumption	PKU-FUEL	IEA
Natural	65	Biomass	Forest fire	Dry matter burned	PKU-FUEL	GFED
	66	Biomass	Deforestation fire	Dry matter burned	PKU-FUEL	GFED
	67	Biomass	Peat fire	Dry matter burned	PKU-FUEL	GFED
	68	Biomass	Woodland fire	Dry matter burned	PKU-FUEL	GFED
	69	Biomass	Savanna fire	Dry matter burned	PKU-FUEL	GFED

Note

^aPKU-FUEL (Wang et al. 2013); USEIA (U.S. Energy Information Administration 2012); WSA (World Steel Association 2012); IEA (International Energy Agency 2011); UNIDO (United Nations Industrial Development Organization 2008); USGS (U.S. Geological Survey 2012a, b); NOAA (National Oceanic and Atmospheric Administration 2012); UNSD (United Nations Statistics Division 2011); FAO (Food and Agriculture Organization of the United Nations 2012); TERI (The Energy and Resources Institute 2008); Endresen (Endresen et al. 2007); GFED (van der Werf et al. 2010)

^bCountry-level activity data for petroleum catalytic cracking was derived from USEIA (2012). The spatial allocation for each country was based on gas flaring source from PKU-FUEL, due to a lack of facility location information

^cCountry-level activity data for iron and steel sources was derived from WSA (2012). The spatial allocation for each country was based on industrial coal combustion from PKU-FUEL, due to a lack of facility location information

The tables are reproduced with permission from Shen et al. (2013). Copyright 2013, American Chemical Society

emission inventories can be improved using PKU-FUEL-2007. 63 of the 64 sources from PKU-FUEL-2007 were directly used to develop PAHs emission inventory (Table 3.1). For the remaining sources that are not involved in PKU-FUEL-2007, including catalytic cracking (USEIA 2012) and five processes in iron-steel industry (iron sintering, open hearth furnace, convertor, arc furnace, and hot rolling) (WSA 2012), activity data for individual countries were derived from the above-mentioned historical data and disaggregated to 0.1×0.1 grids using gas flaring and industrial coal consumptions as proxies, respectively. The source classification was consistent between country-level and spatially resolved activity data.

Monthly Variation. Monthly variation of residential activity data was predicted using heating day (*HD*) and power-function-based heating degree day (HDD_p) as independent variables (Zhu et al. 2013). The equation is as follows:

Table 3.2 Parameters recorded for EF_{PAH} measurements

Parameters	Categories
Fuel type	Gasoline, diesel, liquefied petroleum gases
Vehicle type	Light-duty gasoline vehicle, heavy-duty gasoline vehicle, light-duty diesel vehicle, heavy-duty diesel vehicle or truck, motorcycle
Testing year	1961–2008
Model year (Y_m)	1956–2005
Measurement method	Dynamometer test, tunnel test, freeway measurement
Country where the vehicle was marketed and operated	Australia, Belgium, Brazil, Canada, China, Denmark, France, Germany, Greece, Japan, Mexico, Netherlands, Sweden, Switzerland, Taiwan (China), USA
Catalytic converter	None, three-way, oxidation
Driving cycle	The federal test procedure, inspection and maintenance 240 driving cycle, new European driving cycle, extra-urban driving cycle, ECE European driving cycle, composite urban emission drive cycle, Athens driving cycle, and ARTEMIS cycle, etc.
Starting mode	Cold- or warm-start
Odometer reading	270–64000 km
Particulate matter fraction	PM1.3, PM1.8, PM2.5, PM10, TSP

Reprinted from Shen et al. (2011). Copyright 2011, with permission from Elsevier

$$F_{cap} = 5.95 \times 10^{-5} HDD_p + 3.92 \times 10^{-4} HD + 0.147 \quad R^2 = 0.66$$

where n in the HDD_p definition equals to 0.9; 5.95, 3.92, and 0.147 were regression coefficients derived from least-square fitting based on provincial-level data in China (Zhu et al. 2013). The model was extended to a global scale.

Monthly variation of deforestation/wildfire and agricultural waste burning were from the GFED dataset (van der Werf et al. 2010). For all other sources, it was assumed that seasonal variations were not significant.

3.1.2 Emission Factor Analysis

Through a thorough literature review, the EF_{PAHs} database was established containing 5822 EFs from actual measurements. The database was used in three ways: (1) regression modeling for on-road motor vehicles and other sources in transportation sector (13 sources), (2) technology splitting for industrial sources and anthropogenic biomass burning (28 sources), and (3) medians and frequency distributions for all other sources (28 sources). Time- and country-specific EF_{PAHs} can be derived using the first two approaches.

Regression Analysis. Abundant EF_{PAHs} measurements for on-road motor vehicles allow for regression analysis to address key factors influencing EF variations and to develop empirical models for this specific emission source. During data collection, if the tests were conducted under extreme driving modes, or burning uncommon fuels, or using modified vehicles, the data were excluded. Grubb's test was applied to test statistical outliers for each of the 16 PAHs after log transformation. No outlier was detected at a significant level of 0.05. A total of 2855 EF_{PAHs} from 282 individual tests conducted in 16 countries were adopted (Alsberg et al. 1985; Bartlett et al. 1992; Benner et al. 1989; Bergvall and Westerholm 2009; Beyea et al. 2008; Cadle et al. 1999; Chellam et al. 2005; De Abrantes et al. 2004; Durbin et al. 1998; EA 2003; Fraser et al. 1998; Fujita et al. 2007; HARP-HAZ 2000; Handa et al. 2002; Kado et al. 2005; Karavalakis et al. 2009; Kristensson et al. 2004; Leonidas and Zissis 2000; Lim et al. 2007; Marr et al. 1999; Mi et al. 2001; Miguel et al. 1998; National Academy of Sciences 1983; Nelson et al. 2008; Ning et al. 2008; Norbeck et al. 1998; Pakbin et al. 2009; Phuleria et al. 2006; Riddle et al. 2007a, b, c; Rogge et al. 1993; Sagebiel et al. 1997; Schauer et al. 1999, 2002; Siegl et al. 1999; Staehelin et al. 1998; Tang et al. 2007; Wang et al. 2002, 2007; Westerholm et al. 1988, 1991, 1992, 1996, 2001; Westerholm and Egeback 1994; Westerholm and Li 1994; Wingfors et al. 2001; Yang et al. 2005; Zielinska et al. 2003). The vehicles used for these tests were produced from 1956 to 2005. The EF_{PAHs} reported in different units were converted to mg PAH per ton fuel consumed (mg/t). For a few values reported as mass per distance traveled, vehicle fuel consumption efficiencies as functions of year and vehicle type were adopted to convert them into mg/t (Davis et al. 2010; EA 2003; USEPA 1995).

A number of test conditions were recorded for EF_{PAHs} measurements in the literature. The often reported parameters include fuel type, vehicle type, testing year, model year (Y_m), measurement method, country where the vehicle was marketed and operated, driving speed, catalytic converter, driving cycle, fuel consumption, starting mode, odometer reading, and particulate matter fraction. (see Table 3.2). For those measured in a tunnel test, the Y_m was derived by subtracting the average vehicle age of the country from the testing year (Infobank 2010; USEPA 1995).

Among the above-mentioned factors, those recorded by most studies were country, Y_m , and vehicle type. These factors were analyzed for their effects on EF_{PAHs} . Both bivariate and univariate regression model were conducted using ordinary least-square method. For quantifying country variables, a number of socioeconomic parameters were tested by trial-and-error, and it was found that gross domestic production per capita (purchasing power parity, GDP_c) is the best indicator for describing the difference in developing status among countries. In fact, GDP_c can also be used for describing temporal trends of developing status of a given country over time. Based on these results, a set of univariate regression model were developed for EF_{PAHs} of all individual PAHs based on log-transformed EF_{PAHs} and GDP_c . Data of GDP_c were derived from the World Bank (The World Bank 2010). The robustness of these models was further confirmed using a jack-knife test (see Fig. 3.1). These models were then utilized to extrapolate EF s for

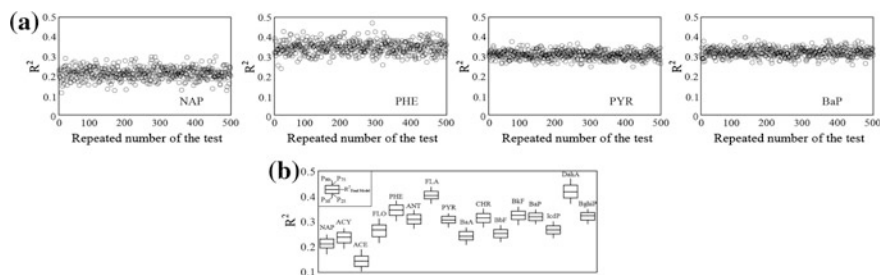


Fig. 3.1 Jackknifed R^2 by removing 20 % randomly selected data points each time for 500 times. **a** The results for NAP, PHE, PYR, and BaP are presented as four representative compounds. The red horizontal line represents the R^2 derived from the final model without deletion. **b** Means, 10th, 25th, 75th, and 90th percentiles of the resulting jackknifed coefficients of the determination for each PAH compound. Reproduced with permission from Shen et al. (2013). Copyright (2013) American Chemical Society

other transportation sources including shipping and aviation, where same slopes but distinguished intercepts were used for the same compounds.

Technology Splits. For 28 out of the 69 sources, a technology split method was applied to reduce the estimate uncertainty introduced by *EFs*. For the technology splitting approach, each source was divided into 2 or more technology divisions, assuming that *EFs* for each technology division remain stable, and fractions of various technology divisions changed over time (Bond et al. 2007). The 222 countries/territories were classified into 5 categories: (1) the USA and Canada, (2) other developed countries (39 countries), (3) former USSR federals (14 countries), (4) China, and (5) all other developing countries (166 countries). For each country category, the time-dependent fractions of the technology divisions were either derived from the literature or calculated using a series of S-shaped curves. The S-curve being often used is as follows:

$$X(t) = (X_0 - X_f)e^{-(t-t_0)^2/2s^2} + X_f,$$

where X_0 and X_f are initial and final fractions of a certain technology division, respectively; t_0 is the start time of the technology transition, and s is a rate (Bond et al. 2007). The smaller the s value is, the faster the transition process will be. All parameters of S-shaped curves for technology splitting were listed in Table 3.3 and Table 3.4. Although, for each compound, one technology division associates with one constant *EF* value, the combined *EF* for a certain source may change over time due to change of fractions of its technology divisions. Figure 3.2 illustrated these kinds of changes of combined *EFs* for some typical sources. The parameterization in this work could be also applied to emission estimates for other compounds with washout mechanism similar to PAHs. However, it should be noticed that these parameters only provide a regional-level technology transition framework. The simulated results should be refined, if detail information could be obtained. In the case of coke production in China, the ratio of beehive coking to mechanical one can

Table 3.3 List of 28 emission sources with technology splits

No.	Sector	Category	Fuel and process	All sub-sources	Ratio description	The United States and Canada				Former USSR			
						X0	Xf	t0	s	X0	Xf	t0	s
1	Energy	Coal	Anthracite	a. Uncontrol b. Efficient control	a/(a+b)	1	0	1907	35	1	0	1955	26
2	Energy	Coal	Bituminous coal										
3	Energy	Coal	Lignite										
4	Energy	Coal	Coking coal										
5	Energy	Coal	Peat										
8	Energy	Biomass	Solid biomass										
10	Energy	Waste	Municipal waste										
11	Energy	Waste	Industrial waste										
25	Industry	Coal	Anthracite	a. Uncontrol b. Efficient control	a/(a+b)	1	0	1907	41	1	0	1955	35
26	Industry	Coal	Coking coal										
27	Industry	Coal	Bituminous coal										
28	Industry	Coal	Lignite										
29	Industry	Coal	Peat										
31	Industry	Biomass	Solid Biomass										
33	Industry	Waste	Municipal waste										
34	Industry	Waste	Industrial waste										
14	Industry	Process	Petroleum catalytic cracking										
19	Industry	Process	Iron sintering										
20	Industry	Process	Electric arc furnace										
21	Industry	Process	Open hearth furnace										
22	Industry	Process	Oxygen blown converter										
23	Industry	Process	Hot rolling										

(continued)

Table 3.3 (continued)

No.	Sector	Category	Fuel and process	All sub-sources	Ratio description	The United States and Canada				Former USSR							
						X0	Xf	t0	s	X0	Xf	t0	s				
17	Industry	Process	Primary Al production ^a	a. Prebaked-uncontrol b. Prebaked-control c. Soderberg-uncontrol d. Soderberg-control	(a+b)/(a+b+c+d) a/(a+b) & c/(c+d)	1	0	1907	41	1	0	1955	35				
15	Industry	Process	Coke production ^b	a. Beehive b. Mechanical-uncontrol c. Mechanical-control	a/(a+b+c) b/(b+c)	1	0.002	1904	12	1	0.002	1887	20				
48	Residential	Biomass	Indoor firewood burning ^c	a. Fireplace b. Improved woodstove c. Traditional woodstove	c/(b+c) a/(a+b+c)	1	0	1988	21	1	0	1985	20				
49	Residential	Biomass	Indoor crop residue burning	a. Improved stove b. Traditional stove	b/(a+b)	1	0	1988	21	1	0	1988	21				
49	Residential	Biomass	Indoor crop residue burning ^d	a. Barley b. Maize c. Rice d. Wheat	a/(a+b+c+d) b/(a+b+c+d) c/(a+b+c+d) d/(a+b+c+d)												
63	Agriculture	Biomass	Open crop residue burning ^d														
No.	Sector	Category	Fuel and Process	All sub-sources	Ratio description	Other developed countries				China				Other developing countries			
						X0	Xf	t0	s	X0	Xf	t0	s	X0	Xf	t0	s
1	Energy	Coal	Anthracite	a. Uncontrol b. Efficient control	a/(a+b)	1	0	1915	40	1	0	1979	18	1	0	1945	31
2	Energy	Coal	Bituminous coal														
3	Energy	Coal	Lignite														
4	Energy	Coal	Coking coal														
5	Energy	Coal	Peat														
8	Energy	Biomass	Solid biomass														
10	Energy	Waste	Municipal waste														
11	Energy	Waste	Industrial waste														

(continued)

Table 3.3 (continued)

No.	Sector	Category	Fuel and Process	All sub-sources	Ratio description	Other developed countries			China			Other developing countries					
						X0	Xf	t0	s	t0	Xf	s	X0	Xf	t0	s	
25	Industry	Coal	Anthracite	a. Uncontrol	a/(a+b)	1	0	1915	55	1	0	1979	25	1	0	1945	52
26	Industry	Coal	Coking coal	b. Efficient control													
27	Industry	Coal	Bituminous coal														
28	Industry	Coal	Lignite														
29	Industry	Coal	Peat														
31	Industry	Biomass	Solid biomass														
33	Industry	Waste	Municipal waste														
34	Industry	Waste	Industrial waste														
14	Industry	Process	Petroleum catalytic cracking														
19	Industry	Process	Iron sintering														
20	Industry	Process	Electric arc furnace														
21	Industry	Process	Open hearth furnace														
22	Industry	Process	Oxygen blown converter														
23	Industry	Process	Hot rolling														
17	Industry	Process	Primary Al production ^a	a. Prebaked-uncontrol	(a+b)/(a+b+c+d)												
				b. Prebaked-control													
				c. Soderberg-uncontrol	a/(a+b) & c/(c+d)	1	0	1915	55	1	0	1979	25	1	0	1945	52
				d. Soderberg-control													
15	Industry	Process	Coke production ^b	a. Beehive	a/(a+b+c)	1	0.002	1894	17					1	0.002	1930	23
				b. Mechanical-uncontrol	b/(b+c)	1	0	1915	55	1	0	1979	25	1	0	1945	52
				c. Mechanical-control													

(continued)

Table 3.3 (continued)

No.	Sector	Category	Fuel and Process	All sub-sources	Ratio description	Other developed countries				China				Other developing countries			
						X0	Xf	t0	s	X0	Xf	t0	s	X0	Xf	t0	s
48	Residential	Biomass	Indoor firewood burning ^c	a. Fireplace b. Improved woodstove c. Traditional woodstove	c/(b+c) a/(a+b+c)	1	0	1985	20	1	0	1985	23	1	0	1985	23
49	Residential	Biomass	Indoor crop residue burning	a. Improved stove b. Traditional stove	b/(a+b)	1	0	1988	21	1	0	1988	21	1	0	1988	21
49	Residential	Biomass	Indoor crop residue burning ^d	a. Barley b. Maize c. Rice d. Wheat	a/(a+b+c+d) b/(a+b+c+d) c/(a+b+c+d) d/(a+b+c+d)												
63	Agriculture	Biomass	Open crop residue burning ^d														

^aThe ratio of prebaked/(prebaked + soderberg) in primary aluminum production was simulated separately for each country based on reported data from two time points, 1998 and 2007.^{16,17} (see Table 3.4)

^bBeehive coke production beyond 2010 was assumed to be 0. The fractions of beehive in China have been reported annually since 1949¹⁵

^cThe ratio of fireplace/(fireplace + woodstove) was assumed to be 1/3 constantly for North America and European countries during the study period, and 0 for other countries

^dCountry crop production was used to calculate the proportions of various kinds of crop residue burned⁹

Reproduced with permission from Shen et al. (2013). Copyright (2013) American Chemical Society

be obtained for the whole study period (China Energy Group 2008), which was considered with better quality and applied instead of S-curve fitting (Table 3.5). Similarly, for primary aluminum production, detailed information on cell technique (prebake or soderberg) can be found by country, and thus, S-curve fitting was conducted for individual countries rather than for regions (Table 3.4).

Table 3.4 List of coefficients to simulate the ratio of prebaked/(prebaked + soderberg) within primary aluminum production for each country^a

Country	X0	Xf	t0	s
Austria	0	1	2000	1.0
Azerbaijan	0	1	2000	1.0
Brazil	0	1	1982	16.7
Cameroon	0	1	1998	2.4
Canada	0	1	1918	51.9
China	0	1	1952	31.9
Croatia	0	1	2000	1.0
Czech Republic	0	1	2000	1.0
Egypt	0	1	1996	3.0
France	0	1	1991	4.2
Germany	0	1	1992	4.2
Hungary	0	1	2000	1.0
India	0	1	1950	31.9
Indonesia	0	1	1998	2.4
Japan	0	1	2000	1.0
North Korea	0	1	2000	1.0
South Korea	0	1	2000	1.0
Kuwait	0	1	2000	1.0
Macedonia	0	1	2000	1.0
Mexico	0	1	2000	1.0
Norway	0	1	1980	17.7
Poland	0	1	1998	6.4
Russia	0	1	1970	53.2
South Africa	0	1	1987	5.3
Spain	0	1	1965	33.2
Suriname	0	1	2000	1.0
Sweden	0	1	1982	21.5
Ukraine	0	1	2000	1.0
United Kingdom	0	1	1965	12.2
USA	0	1	1965	21.5

^aThe simulation coefficients was based on reported data from two time points, 1998 and 2007 (USGS 2012a, b; GENISIM 2012). For other countries, the ratios, prebaked/(prebaked + soderberg), were set to be 1 constantly according to these reports

Reproduced with permission from Shen et al. (2013). Copyright (2013) American Chemical Society

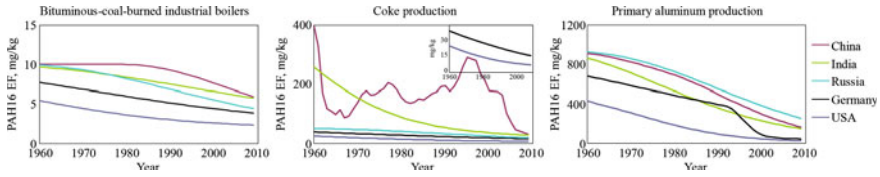


Fig. 3.2 Time trends of PAH16 EF_s of three typical sources for several representative countries including the USA, Germany, Russia, India, and China. The emission sources are Bituminous-coal-burned industrial boilers, coke production, and primary aluminum production from left to right, respectively. Reprinted with permission from Shen et al. (2013). Copyright (2013) American Chemical Society

Table 3.5 The ratios of beehive coke production to total coke production in China from 1949 to 2012

Year	Ratio	Year	Ratio	Year	Ratio
1949	0.018519	1971	0.235197	1993	0.355043
1950	0.14	1972	0.262147	1994	0.435915
1951	0.167488	1973	0.231817	1995	0.500888
1952	0.231834	1974	0.234536	1996	0.490396
1953	0.216901	1975	0.255707	1997	0.479717
1954	0.257778	1976	0.27563	1998	0.393644
1955	0.288321	1977	0.317129	1999	0.347884
1956	0.284144	1978	0.302985	2000	0.28168
1957	0.331325	1979	0.268165	2001	0.280926
1958	0.630635	1980	0.21598	2002	0.2774
1959	0.750444	1981	0.185623	2003	0.256259
1960	0.714893	1982	0.176163	2004	0.135852
1961	0.571734	1983	0.182227	2005	0.083074
1962	0.247392	1984	0.206715	2006	0.034756
1963	0.136528	1985	0.201166	2007	0.025345
1964	0.119497	1986	0.224223	2008	0.017125
1965	0.097524	1987	0.245039	2009	0.009974
1966	0.131579	1988	0.256385	2010	0.003763
1967	0.075318	1989	0.294233	2011	0
1968	0.084699	1990	0.299945	2012	0
1969	0.134845	1991	0.26605		
1970	0.177682	1992	0.298597		

For the remaining 28 sources, fixed EF_{PAH_s} , which are not time and country dependent, were used. Means and standard deviations of collected EF_{PAH_s} for all sources and subsources are listed in Table 3.6

Table 3.6 Geometric means of the collected emission factors of 16 PAHs for various sources

No. ^a	Units	Subsource	NAP	ACY	ACE	FLO	PHE	ANT	FLA
1-5	mg/t fuel consumed	Uncontrol	2.0×10^1	4.3×10^{-1}	1.2×10^0	2.0×10^0	1.3×10^1	1.2×10^0	4.0×10^0
		Control	2.7×10^0	8.2×10^{-2}	2.0×10^{-1}	3.3×10^{-1}	1.2×10^0	1.1×10^{-1}	3.4×10^{-1}
6,7,13	mg/t fuel consumed	Uncontrol	3.3×10^2	2.7×10^0	2.6×10^0	2.0×10^0	6.2×10^0	1.2×10^0	3.8×10^0
		Control	7.6×10^0	2.7×10^{-1}	1.6×10^{-2}	9.8×10^{-2}	8.9×10^{-2}	5.3×10^{-2}	3.5×10^{-2}
8	mg/t fuel consumed	Uncontrol	1.0×10^0	5.2×10^{-2}	2.6×10^{-3}	1.6×10^{-2}	8.4×10^{-3}	4.8×10^{-3}	3.1×10^{-3}
		Control	1.9×10^{-3}	1.4×10^{-4}	1.6×10^{-3}	8.6×10^{-5}	1.6×10^{-4}	1.0×10^{-5}	4.1×10^{-5}
9	g/TJ fuel consumed	Uncontrol	7.2×10^0	2.7×10^0	2.1×10^{-1}	2.4×10^0	5.6×10^{-1}	5.2×10^{-1}	2.3×10^{-1}
		Control	9.9×10^{-1}	5.1×10^{-1}	3.5×10^{-2}	4.0×10^{-1}	5.3×10^{-2}	4.8×10^{-2}	2.0×10^{-2}
10,11	g/TJ fuel consumed	Uncontrol	1.9×10^{-2}	1.4×10^{-3}	1.6×10^{-2}	8.6×10^{-4}	1.6×10^{-3}	1.0×10^{-4}	4.1×10^{-4}
		Control	6.0×10^{-7}	0.0×10^0	0.0×10^0	0.0×10^0	1.3×10^{-4}	6.9×10^{-7}	3.4×10^{-6}
12	kg/barrel capacity	Uncontrol	8.2×10^{-8}	0.0×10^0	0.0×10^0	0.0×10^0	1.2×10^{-5}	6.3×10^{-8}	2.9×10^{-7}
		Control	2.0×10^2	4.3×10^1	1.0×10^1	2.8×10^1	1.0×10^2	1.7×10^1	4.6×10^1
14	g/t coke produced	Mechanical-uncontrol	2.0×10^1	5.5×10^0	5.4×10^{-1}	2.7×10^0	7.6×10^0	2.0×10^0	3.3×10^0
		Mechanical-control	1.6×10^0	5.6×10^{-1}	2.7×10^{-2}	4.0×10^{-1}	4.9×10^{-1}	2.0×10^{-1}	2.3×10^{-1}
15	mg/t brick produced	Uncontrol	4.2×10^2	1.1×10^2	1.1×10^1	5.5×10^1	1.6×10^2	4.2×10^1	6.8×10^1
		Control	3.3×10^1	1.2×10^1	5.6×10^{-1}	8.3×10^0	1.0×10^1	4.0×10^0	4.8×10^0
16	g/t Al produced	Prebaked-uncontrol	4.0×10^{-1}	1.5×10^{-2}	2.4×10^{-1}	3.9×10^{-1}	4.9×10^1	5.6×10^0	1.4×10^2
		Prebaked-control	5.1×10^{-2}	2.9×10^{-2}	1.8×10^{-2}	1.6×10^0	7.9×10^1	1.6×10^{-1}	2.2×10^1
17	g/TJ gas burned	Soderberg-uncontrol	5.5×10^{-2}	2.9×10^{-3}	3.9×10^{-2}	6.4×10^{-2}	4.6×10^0	5.1×10^{-1}	1.2×10^1
		Soderberg-control	7.0×10^{-3}	5.5×10^{-3}	3.0×10^{-3}	2.7×10^{-1}	7.5×10^0	1.5×10^{-2}	1.9×10^0
18	mg/t pig iron produced	Uncontrol	2.9×10^3	2.3×10^{-3}	2.9×10^{-2}	1.1×10^{-3}	1.7×10^{-3}	1.6×10^{-4}	7.4×10^{-4}
		Control	3.3×10^2	1.8×10^2	1.1×10^1	2.3×10^1	1.6×10^1	1.9×10^0	2.3×10^0
19	mg/t crude steel produced	Uncontrol	6.9×10^3	1.2×10^2	6.1×10^1	5.9×10^1	3.4×10^1	4.3×10^2	2.5×10^2
		Control	9.5×10^2	2.3×10^1	9.9×10^0	9.9×10^0	3.2×10^0	3.9×10^1	2.2×10^1

(continued)

Table 3.6 (continued)

No. ^a	Units	Subsource	NAP	ACY	ACE	FLO	PHE	ANT	FLA
21	mg/t crude steel produced	Uncontrol	5.4×10^2	1.3×10^1	6.2×10^0	6.1×10^0	1.2×10^0	2.2×10^1	3.5×10^0
		Control	7.4×10^1	2.4×10^0	1.0×10^0	1.0×10^0	1.2×10^{-1}	2.0×10^0	3.1×10^{-1}
22	mg/t crude steel produced	Uncontrol	2.6×10^3	7.5×10^1	3.7×10^1	4.5×10^1	1.4×10^1	2.8×10^2	1.1×10^2
		Control	3.6×10^2	1.4×10^1	6.1×10^0	7.5×10^0	1.3×10^0	2.5×10^1	9.9×10^0
23	mg/t hot rolled steel produced	Uncontrol	9.6×10^1	3.7×10^1	2.7×10^0	5.5×10^0	6.8×10^0	8.1×10^{-1}	1.0×10^0
		Control	1.3×10^1	7.1×10^0	4.4×10^{-1}	9.1×10^{-1}	6.4×10^{-1}	7.4×10^{-2}	9.1×10^{-2}
24,30,36	mg/t fuel consumed		5.1×10^2	4.5×10^0	4.8×10^0	2.7×10^0	8.6×10^0	1.8×10^0	6.8×10^0
25–29	mg/t fuel consumed	Uncontrol	5.2×10^3	4.0×10^1	9.7×10^1	2.0×10^1	3.2×10^3	2.4×10^1	8.1×10^2
		Control	7.2×10^2	7.6×10^0	1.6×10^1	3.3×10^0	3.0×10^2	2.2×10^0	7.1×10^1
31	mg/t fuel consumed	Uncontrol	2.0×10^3	2.5×10^1	1.2×10^0	9.8×10^{-1}	2.3×10^1	1.1×10^0	7.2×10^0
		Control	2.8×10^2	4.8×10^0	2.0×10^{-1}	1.6×10^{-1}	2.1×10^0	9.6×10^{-2}	6.3×10^{-1}
32	g/TJ fuel consumed	Uncontrol	2.9×10^{-3}	2.3×10^{-4}	2.9×10^{-3}	1.1×10^{-4}	2.2×10^{-4}	1.6×10^{-5}	7.4×10^{-5}
		Control	1.9×10^3	2.4×10^2	1.7×10^1	2.4×10^1	1.4×10^2	1.0×10^1	4.8×10^1
33,34	g/TJ fuel consumed	Uncontrol	2.7×10^2	4.7×10^1	2.8×10^0	4.0×10^0	1.4×10^1	9.5×10^{-1}	4.2×10^0
		Control	2.9×10^{-2}	2.3×10^{-3}	2.9×10^{-2}	1.1×10^{-3}	2.2×10^{-3}	1.6×10^{-4}	7.4×10^{-4}
35	g/TJ fuel consumed		1.1×10^1	7.3×10^0	6.4×10^{-1}	3.0×10^0	5.3×10^0	1.3×10^0	2.8×10^0
37	g/t waste burned		1.3×10^{-1}	2.9×10^{-2}	1.1×10^{-2}	1.0×10^{-2}	1.0×10^{-1}	6.1×10^{-3}	3.0×10^{-2}
38	g/t fuel consumed		1.6×10^1	6.1×10^0	1.1×10^1	4.3×10^0	1.1×10^1	1.9×10^0	4.2×10^0
39–42	g/t fuel consumed		5.3×10^{-2}	1.3×10^{-2}	3.7×10^{-2}	7.7×10^{-3}	3.6×10^{-3}	1.6×10^{-3}	3.4×10^{-2}
44	g/TJ fuel consumed		7.0×10^{-1}	6.0×10^{-2}	6.7×10^{-1}	5.0×10^{-2}	6.2×10^{-2}	4.3×10^{-3}	2.1×10^{-2}
45,46	g/t fuel consumed		5.3×10^{-2}	1.3×10^{-2}	3.7×10^{-2}	7.7×10^{-3}	3.6×10^{-3}	1.6×10^{-3}	3.4×10^{-2}
47	g/TJ fuel consumed		7.0×10^{-2}	6.0×10^{-3}	6.7×10^{-2}	5.0×10^{-3}	6.2×10^{-3}	4.3×10^{-4}	2.1×10^{-3}

(continued)

Table 3.6 (continued)

No. ^a	Units	Subsource	NAP	ACY	ACE	FLO	THE	ANT	FLA	
48	g/t fuel consumed	Traditional woodstove	1.2×10^2	9.4×10^1	2.5×10^1	1.0×10^1	3.0×10^1	5.3×10^0	7.5×10^0	
		Improved woodstove	1.5×10^1	1.0×10^1	5.6×10^0	7.6×10^{-1}	7.9×10^0	2.8×10^0	6.0×10^0	
		Fireplace	1.6×10^1	1.1×10^1	3.9×10^0	1.6×10^0	6.8×10^0	2.0×10^0	3.2×10^0	
49	g/t fuel consumed	Barley-traditional stove	1.1×10^2	2.4×10^1	2.1×10^1	3.3×10^1	6.1×10^1	8.9×10^0	2.5×10^1	
		Maize-traditional stove	1.5×10^1	2.6×10^0	2.4×10^0	3.4×10^0	6.9×10^0	1.1×10^0	2.7×10^0	
		Rice-traditional stove	4.1×10^1	5.5×10^0	5.9×10^0	6.3×10^0	1.0×10^1	1.7×10^0	7.6×10^0	
		Wheat-traditional stove	3.7×10^1	8.3×10^0	7.1×10^0	1.1×10^1	2.1×10^1	3.1×10^0	8.6×10^0	
		Barley-improved stove	1.3×10^1	2.6×10^0	4.7×10^0	2.4×10^0	1.6×10^1	4.6×10^0	2.0×10^1	
		Maize-improved stove	1.9×10^0	2.9×10^{-1}	5.4×10^{-1}	2.5×10^{-1}	1.8×10^0	5.8×10^{-1}	2.1×10^0	
		Rice-improved stove	5.0×10^0	6.0×10^{-1}	1.3×10^0	4.7×10^{-1}	2.7×10^0	9.1×10^{-1}	6.0×10^0	
50	g/t fuel consumed	Wheat-improved stove	4.6×10^0	9.1×10^{-1}	1.6×10^0	8.3×10^{-1}	5.6×10^0	1.6×10^0	6.9×10^0	
		Traditional woodstove	7.9×10^1	4.1×10^1	1.5×10^1	6.3×10^0	2.5×10^1	6.1×10^0	1.2×10^1	
		Improved woodstove	1.9×10^2	5.0×10^0	9.6×10^0	5.3×10^0	5.7×10^1	2.8×10^0	5.2×10^1	
		Barley	1.5×10^2	1.8×10^1	2.2×10^1	2.1×10^0	1.7×10^1	2.4×10^0	2.4×10^0	
		Maize	1.5×10^0	6.3×10^{-1}	5.0×10^{-1}	6.4×10^{-2}	1.8×10^0	2.7×10^{-1}	7.6×10^{-1}	
63	g/t dry matter burned	Rice	7.7×10^0	5.2×10^{-2}	6.1×10^{-1}	2.9×10^{-1}	1.4×10^0	2.4×10^{-1}	4.4×10^{-1}	
		Wheat	4.4×10^1	3.3×10^{-1}	7.0×10^{-1}	2.5×10^{-1}	4.8×10^0	1.2×10^0	6.7×10^0	
		Improved woodstove	1.1×10^1	2.2×10^0	1.8×10^0	7.5×10^{-1}	2.3×10^0	3.7×10^{-1}	1.6×10^0	
65–68	g/t dry matter burned									
69	g/t dry matter burned									
No. ^a	Units	Subsource	BaA	CHR	BHF	BkF	BaP	IcdP	DahA	BghtP
		Uncontrol	2.6×10^0	1.7×10^0	1.1×10^0	8.1×10^{-1}	1.2×10^0	1.1×10^0	3.7×10^{-1}	8.3×10^{-1}
1–5	mg/t fuel consumed	Control	1.7×10^{-1}	5.0×10^{-2}	2.3×10^{-2}	2.3×10^{-2}	1.4×10^{-2}	1.5×10^{-2}	1.1×10^{-2}	1.4×10^{-2}
6,7,13	mg/t fuel consumed		2.9×10^0	4.8×10^{-1}	9.0×10^{-1}	2.0×10^0	1.4×10^0	9.2×10^{-1}	2.2×10^0	1.1×10^0
8	mg/t fuel consumed	Uncontrol	1.9×10^{-1}	5.0×10^{-2}	4.0×10^{-1}	3.7×10^{-1}	2.2×10^{-3}	1.8×10^{-3}	0.0×10^0	4.0×10^{-2}
		Control	1.2×10^{-2}	1.5×10^{-3}	8.9×10^{-3}	1.1×10^{-2}	2.5×10^{-5}	2.5×10^{-4}	0.0×10^0	6.8×10^{-4}

(continued)

Table 3.6 (continued)

No. ^a	Units	Subsource	PYR	BaA	CHR	BbF	BkF	BaP	IcdP	DahA	BghtP	
9	g/TJ fuel consumed		5.2×10^{-5}	8.8×10^{-5}	9.7×10^{-5}	9.7×10^{-5}	9.7×10^{-5}	6.7×10^{-5}	5.2×10^{-5}	3.6×10^{-5}	1.1×10^{-4}	
10,11	g/TJ fuel consumed	Uncontrol	1.5×10^0	1.3×10^0	1.1×10^0	5.8×10^{-1}	3.1×10^0	7.3×10^{-1}	1.1×10^0	6.4×10^{-1}	2.3×10^0	
		Control	9.8×10^{-2}	6.7×10^{-2}	3.1×10^{-2}	1.3×10^{-2}	8.8×10^{-2}	8.3×10^{-3}	1.5×10^{-2}	1.9×10^{-2}	3.9×10^{-2}	
12	g/TJ fuel consumed		5.2×10^{-4}	8.8×10^{-4}	9.7×10^{-4}	9.7×10^{-4}	9.7×10^{-4}	6.7×10^{-4}	5.2×10^{-4}	3.6×10^{-4}	1.1×10^{-3}	
14	kg/barrel capacity	Uncontrol	4.7×10^{-6}	0.0×10^0	0.0×10^0	0.0×10^0	0.0×10^0	9.1×10^{-8}	0.0×10^0	0.0×10^0	8.4×10^{-8}	
		Control	3.1×10^{-7}	0.0×10^0	0.0×10^0	0.0×10^0	0.0×10^0	1.0×10^{-9}	0.0×10^0	0.0×10^0	1.4×10^{-9}	
15	g/t coke produced	Beehive	3.7×10^1	1.4×10^1	9.0×10^0	1.1×10^1	5.5×10^0	1.1×10^1	4.9×10^0	1.1×10^0	5.9×10^0	
		Mechanical-uncontrol	4.4×10^0	9.5×10^{-1}	9.0×10^{-1}	5.8×10^{-1}	4.9×10^{-1}	7.5×10^{-1}	3.0×10^{-1}	4.3×10^{-2}	3.4×10^{-1}	
		Mechanical-control	3.5×10^{-1}	3.8×10^{-2}	4.4×10^{-2}	2.7×10^{-2}	2.4×10^{-2}	3.8×10^{-2}	1.4×10^{-2}	1.4×10^{-2}	2.3×10^{-3}	1.6×10^{-2}
16	mg/t brick produced	Uncontrol	9.2×10^1	2.0×10^1	1.9×10^1	1.2×10^1	1.0×10^1	1.6×10^1	6.2×10^0	8.9×10^1	7.0×10^0	
		Control	7.2×10^0	7.9×10^{-1}	9.0×10^{-1}	5.7×10^{-1}	5.1×10^{-1}	7.9×10^{-1}	3.0×10^{-1}	4.7×10^{-2}	3.4×10^{-1}	
17	g/t Al produced	Prebaked-uncontrol	1.5×10^2	4.8×10^1	2.2×10^2	1.3×10^2	3.1×10^1	3.1×10^1	6.7×10^1	4.6×10^1	8.9×10^0	3.7×10^1
		Prebaked-control	5.3×10^0	5.5×10^{-1}	9.7×10^0	1.2×10^1	2.0×10^0	2.0×10^0	2.6×10^0	7.8×10^0	9.0×10^{-1}	1.5×10^1
		Soderberg-uncontrol	9.5×10^0	2.5×10^0	6.4×10^0	2.9×10^0	8.9×10^{-1}	8.9×10^{-1}	7.6×10^{-1}	6.3×10^{-1}	2.6×10^{-1}	6.3×10^{-1}
		Soderberg-control	3.4×10^{-1}	2.9×10^{-2}	2.8×10^{-1}	2.7×10^{-1}	5.6×10^{-2}	2.9×10^{-2}	2.9×10^{-2}	1.1×10^{-1}	2.7×10^{-2}	2.6×10^{-1}
18	g/TJ gas burned	Uncontrol	7.8×10^{-4}	1.7×10^{-3}	1.8×10^{-3}	2.2×10^{-3}	2.0×10^{-3}	1.3×10^{-3}	1.1×10^{-3}	7.5×10^{-4}	2.4×10^{-3}	
		Control	2.3×10^1	1.3×10^1	1.5×10^1	2.2×10^1	1.3×10^1	1.6×10^1	4.2×10^1	4.2×10^1	4.2×10^1	
19	mg/t pig iron produced	Control	1.5×10^0	6.6×10^{-1}	4.4×10^{-1}	4.9×10^{-1}	3.8×10^{-1}	1.8×10^{-1}	5.7×10^{-1}	5.9×10^{-1}	7.1×10^{-1}	
		Uncontrol	2.7×10^2	2.4×10^1	3.0×10^1	1.5×10^2	1.2×10^1	3.2×10^1	7.5×10^1	8.4×10^0	9.4×10^1	
20	mg/t crude steel produced	Control	1.7×10^1	1.3×10^0	8.7×10^{-1}	3.3×10^0	3.5×10^{-1}	3.6×10^{-1}	1.0×10^0	2.5×10^{-1}	1.6×10^0	
		Uncontrol	2.8×10^0	4.3×10^{-1}	5.2×10^{-1}	5.1×10^{-1}	5.3×10^{-2}	2.4×10^{-1}	2.5×10^{-1}	1.0×10^{-1}	1.4×10^{-1}	
21	mg/t crude steel produced	Control	1.8×10^{-1}	2.3×10^{-2}	1.5×10^{-2}	1.1×10^{-2}	1.5×10^{-3}	2.7×10^{-3}	3.4×10^{-3}	3.0×10^{-3}	2.3×10^{-3}	
		Uncontrol										

(continued)

Table 3.6 (continued)

No. ^a	Units	Subsource	PYR	BaA	CHR	BBF	BkF	BaP	IcdP	DahA	BghtP
22	mg/t crude steel produced	Uncontrol	8.7×10^1	6.4×10^1	3.0×10^1	7.8×10^1	1.0×10^1	1.4×10^1	3.2×10^1	4.1×10^0	6.2×10^1
		Control	5.6×10^0	3.3×10^0	8.6×10^{-1}	1.7×10^0	3.0×10^{-1}	1.6×10^{-1}	3.2×10^{-1}	1.2×10^{-1}	1.1×10^0
23	mg/t hot rolled steel produced	Uncontrol	9.0×10^{-1}	5.0×10^{-1}	6.0×10^{-1}	8.8×10^{-1}	5.2×10^{-1}	6.1×10^{-1}	1.6×10^0	7.8×10^{-1}	1.6×10^0
		Control	5.8×10^{-2}	2.6×10^{-2}	1.7×10^{-2}	1.9×10^{-2}	1.5×10^{-2}	7.0×10^{-3}	2.2×10^{-2}	2.3×10^{-2}	2.8×10^{-2}
24,30,36	mg/t fuel consumed	Uncontrol	4.3×10^0	9.6×10^0	9.0×10^{-1}	2.0×10^0	4.1×10^0	2.8×10^0	1.9×10^0	4.6×10^0	2.4×10^0
25-29	mg/t fuel consumed	Uncontrol	1.2×10^2	7.7×10^0	3.1×10^1	2.0×10^1	6.3×10^0	4.0×10^1	1.0×10^1	3.7×10^0	1.1×10^1
		Control	7.6×10^0	4.0×10^{-1}	9.0×10^{-1}	4.3×10^{-1}	1.8×10^{-1}	4.6×10^{-1}	1.4×10^{-1}	1.1×10^{-1}	1.9×10^{-1}
31	mg/t fuel consumed	Uncontrol	8.5×10^0	5.3×10^{-1}	9.0×10^{-1}	7.5×10^0	2.9×10^0	7.3×10^{-2}	1.7×10^{-1}	0.0×10^0	5.2×10^{-1}
		Control	5.5×10^{-1}	2.8×10^{-2}	2.6×10^{-2}	1.7×10^{-1}	8.3×10^{-2}	8.3×10^{-4}	2.3×10^{-3}	0.0×10^0	8.9×10^{-3}
32	g/TJ fuel consumed	Uncontrol	7.8×10^{-5}	1.7×10^{-4}	1.8×10^{-4}	2.2×10^{-4}	2.0×10^{-4}	1.3×10^{-4}	1.1×10^{-4}	7.5×10^{-5}	2.4×10^{-4}
		Control	6.8×10^1	2.1×10^1	1.9×10^1	1.1×10^1	2.4×10^1	2.5×10^1	1.0×10^1	6.3×10^0	3.0×10^1
33,34	g/TJ fuel consumed	Uncontrol	4.4×10^0	1.1×10^0	5.5×10^{-1}	2.4×10^{-1}	6.9×10^{-1}	2.8×10^{-1}	1.4×10^{-1}	1.9×10^{-1}	5.1×10^{-1}
		Control	7.8×10^{-4}	1.7×10^{-3}	1.8×10^{-3}	2.2×10^{-3}	2.0×10^{-3}	1.3×10^{-3}	1.1×10^{-3}	7.5×10^{-4}	2.4×10^{-3}
35	g/TJ fuel consumed	Uncontrol	3.2×10^0	1.5×10^0	1.8×10^0	1.9×10^0	6.7×10^{-1}	1.4×10^0	1.3×10^0	2.7×10^{-1}	1.3×10^0
		Control	2.2×10^{-2}	5.4×10^{-3}	1.3×10^{-2}	2.5×10^{-3}	1.4×10^{-2}	9.8×10^{-4}	8.9×10^{-4}	6.3×10^{-4}	1.8×10^{-3}
37	g/t waste burned	Uncontrol	2.5×10^0	1.9×10^0	3.7×10^0	1.6×10^0	1.6×10^0	1.1×10^0	9.5×10^{-1}	1.9×10^0	2.1×10^0
		Control	1.5×10^{-2}	3.8×10^{-3}	3.6×10^{-3}	2.4×10^{-3}	2.1×10^{-2}	2.7×10^{-3}	5.5×10^{-3}	8.6×10^{-2}	7.1×10^{-3}
39-42	g/t fuel consumed	Uncontrol	3.0×10^{-2}	4.0×10^{-2}	1.7×10^{-2}	4.2×10^{-2}	4.2×10^{-2}	2.9×10^{-2}	2.2×10^{-2}	1.5×10^{-2}	4.6×10^{-2}
		Control	1.5×10^{-2}	3.8×10^{-3}	3.6×10^{-3}	2.4×10^{-3}	2.1×10^{-2}	2.7×10^{-3}	5.5×10^{-3}	8.6×10^{-2}	7.1×10^{-3}
43	g/t fuel consumed	Uncontrol	1.5×10^{-2}	4.0×10^{-3}	1.7×10^{-3}	4.2×10^{-3}	4.2×10^{-3}	2.9×10^{-3}	2.2×10^{-3}	1.5×10^{-3}	4.6×10^{-3}
		Control	8.8×10^0	6.3×10^0	2.6×10^0	1.6×10^0	7.0×10^{-1}	1.5×10^0	8.7×10^{-1}	5.7×10^{-1}	1.1×10^0
44	g/TJ fuel consumed	Traditional woodstove	2.2×10^0	6.4×10^{-1}	7.4×10^{-1}	4.6×10^{-1}	5.9×10^{-1}	5.6×10^{-1}	2.5×10^{-1}	2.6×10^{-1}	1.8×10^{-1}
		Improved woodstove	2.0×10^0	6.5×10^{-1}	8.6×10^{-1}	4.2×10^{-1}	5.0×10^{-1}	5.5×10^{-1}	1.0×10^{-1}	2.0×10^{-1}	3.6×10^{-1}

(continued)

Table 3.6 (continued)

No. ^a	Units	Subsource	PYR	BaA	CHR	BbF	BkF	BaP	IcdP	DahA	BghtP	
49	g/t fuel consumed	Barley-traditional stove	2.1×10^1	4.4×10^0	4.8×10^0	4.2×10^0	3.3×10^0	4.0×10^0	3.0×10^0	7.5×10^{-1}	2.6×10^0	
		Maize-traditional stove	2.3×10^0	4.8×10^{-1}	5.4×10^{-1}	4.7×10^{-1}	3.7×10^{-1}	4.0×10^{-1}	3.0×10^{-1}	8.7×10^{-2}	2.7×10^{-1}	
		Rice-traditional stove	7.3×10^0	1.3×10^0	1.2×10^0	1.1×10^0	1.0×10^0	1.5×10^0	1.5×10^0	9.5×10^{-1}	1.6×10^{-1}	7.1×10^{-1}
		Wheat-traditional stove	7.3×10^0	1.5×10^0	1.7×10^0	1.4×10^0	1.2×10^0	1.4×10^0	1.4×10^0	1.0×10^0	2.6×10^{-1}	8.9×10^{-1}
		Barley-improved stove	5.2×10^0	4.5×10^{-1}	1.4×10^0	1.2×10^0	2.8×10^0	2.8×10^0	1.5×10^0	8.5×10^{-1}	3.4×10^{-1}	4.3×10^{-1}
		Maize-improved stove	5.5×10^{-1}	4.8×10^{-2}	1.5×10^{-1}	1.3×10^{-1}	3.1×10^{-1}	3.1×10^{-1}	1.5×10^{-1}	8.7×10^{-2}	4.0×10^{-2}	4.5×10^{-2}
50	g/t fuel consumed	Rice-improved stove	1.8×10^0	1.3×10^{-1}	3.5×10^{-1}	3.1×10^{-1}	8.4×10^{-1}	5.8×10^{-1}	2.7×10^{-1}	7.2×10^{-2}	1.2×10^{-1}	
		Wheat-improved stove	1.8×10^0	1.5×10^{-1}	4.7×10^{-1}	4.1×10^{-1}	9.7×10^{-1}	5.3×10^{-1}	2.9×10^{-1}	1.2×10^{-1}	1.5×10^{-1}	
		Traditional woodstove	9.4×10^0	3.1×10^0	1.9×10^0	7.7×10^{-1}	7.0×10^{-1}	1.1×10^0	1.1×10^0	1.9×10^{-1}	4.9×10^{-1}	3.9×10^{-1}
		Improved woodstove	1.3×10^1	2.1×10^{-1}	5.7×10^{-1}	4.4×10^{-1}	9.8×10^{-1}	8.1×10^{-1}	8.1×10^{-1}	2.8×10^{-1}	1.9×10^{-2}	1.1×10^{-1}
63	g/t dry matter burned	Barley	2.4×10^0	1.1×10^0	1.5×10^0	2.5×10^0	6.1×10^{-1}	8.0×10^{-1}	1.0×10^{-2}	5.9×10^{-1}	5.2×10^{-1}	
		Maize	7.9×10^{-1}	7.7×10^{-2}	1.5×10^{-1}	2.9×10^{-2}	1.8×10^{-1}	2.4×10^{-2}	0.0×10^0	0.0×10^0	0.0×10^0	
		Rice	3.4×10^{-1}	8.2×10^{-2}	9.8×10^{-2}	1.3×10^{-1}	3.0×10^{-2}	4.1×10^{-2}	4.1×10^{-2}	0.0×10^0	3.2×10^{-2}	4.3×10^{-2}
		Wheat	3.3×10^0	2.3×10^0	2.3×10^0	9.9×10^{-1}	5.3×10^{-1}	2.8×10^{-1}	2.8×10^{-1}	0.0×10^0	6.7×10^{-1}	1.0×10^0
65-68	g/t dry matter burned	1.1×10^0	1.6×10^{-1}	1.6×10^{-1}	5.3×10^{-2}	1.4×10^{-1}	1.0×10^{-1}	1.0×10^{-1}	3.2×10^{-1}	1.9×10^{-1}	6.9×10^{-2}	
69	g/t dry matter burned	1.0×10^{-1}	1.6×10^{-2}	1.6×10^{-2}	5.1×10^{-3}	1.4×10^{-2}	1.4×10^{-2}	1.0×10^{-2}	3.0×10^{-2}	1.8×10^{-2}	6.6×10^{-3}	

^aIn accord with "No." column in Tables 3.1 and 3.3

Reprinted with permission from Shen et al. (2013). Copyright (2013) American Chemical Society

3.1.3 Uncertainty Analysis

The measured EF_{PAHs} collected for this study were found to be lognormally distributed and distribution statistics of them were calculated based on these data. Figure 4.1 illustrates the distributions of EF s of individual compounds for motor vehicles. Summary of the descriptive statistics information on collected EF values can be found in Tables 3.6 and 3.7. For the lognormal distribution, the expected value that represents the quantity to determine the average EF level is distinct from the exponentiated mean (i.e., $\exp(\mu)$ or the geometric average) of the log-transformed data as discussed by Bond T. C. et al. (2004). The expected value depends on both the mean and the standard deviation of the log-transformed data and can be obtained as follows:

$$E(x) = \exp(\mu + 0.5\sigma^2),$$

where μ and σ are the mean and the standard deviation of log-transformed data, respectively. The confidence interval for the distribution mean is as follows:

$$ci_{1-\alpha} = \exp\left(\mu \pm \frac{\sigma}{\sqrt{n}} t_{\alpha/2, n-1}\right),$$

where n is the total number of observations, α is the significance level (i.e., 1 minus the confidence level). $\alpha = 0.05$ for the confidence level of 95 %; $\alpha = 0.3173$ for the standard deviation range. Based on a Cox's method, the standard deviation of $\log[E(x)]$ can be expressed as follows:

$$SD[E(x)] = \sqrt{\left\{ \frac{\sigma^2}{n} + \frac{\sigma^4}{2(n-1)} \right\}},$$

It can be found that using the geometric average of EF s will underestimated the emissions, and using the geometric standard deviation will overestimate the uncertainty ranges. The expected EF values and standard deviations are listed in Tables 3.8 and 3.9, which are distinguished with the values listed in Tables 3.6 and 3.7. It should be noted that Tables 3.6 and 3.7 show the distributions of EF s from measurements, and these data should be used for emission estimation and uncertainty analysis in specific cases, for example, to estimate emission from a specified industrial boiler. In contrast, data listed in Tables 3.8 and 3.9 can be directly used to estimate regional-aggregate emissions and uncertainty analysis. Actually, in this study, to address country-level emissions, data in Tables 3.8 and 3.9 were applied instead of data in Tables 3.6 and 3.7.

The activity rates were assumed to be uniformly distributed. Based on previous studies, variation intervals of historical consumptions were set to be 20 % of the means for indoor biomass burning and open fires, 15 % for shipping and aviation, 5 % for energy production and industrial sectors, 30 % for non-organized waste

Table 3.7 Standard deviations of the log-transformed emission factors of 16 PAHs for various sources, $SD[\log_{10}(EF_{PAHs})]$

No. ^a	NAP	ACY	ACE	FLO	PHE	ANT	FLA	PYR	BaA	CHR	BbF	BkF	BaP	IcdP	DahA	BghiP
1-5.8	0.51	0.48	0.51	0.75	0.48	0.44	0.46	0.64	0.57	0.56	0.56	0.56	0.84	0.56	0.77	0.75
6.7,13,24,30,36	0.89	1.07	0.90	1.00	1.11	1.35	1.46	1.57	1.13	0.61	1.04	1.03	0.90	0.59	1.48	0.65
9,12,18	0.43	0.49	0.30	0.30	0.28	0.30	0.21	0.69	0.30	0.30	0.30	0.30	0.30	0.30	0.30	0.30
10,11	1.26	1.35	0.87	0.98	0.92	1.24	1.17	1.33	0.69	0.64	0.91	0.70	0.85	1.06	0.84	0.85
14-17, 19-23	0.69	0.69	0.72	0.66	0.71	0.68	0.70	0.70	0.75	0.73	0.73	0.72	0.72	0.73	0.72	0.73
25-29,31	0.51	0.48	0.51	0.75	0.48	0.44	0.46	0.64	0.57	0.56	0.56	0.56	0.84	0.56	0.77	0.75
32,35	0.43	0.49	0.30	0.30	0.28	0.30	0.21	0.69	0.30	0.30	0.30	0.30	0.30	0.30	0.30	0.30
33,34	1.26	1.35	0.87	0.98	0.92	1.24	1.17	1.33	0.69	0.64	0.91	0.70	0.85	1.06	0.84	0.85
37	0.16	0.17	0.11	0.22	0.21	0.26	0.22	0.31	0.22	0.23	0.47	0.27	0.31	0.00	0.35	0.15
38	0.24	0.52	0.18	0.23	0.21	0.43	0.67	0.59	1.07	0.63	0.03	0.33	0.61	0.03	0.03	0.23
39-42	0.33	0.38	0.40	0.48	0.67	0.86	0.45	0.21	0.72	0.67	0.97	0.15	0.42	0.32	0.22	0.48
43-47	0.43	0.49	0.30	0.30	0.28	0.30	0.21	0.69	0.30	0.30	0.30	0.30	0.30	0.30	0.30	0.30
48,50	0.40	0.21	0.28	0.35	0.20	0.59	0.23	0.23	0.25	0.23	0.23	0.21	0.19	0.35	0.28	0.39
49	0.08	0.44	0.14	0.35	0.21	0.30	0.18	0.19	0.18	0.19	0.12	0.18	0.18	0.19	0.10	0.15
63	0.16	0.17	0.11	0.22	0.21	0.26	0.22	0.31	0.22	0.23	0.47	0.27	0.31	0.00	0.35	0.15
65-69	0.27	0.46	0.46	0.61	0.22	0.36	0.36	0.31	0.50	0.50	0.57	0.62	0.77	0.34	0.89	1.03

^aIn accord with "No." column in Tables 3.1 and 3.3

Reprinted with permission from Shen et al. (2013). Copyright (2013) American Chemical Society

Table 3.8 Expected values of the emission factors of 16 PAHs for various sources, $E(EF_{PAHs})$

No. ^a	Units	Subsource	NAP	ACY	ACE	FLO	PHE	ANT	FLA
1-5	mg/t fuel consumed	Uncontrol	3.9×10^1	7.9×10^{-1}	2.5×10^0	8.8×10^0	2.3×10^1	2.0×10^0	6.9×10^0
		Control	5.4×10^0	1.5×10^{-1}	4.0×10^{-1}	1.5×10^0	2.2×10^0	1.9×10^{-1}	6.0×10^{-1}
6,7,13	mg/t fuel consumed	Uncontrol	2.7×10^3	5.6×10^1	2.2×10^1	2.9×10^1	1.7×10^2	1.4×10^2	1.1×10^3
		Control	1.5×10^1	5.0×10^{-1}	3.1×10^{-2}	4.3×10^{-1}	1.6×10^{-1}	8.9×10^{-2}	6.1×10^{-2}
8	mg/t fuel consumed	Uncontrol	2.1×10^0	9.4×10^{-2}	5.1×10^{-3}	7.2×10^{-2}	1.5×10^{-2}	8.1×10^{-3}	5.3×10^{-3}
		Control	3.1×10^{-3}	2.6×10^{-4}	2.0×10^{-3}	1.1×10^{-4}	2.0×10^{-4}	1.3×10^{-5}	4.6×10^{-5}
9	g/TJ fuel consumed	Uncontrol	4.8×10^2	3.4×10^2	1.6×10^0	3.1×10^1	5.3×10^0	3.0×10^1	8.6×10^0
		Control	6.5×10^1	6.5×10^1	2.6×10^{-1}	5.1×10^0	5.0×10^{-1}	2.7×10^0	7.4×10^{-1}
10,11	g/TJ fuel consumed	Uncontrol	3.1×10^{-2}	2.6×10^{-3}	2.0×10^{-2}	1.1×10^{-3}	2.0×10^{-3}	1.3×10^{-4}	4.6×10^{-4}
		Control	1.2×10^{-6}	0.0×10^0	0.0×10^0	0.0×10^0	2.7×10^{-4}	1.4×10^{-6}	6.9×10^{-6}
12	kg/barrel capacity	Uncontrol	1.7×10^{-7}	0.0×10^0	0.0×10^0	0.0×10^0	2.5×10^{-5}	1.3×10^{-7}	6.0×10^{-7}
		Control	4.0×10^2	7.9×10^1	2.3×10^1	5.1×10^1	2.1×10^2	3.5×10^1	9.4×10^1
13	g/t coke produced	Uncontrol	4.1×10^1	1.0×10^1	1.2×10^0	4.8×10^0	1.6×10^1	4.1×10^0	6.7×10^0
		Control	3.2×10^0	1.0×10^0	5.9×10^{-2}	7.3×10^{-1}	1.0×10^0	3.9×10^{-1}	4.7×10^{-1}
14	mg/t brick produced	Uncontrol	8.6×10^2	2.1×10^2	2.5×10^1	1.0×10^2	3.3×10^2	8.4×10^1	1.4×10^2
		Control	6.7×10^1	2.1×10^1	1.2×10^0	1.5×10^1	2.1×10^1	8.1×10^0	9.8×10^0
15	g/t Al produced	Uncontrol	8.2×10^{-1}	2.8×10^{-2}	5.3×10^{-1}	7.1×10^{-1}	1.0×10^2	1.1×10^1	2.8×10^2
		Control	1.0×10^{-1}	5.3×10^{-2}	4.0×10^{-2}	3.0×10^0	1.6×10^2	3.3×10^{-1}	4.4×10^1
16	g/TJ gas burned	Uncontrol	1.1×10^{-1}	5.3×10^{-3}	8.7×10^{-2}	1.2×10^{-1}	9.5×10^0	1.0×10^0	2.5×10^1
		Control	1.4×10^{-2}	1.0×10^{-2}	6.6×10^{-3}	5.0×10^{-1}	1.5×10^1	3.0×10^{-2}	3.8×10^0
17	mg/t pig iron produced	Uncontrol	4.8×10^{-2}	4.4×10^{-3}	3.7×10^{-2}	1.5×10^{-3}	2.7×10^{-3}	2.0×10^{-4}	8.3×10^{-4}
		Control	5.0×10^3	1.7×10^3	1.5×10^2	2.5×10^2	3.5×10^2	4.1×10^1	5.4×10^1
18	mg/t crude steel produced	Uncontrol	6.9×10^2	3.3×10^2	2.4×10^1	4.2×10^1	3.3×10^1	3.7×10^0	4.7×10^0
		Control	1.4×10^4	2.2×10^2	1.3×10^2	1.1×10^2	6.9×10^1	8.5×10^2	5.2×10^2
19	mg/t crude steel produced	Uncontrol	1.9×10^3	4.2×10^1	2.2×10^1	1.8×10^1	6.5×10^0	7.8×10^1	4.5×10^1
		Control							

(continued)

Table 3.8 (continued)

No. ^a	Units	Subsource	NAP	ACY	ACE	FLO	PHE	ANT	FLA
21	mg/t crude steel produced	Uncontrol	1.1×10^3	2.3×10^1	1.4×10^1	1.1×10^1	2.5×10^0	4.4×10^1	7.2×10^0
		Control	1.5×10^2	4.4×10^0	2.2×10^0	1.8×10^0	2.4×10^{-1}	4.0×10^0	6.2×10^{-1}
22	mg/t crude steel produced	Uncontrol	5.3×10^3	1.4×10^2	8.2×10^1	8.2×10^1	2.8×10^1	5.5×10^2	2.3×10^2
		Control	7.3×10^2	2.6×10^1	1.3×10^1	1.4×10^1	2.6×10^0	5.0×10^1	2.0×10^1
23	mg/t hot rolled steel produced	Uncontrol	2.0×10^2	6.9×10^1	5.9×10^0	9.9×10^0	1.4×10^1	1.6×10^0	2.1×10^0
		Control	2.7×10^1	1.3×10^1	9.6×10^{-1}	1.7×10^0	1.3×10^0	1.5×10^{-1}	1.9×10^{-1}
24,30,36	mg/t fuel consumed		4.2×10^3	9.3×10^1	4.1×10^1	3.8×10^1	2.3×10^2	2.2×10^2	1.9×10^3
25–29	mg/t fuel consumed	Uncontrol	1.0×10^4	7.3×10^1	1.9×10^2	8.8×10^1	5.8×10^3	4.1×10^1	1.4×10^3
		Control	1.4×10^3	1.4×10^1	3.2×10^1	1.5×10^1	5.5×10^2	3.7×10^0	1.2×10^2
31	mg/t fuel consumed	Uncontrol	4.0×10^3	4.6×10^1	2.5×10^0	4.3×10^0	4.1×10^1	1.8×10^0	1.3×10^1
		Control	5.5×10^2	8.7×10^0	4.0×10^{-1}	7.2×10^{-1}	3.9×10^0	1.6×10^{-1}	1.1×10^0
32	g/TJ fuel consumed	Uncontrol	4.8×10^{-3}	4.4×10^{-4}	3.7×10^{-3}	1.5×10^{-4}	2.7×10^{-4}	2.0×10^{-5}	8.3×10^{-5}
		Control	1.3×10^5	3.2×10^4	1.2×10^2	3.1×10^2	1.3×10^3	6.0×10^2	1.8×10^3
33,34	g/TJ fuel consumed		1.7×10^4	6.0×10^3	2.0×10^1	5.1×10^1	1.3×10^2	5.5×10^1	1.5×10^2
35	g/TJ fuel consumed		4.8×10^{-2}	4.4×10^{-3}	3.7×10^{-2}	1.5×10^{-3}	2.7×10^{-3}	2.0×10^{-4}	8.3×10^{-4}
37	g/t waste burned		1.2×10^1	7.9×10^0	6.6×10^{-1}	3.4×10^0	6.0×10^0	1.5×10^0	3.2×10^0
38	g/t fuel consumed	Uncontrol	1.5×10^{-1}	6.0×10^{-2}	1.2×10^{-2}	1.2×10^{-2}	1.1×10^{-1}	9.8×10^{-3}	1.0×10^{-1}
		Control	2.1×10^1	8.9×10^0	1.7×10^1	7.9×10^0	3.8×10^1	1.3×10^1	7.3×10^0
39–42	g/t fuel consumed	Uncontrol	8.7×10^{-2}	2.5×10^{-2}	4.7×10^{-2}	9.7×10^{-3}	4.4×10^{-3}	2.1×10^{-3}	3.8×10^{-2}
		Control	1.2×10^0	1.1×10^{-1}	8.5×10^{-1}	6.3×10^{-2}	7.6×10^{-2}	5.5×10^{-3}	2.4×10^{-2}
45,46	g/t fuel consumed	Uncontrol	8.7×10^{-2}	2.5×10^{-2}	4.7×10^{-2}	9.7×10^{-3}	4.4×10^{-3}	2.1×10^{-3}	3.8×10^{-2}
		Control	1.2×10^{-1}	1.1×10^{-2}	8.5×10^{-2}	6.3×10^{-3}	7.6×10^{-3}	5.5×10^{-4}	2.4×10^{-3}
47	g/TJ fuel consumed	Traditional woodstove	1.9×10^2	1.1×10^2	3.1×10^1	1.4×10^1	3.3×10^1	3.3×10^1	8.7×10^0
		Improved woodstove	2.3×10^1	1.2×10^1	7.0×10^0	1.1×10^0	8.8×10^0	7.0×10^0	6.9×10^0
48	g/t fuel consumed	Fireplace	2.5×10^1	1.3×10^1	4.9×10^0	2.3×10^0	7.5×10^0	5.1×10^0	3.7×10^0

(continued)

Table 3.8 (continued)

No. ^a	Units	Subsource	NAP	ACY	ACE	FLO	PHE	ANT	FLA	
49	g/t fuel consumed	Barley-traditional stove	1.1×10^2	4.0×10^1	2.2×10^1	4.5×10^1	6.9×10^1	1.1×10^1	2.7×10^1	
		Maize-traditional stove	1.6×10^1	4.4×10^0	2.5×10^0	4.7×10^0	7.8×10^0	1.4×10^0	2.9×10^0	
		Rice-traditional stove	4.2×10^1	9.2×10^0	6.2×10^0	8.7×10^0	1.1×10^1	2.2×10^0	8.2×10^0	
		Wheat-traditional stove	3.8×10^1	1.4×10^1	7.5×10^0	1.6×10^1	2.4×10^1	3.9×10^0	9.4×10^0	
		Barley-improved stove	1.3×10^1	4.4×10^0	4.9×10^0	3.3×10^0	1.8×10^1	5.9×10^0	2.1×10^1	
		Maize-improved stove	1.9×10^0	4.9×10^{-1}	5.7×10^{-1}	3.4×10^{-1}	2.1×10^0	7.3×10^{-1}	2.3×10^0	
		Rice-improved stove	5.1×10^0	1.0×10^0	1.4×10^0	6.4×10^{-1}	3.1×10^0	1.1×10^0	6.6×10^0	
		Wheat-improved stove	4.7×10^0	1.5×10^0	1.7×10^0	1.1×10^0	6.3×10^0	2.0×10^0	7.5×10^0	
50	g/t fuel consumed	Traditional woodstove	1.2×10^2	4.6×10^1	1.8×10^1	8.7×10^0	2.8×10^1	1.5×10^1	1.4×10^1	
		Improved woodstove	2.9×10^2	5.6×10^0	1.2×10^1	7.3×10^0	6.3×10^1	7.0×10^0	6.0×10^1	
		Barley	1.6×10^2	1.9×10^1	2.3×10^1	2.4×10^0	1.9×10^1	2.8×10^0	2.7×10^0	
63	g/t dry matter burned	Maize	1.6×10^0	6.8×10^{-1}	5.1×10^{-1}	7.2×10^{-2}	2.0×10^0	3.2×10^{-1}	8.7×10^{-1}	
		Rice	8.2×10^0	5.6×10^{-2}	6.3×10^{-1}	3.3×10^{-1}	1.6×10^0	2.9×10^{-1}	5.0×10^{-1}	
		Wheat	4.7×10^1	3.5×10^{-1}	7.3×10^{-1}	2.8×10^{-1}	5.4×10^0	1.5×10^0	7.6×10^0	
65–68	g/t dry matter burned		1.3×10^1	3.9×10^0	3.2×10^0	2.0×10^0	2.6×10^0	5.2×10^{-1}	2.2×10^0	
69	g/t dry matter burned		1.3×10^0	3.7×10^{-1}	3.0×10^{-1}	1.9×10^{-1}	2.5×10^{-1}	4.9×10^{-2}	2.1×10^{-1}	
No. ^a	Units	Subsource	BaA	CHR	BbF	BkF	BaP	IcdP	DahA	BghIP
1–5	mg/t fuel consumed	Uncontrol	1.1×10^0	4.0×10^0	2.5×10^0	1.9×10^0	7.8×10^0	2.4×10^0	1.8×10^0	3.6×10^0
		Control	5.8×10^{-2}	1.2×10^{-1}	5.4×10^{-2}	5.3×10^{-2}	8.8×10^{-2}	3.3×10^{-2}	5.4×10^{-2}	6.2×10^{-2}
6,7,13	mg/t fuel consumed		1.5×10^2	1.3×10^0	1.6×10^1	3.3×10^1	1.3×10^1	2.3×10^0	7.2×10^2	3.4×10^0
8	mg/t fuel consumed	Uncontrol	7.7×10^{-2}	1.2×10^{-1}	9.4×10^{-1}	8.5×10^{-1}	1.4×10^{-2}	4.1×10^{-2}	0.0×10^0	1.7×10^{-1}
		Control	4.0×10^{-3}	3.4×10^{-3}	2.1×10^{-2}	2.4×10^{-2}	1.6×10^{-4}	5.6×10^{-4}	0.0×10^0	2.9×10^{-3}
9	g/TJ fuel consumed		1.1×10^{-4}	1.2×10^{-4}	1.2×10^{-4}	1.2×10^{-4}	8.6×10^{-5}	6.7×10^{-5}	4.5×10^{-5}	1.4×10^{-4}
10,11	g/TJ fuel consumed	Uncontrol	4.5×10^0	3.2×10^0	5.3×10^0	1.1×10^1	4.9×10^0	2.1×10^1	4.2×10^0	1.5×10^1
		Control	2.3×10^{-1}	9.2×10^{-1}	1.2×10^{-1}	3.3×10^{-1}	5.6×10^{-2}	2.9×10^{-1}	1.3×10^{-1}	2.6×10^{-1}

(continued)

Table 3.8 (continued)

No. ^a	Units	Subsource	PYR	BaA	CHR	BbF	BkF	BaP	IcdP	DahA	BghtP
12	g/TJ fuel consumed	Uncontrol	1.9×10^{-3}	1.1×10^{-3}	1.2×10^{-3}	1.2×10^{-3}	1.2×10^{-3}	8.6×10^{-4}	6.7×10^{-4}	4.5×10^{-4}	1.4×10^{-3}
14	kg/barrel capacity	Control	9.2×10^{-6}	0.0×10^0	0.0×10^0	0.0×10^0	0.0×10^0	2.0×10^{-7}	0.0×10^0	0.0×10^0	1.8×10^{-7}
15	g/t coke produced	Control	5.9×10^{-7}	0.0×10^0	0.0×10^0	0.0×10^0	0.0×10^0	2.2×10^{-9}	0.0×10^0	0.0×10^0	3.2×10^{-9}
		Beehive	7.1×10^1	2.9×10^1	2.0×10^1	2.4×10^1	1.2×10^1	2.3×10^1	1.1×10^1	2.4×10^0	1.3×10^1
		Mechanical-uncontrol	8.6×10^0	2.0×10^0	2.0×10^0	1.3×10^0	1.1×10^0	1.6×10^0	6.6×10^{-1}	9.4×10^{-2}	7.5×10^{-1}
		Mechanical-control	6.7×10^{-1}	8.2×10^{-2}	9.6×10^{-2}	6.0×10^{-2}	5.4×10^{-2}	8.4×10^{-2}	3.2×10^{-2}	4.9×10^{-3}	3.6×10^{-2}
16	mg/t brick produced	Uncontrol	1.8×10^2	4.2×10^1	4.1×10^1	2.6×10^1	2.2×10^1	3.4×10^1	1.4×10^1	1.9×10^0	1.5×10^1
		Control	1.4×10^1	1.7×10^0	2.0×10^0	1.3×10^0	1.1×10^0	1.7×10^0	6.6×10^{-1}	1.0×10^{-1}	7.4×10^{-1}
17	g/t Al produced	Prebaked-uncontrol	2.9×10^2	1.0×10^2	4.9×10^2	2.9×10^2	6.8×10^1	1.5×10^2	1.0×10^2	1.9×10^1	8.2×10^1
		Prebaked-control	1.0×10^1	1.2×10^0	2.1×10^1	2.7×10^1	4.3×10^0	5.6×10^0	1.7×10^1	2.0×10^0	3.3×10^1
		Soderberg-uncontrol	1.8×10^1	5.4×10^0	1.4×10^1	6.4×10^0	2.0×10^0	1.7×10^0	1.4×10^0	5.7×10^{-1}	1.4×10^0
		Soderberg-control	6.6×10^{-1}	6.2×10^{-2}	6.2×10^{-1}	6.0×10^{-1}	1.2×10^{-1}	6.3×10^{-2}	2.3×10^{-1}	5.8×10^{-2}	5.6×10^{-1}
18	g/TJ gas burned	Control	2.8×10^{-3}	2.2×10^{-3}	2.3×10^{-3}	2.8×10^{-3}	2.6×10^{-3}	1.7×10^{-3}	1.4×10^{-3}	9.6×10^{-4}	3.0×10^{-3}
19	mg/t pig iron produced	Uncontrol	4.4×10^1	2.7×10^1	3.3×10^1	4.9×10^1	2.9×10^1	3.4×10^1	9.1×10^1	4.3×10^1	9.1×10^1
		Control	2.8×10^0	1.4×10^0	9.6×10^{-1}	1.1×10^0	8.3×10^{-1}	3.9×10^{-1}	1.2×10^0	1.3×10^0	1.6×10^0
20	mg/t crude steel produced	Uncontrol	5.2×10^2	5.2×10^1	6.6×10^1	3.4×10^2	2.7×10^1	6.9×10^1	1.7×10^2	1.8×10^1	2.1×10^2
		Control	3.3×10^1	2.7×10^0	1.9×10^0	7.4×10^0	7.6×10^{-1}	7.8×10^{-1}	2.3×10^0	5.5×10^{-1}	3.5×10^0
21	mg/t crude steel produced	Uncontrol	5.5×10^0	9.4×10^{-1}	1.1×10^0	1.1×10^0	1.2×10^{-1}	5.3×10^{-1}	5.4×10^{-1}	2.2×10^{-1}	3.0×10^{-1}
		Control	3.5×10^{-1}	4.9×10^{-2}	3.3×10^{-2}	2.5×10^{-2}	3.3×10^{-3}	6.0×10^{-3}	7.4×10^{-3}	6.5×10^{-3}	5.1×10^{-3}
22	mg/t crude steel produced	Uncontrol	1.7×10^2	1.4×10^2	6.5×10^1	1.7×10^2	2.3×10^1	3.0×10^1	5.2×10^1	9.0×10^0	1.4×10^2
		Control	1.1×10^1	7.2×10^0	1.9×10^0	3.8×10^0	6.6×10^{-1}	3.4×10^{-1}	7.0×10^{-1}	2.7×10^{-1}	2.3×10^0
23	mg/t hot rolled steel produced	Uncontrol	1.7×10^0	1.1×10^0	1.3×10^0	1.9×10^0	1.1×10^0	1.3×10^0	3.6×10^0	1.7×10^0	3.6×10^0
		Control	1.1×10^{-1}	5.6×10^{-2}	3.8×10^{-2}	4.3×10^{-2}	3.3×10^{-2}	1.5×10^{-2}	4.9×10^{-2}	5.1×10^{-2}	6.2×10^{-2}

(continued)

Table 3.8 (continued)

No. ^a	Units	Subsource	PYR	BaA	CHR	BbF	BkF	BaP	IcdP	DahA	BghiP
24,30,36	mg/t fuel consumed		3.1×10^3	2.9×10^2	2.4×10^0	3.5×10^1	6.8×10^1	2.5×10^1	4.9×10^0	1.5×10^3	7.3×10^0
25–29	mg/t fuel consumed	Uncontrol	3.6×10^2	1.8×10^1	7.2×10^1	4.6×10^1	1.5×10^1	2.6×10^2	2.3×10^1	1.8×10^1	4.8×10^1
		Control	2.3×10^1	9.6×10^{-1}	2.1×10^0	1.0×10^0	4.2×10^{-1}	3.0×10^0	3.1×10^{-1}	5.4×10^{-1}	8.2×10^{-1}
31	mg/t fuel consumed	Uncontrol	2.6×10^1	1.3×10^0	2.1×10^0	1.7×10^1	6.7×10^0	4.8×10^{-1}	3.9×10^{-1}	0.0×10^0	2.3×10^0
		Control	1.6×10^0	6.7×10^{-2}	6.1×10^{-2}	3.9×10^{-1}	1.9×10^{-1}	5.4×10^{-3}	5.3×10^{-3}	0.0×10^0	3.9×10^{-2}
32	g/TJ fuel consumed		2.8×10^{-4}	2.2×10^{-4}	2.3×10^{-4}	2.8×10^{-4}	2.6×10^{-4}	1.7×10^{-4}	1.4×10^{-4}	9.6×10^{-5}	3.0×10^{-4}
33,34	g/TJ fuel consumed	Uncontrol	7.6×10^3	7.4×10^1	5.7×10^1	9.9×10^1	8.9×10^1	1.7×10^2	2.0×10^2	4.2×10^1	2.0×10^2
		Control	4.9×10^2	3.9×10^0	1.7×10^1	2.2×10^0	2.6×10^0	1.9×10^0	2.7×10^0	1.3×10^0	3.5×10^0
35	g/TJ fuel consumed		2.8×10^{-3}	2.2×10^{-3}	2.3×10^{-3}	2.8×10^{-3}	2.6×10^{-3}	1.7×10^{-3}	1.4×10^{-3}	9.6×10^{-4}	3.0×10^{-3}
37	g/t waste burned		4.1×10^0	1.7×10^0	2.1×10^0	3.3×10^0	8.1×10^{-1}	1.8×10^0	1.3×10^0	3.7×10^{-1}	1.4×10^0
38	g/t fuel consumed		5.5×10^{-2}	1.1×10^{-1}	3.8×10^{-2}	2.5×10^{-3}	1.9×10^{-2}	2.6×10^{-3}	8.9×10^{-4}	6.4×10^{-4}	2.1×10^{-3}
39–42	g/t fuel consumed		2.8×10^0	7.5×10^0	1.2×10^1	1.9×10^1	1.7×10^0	1.7×10^0	1.2×10^0	2.2×10^0	3.9×10^0
43	g/t fuel consumed		5.3×10^{-2}	4.9×10^{-3}	4.6×10^{-3}	3.1×10^{-3}	2.7×10^{-2}	3.5×10^{-3}	7.0×10^{-3}	1.1×10^{-1}	9.1×10^{-3}
44	g/TJ fuel consumed		1.1×10^{-1}	5.1×10^{-2}	2.2×10^{-2}	5.3×10^{-2}	5.3×10^{-2}	3.7×10^{-2}	2.8×10^{-2}	1.9×10^{-2}	5.9×10^{-2}
45,46	g/t fuel consumed		5.3×10^{-2}	4.9×10^{-3}	4.6×10^{-3}	3.1×10^{-3}	2.7×10^{-2}	3.5×10^{-3}	7.0×10^{-3}	1.1×10^{-1}	9.1×10^{-3}
47	g/TJ fuel consumed		1.1×10^{-2}	5.1×10^{-3}	2.2×10^{-3}	5.3×10^{-3}	5.3×10^{-3}	3.7×10^{-3}	2.8×10^{-3}	1.9×10^{-3}	5.9×10^{-3}
48	g/t fuel consumed	Traditional woodstove	1.0×10^1	7.5×10^0	3.0×10^0	1.9×10^0	7.9×10^{-1}	1.6×10^0	1.2×10^0	7.0×10^{-1}	1.6×10^0
		Improved woodstove	2.5×10^0	7.6×10^{-1}	8.5×10^{-1}	5.3×10^{-1}	6.6×10^{-1}	6.1×10^{-1}	3.4×10^{-1}	3.2×10^{-1}	2.7×10^{-1}
		Fireplace	2.3×10^0	7.8×10^{-1}	9.8×10^{-1}	4.8×10^{-1}	5.6×10^{-1}	6.0×10^{-1}	1.4×10^{-1}	2.5×10^{-1}	5.4×10^{-1}

(continued)

Table 3.8 (continued)

No. ^a	Units	Subsource	PYR	BaA	CHR	BbF	BkF	BaP	IcdP	DahA	BghtP	
49	g/t fuel consumed	Barley-traditional stove	2.3×10^1	4.8×10^0	5.3×10^0	4.3×10^0	3.6×10^0	4.4×10^0	3.3×10^0	7.7×10^{-1}	2.7×10^0	
		Maize-traditional stove	2.5×10^0	5.2×10^{-1}	5.9×10^{-1}	4.9×10^{-1}	4.0×10^{-1}	4.4×10^{-1}	3.3×10^{-1}	8.9×10^{-2}	2.8×10^{-1}	
		Rice-traditional stove	8.0×10^0	1.4×10^0	1.3×10^0	1.1×10^0	1.1×10^0	1.7×10^0	1.0×10^0	1.0×10^0	1.6×10^{-1}	7.6×10^{-1}
		Wheat-traditional stove	8.1×10^0	1.7×10^0	1.8×10^0	1.5×10^0	1.3×10^0	1.5×10^0	1.5×10^0	1.1×10^0	2.7×10^{-1}	9.4×10^{-1}
		Barley-improved stove	5.7×10^0	4.9×10^{-1}	1.5×10^0	1.2×10^0	3.1×10^0	1.7×10^0	9.3×10^{-1}	9.3×10^{-1}	3.5×10^{-1}	4.6×10^{-1}
		Maize-improved stove	6.1×10^{-1}	5.3×10^{-2}	1.7×10^{-1}	1.4×10^{-1}	3.4×10^{-1}	1.7×10^{-1}	9.6×10^{-2}	4.1×10^{-2}	4.1×10^{-2}	4.8×10^{-2}
		Rice-improved stove	2.0×10^0	1.5×10^{-1}	3.8×10^{-1}	3.2×10^{-1}	9.2×10^{-1}	6.4×10^{-1}	3.0×10^{-1}	3.0×10^{-1}	7.4×10^{-2}	1.3×10^{-1}
		Wheat-improved stove	2.0×10^0	1.7×10^{-1}	5.2×10^{-1}	4.3×10^{-1}	1.1×10^0	5.8×10^{-1}	3.2×10^{-1}	3.2×10^{-1}	1.2×10^{-1}	1.6×10^{-1}
50	g/t fuel consumed	Traditional woodstove	1.1×10^1	3.7×10^0	2.1×10^0	8.9×10^{-1}	7.9×10^{-1}	1.2×10^0	2.6×10^{-1}	6.1×10^{-1}	5.9×10^{-1}	
		Improved woodstove	1.5×10^1	2.4×10^{-1}	6.6×10^{-1}	5.1×10^{-1}	1.1×10^0	8.9×10^{-1}	3.9×10^{-1}	2.3×10^{-2}	1.6×10^{-1}	
63	g/t dry matter burned	Barley	3.2×10^0	1.3×10^0	1.7×10^0	4.4×10^0	7.4×10^{-1}	1.0×10^0	1.0×10^{-2}	8.1×10^{-1}	5.5×10^{-1}	
		Maize	1.0×10^0	8.7×10^{-2}	1.7×10^{-1}	5.2×10^{-2}	2.2×10^{-1}	3.1×10^{-2}	0.0×10^0	0.0×10^0	0.0×10^0	
		Rice	4.4×10^{-1}	9.3×10^{-2}	1.1×10^{-1}	2.3×10^{-1}	3.6×10^{-2}	5.3×10^{-2}	0.0×10^0	0.0×10^0	4.3×10^{-2}	4.6×10^{-2}
		Wheat	4.2×10^0	2.6×10^0	2.7×10^0	1.8×10^0	6.5×10^{-1}	3.6×10^{-1}	3.6×10^{-1}	0.0×10^0	9.2×10^{-1}	1.1×10^0
65-68	g/t dry matter burned		3.2×10^{-1}	3.2×10^{-1}	1.3×10^{-1}	3.9×10^{-1}	5.0×10^{-1}	4.3×10^{-1}	1.5×10^0	1.2×10^0		
69	g/t dry matter burned		1.4×10^{-1}	3.1×10^{-2}	1.2×10^{-2}	3.8×10^{-2}	4.8×10^{-2}	4.1×10^{-2}	1.4×10^{-1}	1.1×10^{-1}		

Note

^aIn accord with "No." column in Tables 3.1 and 3.3

Table 3.9 Standard deviations of the log-transformed expected values of emission factors of 16 PAHs for various sources, $SD[\log_{10}(E(F_{PAHs}))]$

No. ^a	NAP	ACY	ACE	FLO	PHE	ANT	FLA	PYR	BaA	CHR	BbF	BkF	BaP	IcdP	DahA	BghiP
1-5	0.12	0.12	0.12	0.20	0.12	0.11	0.11	0.16	0.14	0.14	0.14	0.14	0.23	0.14	0.20	0.19
8	0.40	0.26	0.28	0.39	0.23	0.21	0.22	0.32	0.47	0.36	0.46	0.46	0.78	0.36	0.69	0.44
6,7,13,24,30,36	0.31	0.57	0.41	0.42	0.46	0.64	0.59	0.70	0.53	0.25	0.50	0.50	0.33	0.25	0.92	0.27
9,12,18	0.21	0.23	0.14	0.14	0.13	0.14	0.10	0.35	0.14	0.14	0.14	0.14	0.14	0.14	0.14	0.14
10,11	0.52	0.74	0.37	0.46	0.40	0.56	0.52	0.63	0.35	0.32	0.42	0.30	0.38	0.70	0.51	0.46
14	0.42	-	-	-	0.33	0.28	0.28	0.27	-	-	-	-	0.30	-	-	0.30
15-17	0.17	0.15	0.18	0.15	0.17	0.16	0.17	0.16	0.17	0.18	0.18	0.18	0.18	0.18	0.18	0.18
19-23	0.28	0.23	0.27	0.23	0.25	0.25	0.25	0.24	0.26	0.21	0.22	0.21	0.24	0.27	0.26	0.27
25-29	0.25	0.30	0.32	0.51	0.23	0.27	0.24	0.43	0.26	0.25	0.28	0.27	0.25	0.27	0.37	0.35
31	0.40	0.26	0.28	0.39	0.23	0.21	0.22	0.32	0.47	0.36	0.46	0.46	0.78	0.36	0.69	0.44
32,35	0.21	0.23	0.14	0.14	0.13	0.14	0.10	0.35	0.14	0.14	0.14	0.14	0.14	0.14	0.14	0.14
33,34	0.52	0.74	0.37	0.46	0.40	0.56	0.52	0.63	0.35	0.32	0.42	0.30	0.38	0.70	0.51	0.46
37	0.12	0.12	0.08	0.16	0.15	0.19	0.16	0.23	0.16	0.17	0.37	0.20	0.23	0.00	0.26	0.11
38	0.14	0.25	0.08	0.08	0.08	0.16	0.27	0.23	0.46	0.23	0.02	0.15	0.24	0.02	0.02	0.09
39-42	0.14	0.15	0.25	0.16	0.22	0.31	0.16	0.07	0.25	0.22	0.49	0.06	0.14	0.12	0.09	0.18
43-47	0.27	0.38	0.22	0.22	0.14	0.22	0.10	0.59	0.22	0.22	0.22	0.22	0.15	0.22	0.22	0.22
48,50	0.09	0.05	0.06	0.08	0.04	0.14	0.05	0.05	0.06	0.05	0.05	0.05	0.04	0.08	0.07	0.09
49	0.06	0.34	0.10	0.26	0.15	0.22	0.13	0.14	0.13	0.14	0.09	0.13	0.13	0.14	0.07	0.11
63	0.07	0.07	0.05	0.10	0.10	0.12	0.10	0.14	0.10	0.10	0.22	0.12	0.14	0.00	0.16	0.07
65-69	0.07	0.13	0.15	0.21	0.06	0.11	0.09	0.07	0.14	0.14	0.22	0.19	0.18	0.14	0.55	0.37

Note^aIn accord with "No." column in Tables 3.1 and 3.3

burning, and 10 % for all other sources (Xu et al. 2006; Bond et al. 2007; Endresen et al. 2007; Ciais et al. 2010). Variation intervals of future consumptions were assumed to increase from original intervals of historical consumptions to double of those for the period from 2009 to 2030. Monte Carlo simulation was used to characterize the overall uncertainty of the emission inventory. The emission estimates were repeatedly calculated 10,000 times by randomly drawing all inputs from given distributions with known coefficients of variation.

3.2 Atmospheric Transport Modeling

3.2.1 *Mozart-4*

The Model for Ozone and Related Chemical Tracers, version 4 (MOZART-4) is an offline global chemical transport model developed by the US National Center for Atmospheric Research (Emmons et al. 2010). The source code is available for download from its official Web site (<http://cdp.ucar.edu>). The model is suitable for studies of the troposphere and includes a number of updates over the previous tropospheric version MOZART-2. MOZART-3 is considered as an extension of MOZART-2 with detailed stratospheric chemistry (Emmons et al. 2010). MOZART-4 can be actually driven by any meteorological dataset with any emissions inventory at essentially any resolution. A standard simulation conducted officially was driven by meteorology from the NCAR reanalysis of the National Centers for Environmental Prediction (NCEP) forecasts (NCEP/NCAR reanalysis, Kalnay et al. 1996) at a horizontal resolution of approximately 2.8×2.8 with 28 vertical levels from the surface to approximately 2 hPa. The standard mechanism includes 85 gas-phase species, 12 bulk aerosol compounds, 39 photolysis, and 157 gas-phase reactions. MOZART-4 requires Linux or Unix operating system and can be run on various computing platforms from a single CPU on a desktop machine to more than one hundred CPUs on a supercomputer. The standard simulation requires at least 2-GB main memory per CPU, and one-year simulation casts probably three days under 32-thread parallel computation.

3.2.2 *Incorporation of PAH Module*

Since individual PAH compounds are not originally included in the standard simulation, a PAH module should be incorporated into MOZART-4. In this work, a PAH module was developed with consideration of the major physicochemical processes of PAH in the environment, including gas-particle partitioning,

photochemical reaction with OH radical, wet/dry deposition, and surface–air exchange. The description below will focus on the incorporation of these processes into MOZART-4. Recommended parameters of 16 parent PAHs for modeling are also listed in Table 3.10.

Gas–particle partitioning. As mentioned in Chap. 2, previous researches have suggested the dual black carbon (BC) adsorption and organic matter (OM) absorption scheme as one of the best schemes for PAH partitioning in long-range transport models (Lohmann and Lammel 2004; Lammel et al. 2009). The scheme is adopted in this study. The partitioning coefficient in the scheme can be expressed as follows:

$$K_p = 10^{-12} \times \left(\frac{f_{\text{OM}}}{\rho_{\text{oct}}} \times K_{\text{oa}} + \frac{f_{\text{BC}}}{\rho_{\text{BC}}} \times K_{\text{soot-air}} \right) \quad (3.1)$$

where K_p is the overall partitioning coefficient in $\text{m}^3/\mu\text{g}$, K_{oa} and $K_{\text{soot-air}}$ are the partitioning coefficients between octanol and air and between soot and air, respectively. K_{oa} and $K_{\text{soot-air}}$ in 298 K are shown in Table 3.10, f_{OM} and f_{BC} are the mass fractions of organic matter and black carbon in total suspended particulate matter, ρ_{oct} and ρ_{BC} are the densities of octanol and black carbon, being 0.8 and 1.0 kg/L , respectively. In this study, temperature dependence of K_p was also considered using following equation,

$$K_{p(T)} = K_{p(298)} \cdot e^{mp \cdot \left(\frac{1}{298} - \frac{1}{T} \right)}$$

where $K_{p(T)}$ was the partitioning coefficient in the temperature T , $K_{p(298)}$ was the partitioning coefficient in 298 K and was calculated using Eq. 3.1. mp is the ratio of $\Delta_{\text{O}_A}H$ to R (see Table 3.10), where $\Delta_{\text{O}_A}H$ is the enthalpy of phase change from air to octanol, and R is the ideal gas constant (8.314 J/mol/K).

Oxidation in the air. The photochemical reaction of PAHs in the gaseous phase with OH radical is the major pathway of removing from the atmospheric environment (Esteve et al. 2006; Kahan et al. 2006). In this study, second-order degradation kinetics was assumed for the reaction. The reaction coefficient (k_{OH}) at environment temperature T was calculated based on the measured reaction constant at a temperature of 298 K and the active energy E_a , as follows:

$$k_{\text{OH}(T)} = k_{\text{OH}(298)} \cdot e^{\frac{-E_a}{RT} \cdot \left(\frac{1}{298} - \frac{1}{T} \right)}$$

Wet/dry deposition. The wet/dry deposition is applied to particle-phase PAHs following the default setting of black carbon and organic carbon in the model.

Surface–air exchange. Dynamic exchanges of PAHs from air-to-soil and air-to-sea were included to depict the mass transfer between the lowest layer of the atmosphere and the top soil and ocean layers. The air-to-soil/sea exchange flux was calculated by the following equation:

Table 3.10 Recommended parameterization for PAH transport modelling

Parameter	Description	NAP	ACY	ACE	FLO	PHE	ANT	FLA	PYR
K_{oa}	Octanol-air partition coefficient	1.5×10^5	3.3×10^6	2.6×10^6	6.5×10^6	4.1×10^7	4.3×10^7	6.3×10^8	6.2×10^8
m_p , 1/K	Slope of $\ln K_p - (-1/T)$	-7259	-8885	-9696	-8239	-9077	-8239	-10171	-9176
K_{sa}	Soot-air partition coefficient	3.5×10^6	9.8×10^7	3.7×10^7	2.4×10^8	1.8×10^9	1.1×10^9	8.5×10^{10}	4.5×10^{10}
K_{oh} , $\text{cm}^3/\text{molec/s}$	Reaction rate constant for oxidation of gas phase with OH	2.4×10^{-11}	9.3×10^{-11}	9.3×10^{-11}	2.3×10^{-11}	1.4×10^{-11}	1.3×10^{-10}	2.1×10^{-10}	5.0×10^{-11}
E_a , J/mol	Activation energy	40	1200	1200	1400	-1600	-900	7300	0
v_m , cm^3/mol	Molecular volume	1.3×10^2	1.4×10^2	1.5×10^2	1.6×10^2	1.7×10^2	1.7×10^2	1.8×10^2	1.8×10^2
pk_{ow}	Octanol-water partition coefficient	3.5×10^3	4.7×10^3	1.1×10^4	2.0×10^4	2.6×10^4	1.5×10^5	5.1×10^4	6.3×10^4
pk_r , 1/s	Degradation rate in soil	4.3×10^{-7}	1.6×10^{-7}	1.3×10^{-7}	3.5×10^{-8}	2.4×10^{-7}	1.1×10^{-7}	4.6×10^{-8}	9.5×10^{-8}
pk_w , 1/s	Degradation rate in water	4.1×10^{-6}	1.6×10^{-7}	2.4×10^{-6}	3.5×10^{-7}	1.4×10^{-6}	1.9×10^{-5}	2.8×10^{-6}	2.3×10^{-5}
ah , $\text{Pa} \cdot \text{K}/\text{m}^3/\text{mol}$	Slope of $\log(\text{Henry}) - (-1/T)$	9.2×10^2	2.2×10^3	1.2×10^3	1.6×10^3	2.1×10^3	1.4×10^3	2.3×10^3	2.5×10^3
bh , $\text{Pa}/\text{m}^3/\text{mol}$	Intercept of $\log(\text{Henry}) - (-1/T)$	5.1×10^0	8.2×10^0	5.6×10^0	7.0×10^0	8.1×10^0	6.9×10^0	8.2×10^0	9.2×10^0
asp , Pa·K	Slope of $\log(P_{solid}) - (-1/T)$	2.9×10^3	3.3×10^3	3.5×10^3	3.6×10^3	3.8×10^3	4.4×10^3	4.3×10^3	4.3×10^3
bsp , Pa	Intercept of $\log(P_{solid}) - (-1/T)$	1.1×10^1	1.1×10^1	1.1×10^1	1.1×10^1	1.1×10^1	1.2×10^1	1.2×10^1	1.2×10^1

(continued)

Table 3.10 (continued)

Parameter	Description	NAP	ACY	ACE	FLO	PHE	ANT	FLA	PYR
alp, Pa·K	Slope of $\log(P_{\text{liquid}}) - (-1/T)$	1.9×10^3	2.8×10^3	2.4×10^3	2.6×10^3	3.0×10^3	2.9×10^3	3.3×10^3	3.4×10^3
blp, Pa	Intercept of $\log(P_{\text{liquid}}) - (-1/T)$	8.1×10^0	9.5×10^0	8.1×10^0	8.6×10^0	9.1×10^0	8.6×10^0	9.0×10^0	9.5×10^0
asl, mol·K/m ³	Slope of $\log(\text{solubility}) - (-1/T)$	1.0×10^3	5.7×10^2	1.1×10^3	1.0×10^3	8.6×10^2	1.5×10^3	9.9×10^2	9.0×10^2
bsl, mol/m ³	Intercept of $\log(\text{solubility}) - (-1/T)$	3.0×10^0	1.3×10^0	2.5×10^0	1.7×10^0	9.3×10^{-1}	1.7×10^0	8.0×10^{-1}	3.2×10^{-1}
pkstd, 1/m/h	Ocean diffusion constant	2.3×10^{-4}	2.3×10^{-4}	2.3×10^{-4}	2.3×10^{-4}	2.3×10^{-4}	2.3×10^{-4}	2.3×10^{-4}	2.3×10^{-4}
bcf, m ³ /kg	Biological concentration factor	7.5×10^0	9.8×10^0	2.1×10^1	2.9×10^1	3.9×10^1	3.8×10^1	2.1×10^2	1.7×10^2
Parameter	Description	BaA	CHR	BbF	BkF	BaP	IcdP	DahA	BghiP
K_{oa}	Octanol-air partition coefficient	1.9×10^{10}	2.0×10^{10}	2.2×10^{11}	2.3×10^{11}	1.4×10^{11}	2.7×10^{12}	3.9×10^{12}	3.5×10^{12}
$mp, 1/K$	Slope of $\ln K_p - (-1/T)$	-10789	-14866	-8885	-8885	-7496	-8885	-8885	-2730
$K_{\text{sort-air}}$	Soot-air partition coefficient	5.0×10^{12}	4.1×10^{12}	6.7×10^{12}	6.2×10^{12}	1.0×10^{13}	2.6×10^{15}	1.1×10^{15}	3.4×10^{15}
K_{obs} , cm ³ /molec/s	Reaction rate constant for oxidation of gas phase with OH	5.0×10^{-11}	5.0×10^{-11}	1.9×10^{-11}	5.4×10^{-11}	1.5×10^{-10}	6.4×10^{-10}	6.4×10^{-11}	6.4×10^{-11}
E_{a} , J/mol	Activation energy	0	0	0	0	0	0	0	0
vm , cm ³ /mol	Molecular volume	2.1×10^2	2.1×10^2	2.2×10^2	2.2×10^2	2.2×10^2	2.3×10^2	2.5×10^2	2.3×10^2
pk_ow	Octanol-water partition coefficient	3.6×10^5	1.0×10^6	7.9×10^5	1.5×10^6	5.0×10^5	5.3×10^6	1.2×10^7	1.3×10^6

(continued)

Table 3.10 (continued)

Parameter	Description	NAP	ACY	ACE	FLO	PHE	ANT	FLA	PYR
pk_r, 1/s	Degradation rate in soil	1.4×10^{-7}	3.8×10^{-8}	1.6×10^{-8}	3.3×10^{-8}	5.3×10^{-8}	1.2×10^{-8}	1.9×10^{-8}	1.6×10^{-8}
pk_w, 1/s	Degradation rate in water	3.8×10^{-5}	4.2×10^{-6}	8.8×10^{-7}	1.3×10^{-6}	2.4×10^{-5}	4.5×10^{-8}	9.6×10^{-7}	1.3×10^{-8}
ah, Pa·K/m ³ /mol	Slope of log(Henry)–(–1/T)	2.6×10^3	2.8×10^3	3.3×10^3	3.0×10^3	3.6×10^3	3.2×10^3	3.4×10^3	4.0×10^3
bh, Pa/m ³ /mol	Intercept of log (Henry)–(–1/T)	9.7×10^0	1.0×10^1	9.8×10^0	9.8×10^0	1.2×10^1	1.0×10^1	1.1×10^1	1.3×10^1
asp, Pa·K	Slope of log(P _{solid})–(–1/T)	4.9×10^3	5.5×10^3	5.9×10^3	5.9×10^3	5.4×10^3	6.1×10^3	6.1×10^3	5.8×10^3
bsp, Pa	Intercept of log (P _{solid})–(–1/T)	1.2×10^1	1.2×10^1	1.2×10^1	1.2×10^1	1.2×10^1	1.3×10^1	1.3×10^1	1.2×10^1
alp, Pa·K	Slope of log(P _{liquid})–(–1/T)	3.8×10^3	4.1×10^3	4.6×10^3	4.4×10^3	5.0×10^3	4.8×10^3	5.0×10^3	4.9×10^3
blp, Pa	Intercept of log (P _{liquid})–(–1/T)	9.3×10^0	9.7×10^0	9.5×10^0	9.5×10^0	1.2×10^1	9.6×10^0	9.8×10^0	1.1×10^1
asl, mol·K/m ³	Slope of log (solubility)–(–1/T)	1.1×10^3	1.4×10^3	1.3×10^3	1.5×10^3	9.1×10^2	1.6×10^3	1.6×10^3	9.1×10^2
bsl, mol/m ³	Intercept of log (solubility)–(–1/T)	-3.3×10^{-1}	-3.2×10^{-1}	-3.5×10^{-1}	-3.5×10^{-1}	-1.3×10^0	-7.6×10^{-1}	-1.4×10^0	-2.1×10^0
pkstd, 1/m/h	Ocean diffusion constant	2.3×10^{-4}	2.3×10^{-4}	2.3×10^{-4}	2.3×10^{-4}	2.3×10^{-4}	2.3×10^{-4}	2.3×10^{-4}	2.3×10^{-4}
bcf, m ³ /kg	Biological concentration factor	6.8×10^2	6.8×10^2	1.7×10^3	1.7×10^3	1.6×10^3	6.0×10^3	1.3×10^4	1.7×10^3

$$F_{\text{si}} = BCF \times F_{\text{om}} C_w$$

where the D was transport coefficient defined by Ma et al. (2003). $f_{\text{soil/ocean}}$ and f_{air} are the fugacity of soil/sea and air, respectively, which changed dynamically due to the change in flux during the computation.

Degradation in soil and sea water. The soil and sea modules were similar to those in the CanMETOP (Ma et al. 2003), except for the biogeochemical processes in sea water. The water–phytoplankton exchange and the sinking of organic matter were parameterized based on the measurements of Jones et al. (Dachs et al. 2002) and were added to the module:

$$F_{\text{si}} = BCF \times F_{\text{om}} C_w$$

where F_{si} is the sinking flux of PAHs sorbed to organic matter, BCF is the concentration ratio of PAHs associated with organic matter against those dissolved in sea water (C_w), and F_{om} is the sinking flux of organic matter. The initial PAH concentrations in surface soil were derived iteratively and the model was run repeatedly based on PAH emissions in 2007 until the soil concentrations reached a steady state.

The PAH module is incorporated in MOZART-4. Using the three quartiles of the emissions at all grids, the best estimates and uncertainty ranges of concentrations can be generated. We conducted a long-term simulation for the period from 1998 to 2007, and two sets of short-term modeling experiments for the year 2007 with spin-up time of one year. The short-term experiments were either for emission from 12 individual source categories globally or total emissions from 12 individual regions (Fig. 3.4). The 69 sources listed in Table 3.1 were classified into 12 source categories, including residential crop residue burning, residential firewood burning, residential fossil fuel combustion, coke production, primary aluminum production, motor vehicles, industrial boilers, iron industry, agriculture waste burning, deforestation/wildfire, shipping, and others. The world regions were defined based on the definition of the Task Force on Hemispheric Transport of Air Pollution (Task Force on Hemispheric Transport of Air Pollution 2014) (Table 3.17).

3.2.3 Model Validation and Downscaling

Since this study mainly focuses on health assessment of PAH exposure which can be evaluated using benzo[*a*]pyrene as an indicator, the model-calculated BaP concentrations at the surface layer were validated against the field-measured BaP concentrations at more than 200 stations around the world. The observation sites were classified into three categories of background, non-background, and time series, which were used separately for the validation. Locations of background and non-background sites applied for model validation are demonstrated in Fig. 5.1 in Chap. 5. To rectify the bias due to the scale mismatch, we downscaled the

model-calculated concentrations from $1.875^\circ \times 1.895^\circ$ to $0.1^\circ \times 0.1^\circ$. The reason why downscaling process was conducted and the detailed procedure can be found in the Chap. 5.

To emphasize the higher health impact of BaP concentrations in densely populated areas, a population-weighted BaP concentration of each $0.1^\circ \times 0.1^\circ$ grid was calculated as the product of the grid concentration and population density divided by global average population density over land area (Oak Ridge National Laboratory 2014).

3.3 Lung Cancer Risk Assessment

In this study, the BaP-indicator approach is used to evaluate lung cancer risk from PAH inhalation exposure. What is different from previous assessment is that the cancer slope factor (CSF) is adopted instead of the unit risk, since assessment adopting CSF makes it possible to involve factors describing individual susceptibility such as body weight and inhalation rate. Practically, to be precautionary, the 95 % upper bound of the slope of a dose–response regression curve has been commonly adopted as the cancer slope (California Environmental Protection Agency 2014; Health Canada 2014). However, this study used the maximum likelihood, instead of the upper bound, to derive an unbiased best estimate of health outcome, namely the incremental lifetime cancer risk (*ILCR*). Uncertainty due to variation in the dose–response relationship is explicitly quantified in a probabilistic model. In addition, genetic susceptibility is characterized based on frequency distributions generated from the lung cancer-related genetic polymorphism data for the major human races (see detailed descriptions below).

3.3.1 Incremental Lifetime Cancer Risk

ILCR is commonly calculated as the product of lifetime average daily doses (*LADD*) and cancer slope factor (*CSF*) (Ezzati and Lopez 2003). In this study, a term of overall susceptibility (*SUS*) was introduced to describe the effect of individual susceptibility on the *ILCR* induced by exposure to PAHs in ambient air (Boström et al. 2002). *ILCR* was calculated as follows:

$$\begin{aligned} ILCR &= CSF \times LADD \times SUS \\ &= \sum_a \left[CSF \times \frac{(C \times IR_{a,g,r} \times y_{a,g,r})}{BW_{a,g,r} \times LE} \times (GeneSus_e \times EAF_e \times ASF_a) \right] \end{aligned}$$

where a, g, e, and r are subscripts representing age, gender, ethnicity, and geographic region, respectively, suggesting that *LADD* is age, gender, and region

dependent and SUS is ethnicity and region dependent; C (mg/m^3) is BaP exposure concentration; IR (m^3/day) is the inhalation rate; y (year) is the exposure duration; BW (kg) is body weight; LE (70 years) is the average life expectancy of the global population (WHO 2014a, b); SUS is the product of $GeneSus$, EAF , and ASF , which are genetic susceptibility, ethnicity-adjusted factor, and age-sensitivity factor, respectively. $GeneSus$, EAF , and ASF are all dimensionless and either ethnicity or region dependent.

In this study, a CSF of $26.6 \text{ kg}(\text{body weight})\cdot\text{day}/\text{mg}$ for BaP was adopted as the maximum likelihood estimate based on epidemiological data from studies on coke oven workers, using a multistage-type model³¹. Use of BaP as an indicator of PAH exposure risk has been thoroughly investigated previously, and it was found that BaP can serve as an indicator for carcinogenic activity of PAH compounds at various sites (Expert Panel on Air Quality Standards 1999).

The uncertainty of the CSF was derived according to the calculated disparity from different epidemiological studies (Boström et al. 2002). The resulting standard deviation of log-transformed CSF is 0.38. C is downscaled BaP concentrations in 2007 at 0.1×0.1 resolution. Derivation of the distributions of country- and age-specific IR and BW is described below. EAF was calculated based on the lung cancer incidences for individual ethnicities reported by the United States Cancer Statistics (USCS 2014), excluding the influence of smoking. ASF values of 10, 2, and 1 were used for the age groups of <2 , 2–16, and >16 years, respectively (California Environmental Protection Agency 2014). Male to female ratios were assumed to be 1:1 for all countries. Proportions of ethnic groups of each country were derived from a report of the Central Intelligence Agency of the USA (Central Intelligence Agency 2014).

To quantify population $ILCR$ and uncertainty for all countries, $ILCR$ values were calculated for 7 billion individuals in the world. The exposure concentrations were derived based on the spatial distributions of both BaP concentration and population (Oak Ridge National Laboratory 2014). Gender, ethnicity, genotypes, IR , and BW of an individual were randomly drawn from their distributions in given counties.

To characterize genetic susceptibility of the global population, data on genetic polymorphisms of the major human races were collected from the literature. Relative risks for lung cancer of different genotypes from 16 polymorphisms were calculated for major ethnic groups individually. Using the Monte Carlo simulation, 100,000 hypothetical persons for each ethnic group were generated with their genotypes randomly chosen based on genotype frequencies. The relative risk of lung cancer for an individual with the generated gene sequence was calculated as the product of the relative risks of all his/her genotypes. The distribution of the calculated relative risks of the 100,000 hypothetical persons ($GeneSus$) represented the overall distribution of genetic susceptibility of the specified ethnic group. Detailed methods can be found below.

3.3.2 *Quantification of Distributions of Individual Differences*

Determination of distributions of body weights and genetic susceptibilities together with other parameters is described in details below.

Body weight. If available, national exposure factors handbooks were used to derive body weight information by age and gender for each country (Institute for Health and Consumer Protection 2014; The Department of Health 2014; USEPA 2011; Kim et al. 2006; National Institute of Advanced Industrial Science and Technology 2014; Duan 2012) (Table 3.11). Otherwise, regional information reported by Walpole et al. (2012) was applied for each country (Table 3.12). National body weight distributions were generated using Monte Carlo simulation based on this information. The body weight distributions of Chinese population are illustrated in Fig. 3.3a as an example.

Inhalation Rate. Inhalation rates were calculated based on oxygen consumption associated with energy expenditures, using equation (S1) (Layton 1993):

$$\text{Inhalation rate} = \text{BMR} \times A \times H \times VQ$$

where BMR is the basal metabolic rate, MJ/day; A is the ratios of energy expenditure rate to basal metabolic rate, unitless; H is the volume of oxygen consumed in the production of 1 MJ of energy, m³/MJ; VQ is ventilatory equivalent, ratio of the volume of air to the volume of oxygen breathed per unit time, unitless. The parameters can be addressed in Table 3.13. Variations of inhalation rates are associated with variations of the basal metabolic rates which are determined by body weights. The inhalation rate of a hypothetical person is generated according to the above equation based on its gender, age, and body weight.

Exposed year. Exposed year, y , is the duration of each age category until the person reached its life expectancy. Distinguished from the average life expectancy of the global population (LE) which is 70 years in 2011 (WHO 2014a, b), life expectancies of hypothetical persons varied with countries and genders based on the WHO reports (WHO 2014a, b).

Ethnicity-adjusted factor. Information on American lung cancer incidences by ethnicity were derived from the United States Cancer Statistics (USCS 2014). Lung cancer incidences caused by smoking were excluded according to the smoking prevalence of each ethnic group (Centers for Disease Control and Prevention 2014) and the attributable lung cancer risk (Fenelon and Preston 2011). Also, Lung cancer incidence rate of each ethnic group was normalized by average body weight, inhalation rate, and life expectancy of this ethnic group. The ethnicity-adjusted factor (EAF) of a specified ethnic group was calculated as the ratio of lung cancer incidence rate of a specific ethnic group to the overall incidence rate of the mixed population. The resulted EAFs are 1.12, 0.86, 1.19, 0.48, and 1.04 for Caucasian, Asian, African, Amerindian, and Pacific, respectively. These results are similar with those of smoking-related risk of lung cancer in which risks of African American,

Table 3.11 Body weight by country, gender, and age

Sex/Age, years	Sweden	Bulgaria	Czech Republic	Estonia	Finland	Latvia	France	Italy	Germany	Hungary	Ireland
<i>Males</i>											
0-2	9.1	9.3	9.1	10.7	10.9	10.6	9.6	10.1	9.3	8.6	11.3
2-3	13.7	13.4	13.1	15.5	15.7	15.3	13.9	14.6	13.5	12.4	16.3
3-5	18.7	17.5	17.2	20.2	20.5	20.0	18.1	19.1	16.7	16.2	21.3
5-10	30.3	27.0	25.6	31.5	32.0	31.1	27.5	29.5	25.6	24.5	33.2
10-18	58.7	53.9	53.1	58.8	59.7	58.0	54.2	56.1	51.6	50.8	61.8
18-30	79.7	71.8	78.7	77.0	78.2	76.0	73.1	73.2	71.9	76.4	81.0
30-60	82.5	77.8	84.5	81.1	83.8	81.3	78.6	77.8	78.1	80.0	84.8
60+	85.3	73.2	79.5	76.3	78.9	76.5	76.2	72.4	82.0	75.2	79.8
SD _{log10}	0.070	0.066	0.062	0.080	0.074	0.064	0.075	0.067	0.062	0.085	0.074
<i>Females</i>											
0-2	9.0	9.0	8.7	9.5	9.7	9.4	9.1	9.7	8.9	8.2	9.9
2-3	13.5	13.1	12.7	13.9	14.1	13.7	13.4	14.1	13.1	12.0	14.5
3-5	18.2	17.2	16.8	18.2	18.6	18.0	17.6	18.6	16.5	15.8	19.1
5-10	29.1	26.9	25.2	28.5	29.0	28.2	27.0	28.9	25.5	24.2	29.8
10-18	51.2	50.5	49.7	48.9	49.8	48.4	49.4	50.1	49.0	47.2	51.1
18-30	66.2	60.7	62.2	61.7	63.0	61.1	59.8	57.9	59.7	61.2	64.6
30-60	67.7	69.1	69.4	68.8	68.3	70.3	63.7	63.0	66.0	67.6	68.1
60+	69.2	64.5	64.7	64.2	63.7	65.5	59.4	58.8	72.2	63.1	63.5
SD _{log10}	0.085	0.072	0.055	0.078	0.082	0.072	0.092	0.080	0.079	0.098	0.084
Sex/Age, years	Lithuania	Netherlands	Slovakia	Switzerland	United Kingdom	Australia	South Korea	Japan	China	United States	
<i>Males</i>											
0-2	10.7	9.3	9.1	9.3	9.5	10.7	9.6	10.7	10.0	9.8	
2-3	15.5	13.4	13.1	13.5	13.6	15.5	14.0	14.9	14.2	14.1	

(continued)

Table 3.11 (continued)

Sex/Age, years	Lithuania	Netherlands	Slovakia	Switzerland	United Kingdom	Australia	South Korea	Japan	China	United States
3-5	20.2	17.5	17.2	17.6	17.8	20.3	16.8	18.8	16.9	18.6
5-10	31.5	26.6	25.6	27.4	27.7	31.8	26.9	28.3	24.6	29.9
10-18	58.7	52.5	53.1	53.3	51.7	60.7	52.5	51.9	46.2	60.5
18-30	76.9	61.3	65.2	69.8	78.6	76.5	69.7	62.7	64.6	82.3
30-60	84.6	68.7	69.6	77.2	83.9	83.5	70.7	64.0	67.4	89.0
60+	79.7	64.7	65.5	72.6	79.0	78.6	64.3	60.2	62.8	83.0
SD _{log10}	0.054	0.069	0.069	0.068	0.069	0.073	0.069	0.069	0.076	0.085
<i>Females</i>										
0-2	9.4	8.8	8.7	9.3	9.3	10.4	9.5	10.0	9.4	9.4
2-3	13.7	12.9	12.7	13.6	13.6	15.3	14.0	14.1	13.5	13.5
3-5	18.0	16.9	16.8	17.8	17.9	20.2	16.2	17.8	16.3	17.9
5-10	28.2	26.5	25.2	27.9	28.0	31.7	25.5	26.8	23.6	29.4
10-18	48.4	50.3	49.7	48.1	48.1	55.6	46.9	44.8	43.8	56.5
18-30	61.2	57.2	58.2	60.8	65.2	67.2	54.4	51.5	55.1	70.3
30-60	70.1	63.6	62.7	61.4	70.2	69.0	58.1	52.7	59.1	76.5
60+	65.4	59.3	58.5	57.3	65.5	64.4	57.1	49.2	56.6	70.6
SD _{log10}	0.074	0.079	0.079	0.078	0.079	0.101	0.079	0.079	0.069	0.111

National medians of body weights are listed in each age category. SD_{log10} represents the standard deviation of log₁₀(body weight), and is applied to all age categories. Body weight distribution of each country was generated using Monte Carlo simulation Reprinted with permission from Shen et al. (2014). Copyright (2014) Nature Publishing Group

Table 3.12 Body weight by world region, gender, and age

Sex/Age, years	Asia	Europe	Africa	Latin America	Northern America	Oceania
<i>Males</i>						
0–2	10.7	10.7	10.7	10.7	10.7	10.7
2–3	15.0	15.4	15.1	15.3	15.6	15.5
3–5	19.4	20.1	19.5	19.9	20.6	20.3
5–10	29.6	31.3	29.9	30.9	32.6	31.7
10–18	49.4	58.4	51.6	56.4	65.3	60.6
18–30	58.9	72.9	62.5	69.9	83.8	76.3
30–60	62.9	77.9	66.7	74.7	89.5	81.5
60+	59.2	73.3	62.8	70.3	84.2	76.7
SD _{log10}	0.076	0.069	0.075	0.075	0.082	0.073
<i>Females</i>						
0–2	10.0	10.0	10.0	10.0	10.0	10.0
2–3	14.3	14.6	14.3	14.5	14.9	14.7
3–5	18.5	19.2	18.7	19.1	19.8	19.4
5–10	28.3	30.0	28.8	29.7	31.3	30.5
10–18	44.3	51.6	45.8	49.9	56.9	53.5
18–30	50.8	61.7	52.9	59.2	69.7	64.6
30–60	54.7	66.5	57.0	63.8	75.1	69.6
60+	51.1	62.1	53.2	59.5	70.1	64.9
SD _{log10}	0.069	0.079	0.088	0.088	0.102	0.101

Regional medians of body weights are listed in each age category. SD_{log10} represents the standard deviation of log₁₀(body weight), and is applied to all age categories. Body weight distribution of each region was generated using Monte Carlo simulation

Reprinted with permission from Shen et al. (2014). Copyright (2014) Nature Publishing Group

Native Hawaiian, and White are higher than those of Japanese American and Latino, given the same level of smoking exposure (Haiman et al. 2006).

Age. Apart from the changes of body weights and inhalation rates, an age-sensitivity factor (ASF) was adopted (see 3.3.1). Figure 3.3b illustrates the resulting lung cancer risks per unit exposure at different age categories for Chinese female.

Gender. For smokers, the issue whether women are more susceptible to lung cancer than men, given the same level of smoking exposure, remains substantially controversial (Bain et al. 2004; Perneger 2001). For non-smokers, the observed higher levels of incidence rates in women than in men may be raised mainly by women's higher level of cumulative exposure to indoor carcinogens, such as indoor fumes from cooking and heating stoves, environmental tobacco smoke, and radon (Siegfried 2001). As a result, our estimation only included the gender disparities in body weights, inhalation rates, and life expectancies, but not an additional gender-adjusted factor.

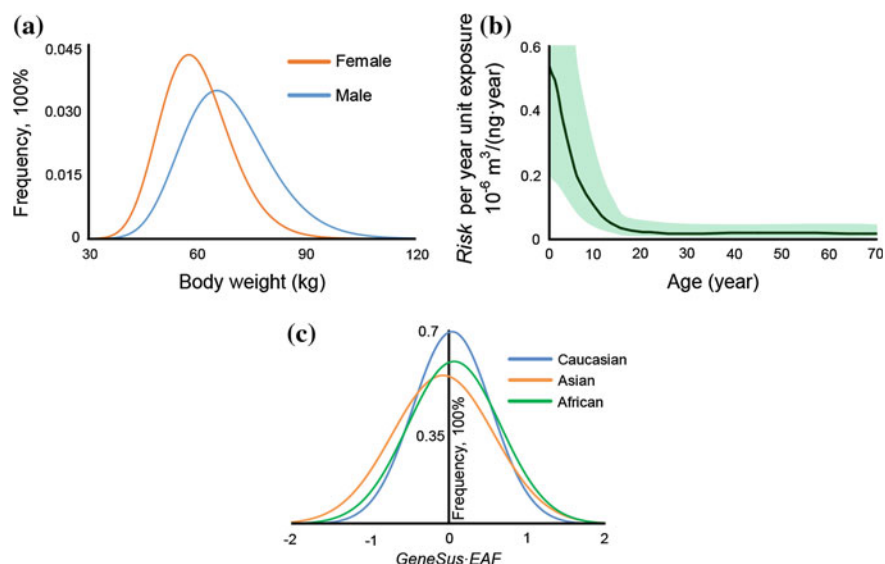


Fig. 3.3 Some examples of individual disparities used as input parameters of risk assessment. **a** Distributions of body weights of Chinese population at ages of 30–60 generated from Monte Carlo simulation. **b** Resulting lung cancer risks per unit exposure per year of Chinese female at different ages. The shadow area demonstrates the individual differences at interquartile range. **c** Distributions of individual susceptibilities due to genetic polymorphisms and ethnic disparities defined as *GeneSus* multiplied by *EAF* in the main text. Reprinted with permission from Shen et al. (2014). Copyright (2014) Nature Publishing Group

Table 3.13 Parameterization for inhalation rate calculation by age and sex

Sex/Age, years	BMR Equation, MJ/day	VQ	A	H, m ³ O ₂ /MJ
<i>Males</i>				
0–3	0.249 BW – 0.127	27	1.6	0.05
3–10	0.095 BW + 2.110	27	1.6	0.05
10–18	0.074 BW + 2.754	27	1.7	0.05
18–30	0.063 BW + 2.896	27	1.59	0.05
30–60	0.048 BW + 3.653	27	1.59	0.05
60+	0.049 BW + 2.459	27	1.59	0.05
<i>Females</i>				
0–3	0.244 BW – 0.130	27	1.6	0.05
3–10	0.085 BW + 2.033	27	1.6	0.05
10–18	0.056 BW + 2.898	27	1.5	0.05
18–30	0.062 BW + 2.036	27	1.38	0.05
30–60	0.034 BW + 3.538	27	1.38	0.05
60+	0.038 BW + 2.755	27	1.38	0.05

Genetic susceptibility. Genetic variations in metabolic enzyme activity, DNA repair capacity, and tumor suppressor genes have been thought to contribute to individual differences in lung cancer susceptibility, following environmental carcinogen exposure (Boström et al. 2002; Kiyohara et al. 2002). The relationship between genetic polymorphisms of related genes and lung cancer has been widely investigated. In this study, 16 polymorphisms in 13 genes potentially related to lung cancer susceptibility was involved, and information on high-risk allele frequencies both in control and case groups by ethnicity was collected from the literature (Zhang et al. 2006, 2011, 2012; Nerurkar et al. 2000; Gaspar et al. 2002; Kiyohara et al. 2005; Dai et al. 2012; Feng et al. 2012; Guan et al. 2011; Duan et al. 2012; Zou et al. 2012; Ding et al. 2012; Matakidou et al. 2003; Boldrini et al. 2008; Kim et al. 2007; Sjölander et al. 1996; Hrstka et al. 2009; Herath et al. 2000) and listed in Tables 3.14 and 3.15. For the first 14 polymorphisms, the high-risk alleles are defined as A1, and the low-risk alleles are defined as A2. Relative risks for lung cancer of genotypes A1/A1, A1/A2, and A2/A2 are calculated as follows, respectively:

$$\begin{aligned} rr_{11} &= \frac{1 - \text{Freq}_{\text{case}}}{1 - \text{Freq}_{\text{control}}} \times \frac{1 - \text{Freq}_{\text{case}}}{1 - \text{Freq}_{\text{control}}} \\ rr_{12} &= \frac{1 - \text{Freq}_{\text{case}}}{1 - \text{Freq}_{\text{control}}} \times \frac{1 - \text{Freq}_{\text{case}}}{1 - \text{Freq}_{\text{control}}} \\ rr_{22} &= \frac{1 - \text{Freq}_{\text{case}}}{1 - \text{Freq}_{\text{control}}} \times \frac{1 - \text{Freq}_{\text{case}}}{1 - \text{Freq}_{\text{control}}} \end{aligned}$$

where subscripts 11, 12, and 22 represent A1/A1, A1/A2, and A2/A2 genotypes, respectively; rr is the relative risk for lung cancer of persons with corresponding genotype compared to population average level; $\text{Freq}_{\text{case}}$ and $\text{Freq}_{\text{control}}$ are high-risk allele (A1) frequencies in case and control groups, which are listed in Table 3.15. For the *GSTM1* and *GSTT1* genes, relative risks of “-” (null) and “+” genotypes are calculated as follows:

$$\begin{aligned} rr_{-} &= \frac{\text{Freq}_{\text{case}}}{\text{Freq}_{\text{control}}} \\ rr_{+} &= \frac{1 - \text{Freq}_{\text{case}}}{1 - \text{Freq}_{\text{control}}} \end{aligned}$$

Table 3.16 shows the relative risks of each genotype by ethnicity, together with genotype frequencies which are derived from Table 3.15 allele frequencies in control groups based on the Hardy–Weinberg Equilibrium.

We notice that 16 polymorphisms cannot demonstrate the overall variations in lung cancer susceptibility. However, allele frequencies of other polymorphisms cannot be fully determined in both control and case groups even for the three main ethnical groups. Landi et al. (2005) suggested that a set of 250 SNPs represents the best candidates as lung cancer risk factors. Thus, for a hypothetical person

Table 3.14 Counts of cases and controls

Genetic polymorphism, at-risk allele (genotype)	Caucasian control/case	Asian control/case	African control/case	India control/case	Amerindian control/case	Pacific control/case	Mestizo control/case
<i>CYP1A1</i> MspI, Var	5292/3944	3706/2411	1364/756	439/409	278/104	106/0	274/103
<i>CYP1A1</i> Ile-Val, Val	6133/3906	4141/2744	1210/646	529/393	275/102	106/0	272/100
<i>GSTP1</i> I105 V, Val	5908/4651	816/896	146/118	110/110	0/0	22/0	90/0
<i>NQO1</i> Pro187Ser, Ser	4387/1705	3329/781	139/116	100/0	0/0	102/83	161/61
<i>MPO</i> G	5107/3411	1660/422	244/157	167/0	0/0	103/80	0/0
<i>ERCC1</i> C118T, T	5249/2128	1696/1589	388/0	100/0	0/0	0/0	90/0
<i>XRCC1</i> 399, Arg	7022/5557	2847/2530	644/524	122/103	0/0	0/0	299/113
<i>XPD</i> 751, Gln	6258/4423	3421/3452	514/408	100/0	0/0	0/0	299/113
<i>hOGG1</i> , G	5413/3713	4100/4246	280/254	0/0	0/0	96/75	296/112
<i>XPA</i> , A	2472/2066	1129/1156	67/81	100/0	0/0	0/0	47/50
<i>TP53</i> -exon4-codon72, Pro	6069/5197	3897/3725	137/80	342/308	257/0	103/85	80/42
<i>TP53</i> -Intron3 16 bp, Ins	2757/2791	371/120	172/64	434/307	257/0	0/0	40/54
<i>TP53</i> -Intron6 MspI, Mt	2637/2703	226/0	172/0	434/0	257/0	0/0	40/0
<i>TP73</i> -exon2, AT	1991/1917	1405/1196	10/0	0/0	0/0	0/0	0/0
<i>GSTM1</i> , null	6735/5008	4248/3208	557/329	0/0	0/0	0/0	114/92
<i>GSTT1</i> , null	581/4405	3561/2823	146/118	186/210	257/0	0/0	178/52

Reprinted with permission from Shen et al. (2014). Copyright (2014) Nature Publishing Group

Table 3.15 High-risk allele frequencies of cases and controls by ethnicity^a

Genetic polymorphism, at-risk allele/genotype	Caucasian		Asian		African		Indian		Amerindian		Pacific		Mestizo	
	Control (%)	Case (%)	Control (%)	Case (%)	Control (%)	Case (%)	Control (%)	Case (%)	Control (%)	Case (%)	Control (%)	Case (%)	Control (%)	Case (%)
<i>CYP1A1</i> MspI, Var	10.8	12.5	38.0	41.1	21.4	21.5	23.7	33.4	37.4	29.3	42.5	—	38.1	39.8
<i>CYP1A1</i> Ile-Val, Val	10.5	11.7	24.6	29.6	2.2	2.9	16.6	28.2	29.6	21.1	16.5	—	31.6	34.0
<i>GSTP1</i> I105 V, Val	31.6	32.2	16.4	15.6	42.8	46.2	28.6	27.3	—	—	25.0	—	55.0	—
<i>NQO1</i> Pro187Ser, Ser	17.6	18.7	43.2	39.3	21.2	18.5	39.8	—	—	—	22.1	15.7	43.2	31.1
<i>MPO</i> , G	76.7	79.0	87.5	90.9	70.1	72.4	95.2	—	—	—	86.9	77.6	—	—
<i>ERCC1</i> C118T, T	60.5	61.9	24.1	25.9	9.2	—	52.3	—	—	—	—	—	27.0	—
<i>XRCC1</i> 399, Arg	34.9	35.2	25.7	26.4	12.3	11.5	42.6	30.1	—	—	45.5	—	14.4	11.1
<i>XPD</i> 751, Gln	36.7	38.8	9.3	10.4	23.6	25.6	35.8	—	—	—	4.3	—	21.9	28.3
<i>hOGGI</i> , G	22.2	21.7	50.4	53.3	15.4	17.7	—	—	—	—	44.8	59.3	32.1	31.7
<i>XPA</i> , A	35.9	37.5	47.1	51.0	29.9	37.0	45.5	—	—	—	—	—	39.4	53.0
<i>TP53</i> -exon4-codon72, Pro	26.2	28.6	39.3	41.3	50.0	48.4	53.5	46.6	15.4	—	48.1	53.5	23.1	27.3
<i>TP53</i> -Intron3 16 bp, Ins	11.8	13.9	2.7	3.5	22.7	25.7	19.8	16.5	0.1	—	22.9	—	6.3	21.7
<i>TP53</i> -Intron6 MspI, Mt	13.8	16.7	4.0	—	20.1	—	20.5	—	0.5	—	—	—	10.0	—
<i>TP73</i> -exon2, AT	20.5	25.0	25.9	24.5	5.0	—	—	—	—	—	—	—	—	—
<i>GSTM1</i> , null	49.6	51.0	51.2	58.1	30.2	30.3	32.8	40.5	21.8	—	63.6	—	23.7	35.9
<i>GSTT1</i> , null	27.2	22.9	41.3	45.7	25.3	23.7	15.1	17.1	13.2	—	—	—	5.1	21.2

^aac.-; no data were obtained from literature

Reprinted with permission from Shen et al. (2014). Copyright (2014) Nature Publishing Group

Table 3.16 Genotype frequencies and relative risks of lung cancer^a

Genotype	Caucasian		Asian		African		Indian		Amerindian		Pacific		Mestizo	
	Freq ^b (%)	rr ^c	Freq (%)	rr	Freq (%)	rr	Freq (%)	rr	Freq (%)	rr	Freq (%)	rr	Freq (%)	rr
<i>CYP1A1</i> MspI,rs4646903														
WT/WT	79.6	0.96	38.5	0.90	61.8	1.00	58.2	0.76	39.2	1.27	33.1	—	38.3	0.95
WT/Var	19.3	1.14	47.1	1.03	33.6	1.00	36.2	1.23	46.8	0.89	48.9	—	47.2	1.02
Var/Var	1.2	1.35	14.4	1.17	4.6	1.01	5.6	1.99	14.0	0.61	18.0	—	14.5	1.09
<i>CYP1A1</i> Ile-Val,rs1048943														
Ile/Ile	80.2	0.97	56.8	0.87	95.6	0.99	69.5	0.74	49.5	1.26	69.7	—	46.8	0.93
Ile/Val	18.7	1.10	37.1	1.12	4.4	1.31	27.7	1.46	41.7	0.80	27.6	—	43.2	1.04
Val/Val	1.1	1.24	6.1	1.45	0.0	1.74	2.8	2.88	8.8	0.51	2.7	—	10.0	1.16
<i>GSTP3</i> III05 V:G,rs1695														
Ile/Ile	46.8	0.98	69.9	1.02	32.7	0.89	50.9	1.04	—	—	56.3	—	20.3	—
Ile/Val	43.2	1.01	27.4	0.96	49.0	1.02	40.9	0.97	—	—	37.5	—	49.5	—
Val/Val	10.0	1.04	2.7	0.91	18.3	1.16	8.2	0.91	—	—	6.3	—	30.3	—
<i>NQO1</i> Pro187Ser:C > T,rs1800566														
Pro/Pro	67.9	0.97	32.3	1.14	62.1	1.07	—	—	—	—	60.7	1.17	32.3	1.47
Pro/Ser	29.0	1.05	49.1	0.97	33.4	0.90	—	—	—	—	34.4	0.77	49.1	0.87
Ser/Ser	3.1	1.13	18.6	0.83	4.5	0.76	—	—	—	—	4.9	0.50	18.6	0.52
<i>MPO</i> :G > A,rs2333227														
A/A	5.4	0.81	1.6	0.53	9.0	0.85	0.2	—	—	—	1.7	2.91	—	—
A/G	35.7	0.93	21.9	0.76	41.9	0.95	9.1	—	—	—	22.8	1.52	—	—
G/G	58.9	1.06	76.6	1.08	49.1	1.07	90.6	—	—	—	75.5	0.80	—	—

(continued)

Table 3.16 (continued)

Genotype	Caucasian		Asian		African		Indian		Amerindian		Pacific		Mestizo	
	Freq ^b (%)	rr ^c	Freq (%)	rr	Freq (%)	rr	Freq (%)	rr	Freq (%)	rr	Freq (%)	rr	Freq (%)	rr
<i>ERCC1/18T</i>														
C/C	15.6	0.93	57.6	0.95	82.5	0.99 ^d	–	–	–	–	–	–	53.3	–
C/T	47.8	0.99	36.6	1.05	16.7	1.04 ^d	–	–	–	–	–	–	39.4	–
T/T	36.6	1.05	5.8	1.16	0.8	1.10 ^d	–	–	–	–	–	–	7.3	–
<i>XRCC1/399,rs25487</i>														
Gln/Gln	42.3	0.99	55.1	0.98	76.8	1.02	32.9	1.48	–	–	–	–	73.3	1.08
Arg/Gln	45.5	1.00	38.2	1.02	21.6	0.94	48.9	0.86	–	–	–	–	24.6	0.80
Arg/Arg	12.2	1.01	6.6	1.05	1.5	0.87	18.2	0.50	–	–	–	–	2.1	0.59
<i>XPD751:A > C,rs13181</i>														
Lys/Lys	40.1	0.93	82.3	0.98	58.3	0.95	41.2	–	–	–	–	–	61.0	0.84
Lys/Gln	46.5	1.02	16.9	1.10	36.1	1.06	46.0	–	–	–	–	–	34.2	1.19
Gln/Gln	13.5	1.12	0.9	1.24	5.6	1.17	12.8	–	–	–	–	–	4.8	1.67
<i>XPD751:A > C,rs13181</i>														
Lys/Lys	40.1	0.93	82.3	0.98	58.3	0.95	41.2	–	–	–	–	–	61.0	0.84
Lys/Gln	46.5	1.02	16.9	1.10	36.1	1.06	46.0	–	–	–	–	–	34.2	1.19
Gln/Gln	13.5	1.12	0.9	1.24	5.6	1.17	12.8	–	–	–	–	–	4.8	1.67
<i>hOGGI:C > G,rs1052133</i>														
C/C	60.6	1.01	24.6	0.88	71.6	0.95	–	–	–	–	–	–	0.54	1.01
C/G	34.5	0.98	50.0	1.00	26.0	1.12	–	–	–	–	–	–	0.98	0.99
G/G	4.9	0.96	25.4	1.12	2.4	1.33	–	–	–	–	–	–	1.75	0.98

(continued)

Table 3.16 (continued)

Genotype	Caucasian		Asian		African		Indian		Amerindian		Pacific		Mestizo	
	Freq ^b (%)	rr ^c	Freq (%)	rr	Freq (%)	rr	Freq (%)	rr	Freq (%)	rr	Freq (%)	rr	Freq (%)	rr
<i>XPA,rs1800975</i>														
G/G	41.1	0.95	28.0	0.86	49.2	0.81	29.7	-	-	-	-	-	36.8	0.60
G/A	46.0	1.02	49.8	1.00	41.9	1.11	49.6	-	-	-	-	-	47.7	1.04
A/A	12.9	1.09	22.2	1.17	8.9	1.54	20.7	-	-	-	-	-	15.5	1.81
<i>TP53-exon4-codon72:G > C,rs1042522</i>														
Arg/Arg	54.5	0.93	36.9	0.93	25.0	1.07	21.7	1.32	71.6	-	27.0	0.80	59.1	0.90
Arg/Pro	38.6	1.06	47.7	1.02	50.0	1.00	49.8	1.00	26.1 %	-	49.9	1.00	35.6	1.12
Pro/Pro	6.9	1.20	15.4	1.11	25.0	0.94	28.6	0.76	2.4	-	23.1	1.24	5.3	1.39
<i>TP53-Intron3 16 bp</i>														
Del/Del	77.8	0.95	94.7	0.98	59.8	0.92	64.3	1.09	99.8	-	59.4	-	87.9	0.70
Del/Ins	20.8	1.16	5.2	1.31	35.1	1.09	31.8	0.87	0.2	-	35.3	-	11.7	2.90
Ins/Ins	1.4	1.40	0.1	1.74	5.1	1.28	3.9	0.69	0.0	-	5.2	-	0.4	12.10
<i>TP53-Intron6 MspI</i>														
W/W	74.2	0.94	92.2	0.98 ^d	63.9	0.90 ^d	63.2	-	99.0	-	-	-	81.0	-
W/M	23.9	1.17	7.6	1.20 ^d	32.1	1.14 ^d	32.6	-	1.0	-	-	-	18.0	-
M/M	1.9	1.45	0.2	1.45 ^d	4.0	1.45 ^d	4.2	-	0.0	-	-	-	1.0	-
<i>TP73-exon2</i>														
GC/GC	63.1	0.89	54.8	1.04	90.3	0.99 ^d	-	-	-	-	-	-	-	-
GC/AT	32.6	1.15	38.4	0.96	9.5	1.08 ^d	-	-	-	-	-	-	-	-
AT/AT	4.2	1.48	6.7	0.89	0.3	1.17 ^d	-	-	-	-	-	-	-	-

(continued)

Table 3.16 (continued)

Genotype	Caucasian		Asian		African		Indian		Amerindian		Pacific		Mestizo	
	Freq ^b (%)	rr ^c	Freq (%)	rr	Freq (%)	rr	Freq (%)	rr	Freq (%)	rr	Freq (%)	rr	Freq (%)	rr
<i>GSTM1</i>														
substitution	50.4	0.97	48.8	0.86	69.8	1.00	67.2	0.89	78.2	–	36.4	–	76.3	0.84
deletion	49.6	1.03	51.2	1.13	30.2	1.00	32.8	1.23	21.8	–	63.6	–	23.7	1.51
<i>GSTT1</i>														
substitution	72.8	1.06	58.7	0.92	74.7	1.02	84.9	0.98	86.8	–	–	–	94.9	0.83
deletion	27.2	0.84	41.3	1.11	25.3	0.94	15.1	1.14	13.2	–	–	–	5.1	4.18

^a–^c–: no data were obtained from literature

^bfreq: genotype frequencies of certain ethnicity

^crr: relative risks for lung cancer of persons with the genotype compared to average risk level of ethnical population, of which the overall genotype frequencies follow the values listed in this table

^dNo frequency data were obtained in case groups. Data gaps were filled using information from other ethnicities assuming that the relative risk of a single at-risk allele was unchanged. Sensitivity tests indicated that the distributions of individual susceptibilities of Asian and African populations were not sensitive to these missing data

Reprinted with permission from Shen et al. (2014). Copyright (2014) Nature Publishing Group

Table 3.17 Classification of world regions (Task Force on Hemispheric Transport of Air Pollution 2014)

Tier-1 region No.	Tier 1	Tier-2 region No.	Tier 2
1	World		
2	Non-arctic/Antarctic Ocean	020	Baltic Sea
		021	North Atlantic
		022	South Atlantic
		023	North Pacific
		024	South Pacific
		025	Indian Ocean
		026	Hudson Bay
		027	Mediterranean Sea
		028	Black and Caspian Sea
		150	Arctic seas are included in the Arctic receptor region
		160	Antarctic seas are included in Antarctic receptor as Southern Ocean
3	The United States and Canada (upto 66 N; polar circle)	031	Northeast of the United States (all divided on state or provincial lines)
		032	Southeast of the United States
		033	Northwest of the United States
		034	Southwest of the United States
		035	East of Canada
		036	West of Canada, Alaska up to 66 N
4	Western and Eastern Europe, Turkey (upto 66 N polar circle)	041	Northwest Europe
		042	Southwest Europe (France follows provinces level at ca. 46 N)
		043	Eastern Europe
		044	Greece, Turkey, Cyprus
5	South Asia: India, Pakistan, Nepal, Bangladesh, Sri Lanka	051	North India, Pakistan, Nepal, Bangladesh
		052	South India, Sri Lanka
		053	Indian Himalaya (above an elevation of 1500 m)
6	E Asia: China, Korea, Japan	061	North East China
		062	South East China
		063	West China, Mongolia (excl. Himalaya)
		064	North/South Korea
		065	Japan
		066	China/Tibet Himalaya (above an elevation of 1500 m)
7	South East Asia	071	Indonesia, Malaysia, Singapore
		072	Thailand, Myanmar, Vietnam

(continued)

Table 3.17 (continued)

Tier-1 region No.	Tier 1	Tier-2 region No.	Tier 2
8	Pacific, Australia, and New Zealand	081	Pacific
		082	Australia
		083	New Zealand
9	Northern Africa	091	091 Egypt
		092	092 Rest of Northern Africa
10	Sub Saharan Africa	101	West and Central Africa: Côte d'Ivoire, Angola, Benin, Burkina Faso, Cameroon, Cape Verde, Chad, Congo Brazzaville, Democratic Republic of Congo, Equatorial Guinea, Gambia, Ghana, Guinea, Guinea Bissau, Liberia, Mali, Niger, Nigeria, Senegal, Sierra Leone and Togo
		102	East Africa: Burundi, Djibouti, Eritrea, Ethiopia, Kenya, Sudan, Rwanda, Uganda, Somalia and Tanzania
		103	Southern Africa: Angola, Botswana, Lesotho, Madagascar, Malawi, Mauritius, Mozambique, Namibia, South Africa, Swaziland, Tanzania, Zambia, and Zimbabwe
11	Middle East, S. Arabia etc, Iran, and Iraq	111	Middle East
		112	S.Arabia, Yemen, Oman, etc
		113	Iran, Iraq
12	Mexico, Central America, Caribbean, Guyanas, Venezuela, and Columbia	121	Mexico
		122	Central America
		123	Caribbean
		124	Guyanans, Columbia, Venezuela
13	South America	131	South Brazil
		132	Rest of Brazil
		133	Uruguay, Paraguay, Argentina, Chile
		134	Peru, Ecuador
14	Russia, Belarus, Ukraine, and Central Asia	141	Russia West
		142	Russia East
		143	Belarus, Ukraine
		144	Uzbekistan, Kazakhstan, Kyrgyzstan, Tajikistan, Turkmenistan
		145	Himalaya part of "Stans" (above an elevation of 1500 m)
15	Arctic Circle (North of 66 N) and Greenland	150	Arctic (includes ocean and all of Greenland)
16	Antarctic	160	Antarctic
		161	Southern Ocean, south of 60S

Reprinted with permission from Shen et al. (2014). Copyright (2014) Nature Publishing Group

generated from Monte Carlo simulation, each of the 16 polymorphisms was repeated 16 times to perform a combination of hypothetical polymorphic traits with up to 256 hypothetical polymorphisms. As the person was born, 256 genotypes were randomly chosen according to their frequencies (Table 3.15), and the overall relative risk for lung cancer due to genetic differences was assumed to be the consequence of the combination of various polymorphisms and determined as the product of relative risks of all genotypes. Distribution of all hypothetical persons' relative risks illustrates the variations in individual susceptibility, namely *GeneSus* defined above. The calculation was only conducted for three ethnic groups including Caucasian, Asian, and African, since information of other groups is inadequate (see Table 3.14). Variations of genetic susceptibility in other ethnicities were substituted with those in one of the three main groups according to population similarities (Jorde and Wooding 2004). The resulting distributions of *GeneSus* follow lognormal distributions (see Fig. 3.3c), and the standard variations of distributions of log₁₀-transformed individual *GeneSus* for Caucasian, Asian, and African are 0.50, 0.65, and 0.59, respectively.

It should be pointed out that thousands of SNPs are reported potentially related to lung cancer (Yu et al. 2010), and replacement of all these sites with the 16 reported polymorphisms would lead to significant overestimation of the overall variations of susceptibility, considering that the well-investigated polymorphisms should be associated with lung cancer more intensively than most of the others. Thus, the count of 256 is thought to be a middle measure for an appropriate estimation. Hopefully, in the future, robust results of relative risks of other polymorphic sites will be filled in together with an improved understanding of interaction among different polymorphisms at multiple loci so that not only the variations but also a full screen of genetic susceptibility will be addressed.

3.3.3 Evaluation of Source-Specific Health Risks

69 source types defined by PKU-PAH inventory (Shen et al. 2013) were summed up into 12 major source categories. 12 2-year modeling experiments (2006 to 2007) were conducted opening only one source category for each performance. Near-surface BaP concentrations from model performances were downscaled. Global *ILCRs* were calculated for population exposure to PAHs emitted from individual source types.

3.3.4 Evaluation of Transboundary Pollution

The Task Force on Hemispheric Transport of Air Pollution (Task Force on Hemispheric Transport of Air Pollution 2014) has defined 15 Tier-1 regions and 59 Tier-2 regions (Table 3.17 and Fig. 3.4). In this study, we classified the world

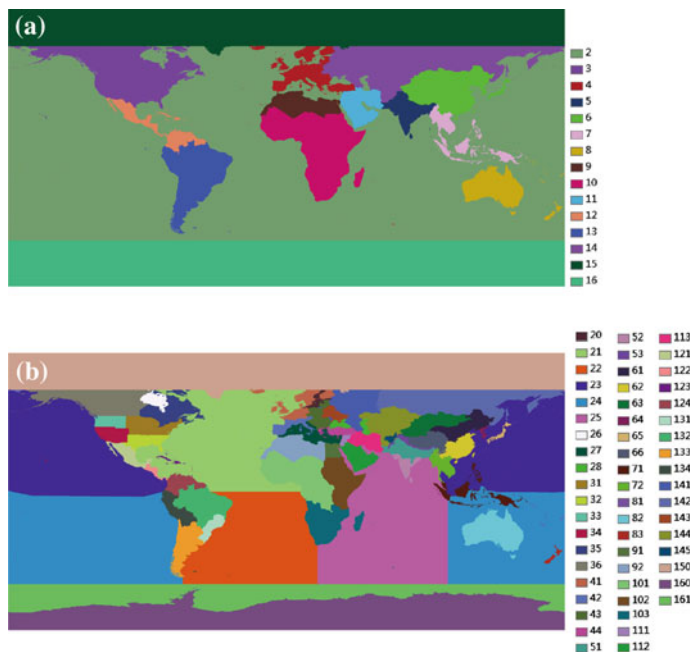


Fig. 3.4 Classification of the world regions. **a** Tier-1 region classification. **b** Tier-2 region classification. Region numbers are consistent with the region No. in Table 3.13. BaP emissions from individual Tier-1 regions shown in (a) were submitted separately to MOZART-4. Long-range transport of BaP emitted from individual regions was performed. Given external pollution promoted by long-range transport, their influences on local health were evaluated for individual Tier-1 and Tier-2 regions based on these model performances. This figure was generated using ESRI® ArcMap and Microsoft® Office Word (ESRI 2014; Microsoft Corporation 2014). Reprinted with permission from Shen et al. (2014). Copyright (2014) Nature Publishing Group

regions based on this definition. 12 2-year model performances (2006 to 2007) were conducted under emissions from individual source regions excluding ocean areas and Polar areas. Concentrations from model performances were not downscaled. Overall *ILCRs* of individual source regions and receptor regions were calculated for each performance so that the influences of emissions from individual source regions on other regions can be addressed.

3.3.5 The Uncertainty and the Distribution of Risks

The risk uncertainty and the risk distribution in population are two different concepts. The uncertainty provides information on the potential bias of the risk estimate, which is mainly raised by the inherent uncertainties in the emission factors, energy statistics, the cancer slope factor, etc. The risk distribution illustrates how

different the individual risks in the population are, which is mostly caused by the differences in ambient concentrations and individual susceptibilities. In this study, both the uncertainty and the population distribution of *ILCRs* are addressed. The uncertainty is addressed based on the uncertainty ranges of modeled concentrations and the CSF mentioned above, while the risk distribution is simulated based on the distributions of various individual susceptibility factors in the population and geographic distribution of BaP concentrations.

References

- Alsberg, T., Stenberg, U., Westerholm, R., Strandell, M., Rannug, U., Sundvall, A., et al. (1985). Chemical and biological characterization of organic material from gasoline exhaust particles. *Environmental Science and Technology*, 19(1), 43–50.
- Bain, C., Feskanich, D., Speizer, F. E., Thun, M., Hertzmark, E., Rosner, B. A., et al. (2004). Lung cancer rates in men and women with comparable histories of smoking. *Journal of the National Cancer Institute*, 96, 826–834.
- Bartlett, C. J. S., Betts, W. E., Giavazzi, F., Guttmann, H., Heinze, P., Mayers, R. F., et al. (1992). *The chemical composition of diesel particulate emissions*. CONCAWE, Brussels, Report no. 92/51.
- Benner, B. A., Gordon, G. E., & Wise, S. A. (1989). Mobile sources of atmospheric polycyclic aromatic hydrocarbons: A roadway tunnel study. *Environmental Science and Technology*, 23 (10), 1269–1278.
- Bergvall, C., & Westerholm, R. (2009). Determination of highly carcinogenic dibenzopyrene isomers in particulate emissions from two diesel- and two gasoline-fuelled light-duty vehicles. *Atmospheric Environment*, 43(25), 3883–3890.
- Beyea, J., Stellman, S. D., Hatch, M., & Gammon, M. D. (2008). Airborne emissions from 1961 to 2004 of benzo[a]pyrene from U.S. vehicles per km of travel based on tunnel studies. *Environmental Science and Technology*, 42(19), 7315–7320.
- Boldrini, L., Gisfredi, S., Ursino, S., Lucchi, M., Greco, G., Mussi, A., et al. (2008). Effect of the p53 codon 72 and intron 3 polymorphisms on non-small cell lung cancer (NSCLC) prognosis. *Cancer Investigation*, 26, 168–172.
- Bond, T. C., Bhardwaj, E., Dong, R., Jogani, R., Jung, S., Roden, C., et al. (2007). Historical emissions of black and organic carbon aerosol from energy-related combustion. *Global Biogeochemical Cycles*, 21, 1850–2000, GB2018, doi:10.1029/2006GB002840.
- Boström, C. E., Gerde, P., Hanberg, A., Jernstrom, B., Johansson, C., Kyrklund, T., et al. (2002). Cancer risk assessment, indicators, and guidelines for polycyclic aromatic hydrocarbons in the ambient air. *Environmental Health Perspectives*, 110, 451–488.
- Cadle, S. H., Mulawa, P. A., Hunsanger, E. C., Nelson, K., Ragazzi, R. A., Barrett, R., et al. (1999). Composition of light-duty motor vehicle exhaust particulate matter in the Denver, Colorado area. *Environmental Science and Technology*, 33(14), 2328–2339.
- California Environmental Protection Agency (2014). *Technical support document for cancer potency factors: Methodologies for derivation, listing of available values, and adjustments to allow for early life stage exposures*. Retrieved from http://oehha.ca.gov/air/hot_spots/2009/TSDCancerPotency.pdf.
- Carbon Monitoring for Action (CARMA) (2013). *CARMA Notes: Data Accuracy*. Retrieved from <http://www.carma.org>.
- Centers for Disease Control and Prevention (2014). *CDC health disparities and inequalities report—United States, 2011*. Retrieved from <http://www.cdc.gov/mmwr/pdf/other/su6001.pdf>.

- Chellam, S., Kulkarni, P., & Fraser, M. P. (2005). Emissions of organic compounds and trace metals in fine particulate matter from motor vehicles: A tunnel study in Houston, Texas. *Journal of the Air and Waste Management Association*, 55(1), 60–72.
- China Energy Group (2008). *China Energy Databook Version 7.0*. Berkeley, California: Lawrence Berkeley Laboratory and Energy Research Institute.
- Ciais, P., Paris, J. D., Marland, G., Peylin, P., Piao, S. L., Piegler, T., et al. (2010). The European carbon balance. Part 1: Fossil fuel emissions. *Global Change Biology*, 16, 1395–1408.
- Dachs, J., Lohmann, R., Ockenden, W. A., Méjanelle, L., Eisenreich, S. J., & Jones, K. C. (2002). Oceanic biogeochemical controls on global dynamics of persistent organic pollutants. *Environmental Science Technology*, 36(20), 4229–4237.
- Dai, L., Duan, F., Wang, P., Song, C., Wang, K., & Zhang, J. (2012). XRCC1 gene polymorphisms and lung cancer susceptibility: A meta-analysis of 44 case-control studies. *Molecular Biology Reports*, 39, 9535–9547.
- Davis, S. C., Diegel, S. W., & Boundy, R. G. (2010). *Transportation Energy Data Book: Edition 28*. U.S. Department of Energy. Retrieved from <http://cta.oml.gov/data/download28.shtml>.
- De Abrantes, R., De Assuncao, J. V., & Pesquero, U. R. (2004). Emission of polycyclic aromatic hydrocarbons from light-duty diesel vehicles exhaust. *Atmospheric Environment*, 38(11), 1631–1640.
- Ding, D., Zhang, Y., Yu, H., Guo, Y., Jiang, L., He, X., et al. (2012). Genetic variation of XPA gene and risk of cancer: A systematic review and pooled analysis. *International Journal of Cancer*, 131, 486–488.
- Duan, W. X., Hua, R. X., Yi, W., Shen, L. J., Jin, Z. X., Zhao, Y. H., et al. (2012). The association between OGG1 Ser326Cys polymorphism and lung cancer susceptibility: A meta-analysis of 27 studies. *PLoS ONE*, 7, e35970.
- Duan, X. L. (2012). *Research methods of exposure factors and its application in environmental health risk assessment* (pp. 122–129). Beijing, China: Beijing Science Press.
- Durbin, T. D., Truex, T. J., & Norbeck, J. M. (1998). *Particulate measurements and emissions characterization of alternative fuel vehicle exhaust*. National Renewable Energy Laboratory, Golden, Colorado, NREL/SR-540-25741.
- Emmons, L. K., Apel, E. C., Lamarque, J. F., Hess, P. G., Avery, M., Blake, D., et al. (2010). Impact of Mexico City emissions on regional air quality from MOZART-4 simulations. *Atmospheric Chemistry and Physics*, 10(13), 6195–6212.
- Endresen, Ø. E., Sørgård, H. L., Behrens, P. O., Brett, P. O., & Isaksen, I. S. A. (2007). A historical reconstruction of ships' fuel consumption and emissions. *Journal of Geophysical Research*, 112, D12301. doi:10.1029/2006JD007630.
- Environment Australia (EA) (2003). *Technical report No. 1: Toxic emissions from diesel vehicles in Australia*. Retrieved from <http://www.environment.gov.au/atmosphere/airquality/publications/report1/index.html>.
- ESRI Inc (2014). *ArcGIS for Desktop*. Retrieved from <http://www.esri.com>.
- Esteve, W., Budzinski, H., & Villenave, E. (2006). Relative rate constants for the heterogeneous reactions of NO₂ and OH radicals with polycyclic aromatic hydrocarbons adsorbed on carbonaceous particles. Part 2: PAHs adsorbed on diesel particulate exhaust SRM 1650a. *Atmospheric Environment*, 40(2), 201–211.
- Expert Panel on Air Quality Standards (1999). *Choice of a marker compound for polycyclic aromatic hydrocarbon*. Retrieved from <http://webarchive.nationalarchives.gov.uk/20060715141954/http://www.defra.gov.uk/environment/airquality/aqs/poly/6.htm>.
- Ezzati, M., & Lopez, A. D. (2003). Estimates of global mortality attributable to smoking in 2000. *Lancet*, 362, 847–852.
- Fenelon, A. & Preston, S. H. (2011). Estimating smoking-attributable mortality in the United States. *Demography*, 49.
- Feng, Z., Ni, Y., Dong, W., Shen, H., & Du, J. (2012). Association of ERCC2/XPD polymorphisms and interaction with tobacco smoking in lung cancer susceptibility: A systemic review and meta-analysis. *Molecular Biology Reports*, 39, 59–69.

- Food and Agriculture Organization of the United Nations (FAO) (2012). *FAOSTAT*. Retrieved from <http://faostat.fao.org/site/291/default.aspx>.
- Fraser, M. P., Cass, G. R., & Simoneit, B. R. T. (1998). Gas-phase and particle-phase organic compounds emitted from motor vehicle traffic in a Los Angeles roadway tunnel. *Environmental Science and Technology*, 32(14), 2051–2060.
- Fujita, E. M., Campbell, D. E., Arnott, W. P., Chow, J. C., & Zielinska, B. (2007). Evaluations of the chemical mass balance method for determining contributions of gasoline and diesel exhaust to ambient carbonaceous aerosols. *Journal of the Air and Waste Management Association*, 57(6), 721–740.
- Gaspar, P. A., Hutz, M. H., Salzano, F. M., Hill, K., Hurtado, A. M., Petzl-Erler, M. L., et al. (2002). Polymorphisms of CYP1A1, CYP2E1, GSTM1, GSTT1, and TP53 genes in Amerindians. *American Journal of Physical Anthropology*, 119(3), 249–256.
- GENISIM (2012). *Aluminum Smelters*. Retrieved from <http://www.genisim.com/aluminum/smelters/smelters.htm>.
- Guan, P., Huang, D., Yin, Z., & Zhou, B. (2011). Association of the hOGG1 Ser326Cys polymorphism with increased lung cancer susceptibility in Asians: A meta-analysis of 18 studies including 7592 cases and 8129 controls. *Asian Pacific Journal of Cancer Prevention*, 12, 1067–1072.
- Haiman, C. A., Stram, D. O., Wilkens, L. R., Pike, M. C., Kolonel, L. N., Henderson, B. E., et al. (2006). Ethnic and racial differences in the smoking-related risk of lung cancer. *The New England Journal of Medicine*, 354, 333–342.
- Handa, T., Yamauchi, T., Sawai, K., Yamamura, T., Koseki, Y., & Ishii, T. (2002). In situ emission levels of carcinogenic and mutagenic compounds from diesel and gasoline engine vehicles on an expressway. *Environmental Science and Technology*, 18(12), 895–902.
- HARP-HAZ (2000). *Guidance document on quantification and reporting on discharges/emissions/losses of polycyclic aromatic hydrocarbons (PAH)*. Norway: HARP-HAZ project.
- Health Canada (2014). *Federal contaminated site risk assessment in Canada, part I: guidance on human health preliminary quantitative risk assessment (PQRA), Version 2.0*. Retrieved from <http://www.healthcanada.gc.ca/>.
- Herath, N. I., Kew, M. C., Whitehall, V. L., Walsh, M. D., Jass, J. R., Khanna, K. K., et al. (2000). p73 is up-regulated in a subset of hepatocellular carcinomas. *Hepatology*, 31, 601–605.
- Hrstka, R., Coates, P. J., & Vojtesek, B. (2009). Polymorphisms in p53 and the p53 pathway: Roles in cancer susceptibility and response to treatment. *Journal of Cellular and Molecular Medicine*, 13, 440–453.
- Infobank (2010). *China content provider*. Retrieved from <http://www.bjinfobank.com>.
- Institute for Health and Consumer Protection (2014). *European Exposure Factors Database*. Retrieved from http://ihcp.jrc.ec.europa.eu/our_databases/expofacts.
- International Energy Agency (2011). *IEA World Energy Statistics and Balances*. Retrieved from <http://www.oecd-ilibrary.org/statistics>.
- Jorde, L. B., & Wooding, S. P. (2004). Genetic variation, classification and ‘race’. *Nature Genetics*, 36, S28–S33.
- Kado, N. Y., Okamoto, R. A., Kuzmicky, P. A., Kobayashi, R., Ayala, A., Gebel, M. E., et al. (2005). Emissions of toxic pollutants from compressed natural gas and low sulfur diesel-fueled heavy-duty transit buses tested over multiple driving cycles. *Environmental Science and Technology*, 39(19), 7638–7649.
- Kahan, T. F., Kwamena, N.-O. A., & Donaldson, D. J. (2006). Heterogeneous ozonation kinetics of polycyclic aromatic hydrocarbons on organic films. *Atmospheric Environment*, 40, 3448–3459.
- Kalnay, E., Kanamitsu, K., Kistler, R., Collins, W., Deaven, D., Gandin, L., et al. (1996). The NCEP/NCAR 40-year reanalysis project. *Bulletin of the American Meteorological Society*, 77, 437–471.
- Karavalakis, G., Alvanou, F., Stournas, S., & Bakeas, E. (2009). Regulated and unregulated emissions of a light duty vehicle operated on diesel/palm-based methyl ester blends over NEDC and a non-legislated driving cycle. *Fuel*, 88(6), 1078–1085.

- Kim, J. M., Lee, O. Y., Lee, C. G., Kwon, S. J., Kim, K. S., Moon, W., et al. (2007). p53 codon 72 and 16-bp duplication polymorphisms of gastric cancer in Koreans. *The Korean Journal of Gastroenterology*, 50(5), 292–298.
- Kim, S., Cheong, H. K., Choi, K., Yang, J. Y., Kim, S. J., Jo, S. N., & Jang, J. Y. (2006). Development of Korean exposure factors handbook for exposure assessment. *Epidemiology*, 17, S460.
- Kiyohara, C., Otsu, A., Shirakawa, T., Fukuda, S., & Hopkin, J. M. (2002). Genetic polymorphisms and lung cancer susceptibility: A review. *Lung Cancer*, 37, 241–256.
- Kiyohara, C., Yoshimasu, K., Takayama, K., & Nakanishi, Y. (2005). NQO1, MPO, and the risk of lung cancer: A HuGE review. *Genetics IN Medicine*, 7, 463–478.
- Kristensson, A., Johansson, C., Westerholm, R., Swietlicki, E., Gidhagen, L., Wideqvist, U., et al. (2004). Real-world traffic emission factors of gases and particles measured in a road tunnel in Stockholm. *Sweden Atmospheric Environment*, 38(5), 657–673.
- Lammel, G., Sehili, A. M., Bond, T. C., Feichter, J., & Grassl, H. (2009). Gas/particle partitioning and global distribution of polycyclic aromatic hydrocarbons—a modelling approach. *Chemosphere*, 76, 98–106.
- Landi, S., Gemignani, F., Monnier, S., & Canzian, F. (2005). A database of single-nucleotide polymorphisms and a genotyping microarray for genetic epidemiology of lung cancer. *Experimental Lung Research*, 31, 223–257.
- Layton, D. W. (1993). Metabolically consistent breathing rates for use in dose assessments. *Health Physics*, 64, 23–36.
- Leonidas, N., & Zissis, S. (2000). *COPERT III* (pp. 76–77). Copenhagen: Computer programme to calculate emissions from road transport. European Environment Agency.
- Lim, M. C. H., Ayoko, G. A., Morawska, L., Ristovski, Z. D., & Jayaratne, E. R. (2007). Influence of fuel composition on polycyclic aromatic hydrocarbon emissions from a fleet of in-service passenger cars. *Atmospheric Environment*, 41(1), 150–160.
- Lohmann, R., & Lammel, G. (2004). Adsorptive and absorptive contributions to the gas-particle partitioning of polycyclic aromatic hydrocarbons: State of knowledge and recommended parametrization for modeling. *Environmental Science and Technology*, 38(14), 3793–3803.
- Ma, J. M., Daggupaty, S., Harner, T., & Li, Y. F. (2003). Impacts of lindane usage in the Canadian prairies on the Great Lakes ecosystem. 1. Coupled atmospheric transport model and modeled concentrations in air and soil. *Environmental Science Technology*, 37(17), 3774–3781.
- Marr, L. C., Kirchstetter, T. W., Harley, R. A., Miguel, A. H., Hering, S. V., & Hammond, S. K. (1999). Characterization of polycyclic aromatic hydrocarbons in motor vehicle fuels and exhaust emissions. *Environmental Science and Technology*, 33(18), 3091–3099.
- Matakidou, A., Eisen, T., & Houlston, R. S. (2003). TP53 polymorphisms and lung cancer risk: A systematic review and meta-analysis. *Mutagenesis*, 18, 377–385.
- Mi, H.-H., Lee, W.-J., Tsai, P.-J., & Chen, C.-B. (2001). A comparison on the emission of polycyclic aromatic hydrocarbons and their corresponding carcinogenic potencies from a vehicle engine using leaded and lead-free gasoline. *Environmental Health Perspectives*, 109(12), 1285.
- Microsoft Corporation (2014). *All Office products*. Retrieved from <http://office.microsoft.com>.
- Miguel, A. H., Kirchstetter, T. W., Harley, R. A., & Hering, S. V. (1998). On-road emissions of particulate polycyclic aromatic hydrocarbons and black carbon from gasoline and diesel vehicles. *Environmental Science and Technology*, 32(4), 450–455.
- Nakićenović, N., Alcamo, J., Davis, G., Vries, B. D., Fenhann, J., Gaffin, S., et al. (2000). *Emissions scenarios: A special report of working Group III of the Inter-governmental panel on climate change*. New York: Cambridge University Press.
- National Academy of Sciences (1983). *Polycyclic aromatic hydrocarbons: evaluation of sources and effects*. Washington, DC. ISBN 978-0-309-07758-3.

- National Institute of Advanced Industrial Science and Technology (2014). *Japanese Exposure Factors Handbook*. Retrieved from http://unit.aist.go.jp/riss/crm/exposurefactors/english_summary.html.
- National Oceanic and Atmospheric Administration (NOAA) (2012). *Global Gas Flaring Estimates*. Retrieved from http://www.ngdc.noaa.gov/dmsp/interest/gas_flares.html.
- Nelson, P. F., Tibbett, A. R., & Day, S. J. (2008). Effects of vehicle type and fuel quality on real world toxic emissions from diesel vehicles. *Atmospheric Environment*, 42(21), 5291–5303.
- Nerurkar, P. V., Okinaka, L., Aoki, C., Seifried, A., Lum-Jones, A., Wilkens, L. R., et al. (2000). CYP1A1, GSTM1, and GSTP1 genetic polymorphisms and urinary 1-hydroxypyrene excretion in non-occupationally exposed individuals. *Cancer Epidemiology, Biomarkers and Prevention*, 9, 1119–1122.
- Ning, Z., Polidori, A., Schauer, J. J., & Sioutas, C. (2008). Emission factors of PM species based on freeway measurements and comparison with tunnel and dynamometer studies. *Atmospheric Environment*, 42(13), 3099–3114.
- Norbeck, J. M., Durbin, T. D., & Truex, T. J. (1998). *Measurement of primary particulate matter emissions from light-duty motor vehicles*. Coordinating Research Council, Inc. and South Coast Air Quality Management District, CRC Project no. E-24-2.
- Oak Ridge National Laboratory (ORNL) (2014). *LandScan Global Population 2007 Database*. Retrieved from <http://www.ornl.gov/sci/landscan/>.
- Pakbin, P., Ning, Z., Schauer, J. J., & Sioutas, C. (2009). Characterization of Particle Bound Organic Carbon from Diesel Vehicles Equipped with Advanced Emission Control Technologies. *Environmental Science and Technology*, 43(13), 4679–4686.
- Perneger, T. V. (2001). Sex, smoking, and cancer: a reappraisal. *Journal of the National Cancer Institute*, 93, 1600–1602.
- Phuleria, H. C., Geller, M. D., Fine, P. M., & Sioutas, C. (2006). Size-resolved emissions of organic tracers from light- and heavy-duty vehicles measured in a California roadway tunnel. *Environmental Science and Technology*, 40(13), 4109–4118.
- Riddle, S. G., Jakober, C. A., Robert, M. A., Cahill, T. M., Charles, M. J., & Kleeman, M. J. (2007a). Large PAHs detected in fine particulate matter emitted from light-duty gasoline vehicles. *Atmospheric Environment*, 41(38), 8658–8668.
- Riddle, S. G., Robert, M. A., Jakober, C. A., Hannigan, M. P., & Kleeman, M. J. (2007b). Size distribution of trace organic species emitted from heavy-duty diesel vehicles. *Environmental Science and Technology*, 41(6), 1962–1969.
- Riddle, S. G., Robert, M. A., Jakober, C. A., Hannigan, M. P., & Kleeman, M. J. (2007c). Size distribution of trace organic species emitted from light-duty gasoline vehicles. *Environmental Science and Technology*, 41(21), 7464–7471.
- Rogge, W. F., Hildemann, L. M., Mazurek, M. A., Cass, G. R., & Simoneit, B. R. T. (1993). Sources of fine organic aerosol. 2. noncatalyst and catalyst-equipped automobiles and heavy-duty diesel trucks. *Environmental Science and Technology*, 27(4), 636–651.
- Sagebiel, J. C., Zielinska, B., Walsh, P. A., Chow, J. C., Cadle, S. H., Mulawa, P. A., et al. (1997). PM-10 exhaust samples collected during IM-240 dynamometer tests of in-service vehicles in Nevada. *Environmental Science and Technology*, 31(1), 75–83.
- Schauer, J. J., Kleeman, M. J., Cass, G. R., & Simoneit, B. R. T. (1999). Measurement of emissions from air pollution sources. 2. C-1 through C-30 organic compounds from medium duty diesel trucks. *Environmental Science & Technology*, 33(10), 1578–1587.
- Schauer, J. J., Kleeman, M. J., Cass, G. R., & Simoneit, B. R. T. (2002). Measurement of emissions from air pollution sources. 5. C-1-C-32 organic compounds from gasoline-powered motor vehicles. *Environmental Science and Technology*, 36(6), 1169–1180.
- Shen, H. Z., Huang, Y., Wang, R., Zhu, D., Li, W., Shen, G., et al. (2013). Global atmospheric emissions of polycyclic aromatic hydrocarbons from 1960 to 2008 and future predictions. *Environmental Science and Technology*, 47, 6415–6424.
- Shen, H. Z., Tao, S., Liu, J., Huang, Y., Chen, H., Li, W., et al. (2014). Global lung cancer risk from PAH exposure highly depends on emission sources and individual susceptibility. *Scientific Reports*,. doi:10.1038/srep06561.

- Shen, H. Z., Tao, S., Wang, R., Wang, B., Shen, G. F., Li, W., et al. (2011). Global time trends in PAH emissions from motor vehicles. *Atmospheric Environment*, *45*, 2067–2073.
- Siegfried, J. M. (2001). Women and lung cancer: Does oestrogen play a role? *The Lancet Oncology*, *2*, 506–513.
- Siegl, W. O., Hammerle, R. H., Herrmann, H. M., Wenclawiak, B. W., & Luers-Jongen, B. (1999). Organic emissions profile for a light-duty diesel vehicle. *Atmospheric Environment*, *33*(5), 797–805.
- Själänder, A., Birgander, R., Saha, N., Beckman, L., & Beckman, G. (1996). p53 polymorphisms and haplotypes show distinct differences between major ethnic groups. *Human Heredity*, *46*(1), 41–48.
- Staelin, J., Keller, C., Stahel, W., Schlapfer, K., & Wunderli, S. (1998). Emission factors from road traffic from a tunnel study (Gubrist tunnel, Switzerland). Part III: Results of organic compounds, SO₂ and speciation of organic exhaust emission. *Atmospheric Environment*, *32* (6), 999–1009.
- Tang, S., Frank, B. P., Lanni, T., Rideout, G., Meyer, N., & Beregszaszy, C. (2007). Unregulated emissions from a heavy-duty diesel engine with various fuels and emission control systems. *Environmental Science and Technology*, *41*(14), 5037–5043.
- Task Force on Hemispheric Transport of Air Pollution (2014). *Theme 2: Source apportionment and source/receptor analysis*. Retrieved from <http://www.htap.org/>.
- The Department of Health (2014). *Australian exposure factor guidance*. Retrieved from www.health.gov.au.
- The Energy and Resources Institute (TERI). (2008). *TERI Energy data directory and yearbook, 2007*. New Delhi, India: TERI Press.
- The World Bank (2010). *World Development Indicators*. Retrieved from <http://ddp-ext.worldbank.org/ext/DDPQQ/member.do?method=getMembers&userid=1&queryId=6>.
- The World Factbook (2014). *Central Intelligence Agency*. Retrieved from <https://www.cia.gov/library/publications/the-world-factbook/>.
- U.S. Energy Information Administration (2012). *International Energy Statistics*. Retrieved from <http://www.eia.gov/countries/data.cfm>.
- U.S. Geological Survey (USGS) (2012). *Commodity Statistics and Information*. Retrieved from <http://minerals.usgs.gov/minerals/pubs/commodity>.
- U.S. Geological Survey (USGS) (2012). *Primary Aluminum Plants Worldwide-1998*. Retrieved from <http://minerals.usgs.gov/minerals>.
- United Nations Industrial Development Organization (UNIDO). (2008). *International yearbook of industrial statistics 2008*. Cheltenham, U.K: Edward Elgar Publishing.
- United Nations Statistics Division (UNSD) (2011). *Environmental Indicators: Waste*. Retrieved from <http://unstats.un.org/unsd/environment/qindicators.htm>.
- United States Cancer Statistics (USCS) (2014). *National Program of Cancer Registries*. Retrieved from http://www.cdc.gov/cancer/npcr/uscs/download_data.htm.
- United States Environmental Protection Agency (USEPA) (1995). *Appendix H: Highway Mobile Source Emission Factors Tables*. Retrieved from <http://www.epa.gov/otaq/ap42.htm>.
- United States Environmental Protection Agency (USEPA) (2011). *Exposure factors handbook* (2011 ed.). EPA/600/R-09/052F.
- van der Werf, G. R., Randerson, J. T., Giglio, L., Collatz, G. J., Mu, M., Kasibhatla, P. S., et al. (2010). Global fire emissions and the contribution of deforestation, savanna, forest, agricultural, and peat fires (1997-2009). *Atmospheric Chemistry and Physics*, *10*, 11707–11735.
- Walpole, S. C., Prieto-Merino, D., Edwards, P., Cleland, J., Stevens, G., & Roberts, L. (2012). The weight of nations: An estimation of adult human biomass. *BMC Public Health*, *12*, 439.
- Wang, B. G., Lu, W. M., Zhou, Y., Shao, M., & Zhang, Y. H. (2007). Emission characteristic of PAHs composition in motor vehicles exhaust of city tunnel. *China Environmental Science*, *27* (4), 482–487.
- Wang, R., Tao, S., Ciais, P., Shen, H. Z., Huang, Y., Chen, H., et al. (2013). High-resolution mapping of combustion processes and implications for CO₂ emissions. *Atmospheric Chemistry and Physics*, *13*(10), 5189–5203.

- Wang, W., Li, H., Liu, H. J., Yue, X., Pan, Z., Wang, Y., et al. (2002). In *Characterization of polycyclic aromatic hydrocarbons in PM exhaust from light-duty vehicles*. The Ninth Nation Conference on Atmospheric Environment, Beijing.
- Westerholm, R. N., Almen, J., Li, H., Rannug, J. U., Egebaeck, K. E., & Graegg, K. (1991). Chemical and biological characterization of particulate-, semivolatile-, and gas-phase-associated compounds in diluted heavy-duty diesel exhausts: A comparison of three different semivolatile-phase samplers. *Environmental Science and Technology*, 25(2), 332–338.
- Westerholm, R. N., Alsberg, T. E., Frommelin, A. B., Strandell, M. E., Rannug, U., Winquist, L., et al. (1988). Effect of fuel polycyclic aromatic hydrocarbon content on the emissions of polycyclic aromatic hydrocarbons and other mutagenic substances from a gasoline-fueled automobile. *Environmental Science and Technology*, 22(8), 925–930.
- Westerholm, R., & Egeback, K. E. (1994). Exhaust emissions from light-duty and heavy-duty vehicles—chemical-composition, impact of exhaust after treatment, and fuel parameters. *Environmental Health Perspectives*, 102, 13–23.
- Westerholm, R., & Li, H. (1994). A multivariate statistical-analysis of fuel-related polycyclic aromatic hydrocarbon emissions from heavy-duty diesel vehicles. *Environmental Science and Technology*, 28(5), 965–972.
- Westerholm, R., Almen, J., Li, H., Rannug, U., & Rosen, A. (1992). Exhaust emissions from gasoline-fueled light duty vehicles operated in different driving conditions—a chemical and biological characterization. *Atmospheric Environment Part B*, 26(1), 79–90.
- Westerholm, R., Christensen, A., & Rosen, A. (1996). Regulated and unregulated exhaust emissions from two three-way catalyst equipped gasoline fuelled vehicles. *Atmospheric Environment*, 30(20), 3529–3536.
- Westerholm, R., Christensen, A., Tornqvist, M., Ehrenberg, L., Rannug, U., Sjogren, M., et al. (2001). Comparison of exhaust emissions from Swedish environmental classified diesel fuel (MK1) and European Program on Emissions, Fuels and Engine Technologies (EPEFE) reference fuel: A chemical and biological characterization with viewpoints on cancer risk. *Environmental Science and Technology*, 35(9), 1748–1754.
- Wingfors, H., Sjodin, A., Haglund, P., & Brorstrom-Lunden, E. (2001). Characterisation and determination of profiles of polycyclic aromatic hydrocarbons in a traffic tunnel in Gothenburg. *Sweden Atmospheric Environment*, 35(36), 6361–6369.
- World Health Organization (2014). *Global Health Observatory Data Repository*. Retrieved from <http://apps.who.int/gho/data/node.main>.
- World Health Organization (2014). *Global Health Observatory Data Repository*. Retrieved from <http://apps.who.int/gho/data/node.main?lang=en>.
- World Steel Association (2012). Retrieved from <http://www.worldsteel.org>.
- Xu, S. S., Liu, W. X., & Tao, S. (2006). Emission of polycyclic aromatic hydrocarbons in China. *Environmental Science and Technology*, 40(3), 702–708.
- Yang, H. H., Hsieh, L. T., Liu, H. C., & Mi, H. H. (2005). Polycyclic aromatic hydrocarbon emissions from motorcycles. *Atmospheric Environment*, 39(1), 17–25.
- Yu, W., Clyne, M., Khoury, M. J., & Gwinn, M. (2010). Phenopedia and genopedia: Disease-centered and gene-centered views of the evolving knowledge of human genetic associations. *Bioinformatics*, 26, 145–146 (2010).
- Zhan, P., Wang, Q., Qian, Q., Wei, S. Z., & Yu, L. K. (2011). CYP1A1 MspI and exon7 gene polymorphisms and lung cancer risk: An updated meta-analysis and review. *Journal of Experimental and Clinical Cancer Research*, 30, 99.
- Zhang, L., Wang, J., Xu, L., Zhou, J., Guan, X., Jiang, F., et al. (2012). Nucleotide excision repair gene ERCC1 polymorphisms contribute to cancer susceptibility: A meta-analysis. *Mutagenesis*, 27, 67–76.
- Zhang, Y., Song, H., Higgins, J. P. T., Pharoah, P., & Danesh, J. (2006). Five Glutathione S-Transferase gene variants in 23,452 cases of lung cancer and 30,397 controls: Meta-analysis of 130 studies. *PLoS Medicine*, 3, 0524–0534.

- Zhu, D., Tao, S., Wang, R., Shen, H. Z., Huang, Y., Shen, G. F., et al. (2013). Temporal and spatial trends of residential energy consumption and air pollutant emissions in China. *Applied Energy*, *106*, 17–24.
- Zielinska, B., Sagebiel, J., McDonald, J. D., Whitney, K., & Lawson, D. R. (2003). Emission rates and comparative chemical composition from selected in-use diesel and gasoline-fueled vehicles. *4th Colloquium on PM and Human Health*, *54*, 1138–1150.
- Zou, J. H., An, L., Chen, S., & Ren, L. Q. (2012). XPA A23G polymorphism and lung cancer risk: A meta-analysis. *Molecular Biology Reports*, *39*, 1435–1440.

Chapter 4

Global Atmospheric Emissions of PAH Compounds

The emission inventory (PKU-PAH) was built upon a global high-resolution combustion inventory (PKU-FUEL), historical energy statistical data, and a spatiotemporally informed emission factor (EF) database. Sixty-nine sources are considered in the emission inventory. Due to lack of EF measurement, some sources such as volcanic eruption and non-ferrous metal smelting rather than aluminum production were not included in the study. However, these sources are supposed to contribute little proportion to overall atmospheric PAH emissions. The emission inventory developed in this study can be regarded as a comprehensive estimate for all sources on a global scale. The emission inventory contains two products: One is country-level emission estimates covering the period 1960–2008 with future prediction by 2030; another is spatially highly resolved emission inventory for 2007. Detailed information and discussion can be found in this chapter.

4.1 Global High-Resolution Fuel Combustion Inventory

This high-resolution combustion inventory (PKU-FUEL) was developed based on subnational energy statistical data of more than 8000 administrative units, such as China, USA, and Mexico by county, India, Brazil, Canada, Australia, Turkey, and South Africa by province. Introduction of the subnational data can substantially reduce the spatial bias caused by uneven distribution of per-capita fuel consumption within countries. Methodology on the development of PKU-FUEL was described in a previous paper (Wang et al. 2013).

4.2 Global Time Trend of Emissions from Motor Vehicles

Thanks to the efforts of many laboratories, PAH EFs (EF_{PAH}) were measured for various activities including motor vehicle exhaust, which were used for developing PAH emission inventories (Galarneau et al. 2007; Pacyna et al. 2003; Zhang et al. 2007). In most cases, if not all, means of available EF_{PAH} with acceptable quality were adopted assuming that they are the best estimates for an average condition (Xu et al. 2006; Zhang et al. 2007). Occasionally, frequency distributions of measured EF_{PAH} were used for uncertainty analysis using Monte Carlo simulation (Xu et al. 2006; Zhang et al. 2007). A thorough review on EF_{PAH} for motor vehicles is conducted in this work, and it is revealed that EF_{PAH} of individual compounds reported by different laboratories varied more than 4 orders of magnitude, primarily due to the influences of many factors including country where the test performed, vehicle model year (Y_m), vehicle type, fuel type, operation mode, and ambient temperature (Baek et al. 1991). Due to such a large variation, uncertainty in EF_{PAH} was the primary source of the overall uncertainty in PAH emission inventories (Xu et al. 2006).

For a better assessment on air quality and exposure risk, it is necessary to develop emission inventories with lower uncertainty. Meantime, inventories with spatial and temporal resolutions are powerful in such assessment. The best way of reducing the overall uncertainty in emission inventories is to reduce the variation in EF_{PAH} . For instance, if the total variation in EF_{PAH} could be reduced by one or two orders of magnitude, 90 or 99 % of the overall uncertainty in an inventory would be removed. It was proposed that if the main factors affecting EF_{PAH} can be identified and quantified, the reduction in EF_{PAH} variation would be realized by rectifying EF_{PAH} based on these factors. An additional advantage of this approach is that the rectified EF_{PAH} can be adopted for developing spatially and/or temporally resolved emission inventories, given that the detailed information on these factors is available. The analysis procedure for emission factors from motor vehicles is different from other sources, since the data size of the collected EFs is large enough to conduct regression analysis that contains major factors effecting EF levels. Hence, this source is discussed separately.

4.2.1 Variations in EF_{PAH} for Motor Vehicles

Numerous tests have been conducted to measure EF_{PAH} for motor vehicles in many countries over the past 50 years. Table 4.1 lists the statistical information of the EF_{PAH} collected in this study, including sample size (n), arithmetic mean (m), standard deviation (s), coefficient of variance (CV), geometric mean (m_g), geometric standard deviation (s_g), coefficients of skewness (g_1) and kurtosis (g_2) of raw data, coefficients of skewness (g_{1g}) and kurtosis (g_{2g}) of log-transformed data, minimum (min), maximum (max), and a number of percentiles (p_{10} , p_{25} , p_{50} , p_{75} , and p_{90}).

Table 4.1 Statistics of PAH EFs for motor vehicles collected from the literature, mg/t

PAH	n	m	s	CV, %	m _g	s _g	g ₁	g ₂	g _{1g}	g _{2g}	P ₉₀	
											min	max
NAP	138	6.56 × 10 ⁴	1.31 × 10 ⁵	2.00 × 10 ²	1.92 × 10 ⁴	4.71	3.91	19.5	0.37	-0.38	5.14 × 10 ⁴	2.02 × 10 ⁵
ACY	130	1.77 × 10 ³	3.78 × 10 ³	2.14 × 10 ²	6.04 × 10 ²	4.90	5.34	33.1	-0.44	0.40	1.67 × 10 ³	3.89 × 10 ³
ACE	124	3.45 × 10 ²	4.43 × 10 ²	1.28 × 10 ²	1.49 × 10 ²	4.46	2.33	6.41	-0.57	0.25	4.65 × 10 ²	8.99 × 10 ²
FLO	140	1.30 × 10 ³	2.99 × 10 ³	2.31 × 10 ²	4.62 × 10 ²	4.60	7.38	67.1	-0.31	0.01	1.42 × 10 ³	2.35 × 10 ³
PHE	181	2.17 × 10 ³	5.42 × 10 ³	2.50 × 10 ²	6.19 × 10 ²	5.60	7.21	66.1	-0.39	0.20	1.85 × 10 ³	4.41 × 10 ³
ANT	180	4.15 × 10 ²	7.58 × 10 ²	1.83 × 10 ²	1.23 × 10 ²	5.64	3.63	15.2	-0.25	-0.30	4.52 × 10 ²	1.03 × 10 ³
FLA	220	6.33 × 10 ²	1.75 × 10 ³	2.76 × 10 ²	1.45 × 10 ²	6.00	7.68	77.3	-0.13	0.12	1.46 × 10 ²	4.41 × 10 ²
PYR	255	1.03 × 10 ³	2.47 × 10 ³	2.41 × 10 ²	2.45 × 10 ²	5.99	5.58	41.1	-0.13	-0.04	1.55 × 10 ²	1.49 × 10 ³
BaA	210	1.24 × 10 ²	3.26 × 10 ²	2.63 × 10 ²	2.80 × 10 ¹	6.53	6.43	50.3	-0.27	-0.05	4.52 × 10 ²	1.49 × 10 ³
CHR	201	1.05 × 10 ²	1.93 × 10 ²	1.84 × 10 ²	3.22 × 10 ¹	5.50	3.85	18.2	-0.32	-0.20	1.46 × 10 ²	4.41 × 10 ²
BbF	191	7.94 × 10 ¹	1.73 × 10 ²	2.18 × 10 ²	2.16 × 10 ¹	5.32	4.16	19.2	0.00	-0.26	1.46 × 10 ²	4.41 × 10 ²
BkF	189	6.43 × 10 ¹	1.41 × 10 ²	2.19 × 10 ²	1.58 × 10 ¹	6.17	4.76	27.2	-0.07	-0.74	1.46 × 10 ²	4.41 × 10 ²
BaP	233	9.03 × 10 ¹	1.90 × 10 ²	2.11 × 10 ²	2.32 × 10 ¹	6.19	5.36	40.1	-0.20	-0.47	1.46 × 10 ²	4.41 × 10 ²
IcdP	171	6.94 × 10 ¹	1.83 × 10 ²	2.63 × 10 ²	1.40 × 10 ¹	6.69	5.56	34.7	-0.09	-0.23	1.46 × 10 ²	4.41 × 10 ²
DahA	92	2.08 × 10 ¹	6.10 × 10 ¹	2.93 × 10 ²	2.45 × 10 ⁰	9.36	4.84	25.6	0.00	-0.42	1.46 × 10 ²	4.41 × 10 ²
BghiP	200	1.30 × 10 ²	3.99 × 10 ²	3.06 × 10 ²	2.53 × 10 ¹	6.97	8.44	89.88	-0.21	-0.08	1.46 × 10 ²	4.41 × 10 ²

(continued)

Table 4.1 (continued)

PAH	min	max	p_{10}	p_{25}	p_{50}	p_{75}	p_{90}
PYR	1.09×10^0	2.49×10^4	2.51×10^1	6.75×10^1	2.50×10^2	8.46×10^2	2.20×10^3
BaA	2.49×10^{-1}	3.18×10^3	2.87×10^0	8.18×10^0	3.32×10^1	1.02×10^2	2.88×10^2
CHR	2.73×10^{-1}	1.41×10^3	4.01×10^0	9.13×10^0	4.14×10^1	1.02×10^2	2.72×10^2
BbF	4.03×10^{-1}	1.16×10^3	2.75×10^0	7.32×10^0	2.20×10^1	6.68×10^1	1.62×10^2
BkF	4.03×10^{-1}	1.16×10^3	1.21×10^0	4.00×10^0	1.72×10^1	6.09×10^1	1.38×10^2
BaP	2.04×10^{-1}	1.91×10^3	1.80×10^0	6.13×10^0	2.63×10^1	8.68×10^1	2.43×10^2
IcdP	1.57×10^{-1}	1.40×10^3	1.07×10^0	4.05×10^0	1.24×10^1	5.71×10^1	1.53×10^2
DahA	2.04×10^{-2}	4.19×10^2	1.78×10^{-1}	5.80×10^{-1}	2.77×10^0	1.21×10^1	2.84×10^1
BghiP	2.49×10^{-1}	4.72×10^3	2.00×10^0	7.64×10^0	3.08×10^1	1.08×10^2	2.61×10^2

Reprinted from Atmospheric Environment 45, Shen et al., Global time trends in PAH emissions from motor vehicles, 2067–2073. Copyright 2011, with the permission from Elsevier

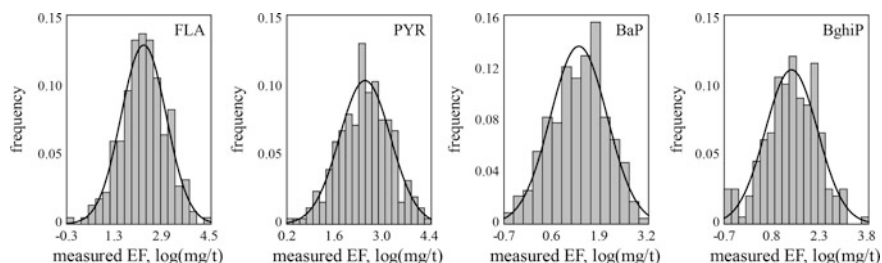


Fig. 4.1 Frequency distributions of log-transformed EFs of FLA, PRY, BaP, and BghiP for motor vehicles. The EFs were log-transformed and fitted with lognormal distribution curves. Modified from Atmospheric Environment 45, Shen et al., Global time trends in PAH emissions from motor vehicles, 2067–2073. Copyright 2011, with the permission from Elsevier

It was found that the reported EF_{PAH} values vary widely for every PAH compounds. For example, 233 BaP EFs range from 0.02 to 1910 mg/t and 220 FLA EFs vary from 0.522 to 20400 mg/t, both showing striking variation of around five orders of magnitude. The coefficients of variance of EF_{PAH} for individual compounds were from 128 % (ACE) to 306 % (BghiP). For the 16 PAHs, the EF_{PAH} were all leptokurtically and right-skewed distributed with coefficients of skewness from 2.33 to 8.44 and the coefficients of kurtosis from 6.4 to 89.9. After log transformation, these coefficients were reduced to values close to zero (t test, $p > 0.05$, see Table 4.1), suggesting that they are all lognormally distributed (see Fig. 4.1).

4.2.2 Factors Affecting EF_{PAH} for Motor Vehicles

Among the many factors investigated, the country where EF_{PAH} were tested is one of the most critical factors affecting EF_{PAH} for vehicles simply because regulations on emission control are very different among countries. Vehicle emission is rigorously regulated in the USA and EU, while there is literally no regulation on vehicle exhaust in poor countries (ADB 2003; Timilsina and Dulal 2009). It is reasonable to expect that a car running in a street of Paris is usually more technically advanced than the one operated in Mexico City at the same time in terms of emission. Such a difference can be clearly seen in the EF_{PAH} database used in this study. For example, arithmetic mean BaP EFs (EF_{BaP}) for vehicles produced from 1994 to 1996 varied widely among the USA (4.56–3.19 mg/t), Sweden (6.13–4.94 mg/t), Denmark (19.6–25.3 mg/t), Australia (70.0–64.4 mg/t), and Brazil (184–73 mg/t) (Cadle et al. 1999; Chellam et al. 2005; De Abrantes et al. 2004; Durbin et al. 1998; EA 2003; Leonidas and Zissis 2000; Nelson et al. 2008; Riddle et al. 2007; Schauer et al. 1999; Wingfors et al. 2001). Apparently, the decreasing gradient is closely related to the socioeconomic development status of these countries.

In a given country, or in a group of countries with similar development status, EF_{PAH} for a specific type of vehicles generally decreased over time due to enforcement of new regulations and development of modern control technologies. From 1992 to 2009, EU has issued five emission standards from Euro I to V for passenger cars and Euro VI was scheduled to be in force in 2014 (Timilsina and Dulal 2009). An important step toward vehicle emission control in the USA was taken in 1970 when the Congress passed the Clean Air Act, which was further amended in 1977 and 1990 (Timilsina and Dulal 2009). Development of most new emission control technologies was primarily driven by these regulations. The first-generation catalytic converter introduced in mid-1970s helped to cut car emission substantially (USEPA 1999). After the three-way catalysts with onboard computer and oxygen sensor hit the market in 1980s, more evident reduction in car emission was achieved (USEPA 1999). Although PAH emission was not regulated directly, the new technologies aiming at other pollutants including particulates and nitrogen oxide helped to trim down PAH emission “unintentionally.” For the same reason, vehicle emission was also gradually reduced in developing countries over years, although the progress was hysteretic (ADB 2003). For example, China III emission standard, which is similar to Euro III, already went into effect in China in 2007 (Timilsina and Dulal 2009).

For instance, the time dependence of EF_{PAH} in the USA and European countries can be clearly observed which is illustrated by plotting EF_{BaP} against model year (Y_m) in Fig. 4.2. Negative correlations are significant at the level of 0.005. Over the last 30 years, in the USA, EF_{BaP} for light-duty gasoline vehicles decreased approximately two orders of magnitude in the USA from 300 mg/t in early 1970s to 1.4 mg/t in 2000. The descending half-life is about 3.9 years, or an equally annual descending rate being 16.4 %. Similarly, EF_{BaP} for all types of vehicles decreased from 113 to 3.0 mg/t in European countries with an annual descending rate of 11.3 % over the past 3 decades. A descending trend was also observed for other countries including Brazil, Australia, and Mexico.

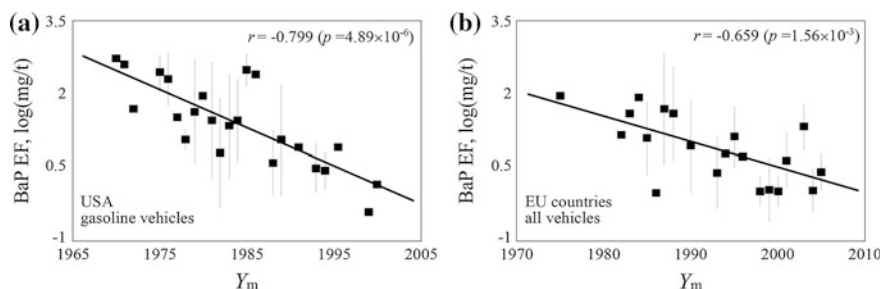


Fig. 4.2 Relationship between the measured EF_{BaP} and Y_m for (a) light-duty gasoline vehicles in the USA from 1970 to 2000 and (b) all types of vehicles in European countries from 1975 to 2005. Annual means and standard deviations of EF_{BaP} are presented in log scale. Reprinted from Atmospheric Environment 45, Shen et al., Global time trends in PAH emissions from motor vehicles, 2067–2073. Copyright 2011, with the permission from Elsevier

Evidences have shown significant difference in EF_{PAH} among different types of vehicles. For example, measured EFs of PHE, FLA, and PYR among vehicles in the USA with model years around late 1990s were 3.01, 1.02, and 2.01 mg/t for light-duty gasoline vehicles and were 91.4, 47.6, and 67.1 mg/t for heavy-duty diesel vehicles, respectively (Riddle et al. 2007). Except for vehicle types, EF_{PAH} measured using different methods could be very different. For instance, it was reported that EF_{PAH} derived from dynamometer tests tended to be lower than those measured in the real-world tests (Kristensson et al. 2004). Among the real-world tests, those observed in the tunnel tests were considerably higher than those measured in roadside tests (Wingfors et al. 2001). Based on the result of an investigation on the influences of fuel type and driving conditions on PAH emission, it was revealed that the emission increased with either higher PAH content in the fuel or higher cruising speed (Westerholm et al. 1992; Westerholm and Li 1994). It was also found that PAH emission over transient driving cycles was higher than that over steady-state driving cycles (Kado et al. 2005). Partition of PAHs between gaseous and particulate phases is temperature dependent (Grieshop et al. 2006), leading to different EF_{PAH} at different ambient temperatures (Cadle et al. 1999). Other factors affecting EF_{PAH} include vehicle age and load, lubricant oil (Ravindra et al. 2008), cold starting (Paturel et al. 1996), and the errors associated with sample collection and analysis.

4.2.3 Prediction of EF_{PAH} for Motor Vehicles

Although a dozen of factors were found to have significant effects on EF_{PAH} , country where vehicles operated and Y_m are the most important. For this reason, records on these two factors are available for almost all EF_{PAH} measurements in the database. The factor of “country” is an attribute reflecting the socioeconomic technical development status. A number of relevant quantitative variables including GDP_c , energy consumption, population density, and income were evaluated for their relationship with EF_{PAH} . Among them, GDP_c was found to be the best one in terms of predicting log-transformed EF_{PAH} . Therefore, bivariate linear regression models were developed for predicting EF_{PAH} (log(mg/t)) using GDP_c (1000 USD) and Y_m (AD) as two independent variables for the 16 PAHs individually at the first place:

$$\log(EF_{PAH}) = a \times GDP_c + b \times Y_m + C,$$

where a (log (mg/t)/(1000 USD)), b (log (mg/t)), and C (log (mg/t)) are regression coefficients of the bivariate regression models and the calculated results of these coefficients, together with p values and coefficients of determination, are found in Table 4.2.

Although Y_m is also a critical factor affecting EF_{PAH} (Fig. 4.2), the results of the regression modeling revealed that this variable was not significant in most cases

Table 4.2 Regression coefficients, p , and R^2 of the bivariate regression models for predicting EF of individual PAHs based on GDP_c and Y_m

PAH	NAP	ACY	ACE	FLO	PHE	ANT	FLA	PYR
a	-0.041	-0.032	-0.038	-0.066	-0.076	-0.057	-0.060	-0.041
b	-0.014	-0.023	-0.001	0.015	0.017	-0.008	-0.008	-0.021
C	32.2	50.1	5.74	-26.2	-29.5	19	19.3	44.8
p_a	2×10^{-3}	3×10^{-1}	2×10^{-2}	2×10^{-8}	$<10^{-10}$	2×10^{-6}	1×10^{-10}	5×10^{-5}
p_b	7×10^{-2}	1×10^{-2}	7×10^{-1}	2×10^{-1}	1×10^{-1}	2×10^{-1}	6×10^{-2}	2×10^{-4}
R^2	0.22	0.25	0.14	0.28	0.36	0.31	0.4	0.33
BaA	CHR	BbF	BkF	BaP	IcdP	DahA	BghiP	
-0.060	-0.058	-0.043	-0.048	-0.050	-0.064	-0.067	-0.041	
0.003	0	-0.009	-0.020	-0.008	0.008	-0.008	-0.022	
-3.97	2.59	20.4	42	18.8	-13.9	18.3	45.9	
7×10^{-8}	6×10^{-10}	1×10^{-5}	1×10^{-6}	8×10^{-7}	2×10^{-6}	8×10^{-9}	2×10^{-4}	
5×10^{-1}	8×10^{-1}	3×10^{-1}	6×10^{-2}	3×10^{-1}	6×10^{-1}	4×10^{-1}	2×10^{-2}	
0.24	0.31	0.26	0.34	0.32	0.27	0.42	0.34	

Reprinted from Atmospheric Environment 45, Shen et al., Global time trends in PAH emissions from motor vehicles, 2067–2073. Copyright 2011, with the permission from Elsevier

(mean p values for the 16 PAHs were 0.02 and 0.27 for GDP_c and Y_m , respectively). Moreover, it was found that Y_m was significantly correlated with GDP_c for individual countries ($p < 0.05$ for the USA, European countries, and Australia), indicating non-orthogonality of the two variables. Intrinsically, both factors of country and Y_m represent the status of technical evolution and socioeconomic development, although the former represents the geographic difference while the latter signifies the temporal change. As such, the EF_{PAH} measured in developed countries were generally lower than those in developing countries at the same period, while EF_{PAH} reported for a given country, either developed or developing, generally decreased over time. In fact, both variables were found to be correlated with GDP_c , which was then used as an integrated independent variable for a monivariate regression model for predicting EF_{PAH} . A set of monivariate regression models were developed for predicting EF_{PAH} (mg/t) for individual PAHs based on GDP_c (1000 USD) (Table 4.3):

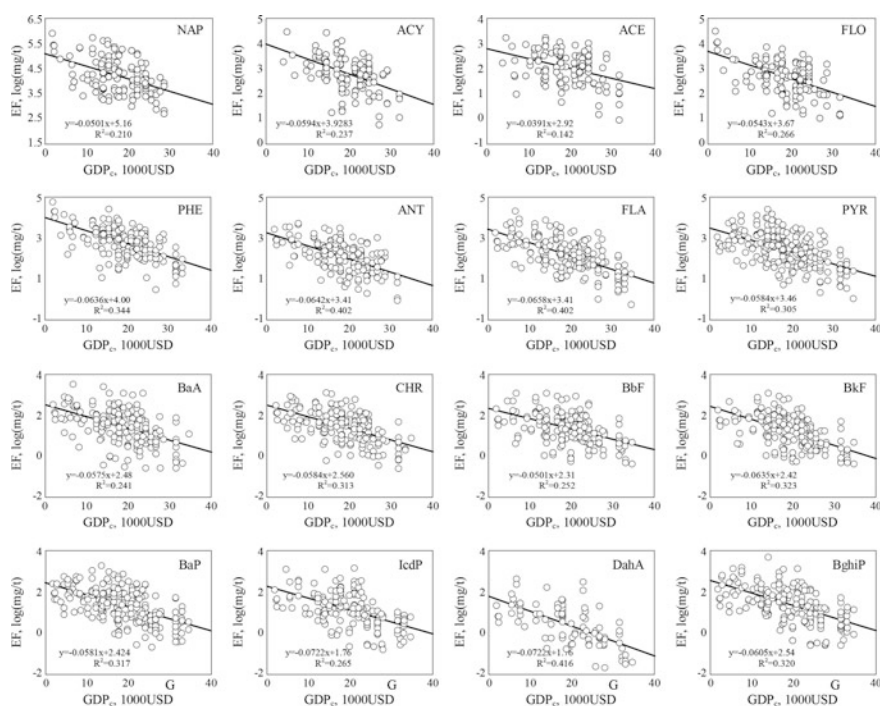
$$\log(EF_{PAH}) = k \times GDP_c + C,$$

where k ($\log(\text{mg/t})/(1000 \text{ USD})$) and C ($\log(\text{mg/t})$) are slope and interception, respectively. Physically, k is a decreasing rate constant of $\log(EF_{PAH})$ as GDP_c increases, while 10^C (mg/t) represents the emission factor of a “prototype vehicle” without emission control. It appears that the relationship between EF_{PAH} and GDP_c follows a typical single exponential function with negative k values, which is universally used to model decay processes. The results of the modeling are presented in Fig. 4.3.

Table 4.3 Regression coefficients, p , and R^2 of the monivariate regression models for predicting EF of individual PAHs based on GDP_c

PAH	NAP	ACY	ACE	FLO	PHE	ANT	FLA	PYR
k	-0.050	-0.059	-0.039	-0.054	-0.064	-0.064	-0.066	-0.058
C	5.16	3.93	2.92	3.67	4	3.25	3.41	3.46
p	2×10^{-8}	4×10^{-9}	2×10^{-5}	$<10^{-10}$	$<10^{-10}$	$<10^{-10}$	$<10^{-10}$	$<10^{-10}$
R^2	0.21	0.237	0.142	0.266	0.344	0.307	0.402	0.305
BaA	CHR	BbF	BkF	BaP	IcdP	DahA	BghiP	
-0.058	-0.058	-0.050	-0.064	-0.058	-0.057	-0.072	-0.060	
2.48	2.56	2.31	2.42	2.42	2.26	1.76	2.54	
$<10^{-10}$	$<10^{-10}$	$<10^{-10}$	$<10^{-10}$	$<10^{-10}$	$<10^{-10}$	$<10^{-10}$	$<10^{-10}$	
0.241	0.313	0.252	0.323	0.317	0.265	0.416	0.32	

Reprinted from Atmospheric Environment 45, Shen et al., Global time trends in PAH emissions from motor vehicles, 2067–2073. Copyright 2011, with the permission from Elsevier

**Fig. 4.3** Linear dependence of $\log(EF_{PAH})$ on GDP_c . Reproduced from Atmospheric Environment 45, Shen et al., Global time trends in PAH emissions from motor vehicles, 2067–2073. Copyright 2011, with the permission from Elsevier

It is evident that the overall uncertainty in EF_{PAH} , subsequently, in emission estimation can be substantially reduced after taking country and model year into account. According to the models developed, r^2 varied from 0.14 for ACE to 0.42 for DahA with a mean value of 0.29 for the 16 PAHs, indicating that almost 30 % of the variation in $\log(EF_{PAH})$ can be explained. It was estimated that for EF_{PAH} with variations of 3–5 orders of magnitude, 29 % variation reduction in log scale is equivalent to over 90 % variation reduction in linear scale.

Although significant difference in PAH emission between light-duty gasoline and heavy-duty diesel vehicles was reported (Riddle et al. 2007), The models were not substantially improved by separating the two types of vehicles in this study. In fact, when the two types of vehicles were modeled separately, the results were similar to each other with only a single exception of NAP (see Table 4.4 and Fig. 4.4). Therefore, a unified model was recommended for both gasoline and diesel vehicles, and further improvement may become possible in the future when more data are available. A number of other factors including method for EF_{PAH} measurement, ambient temperature, and driving mode were also investigated in this study by checking the interrelationship between these factors and the residues of the monivariate regression models. Unfortunately, the sample size reported for these parameters was limited and was not enough for supporting further improvement of the model. Still, there is potential for further improvement of the model if only more data can be collected.

4.2.4 Model Comparison

Based on the model calculated EF_{PAH} and petroleum consumption by motor vehicles, either historically recorded or predicted for years to come (IPCC 2001; IEA 2011; Nakićenović et al. 2000), annual emission of PAHs from motor vehicles for all countries around the world was calculated for a period from 1971 to 2030. It should be noted that the best estimates of EF values for a given country are distinguished from the direct values predicted by regression models. Instead, since the EFs vary on a logarithmic scale, the best estimates are determined by the Equation X using both the predicted values and the model uncertainties and are higher than the predicted values as mentioned in Chap. 3. The models were validated by comparing our results with those reported in the literature for the USA, the UK, Canada, the Netherlands, Italy, France, Germany, and Ireland. Annual emissions of individual PAH compounds in the USA and the UK were reported by US Environmental Protection Agency (USEPA 2011) and National Atmospheric Emissions Inventory (NAEI 2011), respectively, while annual emissions of BbF, BkF, BaP, and IcdP in Canada and five European countries were reported by Environment Canada (Environment Canada 2010) and European Environment Agency (EEA 2010), respectively. The results of the comparison are presented in Fig. 4.5. Unfortunately, our results do not agree with those of some developed European countries such as France, Germany, Italy, and Sweden (EEA 2010). In

Table 4.4 Regression coefficients, p , and R^2 of the monovariate regression models for predicting EF of individual PAHs for gasoline and diesel vehicles based on GDP_c

PAH	NAP	ACY	ACE	FLO	PHE	ANT	FLA	PYR
Gasoline	k	-0.058	-0.071	-0.067	-0.062	-0.046	-0.067	-0.056
	C	5.63	3.38	3.83	3.75	3.11	3.4	3.47
	p	9×10^{-6}	2×10^{-4}	1×10^{-6}	2×10^{-5}	2×10^{-4}	3×10^{-8}	7×10^{-7}
	R^2	0.3	0.28	0.36	0.27	0.18	0.33	0.21
Diesel	k	-0.015	-0.026	-0.047	-0.079	-0.077	-0.071	-0.062
	C	4.27	4.04	3.49	4.42	3.35	3.58	3.58
	p	9×10^{-2}	2×10^{-8}	1×10^{-4}	$<10^{-10}$	$<10^{-10}$	$<10^{-10}$	$<10^{-10}$
	R^2	0.04	0.35	0.07	0.5	0.4	0.49	0.41
BaA	CHR	BbF	BkF	BaP	IcdP	DahA	BghiP	
-0.060	-0.061	-0.048	-0.062	-0.065	-0.059	-0.078	-0.057	
2.36	2.45	2.17	2.28	2.5	2.3	1.72	2.56	
4×10^{-7}	2×10^{-7}	4×10^{-5}	7×10^{-7}	2×10^{-9}	2×10^{-7}	4×10^{-7}	3×10^{-7}	
0.28	0.31	0.23	0.31	0.31	0.3	0.42	0.29	
-0.066	-0.066	-0.061	-0.075	-0.057	-0.061	-0.093	-0.061	
2.81	2.83	2.61	2.74	2.45	2.3	2.16	2.47	
7×10^{-8}	$<10^{-10}$	7×10^{-10}	$<10^{-10}$	7×10^{-10}	8×10^{-6}	8×10^{-8}	3×10^{-8}	
0.24	0.37	0.31	0.38	0.3	0.24	0.7	0.28	

Reprinted from Atmospheric Environment 45, Shen et al., Global time trends in PAH emissions from motor vehicles, 2067–2073. Copyright 2011, with the permission from Elsevier

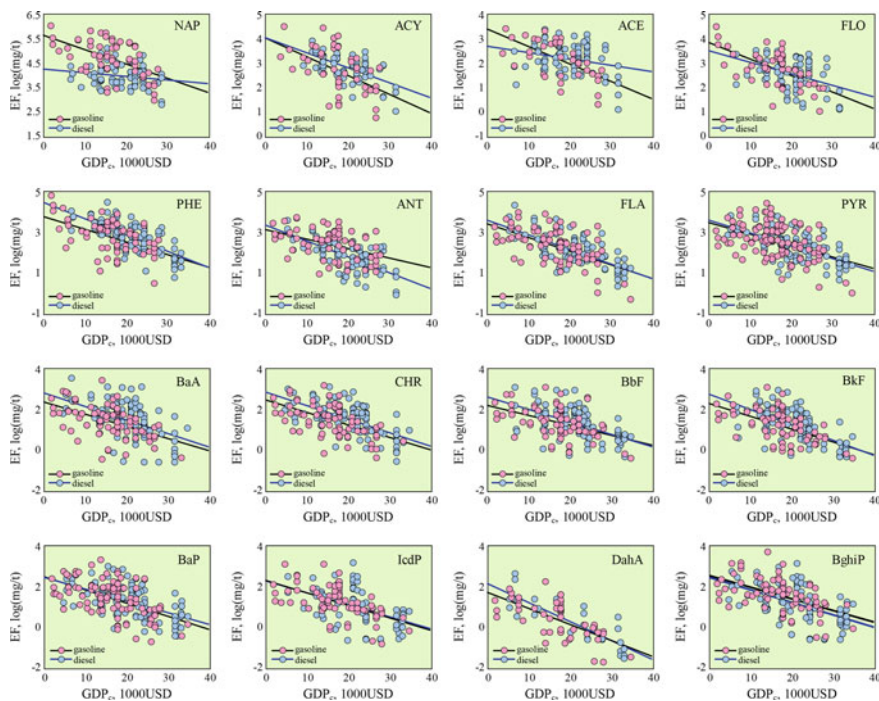


Fig. 4.4 Linear dependence of $\log(EF_{PAH})$ on GDP_c . Gasoline and diesel vehicles were modeled separately. Reprinted from Atmospheric Environment 45, Shen et al., Global time trends in PAH emissions from motor vehicles, 2067–2073. Copyright 2011, with the permission from Elsevier

general, in case of the inconsistency, continuous decrease in annual emission of PAHs over time was predicted by our model for these European countries, while an increasing trend was reported in the literature (France is a typical example). It is very likely that although the numbers of motor vehicles have increased over these years, even quicker decrease in EF_{PAH} has led to decrease in annual emission in all developed countries. For example, the measured EF_{PAH} in Sweden decreased more than one order of magnitude over the last fifteen years, in a pace much faster than the increase rate of vehicle number (Bergvall and Westerholm 2009; Westerholm et al. 1996, 2001; Wingfors et al. 2001). Another piece of evidence was that the ambient air PAH levels in major cities of Western European countries decreased in past decades (Menichini et al. 2006; Schauer et al. 2003; Valerio et al. 2009). For example, total concentrations of several PAHs in ambient air in traffic-oriented sites in two Italian cities including Genoa and Siracusa decreased significantly (Valerio et al. 2009). For major European countries such as the UK, Sweden, Switzerland, the Netherlands, Greece, Germany, France, and Belgium where most EF_{BaP} were measured, the model-predicted half-life of BaP (5.8 year) agrees excellently with that derived directly from the measurements (5.7 year). For this reason, we

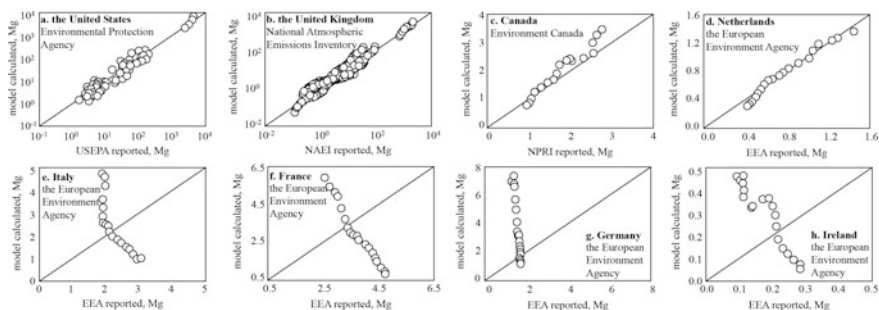


Fig. 4.5 Comparison of annual PAH emissions for motor vehicles between our model estimation and the literature reported values. **a** emissions of individual PAH compounds in the USA (US EPA) in 1999, 2002, 2005, and 2008; **b** emissions of individual PAH compounds in the UK from 1990 to 2007; **c** emissions of BbF, BkF, BaP, and IcdP in Canada from 1990 to 2007; and **d–h** emissions of BbF, BkF, BaP, and IcdP in the Netherlands, Italy, France, Germany, and Ireland from 1990 to 2007. Reproduced from Atmospheric Environment 45, Shen et al., Global time trends in PAH emissions from motor vehicles, 2067–2073. Copyright 2011, with the permission from Elsevier

recommend that the methodology used by the European Environment Agency for PAH emission estimation should be reviewed and updated.

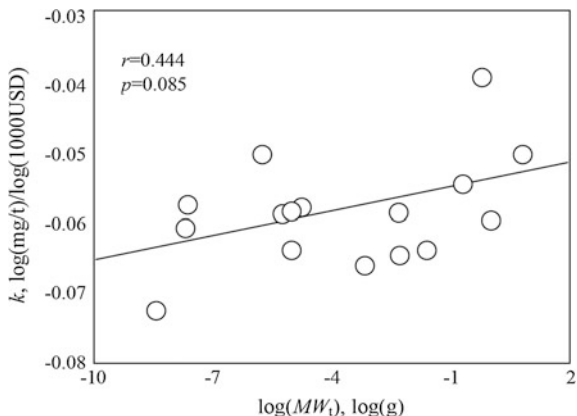
4.2.5 Difference in EF_{PAH} Among PAH Compounds

Although EF_{PAH} of different PAHs for motor vehicles varies widely, the dependence on GDP_c (eventually on country and vehicle model year) follows a similar pattern. Moreover, it was found that the k values of the regression models for individual PAHs were log-transformed vapor pressure $\log(P_s)$ dependent (see Fig. 4.6). Positive correlation between k and $\log(P_s)$ was significant ($p < 0.10$), suggesting that during the course of technical development, the efficiencies of the emission reduction for lower P_s PAHs were higher than those for higher P_s PAHs, likely due to the fact that the particulate matter, which the majority of lower P_s PAHs are bound to, is one of the main targeted pollutants in emission control. Still, more data are needed in the future to confirm this trend.

4.2.6 Time Trends of PAH Emission from Motor Vehicles in the World

Annual emissions of PAHs from motor vehicles are calculated for all countries around the world from 1971 to 2030. The prediction beyond 2008 was based on four IPCC scenarios. Globally, the total annual emissions of 16 PAHs from motor

Fig. 4.6 Linear dependence of k on $\log(P_s)$. Reproduced from Atmospheric Environment 45, Shen et al., Global time trends in PAH emissions from motor vehicles, 2067–2073. Copyright 2011, with the permission from Elsevier



vehicles were 217 (152–313 as interquartile range from Monte Carlo simulation), 225 (158–323), 145 (101–208), 109 (76–157), and 93 (66–135) Gg in 1970, 1980, 1990, 2000, and 2010 and will be 62 (44–90) and 28 (19–40) Gg in 2020 and 2030, respectively, based on a A1B scenario. Time trend of global emission from 1971 to 2030 is presented in Fig. 4.7 (top left panel). In addition, the emission trends in the USA, Germany, Russia, China, and India are also presented in Fig. 4.7. The emissions in the USA and Germany decreased from 91.2 and 9.0 Gg in 1971 to 1.93 and 0.50 Gg in 2010, respectively. Similar trends can be found for the entire developed world. These countries were the major contributors in 1970s and 1980s leading to the peak in global emission during 1970s. On the other hand, PAH emission in China and India increased from 1.81 (1.132–2.394) and 2.42 (1.73–3.62) Gg in 1971 to 21.5 (12.9–34.8) and 7.58 (4.55–10.74) Gg in 2010. Fast increase in PAH emissions during last 10–20 years can also be seen in other developing countries in economic transit periods. Globally, total emission reduced approximately 40 % from 1980 to 1990 after emission control measures were introduced in developed countries, and continuous decrease in these countries has driven the global temporal trend to decrease rapidly. It seems that the global vehicle emission of PAHs will decrease with increasing annual rate, since emissions from developing countries are passing over their peak recently and will decrease in the future. In China, for example, although the number of vehicles increased at annual rate of 21 %, average emission of each vehicle also decreased approximately 18 % each year. In fact, China III emission standard equivalent to Euro III was introduced in 2007 (Timilsina and Dulal 2009), and China IV emission standard equivalent to Euro IV has been enforced in 2011. As a result, the emission from China is approaching its turn point currently and the relative contribution of China to the global motor vehicle PAH emission will decrease rapidly, based on the A1B scenario, if only the current trend of controlling effort would continue. Time trend pattern of EF_{PAH} of India is similar to that of China (the peak between 1995 and 2001 was likely due to error in petroleum consumption data). For comparison, the prediction beyond 2008 was made based on four IPCC energy scenarios of A1B,

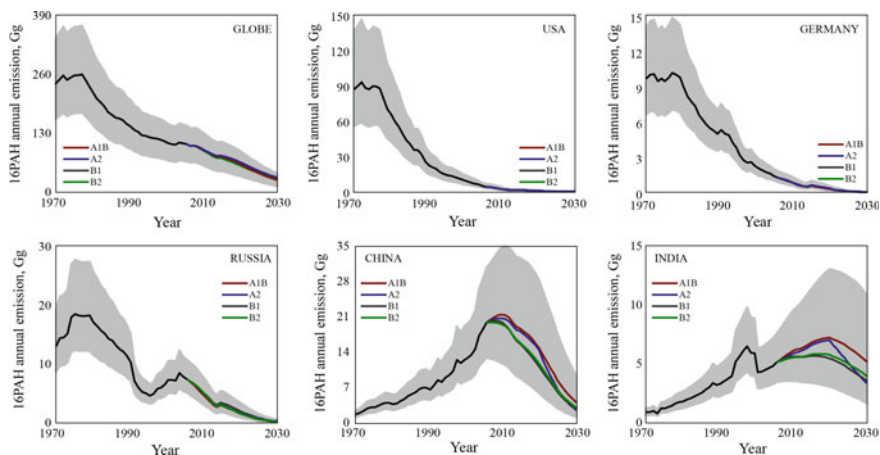


Fig. 4.7 Time trends of motor vehicle emissions of 16 PAHs during a period from 1971 to 2030 for the world and several representative countries including the USA, Germany, China, India, and Russia. The predicted results are presented as medians and interquartile ranges from Monte Carlo simulation, and the latter are used to describe the overall uncertainties of the prediction. Predicted total PAH emissions from motor vehicles from 2009 to 2030 are based on four IPCC energy consumption scenarios of *A1B*, *A2*, *B1*, and *B2*. Reproduced from Atmospheric Environment 45, Shen et al., Global time trends in PAH emissions from motor vehicles, 2067–2073. Copyright 2011, with the permission from Elsevier

A2, *B1*, and *B2* (Nakićenović et al. 2000) and the results are shown in Fig. 4.7 for the globe and individual countries. It appears that under four scenarios, the time trends are similar to one another, and this is particularly true for the developed countries. The relatively large difference can be found in China and India where the emission would be significantly lower at *B1* and *B2* scenarios, which describe slower technology transitions from the developed countries to developing ones.

Since the emission from other major sources including wildfire, biomass burning, and consumer product usage will not change as quickly as those from motor vehicles, the relative contribution of motor vehicles to total PAH emission from all sources is expected to decrease, which would lead to a decrease in inhalation exposure of urban residences to PAHs.

4.3 Global Emissions of Atmospheric PAHs from All Sources

Based on the regression models mentioned above and modified technology splitting described in Chap. 3, a previous EF_{PAHs} database (Zhang and Tao 2009) was fully compiled and updated. Using the newly developed fuel consumption database (PKU-FUEL-2007), a $0.1^\circ \times 0.1^\circ$ gridded global PAH emission inventory was

developed for 2007 (PKU-PAH-2007). The uncertainty in the PAH emission inventory was characterized, and the spatial distributions of the total and per-capita PAH emissions, as well as their potential health effects, were investigated. Historical time trends in PAH emissions from 1960 to 2008 were estimated at country level, and future trends to 2030 were simulated based on the six IPCC (Intergovernmental Panel on Climate Change) scenarios (A1/A1B, A2, B1, B2, A1FI/A1G, and A1T) on future energy consumptions, defined and described in the Special Report on Emissions Scenarios (SRES) (Nakićenović et al. 2000).

4.3.1 Total Emission and Source Profile

The annual global atmospheric emission of the 16 PAHs in 2007 was 655 Gg (521–816 Gg, as interquartile range from the Monte Carlo simulation), which is equivalent to 99 g per capita per year. Emissions of individual PAH compounds, from all sources in various countries, are listed in Tables A1 and A2 in the Appendix. The updated total PAH emission for 2004 in this study (682 Gg) was 31 % higher than previous estimate for 2004 (520 Gg) by Zhang and Tao (2009), mainly because of the updated EF_{PAHs} database and the use of values of the arithmetic means (or the mathematical expectations) instead of the geometric means as the average emission factors for a specified country.

Figure 4.8 shows the relative contributions of various sources to the total PAH emissions for the world and for several countries in 2007. Table 4.5 lists the source specified emissions for individual world regions. Globally, biomass fuels, including

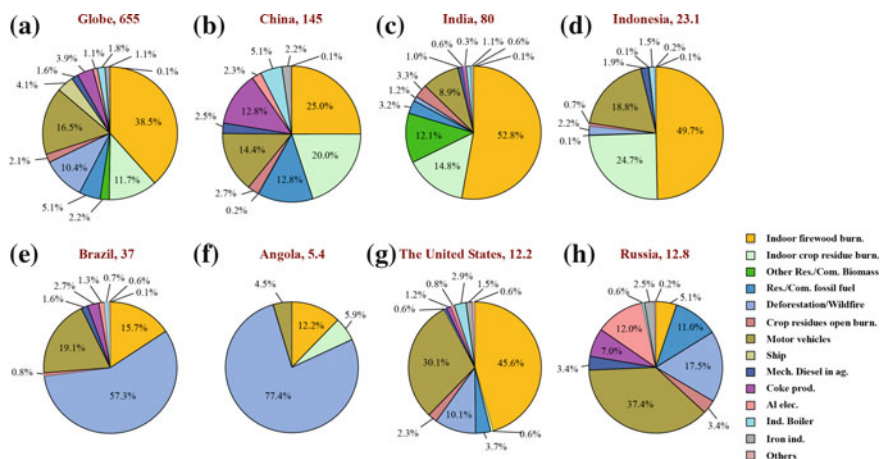


Fig. 4.8 Source profiles of PAH emissions (Gg) in the world (a) and several representative countries including China (b), India (c), Indonesia (d), Brazil (e), Angola (f), the USA (g), and Russia (h) in 2007. Reproduced with the permission from Shen et al. (2013). Copyright (2013) American Chemical Society

Table 4.5 Regional PAH16 emissions by sectors in 2007

Region	Resid./commer.		Deforestation/wildfire		Road trans.		Agriculture		Energy/industry		Total emission		Per-capita total emission		Per-capita anthropogenic emission		Per-capita energy consumption	
	ton	ton	ton	ton	ton	ton	ton	ton	ton	ton	ton	g/cap	g/cap	g/cap	g/cap	toe/cap ^a	toe/cap ^a	
South and Southeast Asia	127573	8133			21351	5849			3238		166145	85	85	85	0.6			
East Asia	85896	508			23155	7532			34918		152009	100	100	100	1.3			
West and Central Asia	3746	70			7358	2511			929		14614	46	46	46	6.1			
West and Central Africa	45602	10174			2859	73			129		58837	180	164	164	1.2			
East and South Africa	30489	12413			6557	329			718		50505	223	155	155	1.9			
Northern Africa	27644	1929			2943	755			292		33564	99	94	94	1.6			
South America	11497	26658			12545	1976			2450		55127	156	134	134	1.9			
North America	10310	3612			8469	733			1376		24499	59	49	49	5.6			
Central America	4970	159			636	15			13		5792	144	144	144	0.4			
Europe	20764	2502			14151	3125			7256		47797	68	63	63	3.4			
Caribbean	742	19			279	37			22		1099	37	37	37	1.9			
Oceania	2007	1238			577	147			348		4317	145	88	88	13.7			

^a“toe” is ton oil equivalent

mainly firewood and crop residues, consumed in residential/commercial sectors were the major PAH sources, contributing 52.4 % of the global total PAH emissions. The consumption of petroleum products in transportation (16.5 %) and deforestation/wildfire (10.4 %) was also important PAH emission sources. Considerable difference in PAH source profiles among individual countries was primarily due to energy structure, development status, and vegetation cover. In many developing countries, such as India, China, and Indonesia, indoor biomass burning was the most important PAH emission source, contributing about half of the total PAH emissions. Indoor firewood combustion was also a major PAH emission source in some developed countries, such as the USA, where certified woodstoves were popular in many rural households (USEPA 1998). Significant deforestation/wildfire emissions occurred primarily in a dozen of countries, including Brazil, Democratic Republic of the Congo, and Angola, where widespread forest or prairie fires occurred every year. Motor vehicle exhaust was also an important source of PAH emissions, accounting for one-sixth of the global total PAH emissions. This source was particularly important in many developed countries. The relative contribution of PAH emissions from motor vehicles is increasing in China and other countries under economic transition. Coke production was also an important source in some countries, including China and Russia. However, because of the rapid decline in the use of beehive coke ovens, PAH emissions from coke production are rapidly declining.

Figure 4.9 compares the PAH emissions from major sources in China, India, Brazil, the USA, and all other countries in 2004 derived from this study (similar to that of 2007) and Zhang's study (Zhang and Tao 2009). It was found that not only the total PAH emission calculated in this study was different from that of Zhang's inventory for 2004, but the differences for individual countries and sources are also much larger between the two inventories. Comparing with those in Zhang's

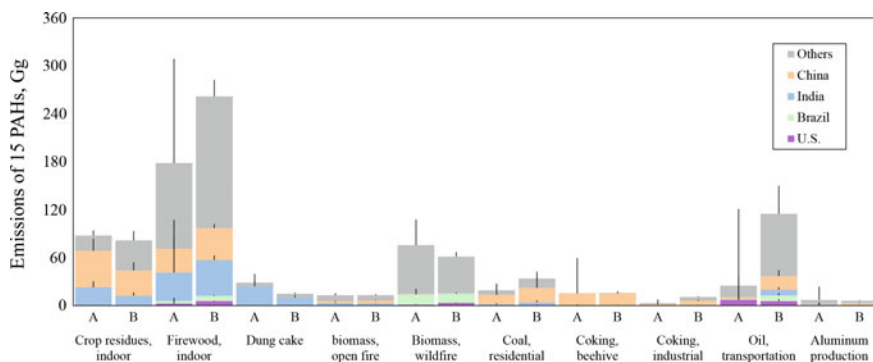


Fig. 4.9 Comparison in total PAH emissions from major sources between two global inventories for 2004: *A* an inventory reported by Zhang and Tao (2009) versus *B* the inventory developed in this study. The *error bars* show upper quartiles for each country derived from Monte Carlo simulations. Reproduced with the permission from Shen et al. (2013). Copyright (2013) American Chemical Society

inventory, the global emissions from indoor firewood burning, on-road motor vehicles, mechanical coke production, and indoor fossil fuel combustion derived in this study were 83 Gg (47 %), 8 Gg (238 %), 9 Gg (359 %), and 140 Gg (77 %) higher, and emissions from biomass open burning, indoor dung cake burning, and indoor crop residue burning were 14 Gg (19 %), 14 Gg (48 %), and 6 Gg (7 %) lower, respectively. The improvement in emission estimation by using country-/region-specific EF_{PAHs} was better demonstrated for individual sources as well as individual countries. In this study, EF_{PAHs} for petroleum consumption by on-road motor vehicles were quantified for individual countries in given years. For example, EF_{PAH16} for on-road gasoline vehicles were 10, 131, and 213 mg/kg for the USA, Brazil, and China in 2004, respectively. As a result, the estimated PAH emissions from motor vehicles in these three countries were 5.1, 5.2, and 140 Gg, respectively, in this study, compared with 6.9, 0.4, and 2.0 Gg in Zhang's inventory, in which a single EF_{PAH} of 17.1 mg/kg was adopted, indicating extraordinary difference between them. Similarly, by using the technology division method, the EF_{PAH} of BaP for primary aluminum production using Soderberg process in 2004 were estimated to be 316 and 47 mg/kg in China and the USA in this study, in contrast to a constant value of 15.1 mg/kg in the previous inventory. Together with prebaked process, the estimated total PAH emissions from aluminum production were updated from 0.7 and 1.5 Gg to 2.1 and 0.1 Gg for China and the USA, respectively. Another example is the emission from residential firewood. By dividing the indoor firewood burning source into three categories of traditional woodstoves, improved woodstoves, and fireplaces with different EF_{PAH} , the global total PAH emission from this source was renewed from 178 Gg in Zhang's inventory to 262 Gg in our inventory. In general, compared with Zhang's study, this 2004 PAH emission inventory showed a reduction in PAH emissions associated with developed countries and an increase in PAH emissions associated with developing countries within technology-based sources due to the use of country-/region-specific EF_{PAHs} . In addition, by dividing the sources to more specific categories, overall uncertainty of the inventory was reduced (error bars in Fig. 4.9), because variations of EF_{PAH} for more specific sources were always smaller than those of more general ones.

4.3.2 Composition Profile

Figure 4.10 shows the PAH emission composition profiles of seven important source categories for global total, developing, and developed countries in 2007. Globally, NAP contributed 45.0 % of the total, followed by ACY (17.1 %) and PHE (10.6 %). The total of eight high molecular weight carcinogenic compounds (Nisbet and LaGoy 1992) (from BaA to BghiP) accounted for 7.7 % of the global total, and this percentage was higher for developing countries (8.0 %) compared to developed countries (6.4 %). Transportation (motor vehicles, ships, and aircrafts) contributed approximately 20 % of the global total PAH emission, with 82.5 % of

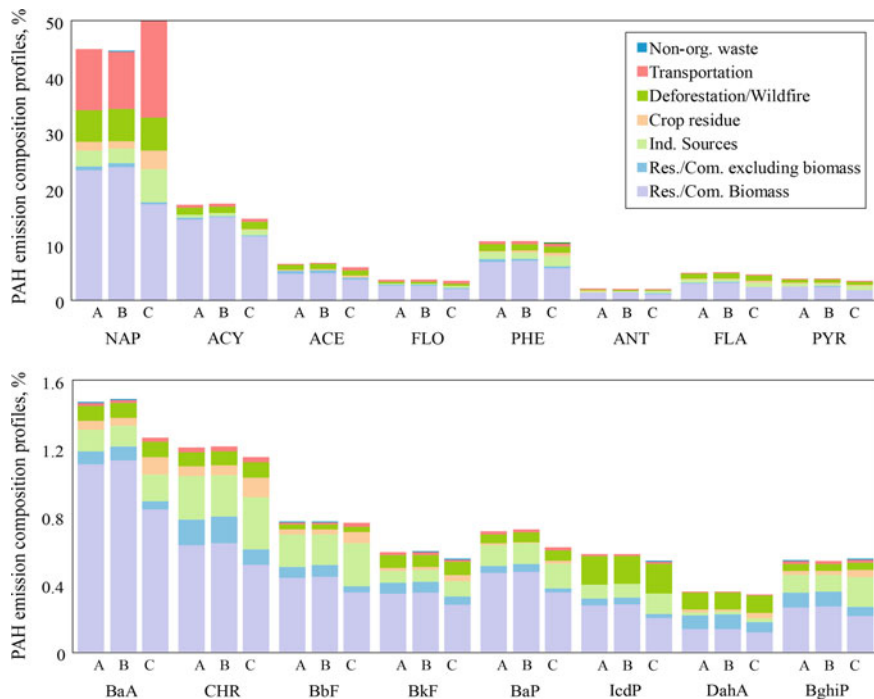


Fig. 4.10 PAH emission composition profiles of seven important source categories for *A* global total, *B* developing countries, and *C* developed countries. The lower molecular weight PAHs are shown in the *top panel*, while the higher molecular weight PAHs are shown in the *bottom panel*. Note the difference in scale between the two panels. Modified with the permission from Shen et al. (2013). Copyright (2013) American Chemical Society

the transportation emissions in the form of NAP. On the other hand, residential fuel consumption, industrial emission, and non-organized waste burning contributed more high molecular weight carcinogenic PAHs, accounting for more of the adverse health effect potential. This is of particular concern in the case of residential biomass fuel combustion because the emission of PAHs from this source can lead to direct human exposure (Ding et al. 2012). In developing countries, the domination of emissions from residential biomass burning led to relatively high percentages of high molecular weight PAHs. In contrast, emission mitigation measures are more strictly implemented in developed countries and are more effective in controlling high molecular weight PAH emissions on fine particulate matter.

To describe and compare the combined toxicities of the emissions of the 16 PAHs from various sources and areas, BaP toxic equivalent quantity (g) per unit mass emission (kg) from individual sources (BaP_{eq}/u) was defined and calculated based on the toxicity equivalent factors (Nisbet and LaGoy 1992) of individual PAHs and emission profiles. On a global scale, the average BaP_{eq}/u from all PAH emission sources was 15.0 g/kg in 2007. The most toxic sources in terms of PAH

composition were aluminum production (80.0 g/kg), residential/commercial coal burning (excluding anthracite) (52.4 g/kg), non-organized waste burning (50.6 g/kg), and coke production (23.7 g/kg). Sources with relatively low BaP_{eq}/u included motor vehicles (3.28 g/kg), industrial boilers (6.26 g/kg), and the iron industry (9.86 g/kg). The average BaP_{eq}/u in developed countries (13.0 g/kg) was lower than that in developing countries (15.1 g/kg), not only due to the differences in energy structures but also the disparities of technology. For example, BaP_{eq}/u for primary aluminum production in developed countries (57.8 g/kg) was much lower than that in developing countries (83.2 g/kg). The reasons for this difference include the following: (1) Emission control devices in aluminum production, as well as in many other processes, are more widely used in developed countries than in developing countries and (2) these emission control devices are more effective in removing high molecular weight carcinogenic PAHs sorbed to fine particulate matter.

Based on the calculated BaP_{eq}/u and total PAH emission mass, BaP toxic equivalent quantities were calculated as indicators to relative health effect potential of all individual sources. The results are shown in Fig. 4.11. Due to significant difference in BaP_{eq}/u, sources with high BaP_{eq}/u, such as primary aluminum production and domestic coal combustion, contributed much more to health effect potential than those to the total PAH emission. Still, solid fuels burned in residential sectors dominated toxic effects on a global scale.

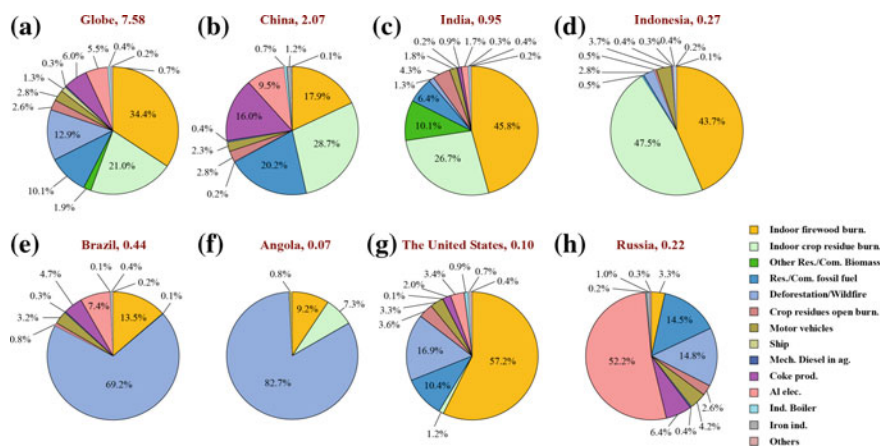


Fig. 4.11 Source profiles of BaP emissions (Gg/year) in 2007 in the world (a) and several representative countries including China (b), India (c), Indonesia (d), Brazil (e), Angola (f), the USA (g), and Russia (h) in 2007. Reprinted with the permission from Shen et al. (2013). Copyright (2013) American Chemical Society

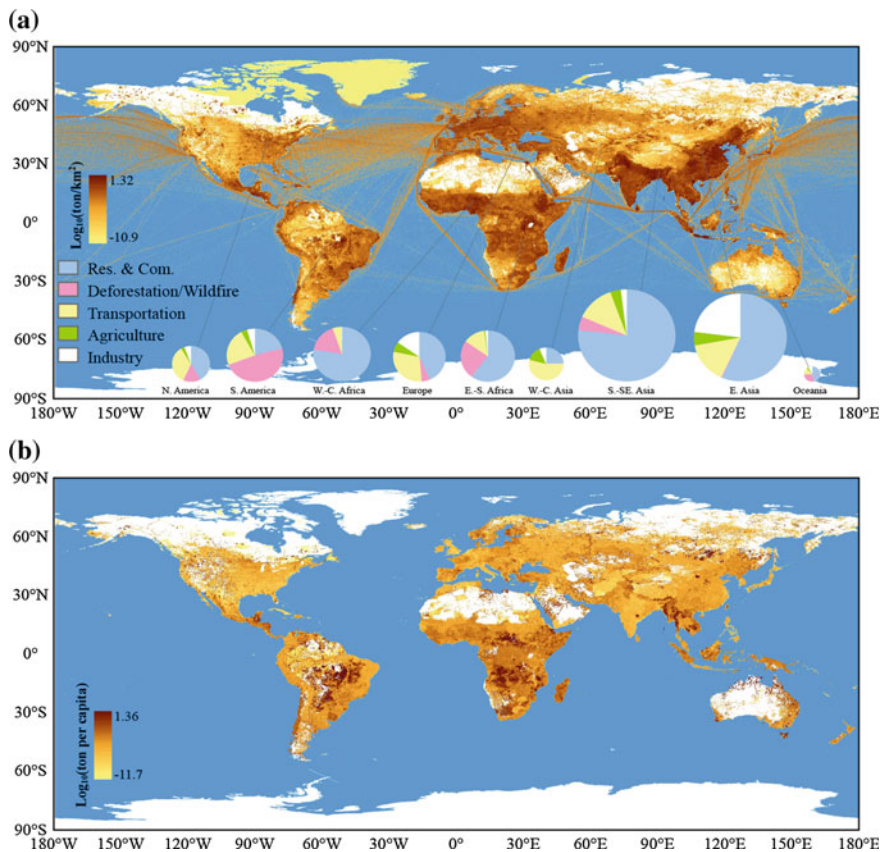


Fig. 4.12 Spatial distributions of total (a) and per-capita (b) PAH emissions globally in 2007 at 0.1×0.1 resolution. For each region, the relative contribution of major sources is shown as *pie charts*, with the areas of the *pie charts* proportional to the total PAH emissions, in a Northern Africa, Central America, and Caribbean not shown in *pie charts*. Reproduced with the permission from Shen et al. (2013). Copyright (2013) American Chemical Society

4.3.3 Geographic Distribution

With the $0.1^\circ \times 0.1^\circ$ resolution fuel combustion inventory (PKU-FUEL-2007) (Wang et al. 2013) and the country-specific EF_{PAHs} available, individual PAH emissions in 2007 were mapped on $0.1^\circ \times 0.1^\circ$ grids. Figure 4.12a shows the global distribution of total PAH emission density in 2007. The annual total PAH emissions from 12 geographic regions are listed in Table 4.5. The relative contributions of the five source sectors (energy/industry, residential/commercial, transportation, agriculture, and deforestation/wildfire) for the main geographic regions are shown as pie charts in the inset of Fig. 4.12a. The areas of the pie charts are proportional to the total PAH emissions in the different geographic regions.

Globally, almost two-thirds (67.4 %) of the total PAH emissions occurred in the residential/commercial sector, and this was particularly true for West–Central Africa (77.5 %), South–Southeast Asia (76.8 %), and South–East Africa (60.4 %), mainly because of the extensive use of biomass fuels in developing countries for cooking and heating (IEA 2011). All Asian countries contributed 53.5 % of the global total PAH emission, with the highest emissions from China (144 Gg) and India (80 Gg) during 2007. The other top PAH emitting countries included Brazil, Indonesia, Nigeria, Ethiopia, Pakistan, Democratic Republic of the Congo, Vietnam, and Russia. The total PAH emission from the above-mentioned top ten emission countries was 378 Gg in 2007, accounting for 57.7 % of the global total PAH emissions. In South America, 48.4 % of the PAH emissions were from deforestation/wildfire, mainly deforestation fires. Other regions with relatively high PAH emission from this sector were Oceania (28.7 %) and East and South Africa (24.6 %). PAH emissions from motor vehicles contributed 16.5 % of the global total, and they were relatively important in Western and Central Asia (51.1 %), North America (34.6 %), and Europe (29.6 %). Although industrial sources contributed only 7.9 % of the global total PAH emissions, they were significant in East Asia (23.0 %) and Europe (15.2 %). The main contributors to the industrial sources were coke production (13.3 %), iron and steel production (2.6 %), and industrial boilers (2.3 %) in East Asia and coke production (6.2 %), primary aluminum production (4.5 %), and iron and steel industry (2.9 %) in Europe, respectively. Compared to developed countries, the relatively large contribution of heavy industries and relatively low level of the application of emission mitigation measures were the main reasons for the higher industrial PAH emissions in China and Eastern European countries.

Figure 4.12b shows the global distribution of per-capita PAH emissions derived from the gridded PAH emission densities and population densities (ORNL 2014). The average per-capita PAH emissions from 12 regions are listed in Table 4.5. The per-capita PAH emissions for the various regions are not proportional to the per-capita energy consumptions, but they appear to be highly dependent on the region's energy structure and status of development. For example, although per-capita energy consumptions in North America (5.6 toe/cap, where toe is short for ton oil equivalent) and Europe (3.4 toe/cap) were relatively high, per-capita PAH emissions in these regions (49 and 63 g/cap) were among the lowest. In contrast, per-capita PAH emissions were much higher in Africa (150 g/cap), Asia (80 g/cap), and South America (134 g/cap), although the per-capita energy consumptions were relatively low (0.8, 1.3, and 1.3 toe/cap, respectively). In general, the proportion of residential/commercial solid biomass burning in the region's energy structure was the key factor affecting per-capita PAH emissions. It is interesting to note that the spatial pattern of per-capita CO₂ emissions (Wang et al. 2013) is very different from that of per-capita PAH emission, because CO₂ was mainly from power generation and industry, while PAHs were largely from residential sectors.

We assumed that the uneven development of urban and rural areas in developing countries, especially those under economic transition, would lead to differences in

energy consumption and structure and, subsequently, to PAH emission density between urban and rural areas. We investigated these differences using the high spatially resolved inventory derived from the subnationally spatialized data. The previously developed method for distinguishing between rural and urban grids was used,¹⁸ and each $0.1^\circ \times 0.1^\circ$ grid point was defined as either “urban” or “rural.” Using this urban–rural mask, the geographic distributions of anthropogenic PAH emissions from urban and rural areas were extracted separately. Globally, the annual total PAH emission from rural areas (413 Gg) was twice as much as that from urban areas (207 Gg). For developing countries, the difference in PAH emissions between rural and urban areas was even larger (321 vs. 135 Gg). With the similarity in global total rural and urban populations, per-capita PAH emission was also significantly higher in global rural areas (130 g/(cap·year)) than that of urban areas (65 g/(cap·year)), mainly due to the wide use of biomass fuels in rural areas. The calculated global BaP_{eq} emissions were 0.46 and 0.20 Gg in rural and urban areas, respectively. This trend was opposite to that of CO₂ and per-capita CO₂ emission—the CO₂ emission in rural areas was only one-third of that in urban areas (Wang et al. 2013).

It should be noted that, due to fast urbanization in countries under economic transition (such as China and India) (Madhukar and Nagarjuna 2011), the spatial distribution patterns of fuel consumption and energy structure have been changing rapidly (National Bureau of Statistics of China 2011a). This trend is expected to continue for years to come (Newgeography 2012). In China alone, 140 million rural residents have resettled in cities and towns during the last two decades (National Bureau of Statistics of China 2011b). Unlike rural residents, who rely largely on biomass fuels for cooking and heating, those migrating to urban areas shift their way of energy use as other city dwellers who rely more on electricity and fossil fuels (Zhang and Song 2003). The potential influence of such large-scale urbanization, occurring in countries like China, on the emissions of PAHs and other incomplete combustion by-products could be considerable. Thus, its effect on the total and spatial distribution patterns of PAH emissions (as well as other combustion by-products, such as CO₂, black carbon, and primary aerosol) should be addressed quantitatively in the future so as to understand the overall impact of urbanization on the environment and health, as well as on climate change.

Using the high spatially resolved inventory, we developed a simple method to roughly assess the potential health impact of PAH emissions based on both emission densities and distances between source and receptor grids. To do this, we assumed that the effects of PAH emissions from a grid were dominated within a 5×5 grid or 50 km \times 50 km area, beyond which the influence could be ignored. Therefore, the overall health effect potential of PAH emissions (as BaP toxic equivalence) on a receiving grid ($0.1^\circ \times 0.1^\circ$) was quantified as the total potential of effects of the PAH emissions from the receiving grid itself, as well as the PAH emissions from the 24 surrounding grids. The individual health effect potential from a source grid was proportional to the total PAH emission of the source grid and the total population of the receiving grid but inversely proportional to the distance between the source and receiving grids. The distance weight factor was 1 when the

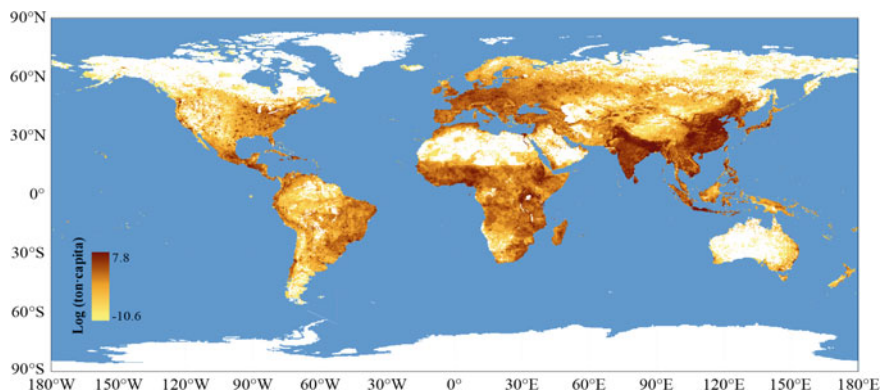


Fig. 4.13 Map of relative potential health effect (*RPHE*) from all sources. It is believed that the effect of a certain emission source on exposed population group is strengthened by increasing emission intensity and weakened by distance. Here, we assume that health effect of PAHs as BaPeq emitted from a given grid ($0.1^\circ \times 0.1^\circ$) was quantified as the effects on the emissions grid and the 24 surrounding grids. The effect on each receiving grid within this area was proportional to the total emissions of the source grid and total population of the receiving grid and inversely proportional to the distance (1 for the source grid itself, $1/4$ for the 8 grids immediately adjacent to the source grid, and $1/9$ for the other 16 grids) between the emissions and receiving grids. *RPHE* of each source category of a source grid was calculated by totalizing the effects of all 25 grids. Reproduced with the permission from Shen et al. (2013). Copyright (2013) American Chemical Society

source grid was the receiving grid itself, $1/4$ for the 8 source grids immediately adjacent to the receiving grid, and $1/9$ for the other 16 grids. The result was a dimensionless indicator, defined as relative potential health effect (*RPHE*) in this study. Because the absolute value of *RPHE* was meaningless, the global *RPHE* for all emission sources was normalized to global total emission for comparative purpose. It should be indicated that this approach is only a rough estimation on the potential of health effect, since the transport processes of PAHs from source to receipts, which depend on meteorological conditions, are not taken into consideration. Atmospheric transport modeling is required for a full assessment on the exposure and risk.

The global distribution of *RPHE* is shown in Fig. 4.13, and the relative contributions of various emission sources are shown in Fig. 4.14. Compared with the global PAH emission map (Fig. 4.12a), the potential health effects in the high PAH emission areas such as East, South, and Southeast Asia were generally intensified, because the higher population density often leads to both higher PAH emissions and higher health effects. The few exceptions were the regions (e.g., South America) with high PAH emissions from aviation, shipping, and deforestation/wildfire which were generally further away from highly populated areas. Although the total PAH emissions from industrial sources and motor vehicles were relatively low, their potential health effects were relatively high because these sources occurred primarily in cities with high population densities. Residential emission

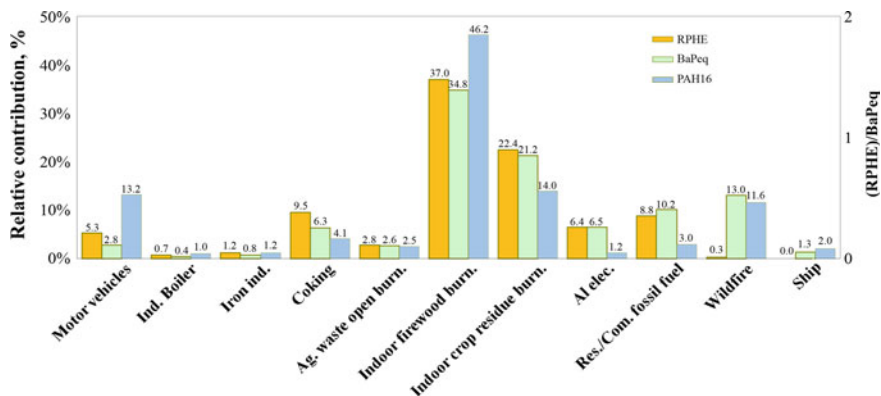


Fig. 4.14 Comparison of relative contributions based on three evaluation methods. PAH16: Emission quantity of 16 PAH compounds was simply aggregated. BaPeq: BaP toxic equivalent quality of each PAH compound was aggregated. *RPHE*: Distance-corrected and population-weighted BaPeq was calculated. Reproduced with the permission from Shen et al. (2013). Copyright (2013) American Chemical Society

sources showed strong potential health effects due to both high PAH emissions and close proximity to people, which in fact could be underestimated, because the PAH emissions from household solid fuel combustion are often very close to receptors in rural settlements. A combined consequence of the relatively high per-capita PAH emissions and biomass source domination in rural areas was that the potential of health effect of the PAH emissions in rural areas was more than double that of urban areas. Unfortunately, this subkilometer proximity could not be well characterized in this study using 10-km resolution.

4.3.4 Historical Time Trends

With the historical fuel consumption data available and time-dependent EF_{PAH} characterized, annual PAH emissions from all countries/territories were calculated from 1960 to 2008. Our results were compared with those previously reported in the literature (USEPA 2011; NAEI 2011; EMEP 2011). The emissions of individual PAHs from all sources in the USA in 2002 and 2005 estimated in this study were plotted against those reported by USEPA (Fig. 4.15a) (USEPA 2011). Similarly, the emissions of individual PAHs from all sources in the UK were compared with those reported by NAEI (National Atmospheric Emissions Inventory) from 1990 to 2009 (Fig. 4.15b) (NAEI 2011). The majority of the data points fell around the 1:1 line, indicating no systematic difference between them. The correspondence between PKU-PAH and that reported by USEPA was further confirmed when individual sources were compared separately (Fig. 4.16) (USEPA 2011). A comparison was also conducted for the total of the four PAHs (BaP, BbF, BkF, and IcdP) with those

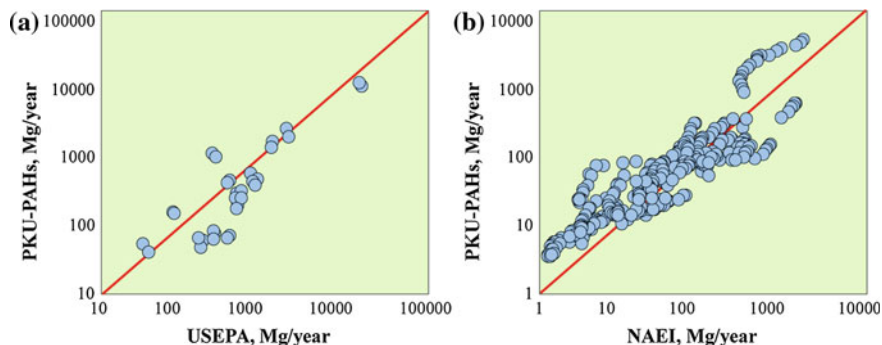
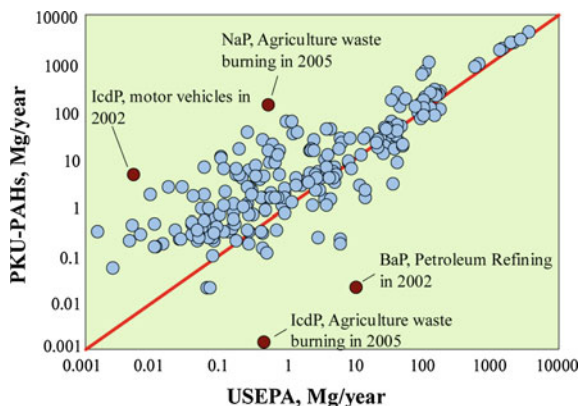


Fig. 4.15 Comparison between the PKU-PAH and the inventories previously published for (a) the USA (16 individual PAHs from all sources from 2002 to 2005) and (b) UK (16 individual PAHs from all sources from 1990 to 2009). Reproduced with the permission from Shen et al. (2013). Copyright (2013) American Chemical Society

Fig. 4.16 Comparison of annual PAH emissions between PKU-PAH and USEPA reported values. Emissions for each of the PAH16 compounds from individual sources in the USA in 2002 and 2005 are plotted in the figure. Reproduced with the permission from Shen et al. (2013). Copyright (2013) American Chemical Society



reported to EMEP (European Monitoring and Evaluation Programme), by each of the 27 European countries from 1990 to 2008 (Fig. 4.17) (EMEP 2011). Although similar trends between PKU-PAH and EMEP were found for many countries, there were striking differences for the Czech Republic, Bulgaria, Belgium, Lithuania, and Romania. The variation in EF_{PAHs} is likely to be one of the reasons for these differences. In PKU-PAH, regression and technology split methods were used to simulate time trends in EF_{PAHs} . The application of the country-specific EF_{PAHs} also caused differences between PKU-PAH and EMEP in Sweden, Germany, and Slovakia, where downward trends in PAH emissions were identified by PKU-PAH, while estimates reported to EMEP show an increasing trend in PAH emissions over the last several years (EMEP 2011). The PKU-PAH prediction was partially verified by the fact that the ambient air PAH concentrations in all European countries have decreased in recent years (Schauer et al. 2003; EMEP 2012).

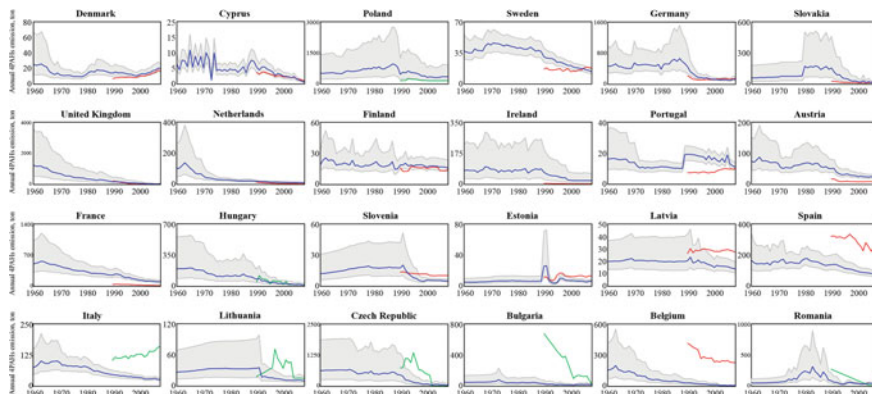


Fig. 4.17 Comparison of emission time trends for the total of 4 high molecular weight PAHs (BaP, BbF, BkF, and IcdP) with those reported by EMEP (European Monitoring and Evaluation Programme) for each of the 27 European countries from 1990 to 2008. The gray areas are interquartile ranges of PKU-PAH estimation. Red lines and green lines are the emission time trends reported by EMEP. Gap-filled time trends are marked with green. Reproduced with the permission from Shen et al. (2013). Copyright (2013) American Chemical Society

Figure 4.18 shows the time trend of global PAH emissions from 1960 to 2008. The results are presented as the global total (a) and the totals of developed (b) and developing countries (c). The PAH emissions of developed countries peaked in the early 1970s and decreased gradually since, primarily due to the introduction of emission mitigation technologies and the subsequent decline in the PAH emissions from on-road motor vehicles (Shen et al. 2011). Although the total number of motor vehicles increased more than five times from 1.2×10^8 to 6.5×10^8 in developed countries during this time period, the total PAH emissions from motor vehicles decreased dramatically. Because the average gas mileage decreased from 0.2 to 0.08 L/km, the mean EF_{PAH16} for on-road motor vehicles decreased from 130 to 7 mg/kg in these countries during the same time period (Dargay et al. 2007). Significant PAH emission decreases in the industrial sectors occurred for similar reasons, while only relatively slow decreases in PAH emissions occurred in the residential/commercial sources. In contrast, the total PAH emissions in developing countries from the transportation sector had increased continuously during the modeled time period. Although both the gas mileage and EF_{PAH} for motor vehicles in developing countries had also decreased during the past three decades (Shen et al. 2011; China Association of Automobile Manufactures 2008), an even faster increase in the number of motor vehicles in these countries, especially in China, Brazil, and India, had negated the decreasing trend (Dargay et al. 2007). For example, the number of motor vehicles in China increased from 3.7×10^6 to 4.4×10^7 from the early 1970s to 2007, while the gas mileage and EF_{PAH} only decreased 27 % from 0.132 to 0.098 L/km and 26 % from 178 to 131 mg/kg, respectively. Fortunately, PAH emissions from motor vehicles in developing countries were predicted to peak around 2010, till then the expansion of vehicle

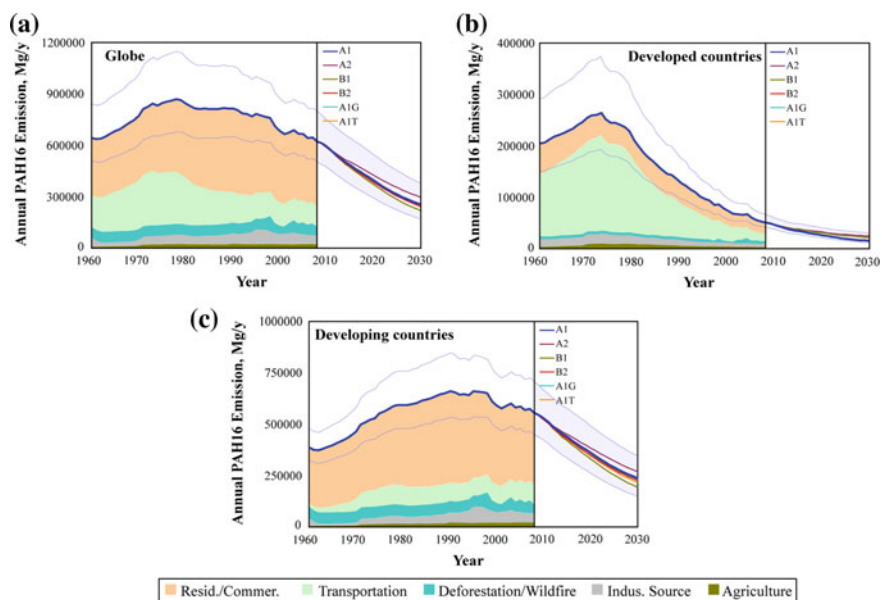


Fig. 4.18 Time trends of PAH emissions during a period from 1960 to 2030 for the world (a), developed countries (b), and developing countries (c). Emissions from the five sectors are marked with different colors (see upper right), and the uncertainties of total emissions, derived from Monte Carlo simulations, are shown as interquartile ranges using light blue curves. Future time trend simulations were conducted based on the six IPCC SRES scenarios and are presented as medians and interquartile ranges derived from Monte Carlo simulations. Reproduced with the permission from Shen et al. (2013). Copyright (2013) American Chemical Society

fleet and reductions in both gas mileage and EF_{PAH} would finally reach a balance (Shen et al. 2011), followed by a declining trend in PAH emissions.

After continuous increases in PAH emissions for decades, the PAH emissions from residential, commercial, and industrial sources in developing countries started to slowly decrease around 1995. As a result, the total PAH emission from developing countries reached its peak around 1995. The main reasons for this decrease include the promotion of centralized heating systems (IEA 2002), replacement of residential coal cooking stoves with natural gas stoves in large and median cities (National Bureau of Statistics of China 2011a), dissemination of improved biomass cookstoves in rural households (Barnes et al. 1994), and the phasing out of beehive coke ovens in China (Coal Law 1996). The global PAH emission reached its peak of 869 Gg in 1978 and gradually decreased afterward. The global peak time came out a little later than the one in developed countries as a result of the rapid increase in developing countries.

4.3.5 Future Time Trends

The annual PAH emissions of individual countries/territories from 2009 to 2030 were simulated using the six IPCC SRES scenarios (Nakićenović et al. 2000). These results are shown in Fig. 4.18 for the global, developed, and developing countries. The uncertainty in these predictions is relatively large because the fuel consumption predictions are not accurate and the changes in EF_{PAHs} and technology splitting fractions can be affected by the changes in socioeconomic development. Even with this significant uncertainty, decreasing trends in PAH emissions are expected in both developed (46–71 % decrease by 2030 compared with 2008) and developing countries (48–64 % decrease by 2030 compared with 2008). A slower decrease in global PAH emissions was associated with the A2 scenario, which described a heterogeneous world with slower technology diffusion (Nakićenović et al. 2000).

In 2007, PAH emissions from residential sources contributed 67.4 % of the global total and a significant reduction in PAH emission in the future will be achieved by taking effective mitigation measures in this sector. Based on the A1 scenario, 34 % of the reduction in PAH emission can be achieved by 2030 due to the optimization of the energy structure in residential consumption (108 Gg) and improvement of residential devices (70 Gg). Moreover, the relatively high percentage of carcinogenic PAH emissions and the close proximity to residents will make the effort in the residential sector more effective in terms of health implications. Unlike industrial and transportation sources, PAH emissions from the residential sector are primarily from millions of residential stoves. Because of this, socioeconomic development is critical in PAH emission mitigation instead of technology development. In China, the percentage of urban population has increased from 36.2 to 51.3 % during the past decade (Infobank 2011). This rapid urbanization has been leading to an extensive change in the ways of energy use in China. Millions of former rural residents have gotten rid of biomass fuel stoves, and the younger generations in rural Eastern China also have started to use electricity and liquid natural gas (National Bureau of Statistics of China 2011a, b). This is one of the major driving forces causing the decrease in PAH emissions in the future projections across all of the IPCC SRES scenarios (Nakićenović et al. 2000). In addition, environmental policy also plays a key role in PAH emission reduction. Rapid decreases in PAH emissions from on-road motor vehicles and industrial processes in developed countries since the early 1970s were due to the promulgation and implementation of a series of legislations which drove the development of energy saving and emission abatement technologies (EEA 2012). Similar legislation occurred in developing countries years later. An example was the implementation of the Coal Law in China in 1996, which banned the use of beehive coke ovens (Coal Law 1996; Yang 2004). Almost all beehive coke ovens have been phased out over the past decade, resulting in a total PAH emission reduction of 18.2 Gg. In the future, legislation on emission abatement in the transportation sector will benefit the developing world. A total reduction of 74 Gg PAH emissions in this sector was estimated by 2030, based on the A1 scenario. Also, the promotion of

cleaner burning fuels such as liquefied petroleum gas, biogas, and pellet biomass fuel (USEPA 1998) in rural areas in developing countries will help to reduce PAH emissions significantly. Both regulations and economic incentives can play important roles in reducing future PAH emissions.

In developing countries, education and risk communication are also important in terms of reducing the PAH emissions from solid fuel burning. Most rural residents are unaware of the potential adverse health effects of PAHs, preventing them from taking the initiative to reduce emissions. For example, open burning of garbage in the household yard is still a common practice in rural China (United Nations Environment Programme 2010), and solid fuel stoves without chimneys can still be seen in poor countries (Click Green 2012). Educating rural primary school students on the health impacts of residential solid fuel combustion can be an inexpensive and effective way to reduce PAH emissions in these countries.

4.4 Summary

In this chapter, global atmospheric emissions of 16 polycyclic aromatic hydrocarbons (PAHs) from 69 major sources were estimated for a period from 1960 to 2030. Regression models and a technology split method were used to estimate country- and time-specific emission factors, resulting in a new estimate of PAH emission factor variation among different countries and over time. PAH emissions in 2007 were spatially resolved to $0.1^\circ \times 0.1^\circ$ grids based on a newly developed global high-resolution fuel combustion inventory (PKU-FUEL-2007). The global total annual atmospheric emission of 16 PAHs in 2007 was 655 Gg (521–816 Gg, as interquartile range), with residential/commercial biomass burning (52.4 %), open-field biomass burning (agricultural waste burning, deforestation, and wildfire, 12.5 %), and petroleum consumption by on-road motor vehicles (16.5 %) as the major sources. South, East, and Southeast Asia were the regions with the highest PAH emission densities, contributing half of the global total PAH emissions. Among the global total PAH emissions, 7.7 % of the emissions were in the form of high molecular weight carcinogenic compounds and the percentage of the carcinogenic PAHs was higher in developing countries (8.0 %) than in developed countries (6.4 %), due to the differences in energy structures and the disparities of technology. The potential health impact of the PAH emissions was greatest in the parts of the world with high anthropogenic PAH emissions, because of the overlap of the high emissions and high population densities. Global total PAH emissions peaked at 869 Gg in 1978 and declined gradually to 624 Gg in 2008. Total PAH emissions from developed countries peaked at 261 Gg in the early 1970s and decreased to 51 Gg in 2008. Emissions from developing countries peaked at 663 Gg in the early 1990s and decreased slowly to 558 in 2008. Simulation of PAH emissions from 2009 to 2030 revealed that PAH emissions in developed and developing countries would decrease by 46–71 % and 48–64 %, respectively, based on the six IPCC SRES scenarios.

References

- Asian Development Bank (ADB) (2003). *Reducing vehicle emissions in Asia*. Manila, Philippines, pp. 14–22.
- Baek, S. O., Field, R. A., Goldstone, M. E., Kirk, P. W., Lester, J. N., & Perry, R. (1991). A review of atmospheric polycyclic aromatic hydrocarbons: sources, fate and behavior. *Water, air, and soil pollution*, 60(3–4), 279–300.
- Barnes, D. F., Openshaw, K., Smith, K. R., & van der Plas, R. (1994). *What makes people cook with improved biomass stoves? A comparative international review of stove programs*. Washington: The World Bank.
- Bergvall, C., & Westerholm, R. (2009). Determination of highly carcinogenic dibenzopyrene isomers in particulate emissions from two diesel- and two gasoline-fuelled light-duty vehicles. *Atmospheric Environment*, 43(25), 3883–3890.
- Cadle, S. H., Mulawa, P. A., Hunsanger, E. C., Nelson, K., Ragazzi, R. A., Barrett, R., et al. (1999). Composition of light-duty motor vehicle exhaust particulate matter in the Denver. *Colorado Area Environmental Science & Technology*, 33(14), 2328–2339.
- Chellam, S., Kulkarni, P., & Fraser, M. P. (2005). Emissions of organic compounds and trace metals in fine particulate matter from motor vehicles: A tunnel study in Houston, Texas. *Journal of the Air and Waste Management Association*, 55(1), 60–72.
- China Association of Automobile Manufactures (CAAM). (2008). *China automotive industry yearbook*. Tianjin, China: China Automotive Industry Yearbook House.
- Click Green. (2012). *Cooking stoves in developing nations*. <http://www.clickgreen.org.uk/research/data/122800-cooking-stoves-in-developing-nations-linked-to-pneumonia.html>.
- Dargay, J., Gately, D., & Sommer, M. (2007). Vehicle ownership and income growth, worldwide: 1960–2030. *Energy Journal*, 28, 143–170.
- De Abrantes, R., De Assuncao, J. V., & Pesquero, U. R. (2004). Emission of polycyclic aromatic hydrocarbons from light-duty diesel vehicles exhaust. *Atmospheric Environment*, 38(11), 1631–1640.
- Ding, J. N., Zhong, J. J., Yang, Y. F., Li, B. G., Shen, G. F., Su, Y. H., et al. (2012). Occurrence and exposure to polycyclic aromatic hydrocarbons and their derivatives in a rural Chinese home through biomass fuelled cooking. *Environmental Pollution*, 169, 160–166.
- Durbin, T. D., Truex, T. J., & Norbeck, J. M. (1998). *Particulate measurements and emissions characterization of alternative fuel vehicle exhaust*. National Renewable Energy Laboratory, Golden, Colorado, NREL/SR-540-25741.
- Environment Australia (EA) (2003). *Technical report No. 1: Toxic emissions from diesel vehicles in Australia*. Retrieved from <http://www.environment.gov.au/atmosphere/airquality/publications/report1/index.html>.
- Environment Canada. (2010). *National pollutant release inventory*. Retrieved from <http://www.ec.gc.ca/inrp-npri/default.asp?lang=%4En&n%0EC58C98e1>.
- European Environment Agency (EEA) (2010). *National emissions reported to the convention on long-range transboundary air pollution (LRTAP Convention)*. Retrieved from <http://www.eea.europa.eu/data-and-maps/data/national-emissions-reported-to-the-convention-on-long-range-transboundary-air-pollution-lrtap-convention-4>.
- European Monitoring and Evaluation Programme (EMEP) (2011). *Centre on emission inventories and projections*. Retrieved from <http://www.ceip.at>.
- European Monitoring and Evaluation Programme (EMEP) (2012). *EMEP POP data*. Retrieved from <http://www.nilu.no/projects/ccc/emepdata.html>.
- Galarneau, E., Makar, P. A., Sassi, M., & Diamond, M. L. (2007). Estimation of atmospheric emissions of six semivolatile polycyclic aromatic hydrocarbons in southern Canada and the United States by use of an emissions processing system. *Environmental Science and Technology*, 41(12), 4205–4213.

- Grieshop, A. P., Lipsky, E. M., Pekney, N. J., Takahama, S., & Robinson, A. L. (2006). Fine particle emission factors from vehicles in a highway tunnel: effects of fleet composition and season. *Atmospheric Environment*, 40, S287–S298.
- Infobank. (2011). *China content provider*. Retrieved from <http://www.bjinfobank.com>.
- Intergovernmental Panel on Climate Change (IPCC) (2001). *Climate Change 2001: The Scientific Basis*. Contribution of Working Group I to the Third Assessment Report of the Intergovernmental Panel on Climate Change (IPCC). New York: Cambridge University Press.
- International Energy Agency. (2011). *IEA world energy statistics and balances*. Retrieved from <http://www.oecd-ilibrary.org/statistics>.
- International Energy Agency (IEA) (2002). *District heating and cooling: Environmental technology for the 21st century*. Retrieved from <http://www.iea-dhc.org/download/Policy%20paper%20District%20Heating%20in%20the%2021st%20century%22FINAL.pdf>.
- Kado, N. Y., Okamoto, R. A., Kuzmicky, P. A., Kobayashi, R., Ayala, A., Gebel, M. E., et al. (2005). Emissions of toxic pollutants from compressed natural gas and low sulfur diesel-fueled heavy-duty transit buses tested over multiple driving cycles. *Environmental Science and Technology*, 39(19), 7638–7649.
- Kristensson, A., Johansson, C., Westerholm, R., Swietlicki, E., Gidhagen, L., Wideqvist, U., et al. (2004). Real-world traffic emission factors of gases and particles measured in a road tunnel in Stockholm. *Sweden Atmospheric Environment*, 38(5), 657–673.
- Law of the People's Republic of China on the Coal Industry. (1996). Order of the president of the people's republic of China, No. 75.
- Leonidas, N., & Zissis, S. (2000). *COPERT III, Computer programme to calculate emissions from road transport* (pp. 76–77). Copenhagen: European Environment Agency.
- Madhukar, S., & Nagarjuna, B. (2011). Inflation and growth rates in India and China: A perspective of transition economies. *2011 International Conference on Economics and Finance Research*, Singapore.
- Menichini, E., Belladonna, V., Bergoglio, F., Gabrieli, C., Ceccanti, M., Rossi, I., et al. (2006). Trend of atmospheric benzo(a)pyrene in Italy before the adoption of the European directive on PAHs. *Polycyclic Aromatic Compounds*, 26, 79–92.
- Nakićenović, N., Alcamo, J., Davis, G., Vries, B. D., Fenhann, J., Gaffin, S., et al. (2000). *Emissions scenarios: A special report of working group iii of the inter-governmental panel on climate change*. New York: Cambridge University Press.
- National Atmospheric Emissions Inventory (NAEI) (2011). Retrieved from http://naei.defra.gov.uk/data_warehouse.php.
- National Bureau of Statistics of China. (2011a). *China energy statistical yearbook 2010*. Beijing: China Statistics Press.
- National Bureau of Statistics of China. (2011b). *China statistical yearbook 2011*. Beijing: China Statistics Press.
- Nelson, P. F., Tibbett, A. R., & Day, S. J. (2008). Effects of vehicle type and fuel quality on real world toxic emissions from diesel vehicles. *Atmospheric Environment*, 42(21), 5291–5303.
- Newgeography. (2012). China's urbanization: It has only just begun. Retrieved from <http://www.newgeography.com/content/001906-china%E2%80%99surbanization-it-has-only-just-begun>.
- Nisbet, I. C. T., & LaGoy, P. K. (1992). Toxic equivalency factors (TEFs) for polycyclic aromatic hydrocarbons (PAHs). *Regulatory Toxicology Pharmacology*, 16, 290–300.
- Oak Ridge National Laboratory (ORNL) (2014). *LandScan global population 2007 database*. Retrieved from <http://www.ornl.gov/sci/landscan/>.
- Pacyna, J. M., Breivik, K., Munch, J., & Fudala, J. (2003). European atmospheric emissions of selected persistent organic pollutants, 1970–1995. *Atmospheric Environment*, 37, S119–S131.
- Paturel, L., Saber, A.-I., Combet, E., & Joumard, R. (1996). Analysis of PAH emissions from passenger cars by high resolution shpol'skii spectrofluorometry. *Polycyclic Aromatic Compounds*, 9, 331–339.
- Ravindra, K., Sokhi, R., & Van Grieken, R. (2008). Atmospheric polycyclic aromatic hydrocarbons: Source attribution, emission factors and regulation. *Atmospheric Environment*, 42(13), 2895–2921.

- Riddle, S. G., Jakober, C. A., Robert, M. A., Cahill, T. M., Charles, M. J., & Kleeman, M. J. (2007). Large PAHs detected in fine particulate matter emitted from light-duty gasoline vehicles. *Atmospheric Environment*, 41(38), 8658–8668.
- Schauer, C., Niessner, R., & Poschl, U. (2003). Polycyclic aromatic hydrocarbons in urban air particulate matter: Decadal and seasonal trends, chemical degradation, and sampling artifacts. *Environmental Science and Technology*, 37, 2861–2868.
- Schauer, J. J., Kleeman, M. J., Cass, G. R., & Simoneit, B. R. T. (1999). Measurement of emissions from air pollution sources. 2. C-1 through C-30 organic compounds from medium duty diesel trucks. *Environmental Science & Technology*, 33(10), 1578–1587.
- Shen, H. Z., Huang, Y., Wang, R., Zhu, D., Li, W., Shen, G., et al. (2013). Global atmospheric emissions of polycyclic aromatic hydrocarbons from 1960 to 2008 and future predictions. *Environmental Science and Technology*, 47, 6415–6424.
- Shen, H. Z., Tao, S., Wang, R., Wang, B., Shen, G. F., Li, W., et al. (2011). Global time trends in PAH emissions from motor vehicles. *Atmospheric Environment*, 45, 2067–2073.
- Timilsina, G. R., & Dulal, H. B. (2009). A review of regulatory instruments to control environmental externalities from the transport sector. *The World Bank*. WPS4867.
- United Nations Environment Programme. (2010). *Hazardous chemicals from open burning of waste in developing countries, final report*. Retrieved from http://www.chem.unep.ch/Pops/pccd_activities/projects/hazardous%20chemicals%20from%20open%20burn%20of%20waste_final%20report%202010.pdf.
- United States Environmental Protection Agency (USEPA) (1998). *Locating and estimating air emission from sources of polycyclic organic matter*. Retrieved from EPA-454/R-98-014. <http://www.epa.gov/ttn/chief>.
- United States Environmental Protection Agency (USEPA) (1999). *The history of reducing tailpipe emissions*. EPA420-F-99-017.
- United States Environmental Protection Agency (USEPA) (2011). *Clearinghouse for Inventories & Emissions factors*. Retrieved from <http://www.epa.gov/ttn/chief/index.html>.
- Valerio, F., Stella, A., Pala, M., Balducci, D., Piccardo, M. T., & Cipolla, M. (2009). The effect of EURO-0 vehicle substitution on polycyclic aromatic hydrocarbon and carbon monoxide concentrations in an urban area. *Atmospheric Environment*, 43, 1520–1526.
- Wang, R., Tao, S., Ciais, P., Shen, H. Z., Huang, Y., Chen, H., et al. (2013). High-resolution mapping of combustion processes and implications for CO₂ emissions. *Atmospheric Chemistry and Physics*, 13(10), 5189–5203.
- Westerholm, R., & Li, H. (1994). A multivariate statistical-analysis of fuel-related polycyclic aromatic hydrocarbon emissions from heavy-duty diesel vehicles. *Environmental Science and Technology*, 28(5), 965–972.
- Westerholm, R., Almen, J., Li, H., Rannug, U., & Rosen, A. (1992). Exhaust emissions from gasoline-fueled light duty vehicles operated in different driving conditions - a chemical and biological characterization. *Atmospheric Environment Part B*, 26(1), 79–90.
- Westerholm, R., Christensen, A., & Rosen, A. (1996). Regulated and unregulated exhaust emissions from two three-way catalyst equipped gasoline fuelled vehicles. *Atmospheric Environment*, 30(20), 3529–3536.
- Westerholm, R., Christensen, A., Tornqvist, M., Ehrenberg, L., Rannug, U., Sjogren, M., et al. (2001). Comparison of exhaust emissions from Swedish environmental classified diesel fuel (MK1) and European Program on Emissions, Fuels and Engine Technologies (EPEFE) reference fuel: A chemical and biological characterization with viewpoints on cancer risk. *Environmental Science and Technology*, 35(9), 1748–1754.
- Wingfors, H., Sjodin, A., Haglund, P., & Brorstrom-Lunden, E. (2001). Characterisation and determination of profiles of polycyclic aromatic hydrocarbons in a traffic tunnel in Gothenburg, Sweden. *Atmospheric Environment*, 35(36), 6361–6369.
- Xu, S. S., Liu, W. X., & Tao, S. (2006). Emission of polycyclic aromatic hydrocarbons in China. *Environmental Science and Technology*, 40(3), 702–708.
- Yang, A. (2004). *Striking at the root of indigenous cooking in Shanxi*. People's Daily.

- Zhang, K. H. L., & Song, S. F. (2003). Rural-urban migration and urbanization in China: Evidence from time-series and cross-section analyses. *China Economic Review, 14*, 386–400.
- Zhang, Y. X., & Tao, S. (2009). Global atmospheric emission inventory of polycyclic aromatic hydrocarbons (PAHs) for 2004. *Atmospheric Environment, 43*(4), 812–819.
- Zhang, Y. X., Tao, S., Cao, J., & Coveney, R. M. (2007). Emission of polycyclic aromatic hydrocarbons in China by county. *Environmental Science and Technology, 41*(3), 683–687.

Chapter 5

Global Atmospheric Transport Modeling of benzo[*a*]pyrene

Based on the PKU-PAHs emission inventory, global atmospheric transport of benzo[*a*]pyrene was simulated with consideration of its major environmental behaviors including gas-particle partitioning, air degradation, dry/wet deposition, and air-surface exchange. A BaP module was incorporated into MOZART-4 (The Model for Ozone and Related Chemical Tracers, version 4). Near-surface concentrations were obtained from the model performance. Previous studies have shown that model performance with coarse resolution tends to underestimate concentrations near emission sources (Zhang et al. 2009; Wang et al. 2014). Large concentration variation can be expected within individual model grids, while areas close to emission sources exhibit higher levels in a specific grid. For PAH compounds, given the observed correlation between population densities and contamination levels, direct use of the model results would result in an underestimate of the overall population exposure level. Therefore, a downscaling process is needed to derive concentrations at a finer resolution. In this study, based on the highly resolved emission inventory, Gauss diffusion equation was applied to downscale the model results to $0.1^\circ \times 0.1^\circ$ resolution. The downscaling method accounts for meteorology condition and degradation rate. Comparing with observation, the concentrations after being downscaled represent better agreement than direct model results do. The downscaling process, model validation, and global BaP concentration distributions were described in this chapter.

5.1 Model Validation

As a class of trace organic pollutants, PAH observations reported by literatures are limited. Most observations were conducted in developed countries as well as in China and in India. Based on a thorough literature review, a database of BaP

observations was compiled including a total of 236 non-background sites and 18 background sites. Non-background sites were all close to emission sources, and most of them were located in urban areas. These sites were highly affected by nearby sources, which cannot be captured by global transport models due to coarse resolution. Background sites were those far from emission areas, such as the Alert site in the Canadian High Arctic. BaP at background sites was mainly from long-range transport which can be accurately captured by transport models with the consideration of necessary environmental behaviors.

5.1.1 Validation at Background Sites

Observation data at background sites were collected from Europe, USA, and the Canadian High Arctic (EMEP 2012; Friedman et al. 2013; Wang et al. 2010). The site distributions are shown in Fig. 5.1a. These data were directly compared with model simulation (see, Fig. 5.2). However, except the Alert and the Spitsbergen sites, other background sites are still located in the model grids where emission activity occurs. Therefore, grid concentrations are reasonably higher than the site measurement. Generally, the model simulation agrees well with observation at background sites. Observed time series were also compared with modeled results (see Fig. 5.3). It can be found that the model can simulate the temporal variation of BaP concentrations well. Higher concentrations were found in winter due to higher emissions, slower air degradation, and stable boundary condition.

Observation at Kosetice site has higher temporal resolution (once a week). Good agreement between weekly observation and modeled simulation can be found at this site (see Fig. 5.3a). Given that only monthly variations of emissions were considered in the model, the modeled fluctuation of concentrations within a month cannot be raised by emissions. At remote sites such as Kosetice, meteorological factors tend to control variation of local BaP levels. However, a large fraction of BaP represents particle phase in the air. Wet deposition is an efficient pathway to wash out BaP during long-range transport. OH degradation is also an important process, which significantly influences long-range transport capacity in the high-latitude areas.

In this study, the model simulation agrees well with observation at the Alert site in the Canadian High Arctic (see, Fig. 5.3g, h). Both concentrations and gas/particle rates are well represented in the model. This is exciting, since the contamination levels in the Arctic area are always difficult to be simulated. A successful simulation depends on both accurate estimates of emissions in the northern hemisphere and proper incorporation of critical processes during long-range transport. The validation indicates that the model can be applied to evaluate transboundary transport among continents which is widely concerned by researchers and governments.

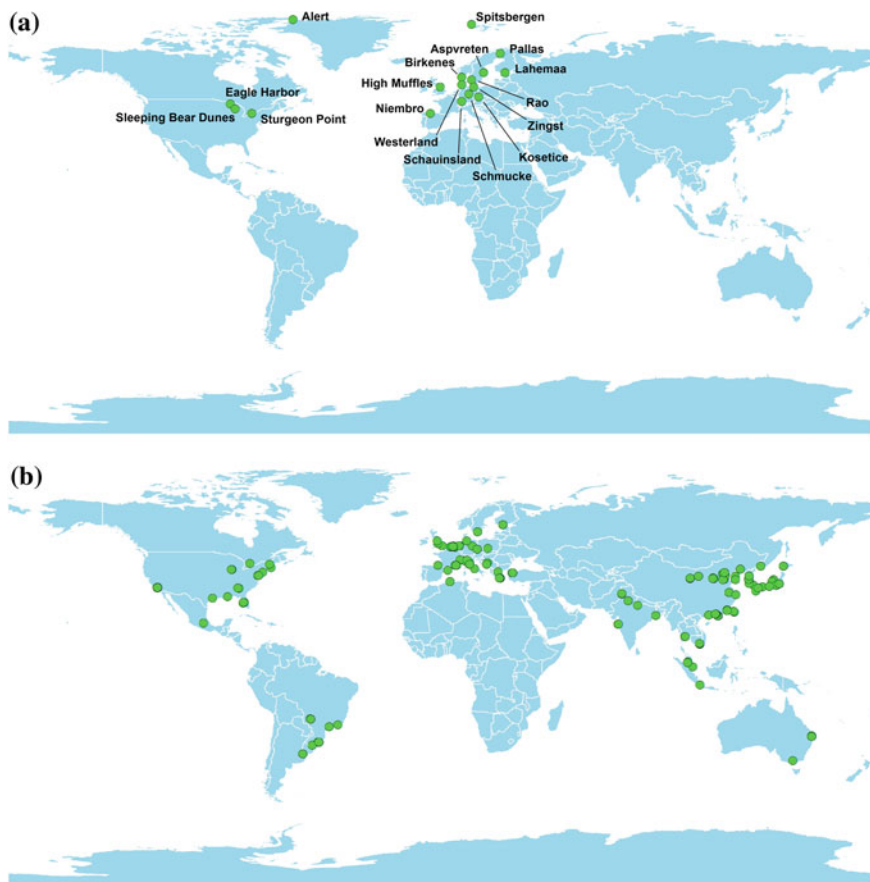


Fig. 5.1 Locations of background and non-background sites applied for model validation. **a** Locations of background sites. **b** Location of non-background sites. Reprinted with the permission from Shen et al. (2014). Copyright (2014) Nature Publishing Group

5.1.2 Validation at Non-background Sites

Locations of non-background sites applied for model validation are demonstrated in Fig. 5.1b. Due to the scale mismatch, model grid concentrations tend to be lower than observations at non-background sites. This kind of mismatch is clearly illustrated in Fig. 5.4, as the high-emission areas are often intensive and only occupy a small part of the model grid. Since the lifetime of BaP is relatively short, spatial variation of emissions in a model grid is believed to highly affect the variation of BaP concentration in this model grid. To address the concentration variation within the model grids, we develop a downscaling method based on wind information and a high-resolution emission inventory, as is described in detail below. Finally, the model concentrations at non-background sites were downscaled to $0.1^\circ \times 0.1^\circ$.

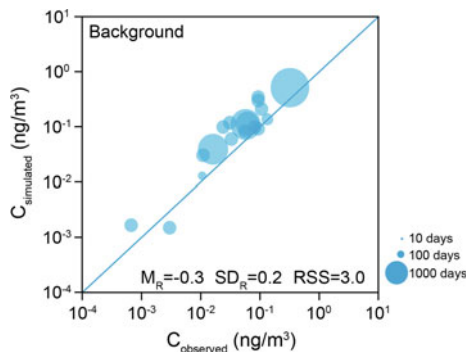


Fig. 5.2 Validation of the model calculated near-surface BaP concentrations against observations at 18 background sites. Residuals are defined as the differences between log-transformed observations and calculations, and the calculated means (M), standard deviations (SD), and square sums (RSS) of residuals are listed in the figure. Reproduced with the permission from Shen et al. (2014). Copyright (2014) Nature Publishing Group

The method takes both emission (source) and wind (dispersion) into consideration to downscale $1.875^\circ \times 1.895^\circ$ model grid BaP concentrations into higher resolution grid cells. Since this method is carried out at a global scale, efforts were made to simplify the calculation processes. The simplest way to get a higher resolution distribution from model grids is to conduct downscaling directly using a higher resolution emission inventory as weighting factors (Zhang et al. 2009; Wang et al. 2014). This method assumes that grid concentrations are proportional to grid emissions raised by a certain exponent and so neglects the influence of transport among emission grids. To address this influence, this study used the Gauss diffusion formula to illustrate the long-term diffusion distribution of BaP from each emission grid. To simplify the calculation, Gauss diffusion formula was reduced to the following approximate expression (Shen 1987):

$$q(x, i) = \sum_j \sum_k \sqrt{\frac{2}{\pi}} \frac{Q f_{ijk}}{\bar{u}_{ik} \sigma_{zk} \left(\frac{2\pi x}{16}\right)} \exp\left(-\frac{H_{jk}^2}{2\sigma_{zk}^2}\right),$$

Wind is classified into 16 directions. i, j, k are subscripts representing wind direction, wind speed, and stability level, respectively; q is the concentration at the receiving point, ng/m^3 ; Q is the emission intensity in units of ng/s ; x is the distance from the emission point to the receiving point in units of m , and, for emission point itself, x is set to be one-eighth of its perimeter; f_{ijk} is the wind frequency at certain wind direction and wind speed under certain air stability level; \bar{u} is the average wind speed, m/s ; H is the emission effective height, m ; σ_z is the vertical standard deviation, m . σ_z can be calculated using the following equation (Sørensen 1998),

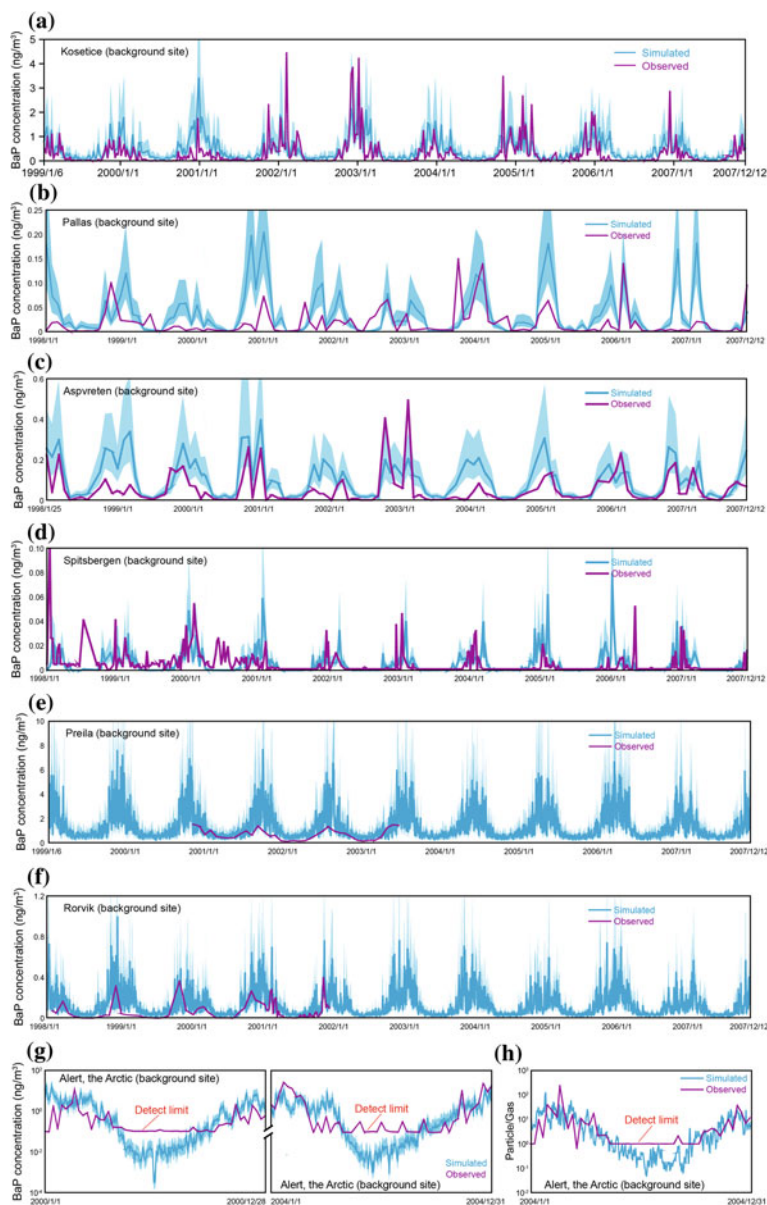


Fig. 5.3 Validation of time series both the model calculated near-surface BaP concentrations and observations. **a–g** The calculated and observed concentrations are shown as *blue* and *purple* lines, respectively. The model calculations at background sites were not downscaled. The model uncertainties as 95 % confidence intervals are shown by shaded areas. **h** Comparison of the time series of the particle/gas partitioning at Alert site. Reproduced with the permission from Shen et al. (2014). Copyright (2014) Nature Publishing Group

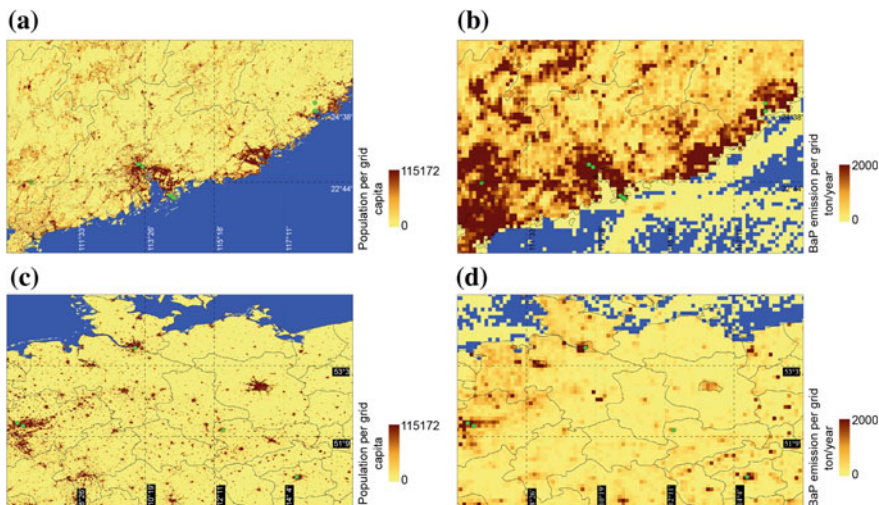


Fig. 5.4 Locations of some typical non-background sites. Each figure contains fifteen 1.875° (longitude) \times 1.895° (latitude) model grids of which the borders are drawn using black dashed lines. The site locations are marked as green points. **a** $30''$ spatial resolved population map of the south coastal region of China. **b** $0.1^\circ \times 0.1^\circ$ BaP emission inventory at the same area of **a**. **c** The population map of part of Central Europe (mainly Germany). **d** BaP emission inventory at the same area of **c**. It can be observed that the population density and BaP emission vary widely within the model grids, and most observation sites are located close to intensively emitted areas at the model grid scale, leading to an underestimation of model grid concentrations compared to observation. Reprinted with the permission from Shen et al. (2014). Copyright (2014) Nature Publishing Group

$$\sigma_z^2 = 2K_z t_L \left\{ \tau - (1 - e^{-\tau}) - \frac{1}{2}(1 - e^{-\tau})^2 \right\},$$

where K_z is the vertical eddy diffusivity; t_L is the Lagrangian timescale of atmospheric turbulence; τ is the travel time in units of t_L ($\tau = t/t_L$). Values of $1 \text{ m}^2/\text{s}$ and $1 \times 10^4 \text{ s}$ are used for K_z and t_L , respectively, on a global scale (Sørensen 1998). To further simplify the calculation, the effective height, H , is set be zero, and seasonal wind frequency and average speed at a certain direction is counted under all atmospheric stability classes. To account for BaP air degradation during the transport from emission point to receiving point, spatial distribution of BaP lose rates in the air was introduced based on MOZART-4 simulation. The final equation is expressed as follows:

$$q(x, i) = \frac{2.03Qf_i}{\bar{u}\sigma_{z,x}} \exp(-r_{\text{lose}}t) \quad (5.1)$$

where r_{lose} is the BaP lose rate, s^{-1} , derived from MOZART-4 with spatial and seasonal variations; t is the transport time, s. Equation (5.1) was used to conduct the downscaling for global BaP concentrations from $1.875^\circ \times 1.895^\circ$ model grid cells into $0.1^\circ \times 0.1^\circ$ grid cells based on PKU-PAH emission inventory. For each model grid, information on wind speeds and frequencies was derived from MOZART-4 wind field. Seasonal wind rose maps of a specified model grid are illustrated in Fig. 5.5a. To carry out the downscaling for this model grid, its surrounding eight model grids are added as a buffer area, assuming that effects of emissions out of this area can be neglected. At the $0.1^\circ \times 0.1^\circ$ resolution, seasonal mean concentration distribution of BaP emitted from a single emission grid can be allocated to the whole area as an effect layer based on Eq. (5.1) (Fig. 5.5b). Effect layers of every emission grid within the 3×3 model grids are calculated and spatially superimposed under the $0.1^\circ \times 0.1^\circ$ resolution (Fig. 5.5c, d). Cut off the buffer area, a map of weighting factors for the grid downscaling is generated. BaP concentration of each $0.1^\circ \times 0.1^\circ$ grid (Fig. 5.5f) is derived from model grid concentration (Fig. 5.5e) multiplied by the $0.1^\circ \times 0.1^\circ$ grid weight divided by average model grid weight (Fig. 5.5d). The global distribution of BaP concentrations can be illustrated by repeating the processes above for all model grids (Fig. 5.6).

For air pollutants with sufficient global surface measurements and remote sensing, regression analysis to combine these data with air transport models is the primary choice to carry out downscaling processes (Brauer 2012). For regional simulations, chemical transport models with higher resolution are preferred, and thus the downscaling method is not necessary. Otherwise, the downscaling method provided in this study has a broad suitability. In the air, most compounds are significantly influenced by emission sources, while emissions varied at a much finer resolution so that global models fail to simulate. The spatial mismatch between model simulation and emission variation directly leads to underestimate near source areas. The downscale method actually reallocates the spatial distribution within a model grid so that the variation affected by emissions can be represented. At the beginning of the evaluation, three different methods was used to downscale the BaP concentrations, including: (1) downscaling directly based on high-resolution emission inventory; (2) downscaling based on high-resolution emission inventory and Gauss diffusion equation as mentioned above; and (3) downscaling with Aerosol Optical Depth (AOD) (Levy et al. 2007). Residues between observation and simulation were obtained using these three different methods separately. Means (M) and standard variations (SD) of residues were calculated. The method using a combination of emission inventory and Gauss diffusion equation represented the optimal validation results (M = -0.06, SD = 0.45), while direct use of emission inventory led to overestimation (M = -0.13, SD = 0.43). Downscaling with AOD significantly underestimated the concentrations (M = 0.57) with the largest uncertainty (SD = 0.64). According to the analysis, the combined method considering

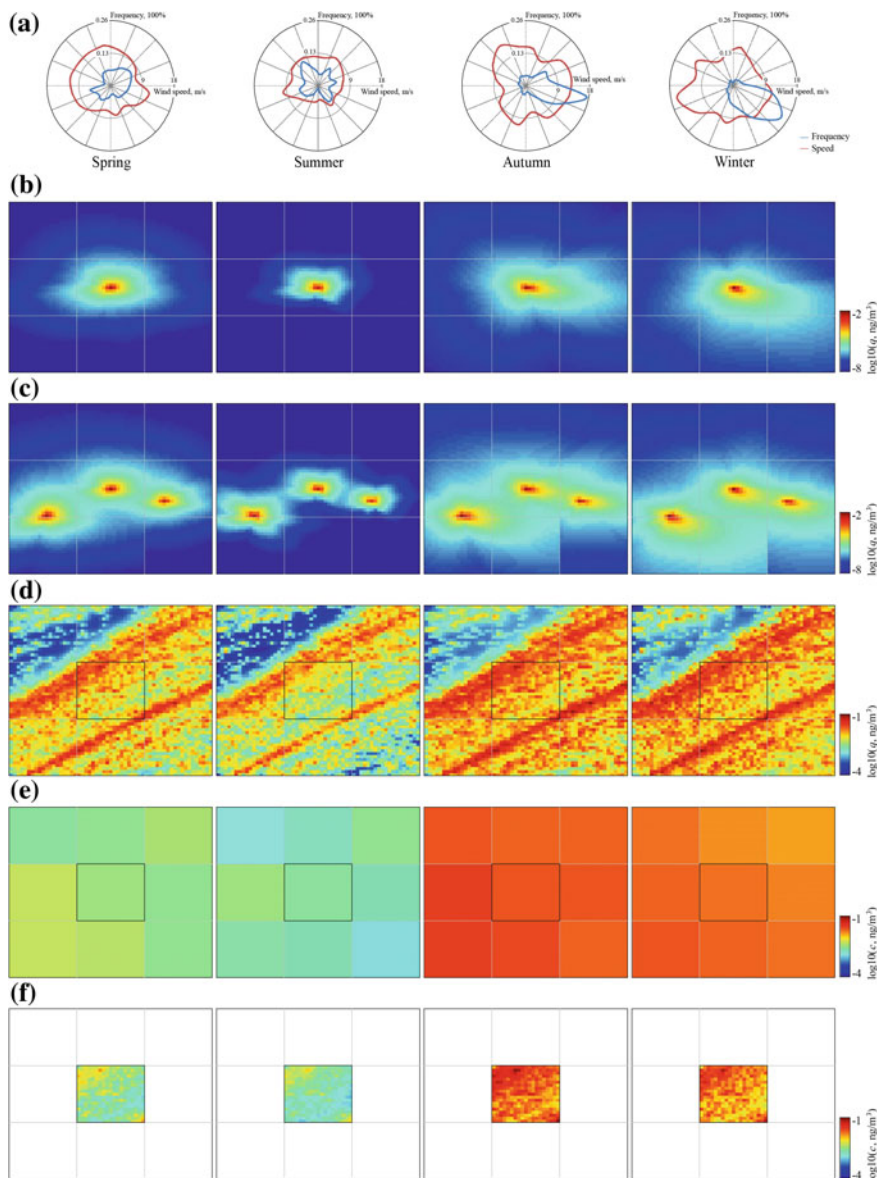


Fig. 5.5 Downscaling processes using Gaussian diffusion formula. **a** Seasonal wind rose maps of a specific model grid. **b** Seasonal diffusion distribution of BaP emitted from an emission grid within this model grid, which is defined as an effect layer of this emission grid. Nine model grids are shown in each map. The one in the middle is the specified model grid for interpolation. Surrounding grids are employed as a buffer area. **c** The process of adding effect layers of other emission grids into the map, including those in the buffer area. **d** The seasonal maps of weighting factors by adding all effect layers together. **e** Model grid seasonal mean BaP concentrations from MOZART-4. **f** Downscaled BaP concentrations at $0.1^\circ \times 0.1^\circ$ resolution. Reproduced with the permission from Shen et al. (2014). Copyright (2014) Nature Publishing Group

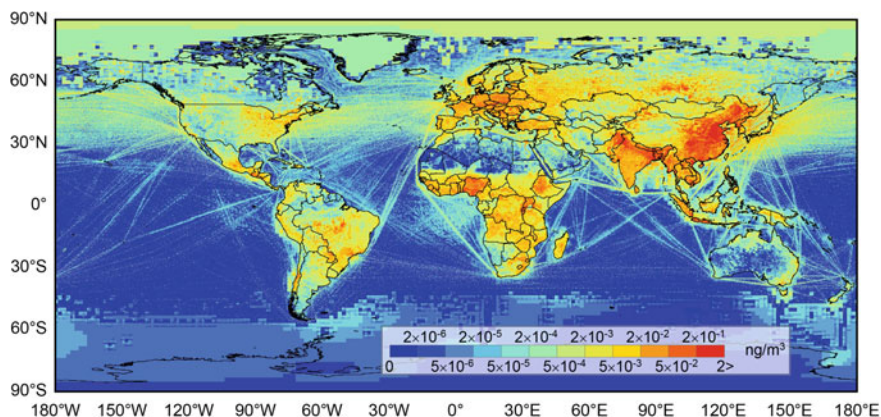


Fig. 5.6 Geographical distributions of $0.1^\circ \times 0.1^\circ$ downscaled BaP concentrations in 2007

both emission and diffusion processes was adopted. In addition, this method is not limited to observation (such as satellite observation) and thus can be used to evaluate the concentration distribution from individual emission sources which benefits the source-specified health assessment in the following study.

Non-background site validation before and after downscaling is shown in Fig. 5.7. It is shown that downscaling process increases the concentrations at

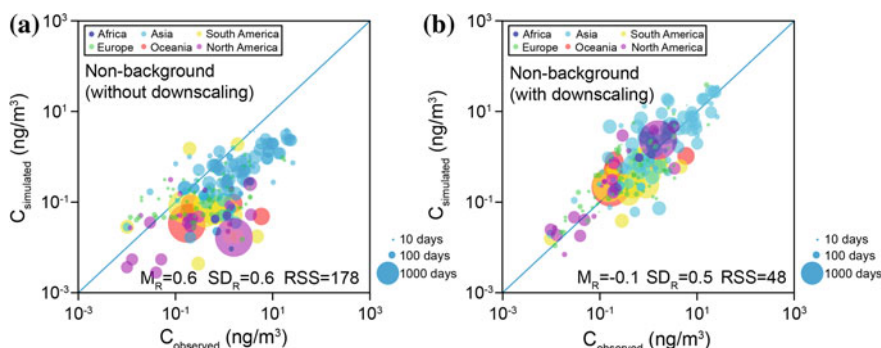


Fig. 5.7 Validation of the model calculated near-surface BaP concentrations against observations at 236 non-background sites without (a) and with downscaling (b), respectively. Sites in different regions are marked with different colors. The areas of the bubbles are proportional to observation durations, so more reliable observations are carried in larger bubbles. 1:1 lines are drawn in blue. Residuals are defined as the differences between log-transformed observations and calculations, and the calculated means (M), standard deviations (SD), and square sums (RSS) of residuals are listed in the figure. Reproduced with the permission from Shen et al. (2014). Copyright (2014) Nature Publishing Group

non-background sites, resulting in a better validation. The sum of residues (RSS) decreased from 177.9 to 48.2 on the log-transformed scale, and the standard variation of residues decreased from 0.62 to 0.45. Notably, in Fig. 5.7, the areas of the bubbles are proportional to observation durations. Large bubbles are generally close to the 1:1 line indicating that long-term model performance tends to provide more reliable results, since short-term observation may be affected by emission fluctuation which cannot be captured by monthly emission inventory. Observation in different world regions is marked by different colors. Both observation and simulation highlight the higher BaP concentrations in Asia, while lower concentrations in Europe and North America. Reprinted with the permission from Shen et al. (2014). Copyright (2014) Nature Publishing Group.

Except for the scatter diagram, model performance was also validated in terms of time series based on observation at two rural sites in Germany. Concentrations were measured every three days. Three-year measurement can be obtained during the model period. The comparison results are shown in Fig. 5.8. Modeled concentration levels agree perfectly with observation at these two sites. Also, the temporal variability can be successfully captured.

The validation shows that the model results after downscaled can simulate BaP concentrations well at non-background sites which is often located in populated areas. The analysis in the previous section indicates the potential capacity in using model performance to evaluate the transboundary pollution, while this section demonstrates that the model combined with downscaling method can be also applied to assess human exposure and health impact.

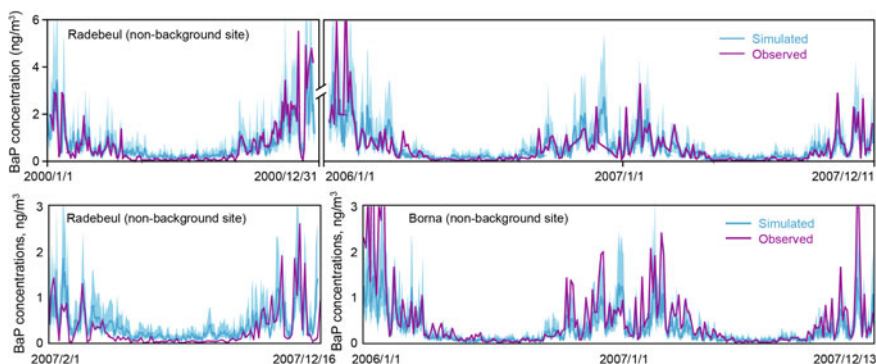


Fig. 5.8 Validation of time series between the model calculated near-surface BaP concentrations and observations at non-background sites. The model results are downscaled. The modeled and observed concentrations are shown as blue and purple lines, respectively. Uncertainties as 95 % confidence intervals are shown by shaded areas. Reproduced with the permission from Shen et al. (2014). Copyright (2014) Nature Publishing Group

5.2 Spatial Distribution

Figure 5.9 shows the global distribution of near-surface BaP concentrations (before downscaled). Grid BaP concentrations over land vary extensively with the three quartiles of 0.00032, 0.0055, and 0.046 ng/m^3 (Table 5.1), respectively. East Asia, South Asia, and Southeast Asia are the major hot regions with the concentration medians of 0.074, 0.21, and 0.086 ng/m^3 , respectively. Among them, the median and 25 % quartile in South Asia are much higher than those in any other regions. South Asia is characterized by large-scale BaP emissions from residential sector, which is more evenly and continuously distributed. Therefore, the BaP contamination widely spreads in a large region of South Asia, although the highly polluted hot spots are fewer than those in East Asia. Due to the uneven distribution of population density in East Asia, BaP concentrations are much higher in the eastern part of this region than in the west. In particular in the eastern China including Northeast China, North China Plain, and eastern coastal areas, the emissions from residential, transportation, and industrial sectors are highly concentrated. Considering high population density, severe health impact from BaP contamination can be expected. Except for East Asia, South Asia, and Southeast Asia, other regions such as Europe, sub-Saharan Africa, and Former Soviet Union regions also see relatively high levels of BaP concentrations with medians of 0.097, 0.024, and 0.014 ng/m^3 , respectively. Eastern Europe exhibits higher BaP concentrations due to emissions from industrial sector. Biomass burning in residential sources and wildfire/deforestation contributes most to local BaP pollution in Africa. Heavy industry, lower degradation due to lower temperature leads to high level of BaP concentrations in the Former Soviet Union regions.

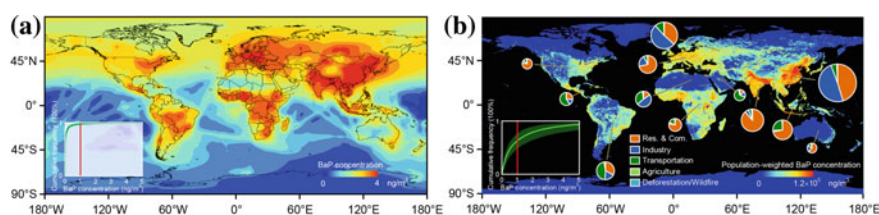


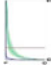
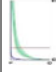
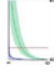
Fig. 5.9 Geographical distributions of BaP concentrations in 2007. **a** Ambient air BaP concentrations calculated from MOZART-4. **b** Population-weighted and spatially downscaled BaP concentrations as indicators of population exposure risk. The relative contributions of various source sectors are shown as pie charts for individual regions. The areas of the pie charts are proportional to the regional mean exposure concentrations. The 12 regions are defined by the Task Force on Hemispheric Transport of Air Pollution (2014) (Table 3.13); the Arctic, Antarctic, and non-Arctic/Antarctic oceans are not shown because of very low values. Cumulative distributions of grid concentrations are also shown together with the European Union target value of 1 ng/m^3 in these two maps, respectively. Uncertainties at 95 % confidence intervals are shown by shaded areas. This figure was generated using ESRI[®] ArcMap, Microsoft[®] Office Excel, and Microsoft[®] Office Word (ESRI 2014; Microsoft Corporation 2014). Reprinted with the permission from Shen et al. (2014). Copyright (2014) Nature Publishing Group

Table 5.1 Spatial variations of global and regional annual mean ambient BaP concentrations

Region	Directly calculated				Population weighted				Cumulative frequency distribution
	$C_{2.5}$ (ng/m ³)	C_{50} (ng/m ³)	C_{75} (ng/m ³)	ER _{EU} 100 (%)	$C_{2.5}$ (ng/m ³)	C_{50} (ng/m ³)	C_{75} (ng/m ³)	ER _{EU} 100 (%)	
World (land area)	0.00032	0.0055	0.046	2.2	0.18	0.57	1.6	36.9	
The United States and Canada	0.00023	0.0014	0.0072	0.1	0.046	0.16	0.42	6.6	
Western and Eastern EU and Turkey (up to 66 N polar circle)	0.033	0.097	0.22	2.1	0.16	0.36	0.86	21.4	
South Asia	0.10	0.21	0.56	14.8	0.29	0.70	1.5	40.1	
East Asia	0.013	0.074	0.58	17.4	0.90	2.0	3.8	72.2	
South East Asia	0.021	0.086	0.26	3.7	0.27	0.68	1.4	35.4	
Pacific, Australia, and New Zealand	0.000012	0.00022	0.0019	0.0	0.039	0.18	0.37	4.5	
Northern Africa	0.000004	0.00007	0.0012	0.0	0.071	0.24	0.47	12.5	
Sub Saharan Africa	0.0039	0.024	0.082	0.3	0.091	0.25	0.59	11.6	
Middle East	0.00012	0.0019	0.0097	0.1	0.030	0.097	0.23	10.6	

(continued)

Table 5.1 (continued)

Mexico, Central America, Caribbean, Guyanas, Venezuela, and Columbia	0.00086	0.0051	0.022	0.1	0.042	0.14	0.46	11.1	
South America	0.0021	0.0081	0.027	0.5	0.038	0.17	0.70	18.7	
Russia, Belarus, Ukraine, and Central Asia	0.0022	0.014	0.049	0.7	0.087	0.36	1.6	32.8	

C_{25} , C_{50} , and C_{75} represent the 25th, 50th, and 75th percentiles of the spatial distributions of annual mean ambient BaP concentrations, respectively. ER_{EU} represents the rates of excess of the European Union target value (1 ng/m^3). For the cumulative distribution curves, x-axis is the ambient BaP concentration (ng/m^3), and y-axis is the accumulative frequency (100 %). The blue curve shows the accumulative frequency distribution of ambient BaP concentrations without population weighted, and the green curve shows that with population weighted. The red line represents the European Union target value for ambient BaP concentration. The uncertainties at 95 % confidence intervals are shown by shaded areas

Reproduced with the permission from Shen et al. (2014). Copyright (2014) Nature Publishing Group

The transboundary pollution is also an important reason for local BaP pollution in this specific region.

As mentioned above, due to a large area with lower emissions in the western part of East Asia, the spatially averaged concentration in East Asia represents a moderate level. However, in terms of human health, this region should be the most concerned considering both the highest BaP concentration levels and intensive population in its eastern part. To highlight the BaP concentrations being exposed by population, population-weighted concentration is adopted which is calculated by averaging the concentrations after being weighted by gridded population counts.

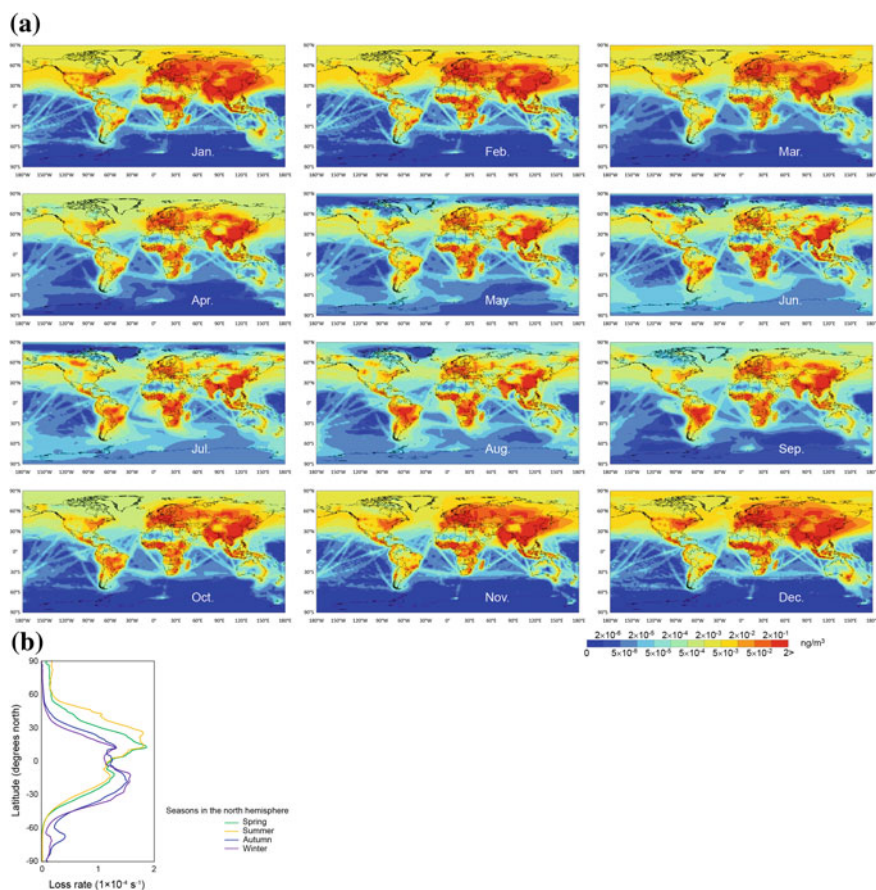


Fig. 5.10 Monthly variations of global BaP concentrations. **a** Geographical distributions of monthly BaP concentrations in 2007. **b** Seasonal variations of BaP's air loss rates. Loss rates are derived from MOZART-4 simulation and averaged along the latitudes. This figure was generated using ESRI[®] ArcMap, Microsoft[®] Office Excel, and Microsoft[®] Office Word (ESRI 2014; Microsoft Corporation 2014). Reprinted with the permission from Shen et al. (2014). Copyright (2014) Nature Publishing Group

Because of the spatial covariation between emission and population, the geographical distribution of population-weighted concentrations as risk indicators shows intensified risk in the hot regions. 25, 50, and 75 % quartiles of population-weighted BaP concentrations by region are shown in Table 5.1, and the global distribution is shown in Fig. 5.9b. Globally, the three quartiles of the population exposure concentrations are 0.18, 0.57, and 1.65 ng/m³, respectively, which are much higher than those of directly calculated ones. East Asia and South Asia represent higher exposure concentrations, being 2.01 and 0.69 ng/m³, respectively. Emission from residential and industrial sectors contributes most to the overall exposure, as a result of both higher emissions and proximity to people. Cumulative frequency distributions of BaP concentrations are also shown in Fig. 5.9b (globe) and Table 5.1 (individual regions) for both directly calculated and population-weighted concentrations. Globally, there is 2.2 % (1.8–2.7 % as R₅₀) of land area with ambient air concentrations exceeding the EU target value (1 ng/m³) (European Union Directive 2013). However, 36.9 % (32.0–41.7 %) of the world's population live in these areas. Among them, 80.3 % live in East, South, and Southeast Asia, where 72.2, 40.1, and 35.4 % of the population, respectively, are exposed to annual mean ambient BaP concentrations above 1 ng/m³. Even with a relatively lenient national standard (Ministry of Environmental Protection of the People's Republic of China 2014) of 2.5 ng/m³, the rate of excess in China is as high as 34.1 %.

Monthly maps suggest a strong seasonality with higher concentrations in winter due to slow degradation in the air and extra emissions from heating (Fig. 5.10a). In higher latitudes in the Northern Hemisphere, promoted capacity of BaP's long-term transport leads to significant transboundary pollutions. The temperature dependence of BaP persistency is confirmed by the strong latitudinal and seasonal variations of BaP's air loss rate (Fig. 5.10b).

5.3 Summary

Based on MOZART-4, the global transport of BaP was simulated. Model validation showed good agreement between observation and simulation at background sites, but an underestimation at non-background sites. Using wind field and high-resolution emission inventory, a Gauss diffusion downscaling method was adopted to generate concentration field with finer resolution. Results from the high-resolution concentration field match observations at non-background sites well. According to the concentration field, global distribution of near-surface BaP concentrations is discussed. Globally, near-surface BaP levels varied widely. The three quartiles of directly calculated concentrations are 0.00032, 0.0055, and 0.046 ng/m³, respectively. East Asia, South Asia, and Southeast Asia are three hot spots with median concentrations being 0.074, 0.21, and 0.086 ng/m³, respectively. Monthly variation of BaP contamination levels is significant. Because of the spatial overlap between emissions and population densities, the population-weighted BaP

concentrations, as an indicator of health risk, are further enhanced in the above regions. Globally, the three quartiles of the population exposure concentrations are 0.18, 0.57, and 1.65 ng/m³, respectively. The medians of exposure concentrations in East Asia and South Asia are as high as 2.01 and 0.69 ng/m³, respectively. Emission from residential and industrial sectors contributes most to the overall exposure, as a result of both higher emissions and proximity to people. Globally, there is 2.2 % (1.8–2.7 % as R₅₀) of land area with ambient air concentrations exceeding the EU target value (1 ng/m³). However, 36.9 % (32.0–41.7 %) of the world's population live in these areas. Among them, 80.3 % live in East, South, and Southeast Asia, where 72.2, 40.1, and 35.4 % of the population, respectively, are exposed to annual mean ambient BaP concentrations above 1 ng/m³. Even with a relatively lenient national standard of 2.5 ng/m³, the rate of excess in China is as high as 34.1 %.

References

- Brauer, M. (2012). Exposure assessment for estimation of the global burden of disease attributable to outdoor air pollution. *Environmental Science and Technology*, 46, 652–660.
- ESRI (2014). *ArcGIS for Desktop*. Retrieved from <http://www.esri.com>.
- European Monitoring and Evaluation Programme (EMEP) (2012). *EMEP POP data*. Retrieved from <http://www.nilu.no/projects/ccc/emepdata.html>.
- European Union Directive (2013). Directive 2004/107/EC of the European Parliament and of the Council. *Official Journal of the European Union*, L23, 3–16. Retrieved from http://eurlex.europa.eu/LexUriServ/site/en/oj/2005/l_023/l_02320050126en00030016.pdf.
- Friedman, C. L., & Selin, N. E. (2013). Long-range atmospheric transport of polycyclic aromatic hydrocarbons: A global 3-D model analysis including evaluation of Arctic sources. *Environmental Science and Technology*, 46, 9501–9510.
- Levy, R. C., Remer, L. A., Mattoo, S., Vermote, E. F., & Kaufman, Y. J. (2007). Second-generation operational algorithm: Retrieval of aerosol properties over land from inversion of Moderate Resolution Imaging Spectroradiometer spectral reflectance. *Journal of Geophysical Research*, 112, D13211.
- Microsoft Corporation (2014). *All Office products*. Retrieved from <http://office.microsoft.com>.
- Ministry of Environmental Protection of the People's Republic of China (2014). *Ambient air quality standards (GB 3095–2012)*. Retrieved from <http://www.zhb.gov.cn/>.
- Shen, H. Z., Tao, S., Liu, J., Huang, Y., Chen, H., Li, W., et al. (2014). Global lung cancer risk from PAH exposure highly depends on emission sources and individual susceptibility. *Scientific Reports*. doi:10.1038/srep06561.
- Shen, Z. Y. (1987). Long period average concentration of single continuous source gas effluent at one and multi-receiving point. *Environment Pollution Control*, 2, 37–41. (in Chinese).
- Sørensen, J. H. (1998). Sensitivity of the derma long-range Gaussian dispersion model to meteorological input and diffusion parameters. *Atmospheric Environment*, 32, 4195–4206.
- Task Force on Hemispheric Transport of Air Pollution (2014). *Theme 2: Source apportionment and source/receptor analysis*. Retrieved from <http://www.htap.org/>.
- Wang, R., Tao, S., Balkanski, Y., Ciais, P., Boucher, O., Liu, J. F., et al. (2014). Exposure to ambient black carbon derived from a unique inventory and high-resolution model. *Proceedings of the National Academy of Sciences of the United States of America*, 111(7), 2459–2463.

- Wang, R., Tao, S., Wang, B., Yang, Y., Lang, C., Zhang, Y. X., et al. (2010). Sources and pathways of polycyclic aromatic hydrocarbons transported to Alert, the Canadian High Arctic. *Environmental Science and Technology*, *44*, 1017–1022.
- Zhang, Y. X., Tao, S., Shen, H. Z., & Ma, J. M. (2009). Inhalation exposure to ambient polycyclic aromatic hydrocarbons and lung cancer risk of Chinese population. *Proceedings of the National Academy of Sciences of the United States of America*, *106*(50), 21063–21067.

Chapter 6

Global Lung Cancer Risks Induced by Inhalation Exposure to PAHs

It has been well illustrated that human exposure to polycyclic aromatic hydrocarbons (PAHs) through various routes is associated with cancer (USEPA 2014; Boffetta et al. 1997; Chen and Liao 2006). Increased lung cancer risks were observed from both occupational exposure and environmental exposure to PAHs and well documented by previous studies (Boffetta et al. 1997; Armstrong et al. 2004; Brüske-Hohlfeld et al. 2000). As a result, one of the high-molecular-weight PAHs, benzo[*a*]pyrene (BaP), has been classified as one of the most carcinogenic agents by the International Agency for Research on Cancer (IARC 2014). Among various exposure routes, inhalation is an important pathway by which humans are exposed to PAH compound. Given that the majority of PAHs in the atmosphere are emitted from incomplete combustion or from pyrolysis (Armstrong et al. 2004; Ravindra et al. 2008), the health impacted being induced by PAH exposure must be strongly related to combustion sources. Different PAH emission sources contribute to PAH exposure to different extents because of their different emission strengths and proximities to people (Shen et al. 2013). The quantification of source–receptor relationships is essential for assessing the health risks associated with different sources and for developing cost-effective abatement strategies.

Their widespread emissions and potential for long-range transport lead to the fact that PAHs can be detected all around the world, including in Polar Regions (Lunde and Björseth 1977). In this study, a global chemical transport model has been used to address the fates of PAHs. A spatial disaggregation method has been used to generate concentration distributions at a higher resolution, which is essential for risk assessment. The high-resolution near-surface concentrations facilitate our following evaluation on lung cancer risk assessment. However, another issue remains to be solved. Evidence from molecular epidemiologic studies has indicated that individual susceptibility plays an important role in cancer development in humans under environmental stress (Perera 1997). Yet, the influences of susceptibility on cancer risks in populations grouped by gender, age, and genetic heritage are difficult to characterize quantitatively. It is a challenge to distinguish the relative

contributions of the exposure dose and individual susceptibility to the risks associated with PAHs (Perera 1997).

In this chapter, the risks in global population of lung cancer being induced by the inhalation of PAHs are evaluated quantitatively. The contributions of different source types, the influences of transboundary pollution, and individual susceptibility on total health risks are quantified and presented.

6.1 Risk Assessment and Influence of Individual Susceptibility

As mentioned in Chap. 3, we used BaP as an indicator for PAH risk assessment, and the maximum likelihood, instead of the upper bound of Cancer Slope Factor, is derived and adopted for an unbiased best estimate of *ILCR* and population attributable fraction (PAF). Globally, overall incremental lifetime lung cancer risk (*ILCR*) induced by inhalation exposure to ambient PAHs is estimated to be 3.1×10^{-5} ($1.6 \times 10^{-5} - 5.9 \times 10^{-5}$ as the interquartile range) with the consideration of individual susceptibility. The corresponding population attributable fraction for lung cancer is 0.13 % (0.07–0.25 %). The R_{50} of the log-scaled variation ($R_{50, \log}$) in individual susceptibility is 0.81, which means that there will be 25 % of the overall population being at least 1.5 times more vulnerable than the population with moderate susceptibility, and the 95 % most vulnerable people will be 8.7 times more vulnerable than common people. The variability associated with individual susceptibility is actually quite close to that of the exposure dose (0.96) we have calculated, suggesting that the relative contribution of individual susceptibility to the overall variation of the risk is comparable to that of the exposure at the global scale. Moreover, on regional or local scales, it is expected that the difference in individual susceptibility can play a more important role in terms of risk variability than variations in exposure dose can; as in local scales, the variation of concentrations will decrease.

Compared to smoking, of which the PAF is as high as 71 % (Ezzati and Lopez 2003), the PAF of PAH exposure is much lower. However, a significantly positive correlation ($p < 0.1$) between the country-specific *ILCRs* and lung cancer incidences (Ferlay et al. 2014) can be found in our study (Fig. 6.1a). A linear regression model built upon *ILCRs* from ambient PAH exposure can explain 7 % of the overall variation (R^2) of country-level lung cancer incidences. After being normalized by smoking prevalence (WHO 2014), the correlation became more significant ($p < 0.01$, Fig. 6.1b). In the smoking-effect-normalized regression model, 12 % of the variation in lung cancer incidences can be explained by the variation in *ILCRs*. It was also found that such a relationship between lung cancer incidences and the *ILCRs* is more robust in developed countries, where 38 % of the variation in lung cancer incidences can be explained. In fact, the correlation was expected to be more significant in developing countries, given lower smoking rates and higher PAH exposure levels there. The opposite trend is mostly caused by the well-established

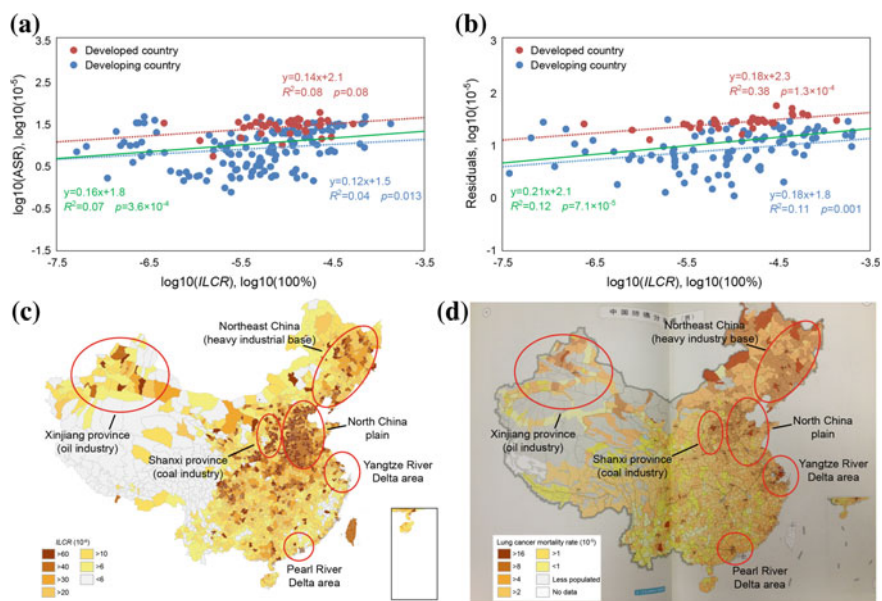


Fig. 6.1 Spatial correlation between *ILCRs* by PAHs exposure and lung cancer incidence rates. **a** Correlation between country-specific *ILCRs* and age-adjusted lung cancer incidence rates (ASR) without smoking effect normalized. **b** Correlation between country-specific *ILCRs* and ASRs with smoking effect normalized. *Red* and *blue circles* represent developed and developing countries, respectively. Regression lines for each country group are shown as *dashed lines* with corresponding colors. Regression lines including all countries are illustrated as *green lines*. **c** Resulting *ILCRs* by county in China in 2007. **d** County-specific lung cancer mortality rates in China over a period 1973–1975. This is a photograph taken from the Chinese Atlas of Cancer Mortality (Editorial Committee for the Atlas of Cancer Mortality 1976). The atlas was prepared based on a 3-year (1973–1975) national survey and was regarded as one of the most celebrated examples because of its highly resolved geographic units. Considering the large temporal discrepancy, ambient PAH levels in China in the 1970s and 2000s should be significantly varied. However, the similarity of spatial patterns of PAHs health impact and overall lung cancer mortality can still be found from **c** and **d**. This figure was generated using ESRI® ArcMap, Microsoft® Office Excel, and Microsoft® Office Word (ESRI 2014; Microsoft Corporation 2014). Reprinted with the permission from Shen et al. (2014). Copyright (2014) Nature Publishing Group

cancer registry systems in developed countries, which provide much more reliable incidence data so as to represent the relationship with less uncertainty.

In China, the geographic similarity of *ILCRs* and lung cancer (LC) mortality can be further illustrated at a county level (Fig. 6.1c, d). Regions with higher *ILCRs* and higher LC mortality are spatially overlapping to a certain extent. Regions such as the North China Plain, the Yangtze River Delta Area, and the Pearl River Delta Area are labeled as the areas with fast-growing economy. Among them, the North China Plain involves the capital which is continuously being regarded as both the economic and the political centers of the nation. The Yangtze River Delta Area and the Pearl River Delta Area are becoming more attractive to light manufacturing due

to convenient transportation. Population gathering leads to highly intensified emissions and high-level exposure in these regions, resulting in higher levels of LC mortality. Additionally, the Shanxi Province with coal and coking industry, the Northeast China as the traditional heavy industrial base, and the Xinjiang Province with oil industry are also regions with high levels of LC mortality. The spatial similarity between *ILCRs* and lung cancer incidences at both national and subnational scales suggests an extremely high correlation between PAH exposure and lung cancer risks, which is actually higher than the estimated PAF indicates. One of the underlying reasons should involve the spatial correlation between PAHs and other pollutants such as the particular matters, since a large fraction of these pollutants are emitted from combustion sources. Hence, the spatial similarity between *ILCRs* and lung cancer incidences is indirectly representing the importance of air pollution as a factor affecting the geographic variability of non-smokers lung cancer mortality rates.

In this work, we calculated *ILCRs* with and without consideration of individual susceptibility separately and compared the difference of *ILCR* distributions between the two cases. The result is quite interesting and inspiring. Figure 6.2 shows the log-scaled frequency distributions of global *ILCR* with (blue curve) and without (green curve) individual susceptibility included. If we considered susceptibility, the cumulative curve became more platykurtic (or fatter), and the population fractions at both high- and low-risk ends increased dramatically, as shown by the ratios of the two frequencies (brown curve) which is 50 times of those without susceptibility when $ILCR = 0.01$. Since the *ILCRs* vary at a log scale, the overall population risk can be very sensitive to the population at the high-risk end. Therefore, excluding susceptibility would lead to a remarkable underestimate of the overall risk. It was

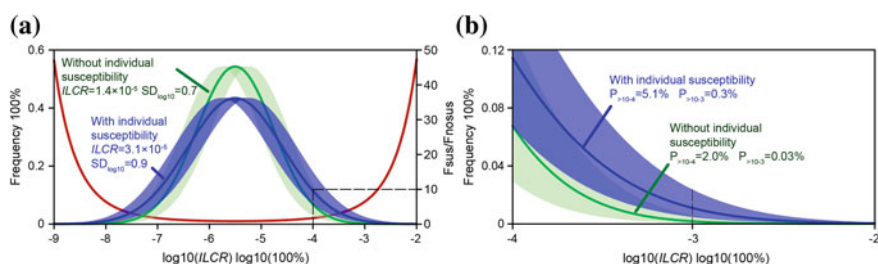


Fig. 6.2 Frequency distributions of global *ILCR* due to inhalation exposure to ambient PAHs. **a** The two curves show the model-calculated frequency distributions with (blue) and without (green) individual susceptibility considered. The distribution of the ratios of the two frequencies (with susceptibility to without susceptibility) is shown as the brown line, indicating accelerated increase in the probabilities at both low- ($ILCR < 10^{-8}$) and high- ($ILCR > 10^{-5}$) risk ends. The overall average *ILCRs* together with standard deviations, with and without susceptibility, are listed. **b** A zoomed-in version of **a** in the high-risk range. The probabilities under the two distribution curves with *ILCR* higher than 10^{-4} and 10^{-3} are labeled as $P_{>10^{-4}}$ and $P_{>10^{-3}}$, respectively. Uncertainty as interquartile range is shown as the shaded area for each frequency–distribution curve. Reprinted with the permission from Shen et al. (2014). Copyright (2014) Nature Publishing Group

found that the risk as *ILCR* of the most vulnerable population would have been underestimated by more than 90 % and the overall population risk would have been underestimated by 55 % (1.4×10^{-5}), if individual susceptibility was not considered.

The Unit Risk (*UR*, m^3/ng), defined as the *ILCR* from exposure to per unit BaP concentration (Boström et al. 2002), was also calculated for all countries (see Fig. 6.3). Large disparity in *UR* can be observed among countries. The disparity is mainly caused by the difference in susceptibility including the body weight, the breathing rate, age–population distributions, the genetic susceptibility, and many other factors that have been described in Chap. 3. Figure 6.3a, b shows that the medians and standard variations of individual susceptibility among countries could be significantly different. Because of this, use of a single *UR* in risk assessment will certainly lead to considerable spatial bias. According to the results, to keep *ILCRs* of 97.5 % population below 10^{-5} , the global average BaP concentration should be $0.1 \text{ ng}/\text{m}^3$. However, the guideline varies widely when coming into individual countries. African people are estimated to be associated with tighter guideline, while in South America, the guideline concentration can be looser. Based on the *ILCRs* and reported country LC incidence rates (Ferlay et al. 2014), relative risk (*RR*) of lung cancer from ambient PAHs exposure was calculated for each country. Globally, the overall *RR* is 1.0013. *RR* of the developing world (1.0017) is higher than that of the developed world (1.0003), which can be explained by the fact that populations in developing countries have much higher levels of exposure concentrations to ambient PAHs and lower levels of lung cancer incidence rates (Ferlay et al. 2014). Using the *RRs*, the unit relative risk (*URR*) (Armstrong et al. 2004) was calculated at a benchmark of $100 \text{ ug}/\text{m}^3$ 3 years of BaP exposure for each country. Also, the *URR* values were calculated for individual persons within each country,

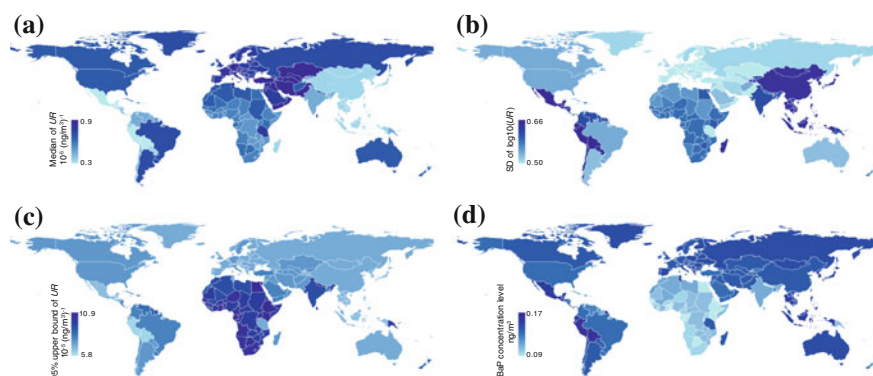


Fig. 6.3 Spatial variations of the resulting unit risks (*UR*). **a** The median of individual *URs* at country level. **b** The standard deviation of \log_{10} -transformed *URs*. **c** The 95 % upper bound of individual *URs*. **d** The resulting BaP concentrations by country under which the 95 % upper bounds of individual *ILCRs* would be less than 10^{-5} . This figure was generated using ESRI® ArcMap and Microsoft® Office Word (ESRI 2014; Microsoft Corporation 2014). Reprinted with the permission from Shen et al. (2014). Copyright (2014) Nature Publishing Group

assuming that different people have different *URRs* due to their differences in susceptibilities. According to our evaluation, the interquartile range of country-level *URRs* is [1.8, 7.0] with the median value of 3.0. It was found that the population overall *URR* of a specific country is higher than the upper bound of interquartile range of individual *URRs*. For example, the overall *URR* of Chinese population is 1.56, whereas the interquartile range of individual *URRs* among Chinese population is merely [1.02, 1.25]. Actually, there are only 13 % of Chinese population exceeding the *URR* value of 1.56, suggesting that this small fraction of people with highest *URRs* can influence the overall *URR* of the population to a very large extent.

It was suggested that the uncertainties in quantifying dose–response relationship are partly attributable to the lack of quantitative information on the level of exposure (Mastrangelo et al. 1996). However, in this study, the uncertainty range of dose–response relationships from epidemiological surveys (R_{50} , $\log = 0.82$) (USEPA 2014) is comparable to the variation of individual susceptibilities (R_{50} , $\log = 0.81$), suggesting that the uncertainties can be also raised by variation in individual susceptibilities, to which genetic polymorphisms contribute most. The adoption of individual susceptibility can not only explain the uncertainties of risk assessments, but also change our insight into the risk outcomes. The air-quality guideline, determined by current risk assessment methodologies, commonly with 97.5 % confidence (upper bound of 95 % confidence interval) in keeping population exposure risks under a specified level, is actually, in this point of view, a guideline to keep exposure risks of 97.5 % population under the specified level. The more susceptible groups (the rest 2.5 % population) are lack of attention. Emphasizing on the high-risk groups, this thesis provides a revised method serving as the first attempt to introduce individual susceptibility into quantitative risk assessments on a global scale. With increasing knowledge of genetic and acquired susceptible factors, this methodology is expected to be more instrumental in evaluating global burden of disease, in developing environmental and health policies, as well as in strengthening individual awareness.

6.2 Source Contributions

Several short-term modeling experiments were conducted using various source types individually to evaluate their contributions to the overall health impact. Globally, biomass fuel burning in residential/commercial sector contributes 40 % of the total *ILCR*, followed by residential/commercial fossil fuel combustion (14 %), coke production (13 %), primary aluminum production (12 %), and motor vehicles (9 %) (see, Fig. 6.4a and Table 6.1). The contribution of a given source to the risk depends not only on the emission strength, but also on the proximity to people. Therefore, relative contributions of a given source to the total emission and to the total risk can be different. The effect of a given source is quantified by specific health effect (*SILCR*, Pg^{-1}), defined as *ILCR* caused by per unit emission. Globally, *SILCRs* for various source types vary extensively from 0.08 to 0.14 Pg^{-1} for

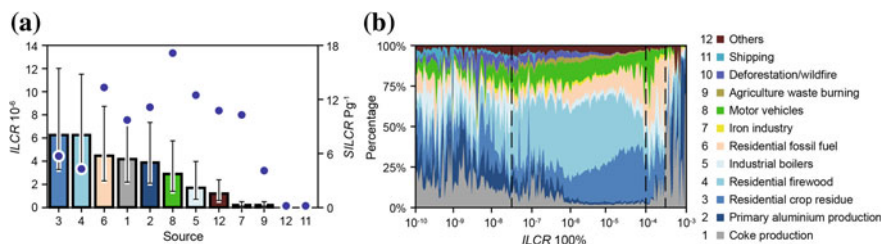


Fig. 6.4 Contributions of various sources to global lung cancer risks. **a** Risks caused by PAH emissions from various sources as *ILCR* (bars) and risks caused by per unit emissions of various sources as *SILCR* (dots). **b** Relative contributions of various sources to the risks for populations facing different risk levels (*ILCR*). Reprinted with the permission from Shen et al. (2014). Copyright (2014) Nature Publishing Group

Table 6.1 Source-specific contributions to global total BaP emission and total *ILCR* in 2007

Source type	BaP emission (ton/year)	Contribution to total BaP emission (100 %)	<i>ILCR</i> (10 ⁻⁶)	Contribution to total <i>ILCR</i> (100 %)	<i>SILCR</i> (Pg ⁻¹)
Residential crop residue burning	1115	24.6	6.3	20.1	5.6
Residential firewood burning	1501	33.1	6.2	19.9	4.2
Residential fossil fuel	339	7.5	4.5	14.4	13.3
Coke production	431	9.5	4.1	13.2	9.6
Primary aluminum production	354	7.8	3.9	12.5	11.0
Motor vehicles	166	3.7	2.8	9.1	17.1
Industrial boilers	134	3.0	1.7	5.3	12.4
Iron industry	24	0.5	0.2	0.8	10.2
Agriculture waste burning	60	1.3	0.2	0.8	4.0
Deforestation/wildfire	339	7.5	0.05	0.2	0.14
Shipping	67	1.5	0.01	0.02	0.08
Others	114	2.5	1.2	3.9	10.7

Reprinted with the permission from Shen et al. (2014). Copyright (2014) Nature Publishing Group

shipping and wildfire to 13 and 17 Pg⁻¹ for residential/commercial fossil fuel usage and motor vehicles (Fig. 6.4a and Table 6.1). Motor vehicles are associated with the highest *SILCR*, due to its spatial intensification in populated areas.

ILCRs also vary dramatically among populations at different risk levels (Fig. 6.4b). For example, a small fraction (1.7 %) of the population facing high risk (*ILCR* > 3 × 10⁻⁴) is largely because of exposure to emissions from coke and aluminum productions. In particular, *ILCRs* of some inhabitants near coking plants in China can reach as high as 1.5 × 10⁻². Long-term situations of these people are

even worse, given their cumulative exposure to continuously high levels of ambient PAHs in the past decades, during which period beehive coking, which is among the severest PAH emission sources, had not been entirely phased out in China (Shen et al. 2013). Emissions from residential solid fuel combustion contribute mainly to the population at risk levels between 3×10^{-8} and 1×10^{-4} . Unlike industrial sources, PAH emissions from residential sources are primarily credited to millions of residential stoves. It is socioeconomic development rather than technical progress that is critical in the abatement of emissions from this sector. The risk-specified source contributions for several representative countries are shown in Fig. 6.5.

These results provide a sound scientific basis for abatement strategy formulation. Globally, residential biomass burning causes the largest overall lung cancer risk and should be the top priority in the emission abatement. On the other hand, control of emissions from motor vehicles and residential coal combustion with the highest *SILCR* is the most effective way of reducing risk. If the objective is to protect the most vulnerable people, emissions from coke and aluminum production should be addressed first. However, the specific strategies should be different among

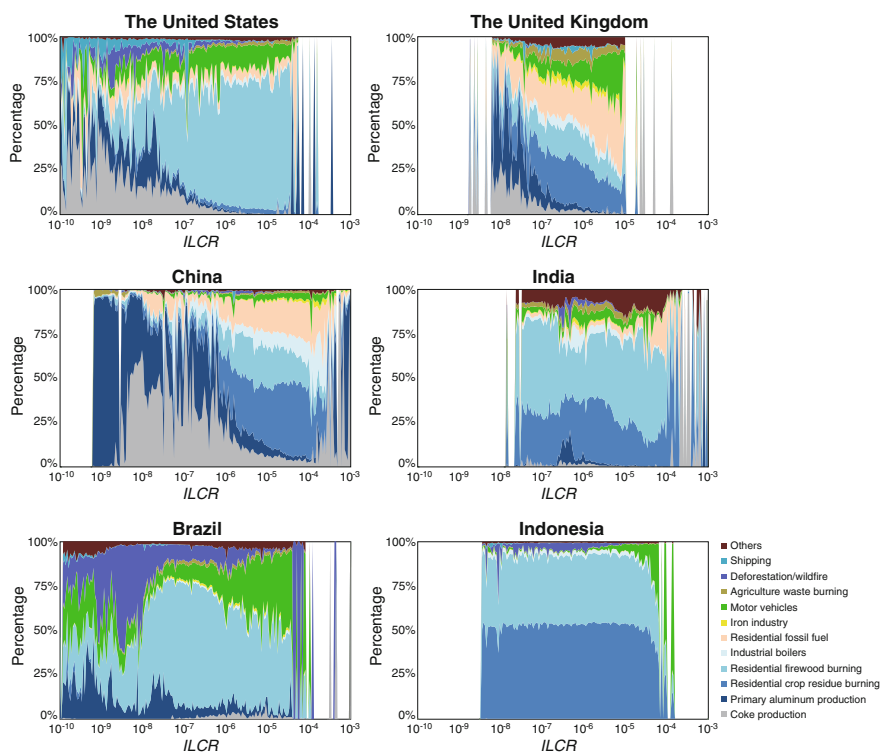


Fig. 6.5 Relative contributions of various sources to the risks for populations facing different risk levels (ILCR) by country. Reprinted with the permission from Shen et al. (2014). Copyright (2014) Nature Publishing Group

countries, depending on local emissions and risks (see, Fig. 6.5). For example, it was found that the spectrums in developing countries tend to be more informative than those in developed countries at higher levels of *ILCRs*, such as those in China and India, since more people were exposed at the higher levels of BaP concentrations. In India, dung-cake burning in residential stoves (included in “Others” source type) contributed a remarkable fraction of health impacts at moderate *ILCR* levels. In Brazil, deforestation/wildfire accounted for a large fraction of health impacts at low *ILCR* levels. The health risks of the most vulnerable populations in Indonesia are dominated by motor vehicles, and primary aluminum production contributed most to the overall risk in Russia. Of course, before the action plan is carried out, abatement costs should be taken into account, since different source types are associated with very different abatement costs. Generally, abatement strategies in residential sector are likely with the cheapest abatement costs, given that improved design of woodstoves can significantly reduce PAH emissions. However, this sector is also the one with high difficulty of policy implementation as a result of wide spread of emissions in every rural household. Notably, in this study, the *ILCR* was calculated from a lifetime exposure to outdoor PAHs, while indoor exposure was not involved due to a lack of linkage between outdoor and indoor concentrations on a global scale. Previous investigation has revealed that indoor exposure could be much higher in some rural areas in developing countries due to the demand for cooking and heating and poorly ventilated conditions, especially for women during cooking period (Mumford et al. 1995). The health impacts contributed by residential/commercial sector should be further promoted by an integrated risk assessment considering both outdoor and indoor exposure.

6.3 Transport Across Continents

To address long-range transport among regions, we conducted short-term modeling experiments in which only emissions from individual regions were opened up so that transboundary pollution can be quantified. *ILCRs* were used as an indicator to evaluate the transboundary pollution. In Fig. 6.6, we illustrated the flows of BaP including directions and quantities among regions and percentages of *ILCRs* contributed by BaP from other regions (the numbers in the black pies). The sizes of the black pies are proportional to the regional *ILCRs*. It appears that interregional transport within the Eurasian continent is relatively active, while America, Oceania, and Africa have much fewer exchanges with other continents. As a result of the westerly wind movement and lower air loss rate in high-latitude area, the transport of BaP from Western/Eastern Europe to the Former Soviet Union region represents the largest *ILCR* flow, leading to a 4.5×10^{-7} increase to local *ILCR* of the latter. The second largest movement occurs from East Asia to Southeast Asia, owing to the extraordinary emission intensity in the source region. Still, even with the active interregional transport, regional risks are predominantly caused by local emissions. The highest external contribution to local *ILCR* is merely 2.6 % (Southeast Asia).

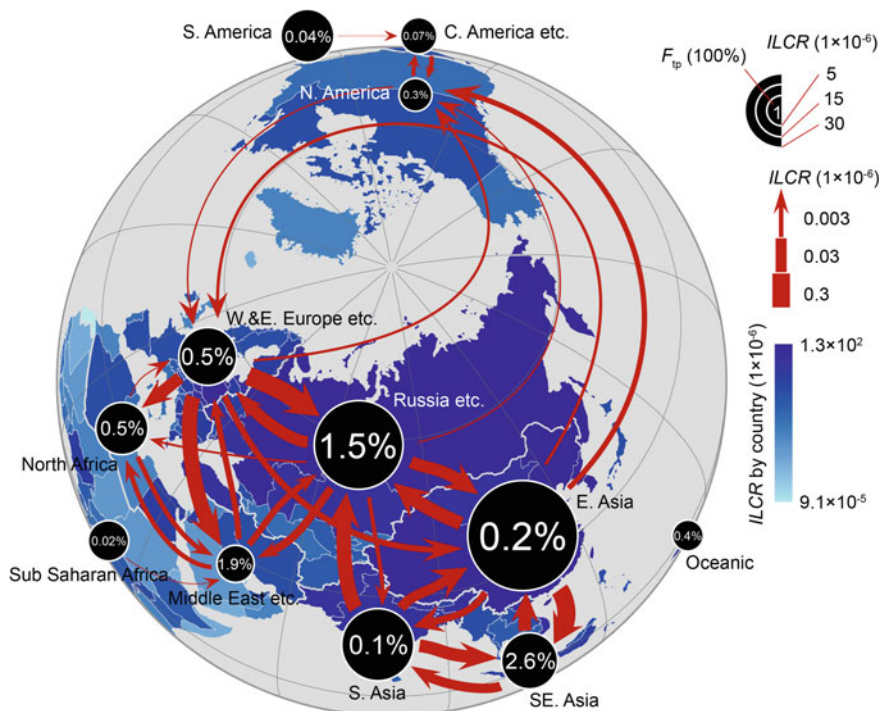


Fig. 6.6 Interregional transport of PAH exposure risk. The sizes of the black pies are proportional to the log-transformed overall *ILCR* of each region. The numbers in the middle (F_{tp}) are percentages of regional *ILCR* contributed by local exposure to PAHs transported from other regions. The *red arrows* indicate the directions of the interregional transport of BaP, and the thicknesses of the arrow shafts are proportional to the enhancement of *ILCR* due to interregional transport in log scale. Unpopulated regions, including the Arctic, Antarctic, and non-Arctic/Antarctic oceans, and transport with *ILCR* influence less than 1×10^{-9} are omitted. The calculated *ILCRs* for individual countries are shown by color codes in the background. This figure was generated using ESRI[®] ArcMap, Microsoft[®] Office Excel, and Microsoft[®] Office Word (ESRI 2014; Microsoft Corporation 2014). Reprinted with the permission from Shen et al. (2014). Copyright (2014) Nature Publishing Group

The net exported risk (*NER*), defined as the difference between the exported and the imported *ILCR* multiplied by regional population, is calculated for each region (Tables 6.2 and 6.3). Western/Eastern Europe ($NER = 145$), South Asia ($NER = 57$), and East Asia ($NER = 42$) are the main export regions of risk, with positive values of exported risk, while Southeast Asia ($NER = -126$), the former Soviet Union ($NER = -92$), and the Middle East ($NER = -19$) are risk passive recipients. The dynamics of the long-range transport of BaP illustrates a strong seasonality with relatively active transport in winter.

Considering rapid degradation of certain substances such as PAHs, their proportions on atmospheric particles must undergo dramatic change during transport. It is estimated that mass fractions of BaP bound on atmospheric organic and black

Table 6.2 PAH transboundary pollution. Transboundary health impact matrix for 12 Tier-1 source regions by 12 Tier-1 receptor regions

Receptor	Source												Risk import (100 % capita)	Risk export (100 % capita)	Net export (100 % capita)		
	03	04	05	06	07	08	09	10	11	12	13	14					
03																	
04	1 × 10⁻⁰⁹																
05	1 × 10 ⁻¹¹	1 × 10 ⁻¹⁰															
06	2 × 10 ⁻¹⁰	6 × 10⁻⁰⁹	2 × 10⁻⁰⁸														
07	8 × 10 ⁻¹²	1 × 10 ⁻¹⁰	6 × 10⁻⁰⁸	4 × 10⁻⁰⁷													
08	1 × 10 ⁻¹⁵	6 × 10 ⁻¹⁶	7 × 10 ⁻¹⁴	3 × 10 ⁻¹³	2 × 10 ⁻¹¹												
09	1 × 10 ⁻¹⁰	5 × 10⁻⁰⁸	6 × 10 ⁻¹¹	4 × 10 ⁻¹⁰	1 × 10 ⁻¹¹	3 × 10 ⁻¹⁶											
10	6 × 10 ⁻¹⁴	7 × 10 ⁻¹²	6 × 10 ⁻¹³	8 × 10 ⁻¹³	1 × 10 ⁻¹²	1 × 10 ⁻¹⁴	2 × 10 ⁻¹¹										
11	9 × 10 ⁻¹¹	1 × 10⁻⁰⁷	2 × 10 ⁻¹⁰	3 × 10 ⁻¹⁰	1 × 10 ⁻¹¹	3 × 10 ⁻¹⁶	3 × 10⁻⁰⁹	8 × 10 ⁻¹⁰									
12	3 × 10⁻⁰⁹	7 × 10 ⁻¹²	1 × 10 ⁻¹¹	8 × 10 ⁻¹¹	9 × 10 ⁻¹²	1 × 10 ⁻¹⁵	1 × 10 ⁻¹³	3 × 10 ⁻¹²	2 × 10 ⁻¹³								
13	8 × 10 ⁻¹⁵	2 × 10 ⁻¹⁵	2 × 10 ⁻¹³	7 × 10 ⁻¹³	2 × 10 ⁻¹²	1 × 10 ⁻¹³	9 × 10 ⁻¹⁷	9 × 10 ⁻¹²	2 × 10 ⁻¹⁶	3 × 10 ⁻¹⁰							
14	4 × 10 ⁻¹⁰	4 × 10⁻⁰⁷	1 × 10⁻⁰⁷	8 × 10⁻⁰⁸	2 × 10 ⁻¹¹	5 × 10 ⁻¹⁶	8 × 10 ⁻¹¹	7 × 10 ⁻¹²	6 × 10⁻⁰⁹	2 × 10 ⁻¹²	3 × 10 ⁻¹³						

The change of *ILCRs* of receptor regions induced by source region emissions is listed in the matrix. Region numbers are consistent with **Tier-1 region number** in Table 3.13. Changes of *ILCRs* more than 10⁻⁹ are highlighted. Ocean areas and Polar Regions are omitted. The risk import and export are calculated as the change of *ILCR* multiplied by population number in the receptor region. Reprinted with the permission from Shen et al. (2014). Copyright (2014) Nature Publishing Group

Table 6.3 PAH transboundary pollution. Transboundary health impact matrix for 12 Tier-1 source regions by 45 Tier-2 receptor regions

Receptor	Source											
	03	04	05	06	07	08	09	10	11	12	13	14
31		3×10^{-09}	2×10^{-10}	5×10^{-09}	4×10^{-11}	8×10^{-16}	6×10^{-12}	1×10^{-11}	2×10^{-11}	2×10^{-11}	5×10^{-13}	2×10^{-09}
32		7×10^{-10}	1×10^{-10}	2×10^{-09}	4×10^{-11}	8×10^{-16}	3×10^{-12}	7×10^{-12}	9×10^{-12}	3×10^{-09}	4×10^{-13}	4×10^{-10}
33		6×10^{-10}	2×10^{-10}	5×10^{-09}	4×10^{-11}	4×10^{-16}	4×10^{-12}	7×10^{-12}	1×10^{-11}	5×10^{-12}	3×10^{-13}	5×10^{-10}
34		3×10^{-10}	2×10^{-10}	3×10^{-09}	5×10^{-11}	5×10^{-16}	3×10^{-12}	7×10^{-12}	9×10^{-12}	2×10^{-08}	3×10^{-13}	2×10^{-10}
35		3×10^{-09}	2×10^{-10}	5×10^{-09}	3×10^{-11}	7×10^{-16}	7×10^{-12}	1×10^{-11}	3×10^{-11}	9×10^{-12}	4×10^{-13}	2×10^{-09}
36		1×10^{-09}	2×10^{-10}	7×10^{-09}	4×10^{-11}	6×10^{-16}	5×10^{-12}	9×10^{-12}	2×10^{-11}	2×10^{-12}	3×10^{-13}	1×10^{-09}
41	2×10^{-09}		1×10^{-10}	2×10^{-09}	2×10^{-11}	5×10^{-16}	1×10^{-10}	8×10^{-12}	2×10^{-11}	3×10^{-12}	3×10^{-13}	2×10^{-08}
42	6×10^{-10}		9×10^{-11}	1×10^{-09}	2×10^{-11}	4×10^{-16}	3×10^{-09}	6×10^{-12}	7×10^{-12}	2×10^{-12}	2×10^{-13}	6×10^{-09}
43	1×10^{-09}		1×10^{-10}	2×10^{-09}	2×10^{-11}	5×10^{-16}	3×10^{-10}	6×10^{-12}	5×10^{-11}	2×10^{-12}	3×10^{-13}	1×10^{-07}
44	4×10^{-10}		1×10^{-10}	1×10^{-09}	2×10^{-11}	5×10^{-16}	1×10^{-09}	6×10^{-12}	4×10^{-08}	2×10^{-12}	3×10^{-13}	4×10^{-08}
51	2×10^{-11}	1×10^{-10}		1×10^{-08}	2×10^{-08}	1×10^{-15}	2×10^{-11}	3×10^{-11}	2×10^{-10}	3×10^{-12}	6×10^{-13}	4×10^{-09}
52	1×10^{-12}	5×10^{-12}		2×10^{-10}	4×10^{-10}	1×10^{-16}	1×10^{-12}	3×10^{-12}	8×10^{-12}	3×10^{-13}	8×10^{-14}	3×10^{-11}
53	4×10^{-11}	5×10^{-10}		2×10^{-08}	2×10^{-08}	2×10^{-15}	5×10^{-11}	4×10^{-11}	6×10^{-10}	6×10^{-12}	1×10^{-12}	3×10^{-08}
61	2×10^{-10}	7×10^{-09}	5×10^{-09}		3×10^{-09}	1×10^{-15}	3×10^{-11}	1×10^{-11}	2×10^{-10}	3×10^{-12}	5×10^{-13}	1×10^{-07}
62	2×10^{-10}	5×10^{-09}	2×10^{-08}		8×10^{-08}	2×10^{-15}	2×10^{-11}	2×10^{-11}	1×10^{-10}	4×10^{-12}	7×10^{-13}	3×10^{-08}
63	7×10^{-11}	3×10^{-09}	1×10^{-07}		3×10^{-11}	6×10^{-16}	2×10^{-11}	1×10^{-11}	4×10^{-10}	2×10^{-12}	4×10^{-13}	8×10^{-08}
64	3×10^{-10}	1×10^{-08}	8×10^{-10}		2×10^{-10}	9×10^{-16}	2×10^{-11}	1×10^{-11}	2×10^{-10}	3×10^{-12}	5×10^{-13}	8×10^{-08}
65	3×10^{-10}	9×10^{-09}	1×10^{-09}		4×10^{-10}	1×10^{-15}	3×10^{-11}	1×10^{-11}	2×10^{-10}	4×10^{-12}	6×10^{-13}	3×10^{-08}
66	4×10^{-11}	5×10^{-10}	3×10^{-07}		2×10^{-07}	2×10^{-15}	3×10^{-11}	6×10^{-11}	9×10^{-11}	6×10^{-12}	1×10^{-12}	1×10^{-09}
71	6×10^{-13}	1×10^{-11}	2×10^{-11}	3×10^{-09}		3×10^{-12}	1×10^{-13}	7×10^{-13}	4×10^{-13}	4×10^{-14}	4×10^{-14}	2×10^{-11}
72	2×10^{-11}	3×10^{-10}	2×10^{-07}	1×10^{-06}		4×10^{-16}	3×10^{-12}	6×10^{-12}	1×10^{-11}	8×10^{-13}	2×10^{-13}	1×10^{-09}
81	3×10^{-15}	3×10^{-15}	5×10^{-13}	2×10^{-12}	1×10^{-10}		1×10^{-16}	4×10^{-12}	3×10^{-16}	2×10^{-13}	2×10^{-12}	4×10^{-15}
82	1×10^{-15}	5×10^{-16}	4×10^{-14}	2×10^{-13}	3×10^{-12}		1×10^{-17}	4×10^{-12}	3×10^{-17}	7×10^{-14}	1×10^{-11}	6×10^{-16}
83	4×10^{-17}	4×10^{-17}	4×10^{-15}	1×10^{-14}	6×10^{-14}		1×10^{-18}	1×10^{-12}	3×10^{-18}	6×10^{-15}	1×10^{-12}	3×10^{-17}

(continued)

Table 6.3 (continued)

Receptor	Source	03	04	05	06	07	08	09	10	11	12	13	14
91	2×10^{-10}	5×10^{-08}	8×10^{-11}	5×10^{-10}	1×10^{-11}	3×10^{-16}		6×10^{-12}	7×10^{-09}	1×10^{-12}	2×10^{-13}	3×10^{-09}	
92	1×10^{-10}	4×10^{-08}	5×10^{-11}	3×10^{-10}	1×10^{-11}	2×10^{-16}		4×10^{-12}	3×10^{-12}	7×10^{-13}	1×10^{-13}	5×10^{-10}	
101	3×10^{-14}	3×10^{-12}	5×10^{-13}	7×10^{-13}	1×10^{-12}	4×10^{-16}	2×10^{-12}		6×10^{-14}	3×10^{-13}	1×10^{-12}	2×10^{-13}	
102	1×10^{-13}	2×10^{-11}	1×10^{-12}	1×10^{-12}	1×10^{-12}	2×10^{-16}	6×10^{-11}		1×10^{-11}	2×10^{-13}	4×10^{-13}	2×10^{-12}	
103	3×10^{-15}	1×10^{-15}	1×10^{-13}	3×10^{-13}	9×10^{-13}	7×10^{-14}	2×10^{-16}		1×10^{-16}	2×10^{-13}	9×10^{-11}	1×10^{-15}	
111	2×10^{-10}	5×10^{-07}	6×10^{-11}	4×10^{-10}	1×10^{-11}	3×10^{-16}	1×10^{-08}		4×10^{-12}		1×10^{-12}	2×10^{-13}	9×10^{-09}
112	2×10^{-11}	3×10^{-09}	6×10^{-11}	6×10^{-11}	3×10^{-12}	1×10^{-16}	5×10^{-10}		3×10^{-09}	5×10^{-13}	9×10^{-14}	4×10^{-10}	
113	1×10^{-10}	5×10^{-08}	4×10^{-10}	5×10^{-10}	2×10^{-11}	3×10^{-16}	8×10^{-10}		5×10^{-12}	1×10^{-12}	2×10^{-13}	2×10^{-08}	
121	6×10^{-09}	2×10^{-11}	3×10^{-11}	2×10^{-10}	2×10^{-11}	2×10^{-15}	2×10^{-13}		4×10^{-12}	6×10^{-13}		6×10^{-12}	9×10^{-12}
122	2×10^{-12}	1×10^{-13}	2×10^{-12}	3×10^{-12}	3×10^{-12}	1×10^{-15}	5×10^{-15}		1×10^{-12}	6×10^{-15}		8×10^{-13}	7×10^{-14}
123	3×10^{-10}	2×10^{-12}	8×10^{-12}	2×10^{-11}	7×10^{-12}	9×10^{-16}	4×10^{-14}		4×10^{-12}	8×10^{-14}		4×10^{-13}	9×10^{-13}
124	6×10^{-14}	8×10^{-15}	2×10^{-13}	6×10^{-13}	7×10^{-13}	1×10^{-15}	3×10^{-16}		2×10^{-12}	5×10^{-16}		3×10^{-09}	6×10^{-15}
131	7×10^{-15}	2×10^{-15}	2×10^{-13}	8×10^{-13}	2×10^{-12}	7×10^{-14}	9×10^{-17}		2×10^{-12}	2×10^{-16}	5×10^{-13}		3×10^{-15}
132	6×10^{-15}	2×10^{-15}	2×10^{-13}	5×10^{-13}	9×10^{-13}	1×10^{-14}	7×10^{-17}		3×10^{-11}	2×10^{-16}	2×10^{-10}		2×10^{-15}
133	9×10^{-15}	2×10^{-15}	2×10^{-13}	8×10^{-13}	2×10^{-12}	4×10^{-13}	1×10^{-16}		2×10^{-12}	2×10^{-16}	7×10^{-13}		3×10^{-15}
134	1×10^{-14}	2×10^{-15}	2×10^{-13}	6×10^{-13}	9×10^{-13}	1×10^{-14}	8×10^{-17}		2×10^{-12}	2×10^{-16}	2×10^{-09}		3×10^{-15}
141	5×10^{-10}	4×10^{-07}	1×10^{-10}	3×10^{-09}	2×10^{-11}	5×10^{-16}	1×10^{-10}		7×10^{-12}	1×10^{-08}	2×10^{-12}	3×10^{-13}	
142	3×10^{-10}	3×10^{-08}	2×10^{-09}	5×10^{-07}	2×10^{-11}	5×10^{-16}	3×10^{-11}		8×10^{-12}	5×10^{-10}	2×10^{-12}	3×10^{-13}	
143	7×10^{-10}	1×10^{-06}	1×10^{-10}	2×10^{-09}	2×10^{-11}	5×10^{-16}	9×10^{-11}		6×10^{-12}	3×10^{-10}	2×10^{-12}	3×10^{-13}	
144	1×10^{-10}	1×10^{-08}	2×10^{-07}	8×10^{-08}	2×10^{-11}	5×10^{-16}	6×10^{-11}		9×10^{-12}	8×10^{-09}	2×10^{-12}	3×10^{-13}	
145	5×10^{-11}	2×10^{-09}	1×10^{-06}	7×10^{-10}	2×10^{-11}	5×10^{-16}	7×10^{-11}		8×10^{-12}	2×10^{-09}	2×10^{-12}	3×10^{-13}	

The change of *ILCRs* of receptor regions induced by source region emissions is listed in the matrix. Region numbers are consistent with **Tier-1** and **Tier-2** region number in Table 3.13. Changes of *ILCRs* more than 10^{-7} are highlighted. Ocean areas and Polar Regions are omitted. The risk import and export are calculated as the change of *ILCR* multiplied by population number in the receptor region.

Reprinted with the permission from Shen et al. (2014). Copyright (2014) Nature Publishing Group

carbon decrease more than 80 % (from 1.6×10^{-4} to 2.7×10^{-5}) over trans-Pacific transportation. Given the ever-changing properties, particles after long-range transport may act with very different health outcomes associated with human exposure.

6.4 Summary

In this chapter, we used BaP as an indicator to evaluate the global lung cancer risk being induced by inhalation exposure to ambient PAHs. The results showed that not only the locations and strengths of emission sources, but also the individual susceptibility can strongly influence the health outcomes. Moreover, model resolution is critical in exposure modeling. The global incremental lifetime lung cancer risk (*ILCR*) being induced by ambient PAH exposure is estimated to be 3.1×10^{-5} which means about 30 persons per million would suffer from lung cancer due to a lifetime PAH exposure. The *ILCR* is in excess of the acceptable level of 1×10^{-5} . If we did not account for the individual susceptibility, the overall risk would be underestimated by 55 %, and the proportion of highly vulnerable population would be underestimated by more than 90 %. Therefore, the difference of individual susceptibility is strongly recommended to be considered in risk assessment. In terms of lung cancer risk, the most important sources are combustion of biomass fuels (40 %) and fossil fuels (14 %) in the residential/commercial sector, coke (13 %) and aluminum (12 %) production, and motor vehicles (9 %). Model performance of emissions from individual regions revealed that PAHs can travel long distance globally especially within the Eurasian continent, but still, the risk is dominantly contributed by local sources.

As well demonstrated in this chapter, model resolution is critical in exposure modeling and risk assessment. Detailed information on spatial variation would be smoothed by coarsely resolved models, leading to significant underestimation of exposure. This problem can be prevented by either using highly resolved models (e.g., 0.5° or even more) or downscaling the model results to a finer resolution as did in this chapter. When computing load is limited, the latter can provide an alternative to the high-resolution modeling. However, the environmental behavior is poorly captured during this procedure. Future study may further focus on the influences of model resolution on the risk assessment and development of more accurate downscaling method.

In this study, long-range transport of BaP among continents is quantified. Detailed study can be carried out to address across-boundary transport of PAHs among countries or even subcountry administrative regions and to focus on sources of PAHs reaching vulnerable regions such as Arctic.

The sectorally resolved emission inventory enables us to exploit the source–receptor relationship linking emissions from individual sources to population exposure risk. The outcome provides critical and quantitative information for decision makers to formulate future strategy on source abatement and risk

reduction. Of course, further cost-effective analysis is also needed for the decision-making process, which cannot be fulfilled without the quantitative source–receptor relationship generated in this study.

One of the major findings of this study is that the lung cancer risk would be underestimated by almost 50 % if individual susceptibility is not taken into consideration in risk assessment. It is a common practice in risk assessment to use upper bound of 95 % confidence interval of risks conservatively in guideline formulation. With individual susceptibility introduced in the model, the goal can be achieved more reasonably by using the statistically best estimates and generate a frequency distribution from which a given risk range can be selected. On the other hand, the susceptibility was modeled with relatively large uncertainty largely due to limited data on genetic susceptibility. In fact, the uncertainty caused by the data limitation in genetic susceptibility is comparable to those introduced by the data limitation in dose–response relationship which is constrained by limitation in epidemiological survey studies. The overall uncertainty can be reduced in the future with a full understanding of the spectrum of genetic susceptibility in the population.

References

- Armstrong, B., Hutchinson, E., Unwin, J., & Fletcher, T. (2004). Lung cancer risk after exposure to polycyclic aromatic hydrocarbons: a review and meta-analysis. *Environmental Health Perspectives*, *112*, 970–978.
- Boffetta, P., Jourenkova, N., & Gustavsson, P. (1997). Cancer risk from occupational and environmental exposure to polycyclic aromatic hydrocarbons. *Cancer Causes and Control*, *8*, 444–472.
- Boström, C. E., Gerde, P., Hanberg, A., Jernstrom, B., Johansson, C., Kyrklund, T., et al. (2002). Cancer risk assessment, indicators, and guidelines for polycyclic aromatic hydrocarbons in the ambient air. *Environmental Health Perspectives*, *110*, 451–488.
- Brüske-Hohlfeld, I., Möhner, M., Pohlabein, H., Ahrens, W., Bolm-Audorff, U., Kreuzer, M., et al. (2000). Occupational lung cancer risk for men in Germany: results from a pooled case-control study. *American Journal of Epidemiology*, *151*, 384–395.
- Chen, S. C., & Liao, C. M. (2006). Health risk assessment on human exposed to environmental polycyclic aromatic hydrocarbons pollution sources. *Science of the Total Environment*, *366*, 112–123.
- Editorial Committee for the Atlas of Cancer Mortality (1976). Atlas of Cancer Mortality in the People's Republic of China. China Map Press.
- ESRI Inc (2014). *ArcGIS for Desktop*. Retrieved from <http://www.esri.com>.
- Ezzati, M., & Lopez, A. D. (2003). Estimates of global mortality attributable to smoking in 2000. *Lancet*, *362*, 847–852.
- Ferlay, J., Soerjomataram, I., Ervik, M., Dikshit, R., Eser, S., Mathers, C., et al. (2014). *GLOBOCAN 2012 v1.0. Cancer incidence and mortality worldwide: IARC cancerbase No. 11* [Internet] Lyon, France: International Agency for Research on Cancer. Retrieved from <http://globocan.iarc.fr>.
- International Agency for Research on Cancer (IARC) (2014). *Agents classified by the IARC monographs, volumes 1–109*. Retrieved from <http://monographs.iarc.fr/ENG/Classification/index.php>.
- Lunde, G., & Björseth, A. (1977). Polycyclic aromatic hydrocarbons in long-range transported aerosols. *Nature*, *268*, 518–519.

- Mastrangelo, G., Fadda, E., & Marzia, V. (1996). Polycyclic aromatic hydrocarbons and cancer in man. *Environmental Health Perspectives*, *104*, 1166–1170.
- Microsoft Corporation (2014). *All Office products*. Retrieved from <http://office.microsoft.com>.
- Mumford, J. L., Li, X., Hu, F., Lu, X. B., & Chuang, J. C. (1995). Human exposure and dosimetry of polycyclic aromatic hydrocarbons in urine from Xuan Wei, China with high lung cancer mortality associated with exposure to unvented coal smoke. *Carcinogenesis*, *16*, 3031–3036.
- Perera, F. P. (1997). Environment and cancer: who are susceptible? *Science*, *278*, 1068–1073.
- Ravindra, K., Sokhi, R., & Grieken, R. V. (2008). Atmospheric polycyclic aromatic hydrocarbons: source attribution, emission factors and regulation. *Atmospheric Environment*, *42*, 2895–2921.
- Shen, H. Z., Huang, Y., Wang, R., Zhu, D., Li, W., Shen, G., et al. (2013). Global atmospheric emissions of polycyclic aromatic hydrocarbons from 1960 to 2008 and future predictions. *Environmental Science and Technology*, *47*, 6415–6424.
- Shen, H. Z., Tao, S., Liu, J., Huang, Y., Chen, H., Li, W., et al. (2014). Global lung cancer risk from PAH exposure highly depends on emission sources and individual susceptibility. *Scientific Reports*,. doi:10.1038/srep06561.
- United States Environmental Protection Agency (USEPA) (2014). *Provisional guidance for quantitative risk assessment of polycyclic aromatic hydrocarbons*. Retrieved from <http://cfpub.epa.gov/ncea/cfm/recorddisplay.cfm?deid=49732>.
- World Health Organization (WHO) (2014). *Global Health Observatory Data Repository*. Retrieved from <http://apps.who.int/gho/data/node.main>.

Chapter 7

Conclusions

Global emissions, transport, exposure, and lung cancer risks of polycyclic aromatic hydrocarbons (PAHs) were quantitatively assessed in this thesis. Emissions of 16 parent PAHs from 69 major sources were estimated. Different methods have been used to estimate country- and time-specific emission factors to reduce the uncertainty in emission estimate. Two types of emission inventories (PKU-PAHs) were established, including country-level emission time series and a spatially resolved emission inventory for the year 2007 with a geographic resolution of $0.1^\circ \times 0.1^\circ$. The global total annual atmospheric emission of 16 PAHs in 2007 was 655 Gg (521–816 Gg, as interquartile range), with residential/commercial biomass burning (52.4 %), open-field biomass burning (agricultural waste burning, deforestation, and wildfire, 12.5 %), and petroleum consumption by on-road motor vehicles (16.5 %) as the major sources. South, East, and Southeast Asia were the regions with the highest PAH emission densities, contributing half of the global total PAH emissions. Among the global total PAH emissions, 7.7 % of the emissions were in the form of high molecular weight carcinogenic compounds and the percentage of the carcinogenic PAHs was higher in developing countries (8.0 %) than in developed countries (6.4 %), due to the differences in energy structures and the disparities of technology. The potential health impact of the PAH emissions was greatest in the parts of the world with high anthropogenic PAH emissions, because of the overlap of the high emissions and high population densities. Global total PAH emissions peaked at 869 Gg in 1978 and declined gradually to 624 Gg in 2008. Total PAH emissions from developed countries peaked at 261 Gg in the early 1970s and decreased to 51 Gg in 2008. Emissions from developing countries peaked at 663 Gg in the early 1990s and decreased slowly to 558 in 2008. Simulation of PAH emissions from 2009 to 2030 revealed that PAH emissions in developed and developing countries would decrease by 46–71 % and 48–64 %, respectively, based on the six IPCC SRES scenarios.

Based on MOZART-4, the global transport of BaP was simulated. Model validation showed good agreement between observation and simulation at background sites, but an underestimation at non-background sites. Using wind field and

high-resolution emission inventory, a Gauss diffusion downscaling method was adopted to generate concentration field with finer resolution. Results from the high-resolution concentration field match observations at non-background sites well. According to the concentration field, global distribution of near-surface BaP concentrations is discussed. Globally, near-surface BaP levels varied widely. The three quartiles of directly calculated concentrations are 0.00032, 0.0055, and 0.046 ng/m³, respectively. East Asia, South Asia, and Southeast Asia are three hot spots with median concentrations being 0.074, 0.21, and 0.086 ng/m³, respectively. Monthly variation of BaP contamination levels is significant. Because of the spatial overlap between emissions and population densities, the population-weighted BaP concentrations, as an indicator of health risk, is further enhanced in the above regions. Globally, the three quartiles of the population exposure concentrations are 0.18, 0.57, and 1.65 ng/m³, respectively. The medians of exposure concentrations in East Asia and South Asia are as high as 2.01 and 0.69 ng/m³, respectively. Emission from residential and industrial sectors contributes most to the overall exposure, as a result of both higher emissions and proximity to people. Globally, there is 2.2 % (1.8–2.7 % as R₅₀) of land area with ambient air concentrations exceeding the EU target value (1 ng/m³). However, 36.9 % (32.0–41.7 %) of the world's population live in these areas. Among them, 80.3 % live in East, South, and Southeast Asia, where 72.2, 40.1, and 35.4 % of the population, respectively, are exposed to annual mean ambient BaP concentrations above 1 ng/m³. Even with a relatively lenient national standard of 2.5 ng/m³, the rate of excess in China is as high as 34.1 %.

Based on the modeled distributions of near-surface BaP concentrations, the lung cancer risk being induced by inhalation exposure to PAHs is evaluated on a global scale, using BaP as an indicator. The results reveal that the health outcomes depend not only on the locations and strengths of emission sources, but also on individual susceptibility. Model resolution is critical in exposure modeling. Globally, incremental lifetime lung cancer risk (*ILCR*) induced by ambient PAH exposure is 3.1×10^{-5} . If the individual susceptibility was not taken into consideration, the overall risk would be underestimated by 55 % and the proportion of highly vulnerable population would be underestimated by more than 90 %. Emphasizing on individual susceptibility, this work provides an instrumental revision of current risk assessment methodology. In terms of lung cancer risk, the most important sources are combustion of biomass fuels (40 %) and fossil fuels (14 %) in the residential/commercial sector, coke (13 %) and aluminum (12 %) production, and motor vehicles (9 %). PAHs can travel long distance globally, especially within the Eurasian continent. Still, the risk is dominantly contributed by local.

Appendix

Based on the PKU-PAH emission inventory, emissions of individual PAH compounds in 2007 are listed in Tables [A.1](#) and [A.2](#) for each country.

Table A.1 World emissions of NAP, ACY, ACE, FLO, PHE, ANT, FLA, and PYR in 2007 (Mg/year)

Country	NAP	ACY	ACE	FLO	PHE	ANT	FLA	PYR
<i>World</i>	3.1×10^5	9.3×10^4	3.9×10^4	2.3×10^4	7.3×10^4	1.5×10^4	3.0×10^4	2.3×10^4
Afghanistan	1.9×10^2	6.9×10^1	2.3×10^1	8.8×10^0	3.6×10^1	6.8×10^0	1.6×10^1	1.2×10^1
Albania	1.2×10^2	1.7×10^1	7.1×10^0	7.0×10^0	1.7×10^1	3.3×10^0	7.2×10^0	5.9×10^0
Algeria	7.2×10^2	5.6×10^1	1.8×10^1	2.3×10^1	6.1×10^1	1.2×10^1	2.2×10^1	2.4×10^1
American Samoa	6.4×10^{-1}	4.2×10^{-1}	1.3×10^{-1}	6.3×10^{-2}	2.0×10^{-1}	3.6×10^{-2}	6.8×10^{-2}	5.5×10^{-2}
Andorra	1.0×10^0	2.7×10^{-1}	1.2×10^{-1}	1.5×10^{-1}	2.9×10^{-1}	5.4×10^{-2}	1.3×10^{-1}	9.5×10^{-2}
Angola	2.6×10^3	6.4×10^2	4.2×10^2	1.9×10^2	5.6×10^2	9.6×10^1	3.7×10^2	2.5×10^2
Anguilla	1.0×10^{-1}	3.6×10^{-3}	1.0×10^{-3}	2.4×10^{-3}	3.9×10^{-3}	6.7×10^{-4}	9.0×10^{-4}	1.6×10^{-3}
Antigua and Barbuda	1.4×10^0	2.2×10^{-1}	7.1×10^{-2}	6.0×10^{-2}	1.5×10^{-1}	2.7×10^{-2}	4.8×10^{-2}	4.7×10^{-2}
Argentina	1.9×10^3	1.6×10^2	1.1×10^2	6.1×10^1	2.1×10^2	4.0×10^1	1.3×10^2	9.7×10^1
Armenia	4.0×10^1	3.7×10^0	1.6×10^0	1.1×10^0	3.5×10^0	6.7×10^{-1}	1.3×10^0	1.2×10^0
Aruba	5.8×10^{-1}	3.5×10^{-1}	1.2×10^{-1}	6.8×10^{-2}	1.9×10^{-1}	3.6×10^{-2}	7.4×10^{-2}	5.9×10^{-2}
Australia	1.4×10^3	3.5×10^2	1.8×10^2	9.3×10^1	3.4×10^2	4.7×10^1	1.7×10^2	1.1×10^2
Austria	3.8×10^2	1.6×10^2	5.5×10^1	3.6×10^1	9.9×10^1	2.0×10^1	4.0×10^1	3.0×10^1
Azerbaijan	2.5×10^2	1.4×10^1	8.1×10^0	6.4×10^0	2.1×10^1	4.7×10^0	6.7×10^0	7.1×10^0
The Bahamas	2.8×10^0	1.6×10^0	5.5×10^{-1}	3.3×10^{-1}	9.3×10^{-1}	1.7×10^{-1}	3.5×10^{-1}	2.7×10^{-1}
Bahrain	2.2×10^1	9.9×10^{-1}	3.9×10^{-1}	1.6×10^0	5.2×10^1	2.6×10^{-1}	1.4×10^1	3.4×10^0
Bangladesh	2.2×10^3	1.1×10^3	3.9×10^2	1.7×10^2	5.8×10^2	1.2×10^2	2.5×10^2	1.9×10^2
Barbados	7.9×10^{-1}	2.9×10^{-1}	1.1×10^{-1}	9.7×10^{-2}	2.3×10^{-1}	4.4×10^{-2}	9.0×10^{-2}	6.9×10^{-2}
Belarus	3.9×10^2	6.8×10^1	2.7×10^1	2.5×10^1	6.2×10^1	1.2×10^1	2.5×10^1	2.0×10^1
Belgium	2.0×10^2	3.4×10^1	1.0×10^1	1.0×10^1	2.9×10^1	6.9×10^0	1.1×10^1	1.1×10^1
Belize	6.4×10^1	3.1×10^1	1.0×10^1	4.1×10^0	1.5×10^1	2.5×10^0	5.1×10^0	4.1×10^0
Benin	4.3×10^2	2.2×10^2	6.9×10^1	2.7×10^1	9.9×10^1	1.7×10^1	3.3×10^1	2.7×10^1

(continued)

Table A.1 (continued)

Country	NAP	ACY	ACE	FLO	PHE	ANT	FLA	PYR
Bermuda	4.6×10^{-2}	1.1×10^{-2}	1.2×10^{-3}	5.9×10^{-3}	1.7×10^{-2}	4.6×10^{-3}	7.2×10^{-3}	9.2×10^{-3}
Bhutan	3.0×10^2	2.0×10^2	6.4×10^1	2.3×10^1	8.9×10^1	1.6×10^1	2.8×10^1	2.3×10^1
Bolivia	1.6×10^3	3.3×10^2	2.4×10^2	9.9×10^1	3.0×10^2	5.0×10^1	2.2×10^2	1.5×10^2
Bosnia and Herzegovina	1.8×10^2	4.1×10^1	2.4×10^1	1.3×10^1	6.1×10^1	1.5×10^1	1.6×10^1	1.0×10^1
Botswana	1.1×10^2	3.8×10^1	1.5×10^1	8.9×10^0	2.6×10^1	4.9×10^0	9.8×10^0	7.4×10^0
Brazil	1.9×10^4	4.1×10^3	2.3×10^3	1.1×10^3	3.4×10^3	5.8×10^2	2.1×10^3	1.5×10^3
British Indian Ocean Territory	0.0×10^0	0.0×10^0	0.0×10^0	0.0×10^0	0.0×10^0	0.0×10^0	0.0×10^0	0.0×10^0
British Virgin Islands	4.9×10^{-2}	1.2×10^{-2}	1.4×10^{-3}	6.3×10^{-3}	1.8×10^{-2}	5.0×10^{-3}	7.8×10^{-3}	9.9×10^{-3}
Brunei	3.8×10^0	1.4×10^0	6.0×10^{-1}	2.3×10^{-1}	8.4×10^{-1}	1.9×10^{-1}	4.7×10^{-1}	3.1×10^{-1}
Bulgaria	3.9×10^2	9.5×10^1	3.6×10^1	2.2×10^1	7.1×10^1	1.6×10^1	2.3×10^1	1.9×10^1
Burkina Faso	8.2×10^2	5.3×10^2	1.7×10^2	6.1×10^1	2.3×10^2	4.0×10^1	7.1×10^1	5.8×10^1
Burundi	5.7×10^2	3.8×10^2	1.2×10^2	4.2×10^1	1.6×10^2	2.8×10^1	4.8×10^1	4.0×10^1
Cambodia	1.4×10^3	5.4×10^2	2.5×10^2	1.1×10^2	3.4×10^2	6.0×10^1	1.9×10^2	1.4×10^2
Cameroon	9.6×10^2	4.7×10^2	1.7×10^2	7.9×10^1	2.6×10^2	4.5×10^1	1.0×10^2	7.8×10^1
Canada	1.9×10^3	3.8×10^2	2.5×10^2	1.4×10^2	4.1×10^2	6.4×10^1	2.5×10^2	1.7×10^2
Cape Verde	6.3×10^0	3.7×10^{-1}	6.6×10^{-2}	1.7×10^{-1}	3.9×10^{-1}	7.6×10^{-2}	1.1×10^{-1}	1.5×10^{-1}
Cayman Islands	2.3×10^{-2}	5.5×10^{-3}	6.1×10^{-4}	2.9×10^{-3}	8.2×10^{-3}	2.3×10^{-3}	3.6×10^{-3}	4.5×10^{-3}
Central African Republic	1.9×10^3	4.5×10^2	3.2×10^2	1.3×10^2	4.0×10^2	6.3×10^1	2.9×10^2	1.9×10^2
Chad	5.8×10^2	3.2×10^2	1.1×10^2	4.2×10^1	1.5×10^2	2.6×10^1	5.8×10^1	4.5×10^1
Chile	1.2×10^3	4.9×10^2	1.8×10^2	6.5×10^1	2.4×10^2	4.7×10^1	7.8×10^1	6.6×10^1
China	6.0×10^4	1.6×10^4	7.7×10^3	6.1×10^3	2.0×10^4	4.4×10^3	7.8×10^3	5.9×10^3
Colombia	1.3×10^3	3.4×10^2	1.1×10^2	6.1×10^1	2.0×10^2	3.5×10^1	6.8×10^1	6.1×10^1
Comoros	1.7×10^1	1.0×10^1	3.2×10^0	1.2×10^0	4.5×10^0	7.8×10^{-1}	1.3×10^0	1.1×10^0
Congo DR	6.4×10^3	3.4×10^3	1.3×10^3	4.7×10^2	1.7×10^3	2.8×10^2	7.1×10^2	5.3×10^2

(continued)

Table A.1 (continued)

Country	NAP	ACY	ACE	FLO	PHE	ANT	FLA	PYR
Congo	1.5×10^2	5.7×10^1	2.4×10^1	8.9×10^0	3.1×10^1	7.0×10^0	1.2×10^1	1.0×10^1
Cook Islands	4.9×10^{-1}	2.0×10^{-2}	4.2×10^{-3}	1.2×10^{-2}	2.3×10^{-2}	4.1×10^{-3}	5.7×10^{-3}	9.2×10^{-3}
Costa Rica	2.3×10^2	7.2×10^1	2.2×10^1	1.1×10^1	3.5×10^1	6.1×10^0	1.0×10^1	9.8×10^0
Cote d'Ivoire	7.4×10^2	4.0×10^2	1.4×10^2	6.2×10^1	2.0×10^2	3.5×10^1	7.8×10^1	6.1×10^1
Croatia	1.8×10^2	3.1×10^1	1.2×10^1	8.3×10^0	2.4×10^1	4.2×10^0	7.6×10^0	7.0×10^0
Cuba	5.9×10^1	4.6×10^0	2.2×10^0	1.8×10^0	5.3×10^0	9.4×10^{-1}	2.3×10^0	2.2×10^0
Cyprus	4.5×10^1	3.6×10^0	3.3×10^0	9.3×10^{-1}	3.8×10^0	6.1×10^{-1}	8.8×10^{-1}	9.6×10^{-1}
Czech Republic	5.1×10^2	1.1×10^2	6.2×10^1	5.5×10^1	1.6×10^2	3.9×10^1	5.5×10^1	3.9×10^1
Denmark	2.1×10^2	6.7×10^1	3.3×10^1	3.7×10^1	7.8×10^1	1.5×10^1	3.7×10^1	2.5×10^1
Djibouti	1.2×10^2	7.9×10^1	2.4×10^1	8.9×10^0	3.4×10^1	5.8×10^0	1.0×10^1	8.4×10^0
Dominica	8.6×10^{-1}	1.1×10^{-1}	3.5×10^{-2}	4.3×10^{-2}	9.8×10^{-2}	1.8×10^{-2}	3.4×10^{-2}	3.2×10^{-2}
Dominican Republic	2.9×10^2	5.7×10^1	1.9×10^1	1.6×10^1	3.7×10^1	7.0×10^0	1.7×10^1	1.5×10^1
Ecuador	5.6×10^2	9.1×10^1	2.6×10^1	2.0×10^1	5.6×10^1	1.0×10^1	1.6×10^1	1.8×10^1
Egypt	2.2×10^3	2.6×10^2	9.8×10^1	7.3×10^1	2.3×10^2	5.4×10^1	8.0×10^1	8.1×10^1
El Salvador	3.5×10^2	1.7×10^2	5.3×10^1	2.3×10^1	8.0×10^1	1.4×10^1	2.5×10^1	2.1×10^1
Equatorial Guinea	1.5×10^1	8.1×10^0	2.5×10^0	9.6×10^{-1}	3.5×10^0	6.1×10^{-1}	1.0×10^0	9.0×10^{-1}
Eritrea	7.9×10^1	5.1×10^1	1.6×10^1	5.7×10^0	2.2×10^1	3.8×10^0	6.5×10^0	5.4×10^0
Estonia	1.2×10^2	4.2×10^1	1.5×10^1	1.2×10^1	3.1×10^1	5.7×10^0	1.2×10^1	8.8×10^0
Ethiopia	7.5×10^3	5.0×10^3	1.6×10^3	5.6×10^2	2.2×10^3	3.7×10^2	6.6×10^2	5.4×10^2
Falkland Islands	4.2×10^{-1}	2.0×10^{-1}	6.2×10^{-2}	2.6×10^{-2}	9.2×10^{-2}	1.6×10^{-2}	2.7×10^{-2}	2.4×10^{-2}
Faroe Islands	1.4×10^0	1.7×10^{-1}	6.7×10^{-2}	1.0×10^{-1}	1.9×10^{-1}	3.5×10^{-2}	7.8×10^{-2}	6.6×10^{-2}
Fiji	1.7×10^1	2.4×10^0	7.9×10^{-1}	7.2×10^{-1}	1.8×10^0	3.3×10^{-1}	6.9×10^{-1}	6.8×10^{-1}
Finland	3.2×10^2	1.5×10^2	5.2×10^1	2.0×10^1	7.8×10^1	1.5×10^1	2.5×10^1	2.0×10^1
France	2.0×10^3	7.9×10^2	2.9×10^2	1.2×10^2	4.6×10^2	8.7×10^1	1.6×10^2	1.2×10^2

(continued)

Table A.1 (continued)

Country	NAP	ACY	ACE	FLO	PHE	ANT	FLA	PYR
French Guiana	6.3×10^0	2.9×10^0	8.9×10^{-1}	3.7×10^{-1}	1.3×10^0	2.3×10^{-1}	3.9×10^{-1}	3.5×10^{-1}
French Polynesia	4.9×10^0	3.9×10^{-1}	1.5×10^{-1}	1.9×10^{-1}	3.5×10^{-1}	6.2×10^{-2}	1.2×10^{-1}	1.3×10^{-1}
Gabon	7.8×10^1	3.4×10^1	1.3×10^1	1.0×10^1	2.5×10^1	4.7×10^0	1.0×10^1	7.6×10^0
Georgia	1.6×10^2	2.8×10^1	1.0×10^1	9.7×10^0	2.4×10^1	4.8×10^0	9.1×10^0	7.6×10^0
Germany	1.9×10^3	4.6×10^2	2.0×10^2	1.9×10^2	4.7×10^2	9.9×10^1	2.0×10^2	1.4×10^2
Ghana	1.2×10^3	6.1×10^2	2.0×10^2	7.9×10^1	2.9×10^2	4.9×10^1	1.0×10^2	8.1×10^1
Gibraltar	4.1×10^0	1.5×10^{-1}	3.9×10^{-2}	9.7×10^{-2}	1.7×10^{-1}	2.9×10^{-2}	3.9×10^{-2}	6.9×10^{-2}
Greece	3.5×10^2	5.3×10^1	2.8×10^1	2.2×10^1	5.9×10^1	9.9×10^0	2.7×10^1	1.9×10^1
Greenland	5.1×10^{-1}	3.2×10^{-1}	1.0×10^{-1}	4.0×10^{-2}	1.5×10^{-1}	2.7×10^{-2}	4.7×10^{-2}	3.8×10^{-2}
Grenada	1.3×10^0	1.4×10^{-1}	4.2×10^{-2}	5.8×10^{-2}	1.3×10^{-1}	2.4×10^{-2}	4.2×10^{-2}	4.4×10^{-2}
Guadeloupe	4.8×10^0	2.2×10^{-1}	3.9×10^{-2}	1.2×10^{-1}	2.6×10^{-1}	4.9×10^{-2}	6.8×10^{-2}	1.0×10^{-1}
Guam	1.6×10^0	1.8×10^{-1}	4.7×10^{-2}	6.2×10^{-2}	1.5×10^{-1}	2.9×10^{-2}	4.7×10^{-2}	5.1×10^{-2}
Guatemala	1.2×10^3	6.6×10^2	2.1×10^2	8.2×10^1	3.0×10^2	5.1×10^1	9.5×10^1	7.9×10^1
Guinea	9.6×10^2	5.3×10^2	1.7×10^2	6.6×10^1	2.4×10^2	4.2×10^1	8.3×10^1	6.7×10^1
Guinea-Bissau	4.6×10^1	2.1×10^1	7.7×10^0	3.0×10^0	1.1×10^1	1.8×10^0	4.4×10^0	3.4×10^0
Guyana	7.7×10^1	3.8×10^1	1.2×10^1	4.7×10^0	1.7×10^1	3.0×10^0	5.1×10^0	4.4×10^0
Haiti	2.1×10^2	1.0×10^2	3.4×10^1	2.0×10^1	5.6×10^1	1.0×10^1	2.2×10^1	1.8×10^1
Honduras	5.6×10^2	2.8×10^2	8.8×10^1	3.5×10^1	1.3×10^2	2.2×10^1	3.9×10^1	3.4×10^1
Hungary	3.7×10^2	8.5×10^1	3.2×10^1	1.7×10^1	6.0×10^1	1.4×10^1	1.9×10^1	1.7×10^1
Iceland	6.9×10^0	1.8×10^0	8.5×10^{-1}	1.3×10^0	1.7×10^1	4.2×10^{-1}	5.1×10^0	1.5×10^0
India	3.3×10^4	1.5×10^4	5.4×10^3	2.9×10^3	9.2×10^3	1.9×10^3	3.9×10^3	2.9×10^3
Indonesia	1.1×10^4	3.7×10^3	1.4×10^3	9.0×10^2	2.4×10^3	4.5×10^2	1.1×10^3	8.8×10^2
Iran	4.0×10^3	2.0×10^2	5.1×10^1	1.0×10^2	2.5×10^2	4.8×10^1	8.7×10^1	1.0×10^2
Iraq	1.5×10^3	7.7×10^1	1.5×10^1	4.0×10^1	9.1×10^1	1.8×10^1	2.7×10^1	3.7×10^1

(continued)

Table A.1 (continued)

Country	NAP	ACY	ACE	FLO	PHE	ANT	FLA	PYR
Ireland	7.7×10^1	1.2×10^1	1.7×10^1	9.0×10^0	3.7×10^1	1.2×10^1	8.1×10^0	4.2×10^0
Israel	7.5×10^1	2.5×10^0	1.1×10^0	1.8×10^0	4.1×10^0	6.1×10^{-1}	1.3×10^0	1.5×10^0
Italy	9.4×10^2	1.7×10^2	6.4×10^1	3.9×10^1	1.2×10^2	2.6×10^1	4.5×10^1	4.1×10^1
Jamaica	1.5×10^2	2.5×10^1	6.9×10^0	5.2×10^0	1.5×10^1	2.6×10^0	4.1×10^0	4.6×10^0
Japan	2.0×10^3	1.9×10^2	6.7×10^1	9.8×10^1	2.8×10^2	7.8×10^1	1.0×10^2	1.1×10^2
Jordan	2.4×10^2	1.2×10^1	2.1×10^0	6.4×10^0	1.4×10^1	2.7×10^0	3.8×10^0	5.5×10^0
Kazakhstan	9.3×10^2	8.2×10^1	7.4×10^1	4.4×10^1	2.0×10^2	5.2×10^1	6.9×10^1	4.6×10^1
Kenya	1.7×10^3	1.0×10^3	3.3×10^2	1.3×10^2	4.8×10^2	8.3×10^1	1.5×10^2	1.2×10^2
Kiribati	5.5×10^{-1}	8.7×10^{-2}	2.9×10^{-2}	3.5×10^{-2}	7.6×10^{-2}	1.4×10^{-2}	3.0×10^{-2}	2.7×10^{-2}
North Korea	7.0×10^2	3.3×10^2	2.2×10^2	9.3×10^1	4.7×10^2	1.3×10^2	1.1×10^2	5.5×10^1
South Korea	1.2×10^3	9.7×10^1	2.7×10^1	3.7×10^1	9.6×10^1	2.5×10^1	3.4×10^1	4.2×10^1
Kuwait	7.5×10^1	1.6×10^1	8.3×10^0	1.4×10^1	2.6×10^1	4.6×10^0	1.2×10^1	8.5×10^0
Kyrgyzstan	1.1×10^2	6.4×10^0	2.7×10^0	2.6×10^0	1.0×10^1	1.6×10^0	3.9×10^0	3.4×10^0
Laos	8.7×10^2	3.6×10^2	1.6×10^2	7.1×10^1	2.2×10^2	3.8×10^1	1.2×10^2	8.4×10^1
Latvia	2.0×10^2	5.5×10^1	2.4×10^1	2.7×10^1	5.8×10^1	1.1×10^1	2.6×10^1	1.8×10^1
Lebanon	1.0×10^2	7.7×10^0	2.2×10^0	2.8×10^0	7.4×10^0	1.2×10^0	2.2×10^0	2.5×10^0
Lesotho	1.5×10^2	9.1×10^1	2.9×10^1	1.1×10^1	4.1×10^1	7.1×10^0	1.3×10^1	1.1×10^1
Liberia	3.9×10^2	2.7×10^2	8.2×10^1	3.0×10^1	1.1×10^2	2.0×10^1	3.4×10^1	2.8×10^1
Libya	2.7×10^2	3.8×10^1	1.1×10^1	8.6×10^0	2.2×10^1	4.3×10^0	6.7×10^0	7.4×10^0
Liechtenstein	6.1×10^{-2}	2.8×10^{-2}	1.1×10^{-2}	1.5×10^{-2}	3.1×10^{-2}	6.0×10^{-3}	1.4×10^{-2}	1.1×10^{-2}
Lithuania	1.9×10^2	4.8×10^1	2.0×10^1	1.4×10^1	4.1×10^1	8.4×10^0	1.4×10^1	1.1×10^1
Luxembourg	1.5×10^1	1.4×10^0	6.9×10^{-1}	7.1×10^{-1}	1.5×10^0	7.8×10^{-1}	9.6×10^{-1}	7.1×10^{-1}
Macedonia	7.2×10^1	2.0×10^1	7.4×10^0	4.0×10^0	1.4×10^1	2.7×10^0	4.6×10^0	3.6×10^0
Madagascar	3.9×10^3	8.0×10^2	2.7×10^2	1.8×10^2	5.1×10^2	9.1×10^1	2.0×10^2	1.8×10^2

(continued)

Table A.1 (continued)

Country	NAP	ACY	ACE	FLO	PHE	ANT	FLA	PYR
Malawi	4.0×10^2	2.4×10^2	7.8×10^1	3.1×10^1	1.1×10^2	1.9×10^1	3.8×10^1	3.1×10^1
Malaysia	1.5×10^3	2.0×10^2	7.0×10^1	5.8×10^1	1.5×10^2	2.7×10^1	5.9×10^1	5.5×10^1
Maldives	4.7×10^1	1.9×10^1	6.0×10^0	3.0×10^0	9.7×10^0	1.7×10^0	3.0×10^0	2.6×10^0
Mali	4.6×10^2	2.4×10^2	7.8×10^1	3.1×10^1	1.1×10^2	1.9×10^1	3.9×10^1	3.1×10^1
Malta	1.4×10^1	5.4×10^0	1.8×10^0	8.2×10^{-1}	2.7×10^0	5.0×10^{-1}	9.3×10^{-1}	7.5×10^{-1}
Marshall Islands	1.2×10^0	1.2×10^{-1}	3.5×10^{-2}	5.2×10^{-2}	1.1×10^{-1}	2.1×10^{-2}	4.0×10^{-2}	4.1×10^{-2}
Martinique	1.9×10^1	8.3×10^{-1}	1.5×10^{-1}	4.8×10^{-1}	9.7×10^{-1}	1.8×10^{-1}	2.5×10^{-1}	3.9×10^{-1}
Mauritania	1.3×10^2	7.4×10^1	2.3×10^1	9.0×10^0	3.3×10^1	5.7×10^0	1.0×10^1	8.6×10^0
Mauritius	4.5×10^1	2.9×10^0	8.9×10^{-1}	1.9×10^0	3.7×10^0	7.0×10^{-1}	1.3×10^0	1.3×10^0
Mayotte	8.8×10^0	2.6×10^{-1}	1.1×10^{-1}	2.0×10^{-1}	2.7×10^{-1}	4.4×10^{-2}	5.8×10^{-2}	1.2×10^{-1}
Mexico	5.4×10^3	1.1×10^3	3.4×10^2	2.1×10^2	6.3×10^2	1.2×10^2	2.0×10^2	2.0×10^2
Moldova	7.0×10^1	7.2×10^0	3.8×10^0	2.9×10^0	9.7×10^0	2.9×10^0	2.7×10^0	2.4×10^0
Monaco	3.2×10^0	1.5×10^{-1}	2.4×10^{-2}	8.5×10^{-2}	1.8×10^{-1}	3.5×10^{-2}	4.9×10^{-2}	7.3×10^{-2}
Mongolia	1.8×10^2	3.4×10^1	2.8×10^1	1.4×10^1	5.1×10^1	1.3×10^1	2.2×10^1	1.4×10^1
Montserrat	4.1×10^{-1}	1.7×10^{-2}	3.4×10^{-3}	1.0×10^{-2}	2.0×10^{-2}	3.7×10^{-3}	5.1×10^{-3}	8.2×10^{-3}
Morocco	7.2×10^2	6.6×10^1	2.2×10^1	3.3×10^1	7.4×10^1	1.4×10^1	2.7×10^1	2.6×10^1
Mozambique	2.6×10^3	1.0×10^3	4.6×10^2	1.9×10^2	6.5×10^2	1.0×10^2	3.4×10^2	2.4×10^2
Myanmar (Burma)	4.0×10^3	1.8×10^3	7.3×10^2	3.0×10^2	1.0×10^3	1.8×10^2	4.9×10^2	3.5×10^2
Namibia	1.5×10^2	2.8×10^1	1.2×10^1	7.0×10^0	1.9×10^1	4.1×10^0	7.9×10^0	6.9×10^0
Nauru	2.8×10^{-1}	1.3×10^{-2}	2.2×10^{-3}	7.4×10^{-3}	1.6×10^{-2}	3.0×10^{-3}	4.1×10^{-3}	6.2×10^{-3}
Nepal	1.3×10^3	6.7×10^2	2.5×10^2	1.6×10^2	4.1×10^2	7.8×10^1	1.9×10^2	1.4×10^2
Netherlands	1.9×10^2	2.6×10^1	1.0×10^1	1.3×10^1	3.9×10^1	6.8×10^0	1.5×10^1	1.1×10^1
Netherlands Antilles	1.6×10^1	2.5×10^0	7.8×10^{-1}	5.4×10^{-1}	3.1×10^0	2.5×10^{-1}	4.3×10^{-1}	4.9×10^{-1}
New Caledonia	5.2×10^0	4.4×10^{-1}	1.6×10^{-1}	1.8×10^{-1}	3.4×10^{-1}	6.0×10^{-2}	1.0×10^{-1}	1.2×10^{-1}

(continued)

Table A.1 (continued)

Country	NAP	ACY	ACE	FLO	PHE	ANT	FLA	PYR
New Zealand	1.8×10^2	3.9×10^1	1.9×10^1	9.3×10^0	4.4×10^1	7.7×10^0	1.2×10^1	7.9×10^0
Nicaragua	4.2×10^2	2.4×10^2	7.3×10^1	2.9×10^1	1.1×10^2	1.8×10^1	3.3×10^1	2.8×10^1
Niger	6.3×10^2	4.0×10^2	1.2×10^2	4.6×10^1	1.7×10^2	3.0×10^1	5.1×10^1	4.3×10^1
Nigeria	8.7×10^3	3.8×10^3	1.4×10^3	1.1×10^3	2.6×10^3	4.9×10^2	1.2×10^3	9.2×10^2
Niue	3.1×10^{-2}	1.6×10^{-3}	2.8×10^{-4}	8.6×10^{-4}	1.9×10^{-3}	3.6×10^{-4}	5.3×10^{-4}	7.3×10^{-4}
Northern Mariana Islands	2.9×10^{-1}	8.6×10^{-2}	3.2×10^{-2}	3.2×10^{-2}	6.9×10^{-2}	1.3×10^{-2}	3.0×10^{-2}	2.4×10^{-2}
Norway	1.3×10^2	6.6×10^1	2.4×10^1	1.5×10^1	8.2×10^1	8.5×10^0	4.9×10^1	3.7×10^1
Oman	1.0×10^2	1.8×10^1	9.0×10^0	1.7×10^1	2.9×10^1	5.2×10^0	1.3×10^1	9.8×10^0
Pakistan	5.2×10^3	1.8×10^3	7.1×10^2	6.1×10^2	1.5×10^3	2.9×10^2	7.1×10^2	5.1×10^2
Palau	5.8×10^{-1}	4.5×10^{-2}	1.3×10^{-2}	2.1×10^{-2}	4.4×10^{-2}	8.3×10^{-3}	1.5×10^{-2}	1.7×10^{-2}
Panama	1.6×10^2	5.0×10^1	1.6×10^1	8.1×10^0	2.5×10^1	4.5×10^0	8.1×10^0	7.5×10^0
Papua New Guinea	3.9×10^2	2.4×10^2	7.5×10^1	2.8×10^1	1.0×10^2	1.8×10^1	3.2×10^1	2.7×10^1
Paraguay	1.1×10^3	3.1×10^2	1.6×10^2	6.9×10^1	2.2×10^2	3.6×10^1	1.4×10^2	9.4×10^1
Peru	9.8×10^2	3.5×10^2	1.2×10^2	6.1×10^1	1.9×10^2	3.3×10^1	7.1×10^1	5.9×10^1
Philippines	2.1×10^3	5.8×10^2	1.8×10^2	1.0×10^2	3.2×10^2	5.8×10^1	1.1×10^2	9.7×10^1
Pitcairn Islands	7.2×10^{-4}	3.5×10^{-5}	5.2×10^{-6}	1.9×10^{-5}	4.2×10^{-5}	8.1×10^{-6}	1.1×10^{-5}	1.6×10^{-5}
Poland	1.9×10^3	3.8×10^2	3.0×10^2	2.2×10^2	7.5×10^2	2.2×10^2	2.1×10^2	1.5×10^2
Portugal	3.1×10^2	4.4×10^1	2.1×10^1	2.4×10^1	5.0×10^1	9.8×10^0	2.3×10^1	1.8×10^1
Puerto Rico	3.8×10^1	7.4×10^0	2.8×10^0	2.7×10^0	5.8×10^0	1.1×10^0	2.2×10^0	1.8×10^0
Qatar	1.3×10^1	1.9×10^0	2.8×10^{-1}	3.6×10^{-1}	2.5×10^0	4.3×10^{-1}	3.5×10^{-1}	3.6×10^{-1}
Reunion	2.9×10^1	1.2×10^0	2.6×10^{-1}	7.2×10^{-1}	1.4×10^0	2.4×10^{-1}	3.4×10^{-1}	5.5×10^{-1}
Romania	8.2×10^2	2.0×10^2	7.3×10^1	7.3×10^1	1.9×10^2	3.4×10^1	7.3×10^1	5.7×10^1
Russia	6.6×10^3	8.2×10^2	5.9×10^2	3.2×10^2	1.1×10^3	2.9×10^2	6.4×10^2	5.6×10^2
Rwanda	6.4×10^2	4.1×10^2	1.3×10^2	4.6×10^1	1.8×10^2	3.0×10^1	5.2×10^1	4.4×10^1

(continued)

Table A.1 (continued)

Country	NAP	ACY	ACE	FLO	PHE	ANT	FLA	PYR
Samoa	7.0×10^0	3.1×10^0	9.6×10^{-1}	4.4×10^{-1}	1.5×10^0	2.6×10^{-1}	4.6×10^{-1}	4.0×10^{-1}
San Marino	2.9×10^0	2.2×10^{-1}	6.1×10^{-2}	1.2×10^{-1}	2.6×10^{-1}	4.9×10^{-2}	8.8×10^{-2}	9.4×10^{-2}
Sao Tome and Principe	7.4×10^1	5.1×10^1	1.6×10^1	5.6×10^0	2.2×10^1	3.7×10^0	6.4×10^0	5.3×10^0
Saudi Arabia	1.1×10^3	4.1×10^1	1.9×10^1	2.5×10^1	4.6×10^1	9.6×10^0	1.5×10^1	2.0×10^1
Senegal	2.7×10^2	1.0×10^2	3.6×10^1	1.5×10^1	5.1×10^1	1.0×10^1	1.8×10^1	1.5×10^1
Serbia and Montenegro	3.3×10^2	1.4×10^2	6.6×10^1	2.8×10^1	1.3×10^2	3.1×10^1	3.4×10^1	2.2×10^1
Seychelles	2.3×10^0	1.9×10^{-1}	8.6×10^{-2}	1.4×10^{-1}	2.6×10^{-1}	5.1×10^{-2}	1.2×10^{-1}	9.9×10^{-2}
Sierra Leone	4.3×10^2	2.5×10^2	8.3×10^1	3.1×10^1	1.1×10^2	1.9×10^1	4.0×10^1	3.2×10^1
Singapore	2.2×10^1	5.9×10^{-1}	3.0×10^{-1}	4.5×10^{-1}	2.0×10^0	2.3×10^{-1}	2.8×10^{-1}	4.0×10^{-1}
Slovakia	2.0×10^2	2.5×10^1	1.3×10^1	1.2×10^1	4.9×10^1	1.2×10^1	1.4×10^1	1.1×10^1
Slovenia	1.0×10^2	2.8×10^1	1.0×10^1	7.4×10^0	2.3×10^1	3.7×10^0	8.4×10^0	5.9×10^0
Solomon Islands	9.7×10^0	5.4×10^0	1.7×10^0	6.7×10^{-1}	2.4×10^0	4.2×10^{-1}	7.4×10^{-1}	6.3×10^{-1}
Somalia	9.1×10^2	5.0×10^2	1.5×10^2	5.9×10^1	2.2×10^2	3.8×10^1	6.5×10^1	5.5×10^1
South Africa	3.2×10^3	8.3×10^2	4.8×10^2	2.8×10^2	1.0×10^3	2.6×10^2	3.0×10^2	2.1×10^2
South Georgia and the South Sandwich Islands	0.0×10^0	0.0×10^0	0.0×10^0	0.0×10^0	0.0×10^0	0.0×10^0	0.0×10^0	0.0×10^0
Spain	1.3×10^3	1.8×10^2	9.8×10^1	1.1×10^2	2.3×10^2	4.6×10^1	1.1×10^2	8.6×10^1
Sri Lanka	8.4×10^2	3.0×10^2	1.2×10^2	6.4×10^1	1.7×10^2	3.9×10^1	8.3×10^1	6.7×10^1
St. Helena	3.9×10^{-2}	2.0×10^{-3}	2.8×10^{-4}	1.0×10^{-3}	2.4×10^{-3}	4.7×10^{-4}	6.5×10^{-4}	9.3×10^{-4}
St. Kitts and Nevis	3.2×10^0	1.6×10^{-1}	4.0×10^{-2}	8.8×10^{-2}	1.7×10^{-1}	3.2×10^{-2}	4.9×10^{-2}	6.8×10^{-2}
St. Lucia	9.1×10^0	5.3×10^{-1}	1.3×10^{-1}	2.7×10^{-1}	5.6×10^{-1}	1.1×10^{-1}	1.7×10^{-1}	2.2×10^{-1}
St. Pierre and Miquelon	2.2×10^{-1}	8.0×10^{-3}	2.1×10^{-3}	5.3×10^{-3}	9.0×10^{-3}	1.6×10^{-3}	2.1×10^{-3}	3.7×10^{-3}
St. Vincent and the Grenadines	5.6×10^0	3.7×10^{-1}	9.1×10^{-2}	1.8×10^{-1}	3.8×10^{-1}	7.3×10^{-2}	1.1×10^{-1}	1.4×10^{-1}
Sudan	2.0×10^3	8.0×10^2	3.2×10^2	1.3×10^2	4.4×10^2	7.4×10^1	2.0×10^2	1.5×10^2

(continued)

Table A.1 (continued)

Country	NAP	ACY	ACE	FLO	PHE	ANT	FLA	PYR
Suriname	2.6×10^1	3.3×10^0	1.0×10^0	9.1×10^{-1}	2.4×10^0	4.3×10^{-1}	8.1×10^{-1}	8.5×10^{-1}
Swaziland	9.1×10^1	4.6×10^1	1.5×10^1	6.2×10^0	2.2×10^1	3.7×10^0	7.1×10^0	5.9×10^0
Sweden	2.6×10^2	8.6×10^1	2.9×10^1	1.3×10^1	4.8×10^1	9.3×10^0	1.9×10^1	1.6×10^1
Switzerland	1.3×10^2	4.1×10^1	1.4×10^1	7.0×10^0	2.3×10^1	4.7×10^0	8.1×10^0	6.6×10^0
Syria	6.8×10^2	3.6×10^1	1.7×10^1	1.7×10^1	4.3×10^1	1.1×10^1	1.6×10^1	1.8×10^1
Tajikistan	5.2×10^1	9.1×10^0	9.3×10^0	5.0×10^0	3.8×10^1	6.7×10^0	1.0×10^1	4.1×10^0
United Republic of Tanzania	2.3×10^3	1.1×10^3	4.1×10^2	2.0×10^2	6.2×10^2	1.1×10^2	2.6×10^2	2.0×10^2
Thailand	3.9×10^3	7.5×10^2	2.6×10^2	1.6×10^2	5.1×10^2	8.4×10^1	1.9×10^2	1.6×10^2
Timor Leste	1.9×10^2	1.2×10^2	3.9×10^1	1.8×10^1	5.7×10^1	1.0×10^1	2.1×10^1	1.7×10^1
Togo	2.3×10^2	1.3×10^2	4.1×10^1	1.6×10^1	5.8×10^1	9.9×10^0	1.9×10^1	1.6×10^1
Tokelau	1.5×10^{-2}	7.4×10^{-4}	1.1×10^{-4}	4.0×10^{-4}	8.7×10^{-4}	1.7×10^{-4}	2.4×10^{-4}	3.5×10^{-4}
Tonga	3.8×10^0	1.9×10^0	5.7×10^{-1}	2.4×10^{-1}	8.5×10^{-1}	1.5×10^{-1}	2.6×10^{-1}	2.2×10^{-1}
Trinidad and Tobago	5.3×10^1	5.2×10^0	1.4×10^0	1.6×10^0	4.1×10^0	7.5×10^{-1}	1.2×10^0	1.4×10^0
Tunisia	3.8×10^2	1.1×10^2	3.7×10^1	3.0×10^1	7.5×10^1	1.4×10^1	2.7×10^1	2.3×10^1
Turkey	3.0×10^3	5.5×10^2	3.7×10^2	3.0×10^2	8.8×10^2	2.2×10^2	3.0×10^2	2.1×10^2
Turkmenistan	1.8×10^2	9.0×10^0	4.2×10^0	5.1×10^0	1.7×10^1	4.1×10^0	7.5×10^0	6.3×10^0
Turks and Caicos Islands	1.1×10^0	3.8×10^{-2}	1.1×10^{-2}	2.5×10^{-2}	4.2×10^{-2}	7.3×10^{-3}	9.9×10^{-3}	1.7×10^{-2}
Tuvalu	1.4×10^{-1}	6.8×10^{-3}	1.0×10^{-3}	3.7×10^{-3}	8.0×10^{-3}	1.6×10^{-3}	2.2×10^{-3}	3.2×10^{-3}
Uganda	2.5×10^3	1.6×10^3	5.1×10^2	1.9×10^2	7.2×10^2	1.2×10^2	2.2×10^2	1.8×10^2
Ukraine	1.9×10^3	2.2×10^2	8.5×10^1	9.3×10^1	2.9×10^2	7.8×10^1	9.6×10^1	9.7×10^1
United Arab Emirates	6.3×10^1	1.1×10^1	6.4×10^0	1.3×10^1	7.2×10^1	3.7×10^0	2.3×10^1	9.9×10^0
United Kingdom	7.6×10^2	6.5×10^1	3.9×10^1	3.5×10^1	1.1×10^2	2.4×10^1	3.6×10^1	3.0×10^1
United States	6.6×10^3	1.7×10^3	7.6×10^2	3.1×10^2	1.1×10^3	2.0×10^2	3.9×10^2	3.2×10^2
Uruguay	1.8×10^2	5.6×10^1	1.9×10^1	8.0×10^0	2.9×10^1	5.2×10^0	9.5×10^0	8.1×10^0

(continued)

Table A.1 (continued)

Country	NAP	ACY	ACE	FLO	PHE	ANT	FLA	PYR
Uzbekistan	5.2×10^2	3.6×10^1	3.5×10^1	1.7×10^1	6.5×10^1	2.5×10^1	2.5×10^1	2.0×10^1
Vanuatu	7.3×10^0	4.0×10^0	1.2×10^0	4.8×10^{-1}	1.8×10^0	3.1×10^{-1}	5.3×10^{-1}	4.5×10^{-1}
Venezuela	1.4×10^3	1.3×10^2	4.7×10^1	4.6×10^1	1.5×10^2	2.0×10^1	5.4×10^1	4.7×10^1
Vietnam	5.0×10^3	1.8×10^3	7.9×10^2	5.0×10^2	1.4×10^3	3.0×10^2	6.4×10^2	4.8×10^2
Wallis and Futuna	1.9×10^{-1}	8.5×10^{-3}	1.4×10^{-3}	4.8×10^{-3}	9.9×10^{-3}	1.9×10^{-3}	2.6×10^{-3}	4.0×10^{-3}
Western Sahara	0.0×10^0	0.0×10^0	0.0×10^0	0.0×10^0	0.0×10^0	0.0×10^0	0.0×10^0	0.0×10^0
Yemen	4.5×10^2	3.8×10^1	8.5×10^0	1.3×10^1	3.2×10^1	6.2×10^0	9.4×10^0	1.2×10^1
Zambia	1.9×10^3	6.4×10^2	3.3×10^2	1.4×10^2	4.4×10^2	7.2×10^1	2.6×10^2	1.8×10^2
Zimbabwe	8.8×10^2	4.6×10^2	1.7×10^2	1.1×10^2	3.0×10^2	5.7×10^1	1.2×10^2	8.6×10^1

The results here are source-aggregated for the base year of 2007 only

Table A.2 World emissions of BaA, CHR, BbF, BaP, IcdP, DahA, and BghiP in 2007 (Mg/year)

Country	BaA	CHR	BbF	BaP	IcdP	DahA	BghiP
World	1.3×10^4	9.6×10^3	8.3×10^3	4.7×10^3	4.1×10^3	2.5×10^3	3.7×10^3
Afghanistan	1.1×10^1	5.5×10^0	3.6×10^0	2.0×10^0	1.1×10^0	1.5×10^0	2.1×10^0
Albania	2.0×10^0	1.6×10^0	1.3×10^0	9.0×10^{-1}	9.7×10^{-1}	4.9×10^{-1}	7.9×10^{-1}
Algeria	7.0×10^0	5.1×10^0	4.6×10^0	3.6×10^0	2.6×10^0	1.5×10^0	3.5×10^0
American Samoa	5.5×10^{-2}	2.1×10^{-2}	1.2×10^{-2}	1.2×10^{-2}	7.6×10^{-3}	4.2×10^{-3}	7.3×10^{-3}
Andorra	3.3×10^{-2}	2.5×10^{-2}	1.9×10^{-2}	1.9×10^{-2}	1.3×10^{-2}	4.1×10^{-3}	1.1×10^{-2}
Angola	6.0×10^1	4.6×10^1	1.7×10^1	2.9×10^1	7.7×10^1	4.0×10^1	1.9×10^1
Anguilla	2.6×10^{-4}	2.0×10^{-4}	1.7×10^{-4}	1.6×10^{-4}	1.4×10^{-4}	1.5×10^{-5}	2.1×10^{-4}
Antigua and Barbuda	2.6×10^{-2}	1.2×10^{-2}	7.8×10^{-3}	7.5×10^{-3}	5.3×10^{-3}	2.2×10^{-3}	6.0×10^{-3}
Argentina	2.6×10^1	2.6×10^1	1.7×10^1	9.7×10^0	1.6×10^1	1.3×10^1	1.4×10^1
Armenia	5.1×10^{-1}	3.9×10^{-1}	4.1×10^{-1}	1.7×10^{-1}	9.2×10^{-2}	1.3×10^{-1}	2.1×10^{-1}
Aruba	4.6×10^{-2}	2.0×10^{-2}	1.3×10^{-2}	1.3×10^{-2}	7.9×10^{-3}	3.7×10^{-3}	7.3×10^{-3}
Australia	4.0×10^1	3.2×10^1	2.3×10^1	1.7×10^1	3.2×10^1	1.5×10^1	2.1×10^1
Austria	2.0×10^1	1.1×10^1	7.3×10^0	6.2×10^0	3.8×10^0	2.1×10^0	4.3×10^0
Azerbaijan	1.8×10^0	2.1×10^0	2.1×10^0	8.0×10^{-1}	6.5×10^{-1}	5.9×10^{-1}	1.4×10^0
The Bahamas	2.0×10^{-1}	9.2×10^{-2}	5.7×10^{-2}	5.3×10^{-2}	4.1×10^{-2}	2.1×10^{-2}	3.3×10^{-2}
Bahrain	4.2×10^{-1}	6.1×10^0	7.7×10^0	1.6×10^0	4.8×10^0	5.7×10^{-1}	9.2×10^0
Bangladesh	1.5×10^2	6.0×10^1	3.4×10^1	3.5×10^1	2.0×10^1	1.3×10^1	2.0×10^1
Barbados	3.8×10^{-2}	2.1×10^{-2}	1.5×10^{-2}	1.4×10^{-2}	9.1×10^{-3}	3.7×10^{-3}	8.2×10^{-3}
Belarus	8.0×10^0	5.8×10^0	5.2×10^0	3.6×10^0	2.3×10^0	1.2×10^0	2.9×10^0
Belgium	4.4×10^0	3.0×10^0	2.5×10^0	2.0×10^0	1.2×10^0	5.6×10^{-1}	1.6×10^0
Belize	3.9×10^0	1.5×10^0	7.8×10^{-1}	7.7×10^{-1}	7.2×10^{-1}	4.2×10^{-1}	5.2×10^{-1}
Benin	2.7×10^1	1.0×10^1	5.4×10^0	5.2×10^0	4.3×10^0	2.6×10^0	3.5×10^0

(continued)

Table A.2 (continued)

Country	BaA	CHR	BbF	BkF	BaP	IcdP	DahA	BghiP
Bermuda	2.0×10^{-3}	2.0×10^{-3}	1.3×10^{-3}	1.1×10^{-3}	1.7×10^{-3}	6.8×10^{-4}	9.8×10^{-5}	7.7×10^{-4}
Bhutan	2.7×10^1	9.5×10^0	5.1×10^0	2.5×10^0	4.8×10^0	3.2×10^0	2.1×10^0	3.0×10^0
Bolivia	2.8×10^1	2.4×10^1	7.7×10^0	2.0×10^1	1.5×10^1	4.7×10^1	2.5×10^1	1.0×10^1
Bosnia and Herzegovina	1.0×10^1	1.2×10^1	1.7×10^1	2.4×10^0	2.9×10^0	2.6×10^0	2.3×10^0	5.6×10^0
Botswana	5.0×10^0	2.8×10^0	2.2×10^0	1.1×10^0	1.4×10^0	1.3×10^0	7.4×10^{-1}	1.1×10^0
Brazil	4.3×10^2	3.8×10^2	1.8×10^2	2.0×10^2	2.0×10^2	4.3×10^2	2.2×10^2	1.5×10^2
British Indian Ocean Territory	0.0×10^0	0.0×10^0	0.0×10^0	0.0×10^0	0.0×10^0	0.0×10^0	0.0×10^0	0.0×10^0
British Virgin Islands	2.2×10^{-3}	2.2×10^{-3}	1.4×10^{-3}	1.2×10^{-3}	1.8×10^{-3}	7.4×10^{-4}	1.1×10^{-4}	8.3×10^{-4}
Brunei	1.7×10^{-1}	7.9×10^{-2}	3.5×10^{-2}	3.5×10^{-2}	4.4×10^{-2}	4.2×10^{-2}	3.2×10^{-2}	2.2×10^{-2}
Bulgaria	1.4×10^1	9.8×10^0	1.0×10^1	2.9×10^0	3.9×10^0	2.6×10^0	2.0×10^0	4.0×10^0
Burkina Faso	6.8×10^1	2.4×10^1	1.3×10^1	6.4×10^0	1.2×10^1	8.6×10^0	5.5×10^0	8.0×10^0
Burundi	4.9×10^1	1.7×10^1	9.4×10^0	4.3×10^0	8.6×10^0	5.6×10^0	3.6×10^0	5.6×10^0
Cambodia	6.3×10^1	3.3×10^1	1.6×10^1	1.8×10^1	2.1×10^1	3.2×10^1	1.7×10^1	1.2×10^1
Cameroon	5.9×10^1	2.6×10^1	1.4×10^1	1.0×10^1	1.4×10^1	1.5×10^1	8.3×10^0	9.8×10^0
Canada	4.3×10^1	5.2×10^1	3.0×10^1	2.5×10^1	2.5×10^1	4.6×10^1	2.2×10^1	2.0×10^1
Cape Verde	2.8×10^{-2}	1.9×10^{-2}	1.4×10^{-2}	1.4×10^{-2}	1.5×10^{-2}	1.2×10^{-2}	3.4×10^{-3}	2.0×10^{-2}
Cayman Islands	9.9×10^{-4}	1.0×10^{-3}	6.5×10^{-4}	5.5×10^{-4}	8.4×10^{-4}	3.4×10^{-4}	4.8×10^{-5}	3.8×10^{-4}
Central African Republic	4.0×10^1	3.3×10^1	1.0×10^1	2.6×10^1	2.0×10^1	6.4×10^1	3.4×10^1	1.3×10^1
Chad	4.0×10^1	1.5×10^1	7.9×10^0	5.3×10^0	8.0×10^0	9.0×10^0	5.3×10^0	5.3×10^0
Chile	6.3×10^1	2.5×10^1	1.4×10^1	7.5×10^0	1.3×10^1	8.5×10^0	5.8×10^0	8.7×10^0
China	3.1×10^3	3.3×10^3	3.5×10^3	1.0×10^3	1.5×10^3	9.2×10^2	5.2×10^2	1.3×10^3
Colombia	4.2×10^1	1.9×10^1	1.2×10^1	6.9×10^0	1.1×10^1	9.4×10^0	5.1×10^0	8.1×10^0
Comoros	1.3×10^0	4.7×10^{-1}	2.6×10^{-1}	1.2×10^{-1}	2.4×10^{-1}	1.5×10^{-1}	9.9×10^{-2}	1.6×10^{-1}
Congo DR	4.1×10^2	1.7×10^2	8.2×10^1	6.4×10^1	8.8×10^1	1.2×10^2	6.9×10^1	5.7×10^1

(continued)

Table A.2 (continued)

Country	BaA	CHR	BbF	BkF	BaP	IcdP	DahA	BghiP
Congo	6.9×10^0	3.0×10^0	1.5×10^0	1.2×10^0	1.6×10^0	1.8×10^0	1.1×10^0	1.1×10^0
Cook Islands	1.3×10^{-3}	1.1×10^{-3}	8.3×10^{-4}	7.5×10^{-4}	8.9×10^{-4}	7.4×10^{-4}	1.2×10^{-4}	1.2×10^{-3}
Costa Rica	9.0×10^0	3.4×10^0	1.9×10^0	1.0×10^0	1.8×10^0	1.2×10^0	7.1×10^{-1}	1.4×10^0
Cote d'Ivoire	5.1×10^1	2.1×10^1	1.2×10^1	7.9×10^0	1.2×10^1	1.0×10^1	5.5×10^0	7.3×10^0
Croatia	3.8×10^0	2.1×10^0	1.5×10^0	9.0×10^{-1}	1.2×10^0	7.6×10^{-1}	4.5×10^{-1}	9.9×10^{-1}
Cuba	4.7×10^{-1}	3.8×10^{-1}	3.3×10^{-1}	2.8×10^{-1}	2.6×10^{-1}	4.3×10^{-1}	2.5×10^{-1}	2.5×10^{-1}
Cyprus	3.6×10^{-1}	3.7×10^{-1}	7.0×10^{-1}	1.6×10^{-1}	2.0×10^{-1}	4.5×10^{-2}	1.6×10^{-1}	1.7×10^{-1}
Czech Republic	2.3×10^1	2.6×10^1	3.3×10^1	8.0×10^0	9.1×10^0	5.8×10^0	4.7×10^0	9.7×10^0
Denmark	8.9×10^0	7.7×10^0	6.9×10^0	5.0×10^0	5.1×10^0	3.3×10^0	1.5×10^0	3.3×10^0
Djibouti	1.0×10^1	3.6×10^0	2.0×10^0	9.1×10^{-1}	1.8×10^0	1.2×10^0	7.5×10^{-1}	1.2×10^0
Dominica	1.2×10^{-2}	7.2×10^{-3}	5.1×10^{-3}	4.3×10^{-3}	4.9×10^{-3}	3.6×10^{-3}	1.3×10^{-3}	4.1×10^{-3}
Dominican Republic	7.0×10^0	3.5×10^0	2.4×10^0	2.0×10^0	2.8×10^0	1.8×10^0	7.3×10^{-1}	1.8×10^0
Ecuador	1.0×10^1	4.4×10^0	2.7×10^0	1.8×10^0	2.6×10^0	2.0×10^0	1.1×10^0	2.4×10^0
Egypt	3.3×10^1	2.2×10^1	1.7×10^1	9.5×10^0	1.2×10^1	8.8×10^0	5.5×10^0	1.4×10^1
El Salvador	2.2×10^1	8.1×10^0	4.6×10^0	2.4×10^0	4.2×10^0	2.8×10^0	1.7×10^0	2.9×10^0
Equatorial Guinea	1.0×10^0	3.7×10^{-1}	2.1×10^{-1}	9.5×10^{-2}	1.9×10^{-1}	1.2×10^{-1}	7.7×10^{-2}	1.3×10^{-1}
Eritrea	6.6×10^0	2.3×10^0	1.3×10^0	5.9×10^{-1}	1.2×10^0	7.6×10^{-1}	5.0×10^{-1}	7.6×10^{-1}
Estonia	5.2×10^0	3.0×10^0	2.2×10^0	1.5×10^0	1.8×10^0	1.1×10^0	5.7×10^{-1}	1.2×10^0
Ethiopia	6.5×10^2	2.3×10^2	1.3×10^2	5.9×10^1	1.2×10^2	7.8×10^1	5.1×10^1	7.5×10^1
Falkland Islands	2.6×10^{-2}	9.4×10^{-3}	5.2×10^{-3}	2.5×10^{-3}	4.8×10^{-3}	3.2×10^{-3}	2.0×10^{-3}	3.3×10^{-3}
Faroe Islands	1.9×10^{-2}	1.5×10^{-2}	1.1×10^{-2}	1.0×10^{-2}	1.1×10^{-2}	8.1×10^{-3}	2.3×10^{-3}	8.1×10^{-3}
Fiji	2.8×10^{-1}	1.4×10^{-1}	1.0×10^{-1}	7.9×10^{-2}	1.1×10^{-1}	7.9×10^{-2}	3.1×10^{-2}	8.3×10^{-2}
Finland	2.0×10^1	9.5×10^0	6.8×10^0	2.8×10^0	4.5×10^0	2.6×10^0	1.9×10^0	3.4×10^0
France	1.1×10^2	5.7×10^1	4.2×10^1	1.8×10^1	2.6×10^1	1.6×10^1	1.2×10^1	2.3×10^1

(continued)

Table A.2 (continued)

Country	BaA	CHR	BbF	BkF	BaP	IcdP	DahA	BghiP
French Guiana	3.7×10^{-1}	1.3×10^{-1}	7.5×10^{-2}	3.7×10^{-2}	7.0×10^{-2}	4.6×10^{-2}	2.8×10^{-2}	4.8×10^{-2}
French Polynesia	4.4×10^{-2}	2.7×10^{-2}	2.1×10^{-2}	1.6×10^{-2}	2.1×10^{-2}	1.5×10^{-2}	3.8×10^{-3}	1.6×10^{-2}
Gabon	4.2×10^0	2.3×10^0	1.5×10^0	1.3×10^0	1.5×10^0	1.2×10^0	5.2×10^{-1}	8.9×10^{-1}
Georgia	3.5×10^0	2.2×10^0	1.8×10^0	1.1×10^0	1.3×10^0	9.2×10^{-1}	4.5×10^{-1}	1.1×10^0
Germany	6.4×10^1	5.5×10^1	5.4×10^1	2.6×10^1	3.0×10^1	2.0×10^1	1.0×10^1	2.6×10^1
Ghana	7.7×10^1	2.9×10^1	1.5×10^1	9.2×10^0	1.5×10^1	1.4×10^1	8.5×10^0	1.0×10^1
Gibraltar	1.1×10^{-2}	8.1×10^{-3}	6.8×10^{-3}	5.4×10^{-3}	6.9×10^{-3}	5.7×10^{-3}	1.0×10^{-3}	8.9×10^{-3}
Greece	6.1×10^0	5.2×10^0	3.9×10^0	3.1×10^0	3.2×10^0	3.9×10^0	1.7×10^0	3.1×10^0
Greenland	4.1×10^{-2}	1.7×10^{-2}	9.2×10^{-3}	5.0×10^{-3}	8.4×10^{-3}	4.9×10^{-3}	3.3×10^{-3}	5.6×10^{-3}
Grenada	1.5×10^{-2}	8.8×10^{-3}	6.3×10^{-3}	5.4×10^{-3}	6.2×10^{-3}	4.6×10^{-3}	1.5×10^{-3}	5.6×10^{-3}
Guadeloupe	1.4×10^{-2}	1.1×10^{-2}	8.6×10^{-3}	8.8×10^{-3}	9.8×10^{-3}	8.1×10^{-3}	1.7×10^{-3}	1.4×10^{-2}
Guam	1.8×10^{-2}	1.0×10^{-2}	7.0×10^{-3}	5.9×10^{-3}	7.0×10^{-3}	5.2×10^{-3}	1.9×10^{-3}	6.9×10^{-3}
Guatemala	8.4×10^1	3.1×10^1	1.7×10^1	8.8×10^0	1.6×10^1	1.2×10^1	7.3×10^0	1.1×10^1
Guinea	6.8×10^1	2.5×10^1	1.3×10^1	7.6×10^0	1.3×10^1	1.2×10^1	7.0×10^0	8.5×10^0
Guinea-Bissau	2.6×10^0	1.1×10^0	5.2×10^{-1}	4.0×10^{-1}	5.6×10^{-1}	7.2×10^{-1}	4.1×10^{-1}	3.8×10^{-1}
Guyana	4.8×10^0	1.7×10^0	9.7×10^{-1}	4.7×10^{-1}	8.9×10^{-1}	5.9×10^{-1}	3.7×10^{-1}	6.1×10^{-1}
Haiti	1.3×10^1	5.7×10^0	3.6×10^0	2.5×10^0	3.7×10^0	2.4×10^0	1.1×10^0	2.2×10^0
Honduras	3.6×10^1	1.3×10^1	7.2×10^0	3.6×10^0	6.7×10^0	4.7×10^0	2.9×10^0	4.6×10^0
Hungary	1.3×10^1	9.2×10^0	9.4×10^0	2.4×10^0	3.3×10^0	1.9×10^0	1.8×10^0	3.5×10^0
Iceland	3.2×10^{-1}	1.8×10^0	2.2×10^0	4.6×10^{-1}	5.5×10^{-1}	1.4×10^0	1.9×10^{-1}	2.5×10^0
India	2.1×10^3	1.1×10^3	8.6×10^2	4.0×10^2	5.8×10^2	3.6×10^2	2.3×10^2	4.1×10^2
Indonesia	4.8×10^2	2.3×10^2	1.6×10^2	1.3×10^2	1.8×10^2	1.2×10^2	4.9×10^1	1.0×10^2
Iran	2.2×10^1	2.1×10^1	2.0×10^1	1.1×10^1	1.2×10^1	9.4×10^0	6.0×10^0	1.8×10^1
Iraq	6.2×10^0	5.1×10^0	4.1×10^0	3.5×10^0	3.6×10^0	2.7×10^0	1.6×10^0	5.2×10^0

(continued)

Table A.2 (continued)

Country	BaA	CHR	BbF	BkF	BaP	IcdP	DahA	BghiP
Ireland	6.9×10^0	1.1×10^1	1.6×10^1	1.7×10^0	1.7×10^0	1.2×10^0	2.1×10^0	3.5×10^0
Israel	3.9×10^{-1}	3.3×10^{-1}	2.8×10^{-1}	1.7×10^{-1}	1.7×10^{-1}	1.2×10^{-1}	1.8×10^{-1}	2.3×10^{-1}
Italy	2.2×10^1	1.3×10^1	1.0×10^1	5.3×10^0	7.3×10^0	5.3×10^0	3.0×10^0	7.1×10^0
Jamaica	2.9×10^0	1.2×10^0	7.0×10^{-1}	4.4×10^{-1}	6.9×10^{-1}	4.9×10^{-1}	2.5×10^{-1}	6.2×10^{-1}
Japan	3.1×10^1	3.2×10^1	3.5×10^1	1.4×10^1	2.1×10^1	1.2×10^1	7.1×10^0	1.7×10^1
Jordan	8.5×10^{-1}	6.5×10^{-1}	5.2×10^{-1}	5.1×10^{-1}	5.4×10^{-1}	4.4×10^{-1}	1.9×10^{-1}	7.6×10^{-1}
Kazakhstan	3.2×10^1	4.3×10^1	5.7×10^1	9.0×10^0	9.9×10^0	6.1×10^0	1.0×10^1	1.6×10^1
Kenya	1.4×10^2	5.0×10^1	2.8×10^1	1.4×10^1	2.6×10^1	1.7×10^1	1.0×10^1	1.7×10^1
Kiribati	9.9×10^{-3}	5.9×10^{-3}	4.1×10^{-3}	3.8×10^{-3}	4.5×10^{-3}	3.1×10^{-3}	1.0×10^{-3}	3.3×10^{-3}
North Korea	9.3×10^1	1.1×10^2	1.6×10^2	1.7×10^1	2.2×10^1	1.4×10^1	2.0×10^1	3.5×10^1
South Korea	8.9×10^0	7.5×10^0	7.5×10^0	4.5×10^0	6.9×10^0	4.4×10^0	1.8×10^0	6.3×10^0
Kuwait	2.0×10^0	2.0×10^0	1.6×10^0	1.6×10^0	1.7×10^0	1.2×10^0	3.9×10^{-1}	9.6×10^{-1}
Kyrgyzstan	9.6×10^{-1}	9.2×10^{-1}	8.2×10^{-1}	4.0×10^{-1}	4.4×10^{-1}	2.1×10^{-1}	3.0×10^{-1}	5.4×10^{-1}
Laos	4.3×10^1	2.1×10^1	1.0×10^1	1.1×10^1	1.3×10^1	1.9×10^1	1.0×10^1	7.8×10^0
Latvia	7.0×10^0	5.6×10^0	4.8×10^0	3.5×10^0	3.6×10^0	2.4×10^0	1.0×10^0	2.5×10^0
Lebanon	8.6×10^{-1}	5.2×10^{-1}	4.0×10^{-1}	2.5×10^{-1}	3.2×10^{-1}	2.2×10^{-1}	1.5×10^{-1}	3.6×10^{-1}
Lesotho	1.2×10^1	4.3×10^0	2.4×10^0	1.2×10^0	2.2×10^0	1.5×10^0	9.5×10^{-1}	1.4×10^0
Liberia	3.5×10^1	1.2×10^1	6.7×10^0	3.0×10^0	6.1×10^0	3.9×10^0	2.6×10^0	4.0×10^0
Libya	4.3×10^0	1.9×10^0	1.3×10^0	7.5×10^{-1}	1.1×10^0	8.3×10^{-1}	5.3×10^{-1}	1.1×10^0
Liechtenstein	3.5×10^{-3}	2.8×10^{-3}	2.1×10^{-3}	1.9×10^{-3}	2.2×10^{-3}	1.4×10^{-3}	4.3×10^{-4}	1.2×10^{-3}
Lithuania	6.9×10^0	5.2×10^0	5.4×10^0	1.9×10^0	2.2×10^0	1.4×10^0	1.0×10^0	2.0×10^0
Luxembourg	1.9×10^{-1}	1.7×10^{-1}	2.8×10^{-1}	9.7×10^{-2}	1.3×10^{-1}	1.4×10^{-1}	3.7×10^{-2}	1.6×10^{-1}
Macedonia	2.7×10^0	1.6×10^0	1.5×10^0	5.1×10^{-1}	7.3×10^{-1}	5.9×10^{-1}	4.0×10^{-1}	6.6×10^{-1}
Madagascar	9.0×10^1	4.2×10^1	2.3×10^1	2.1×10^1	2.6×10^1	3.0×10^1	1.5×10^1	2.1×10^1

(continued)

Table A.2 (continued)

Country	BaA	CHR	BbF	BkF	BaP	IcdP	DahA	BghiP
Malawi	3.0×10^1	1.2×10^1	6.2×10^0	3.8×10^0	5.9×10^0	4.9×10^0	2.9×10^0	3.8×10^0
Malaysia	2.3×10^1	1.2×10^1	7.9×10^0	6.4×10^0	8.7×10^0	8.2×10^0	3.6×10^0	6.9×10^0
Maldives	2.4×10^0	9.4×10^{-1}	5.4×10^{-1}	3.1×10^{-1}	5.1×10^{-1}	3.4×10^{-1}	1.9×10^{-1}	3.6×10^{-1}
Mali	3.0×10^1	1.1×10^1	6.0×10^0	3.6×10^0	5.9×10^0	5.3×10^0	3.1×10^0	4.0×10^0
Malta	6.7×10^{-1}	2.9×10^{-1}	1.6×10^{-1}	1.0×10^{-1}	1.5×10^{-1}	9.1×10^{-2}	6.6×10^{-2}	1.1×10^{-1}
Marshall Islands	1.2×10^{-2}	7.6×10^{-3}	5.4×10^{-3}	5.1×10^{-3}	6.0×10^{-3}	4.3×10^{-3}	1.3×10^{-3}	5.2×10^{-3}
Martinique	5.4×10^{-2}	4.3×10^{-2}	3.3×10^{-2}	3.3×10^{-2}	3.7×10^{-2}	3.1×10^{-2}	5.8×10^{-3}	5.2×10^{-2}
Mauritania	9.6×10^0	3.5×10^0	1.9×10^0	9.6×10^{-1}	1.8×10^0	1.2×10^0	7.5×10^{-1}	1.2×10^0
Mauritius	2.5×10^{-1}	2.2×10^{-1}	1.7×10^{-1}	1.7×10^{-1}	1.7×10^{-1}	1.3×10^{-1}	3.3×10^{-2}	1.7×10^{-1}
Mayotte	2.0×10^{-2}	1.5×10^{-2}	1.4×10^{-2}	8.1×10^{-3}	1.2×10^{-2}	1.0×10^{-2}	7.3×10^{-4}	1.5×10^{-2}
Mexico	1.3×10^2	5.8×10^1	3.4×10^1	2.2×10^1	3.2×10^1	2.6×10^1	1.5×10^1	2.8×10^1
Moldova	1.6×10^0	1.9×10^0	2.7×10^0	4.1×10^{-1}	4.6×10^{-1}	3.6×10^{-1}	3.8×10^{-1}	8.1×10^{-1}
Monaco	9.7×10^{-3}	7.8×10^{-3}	5.8×10^{-3}	6.3×10^{-3}	6.8×10^{-3}	5.6×10^{-3}	1.3×10^{-3}	9.7×10^{-3}
Mongolia	7.4×10^0	9.8×10^0	1.3×10^1	2.6×10^0	2.4×10^0	4.2×10^0	3.2×10^0	3.5×10^0
Montserrat	1.2×10^{-3}	9.2×10^{-4}	7.1×10^{-4}	6.7×10^{-4}	7.8×10^{-4}	6.5×10^{-4}	1.1×10^{-4}	1.1×10^{-3}
Morocco	7.3×10^0	5.7×10^0	5.0×10^0	3.5×10^0	3.8×10^0	2.6×10^0	1.4×10^0	3.7×10^0
Mozambique	1.1×10^2	6.1×10^1	3.0×10^1	3.1×10^1	3.3×10^1	6.6×10^1	3.5×10^1	2.7×10^1
Myanmar (Burma)	2.2×10^2	9.9×10^1	5.0×10^1	4.4×10^1	5.6×10^1	7.8×10^1	4.3×10^1	3.5×10^1
Namibia	3.1×10^0	1.6×10^0	8.6×10^{-1}	8.4×10^{-1}	9.5×10^{-1}	1.2×10^0	6.3×10^{-1}	7.6×10^{-1}
Nauru	8.3×10^{-4}	6.8×10^{-4}	5.0×10^{-4}	5.3×10^{-4}	5.8×10^{-4}	4.8×10^{-4}	1.0×10^{-4}	8.3×10^{-4}
Nepal	8.9×10^1	4.2×10^1	2.7×10^1	2.1×10^1	2.9×10^1	1.8×10^1	8.2×10^0	1.6×10^1
Netherlands	3.8×10^0	4.3×10^0	4.4×10^0	1.9×10^0	2.3×10^0	2.1×10^0	7.2×10^{-1}	3.3×10^0
Netherlands Antilles	3.1×10^{-1}	1.2×10^{-1}	7.5×10^{-2}	4.3×10^{-2}	7.2×10^{-2}	4.9×10^{-2}	3.4×10^{-2}	6.1×10^{-2}
New Caledonia	5.0×10^{-2}	2.7×10^{-2}	2.0×10^{-2}	1.3×10^{-2}	1.8×10^{-2}	1.3×10^{-2}	4.0×10^{-3}	1.5×10^{-2}

(continued)

Table A.2 (continued)

Country	BaA	CHR	BbF	BkF	BaP	IcdP	DahA	BghiP
New Zealand	6.7×10^0	6.6×10^0	8.0×10^0	1.4×10^0	2.0×10^0	2.1×10^0	1.2×10^0	3.8×10^0
Nicaragua	3.0×10^1	1.1×10^1	6.1×10^0	3.1×10^0	5.8×10^0	3.8×10^0	2.4×10^0	3.8×10^0
Niger	5.1×10^1	1.8×10^1	1.0×10^1	4.7×10^0	9.2×10^0	6.0×10^0	3.8×10^0	6.0×10^0
Nigeria	4.9×10^2	2.5×10^2	1.7×10^2	1.5×10^2	1.9×10^2	1.3×10^2	4.8×10^1	1.0×10^2
Niue	1.1×10^{-4}	8.6×10^{-5}	6.2×10^{-5}	6.8×10^{-5}	7.3×10^{-5}	5.9×10^{-5}	1.5×10^{-5}	9.7×10^{-5}
Northern Mariana Islands	1.1×10^{-2}	6.2×10^{-3}	4.3×10^{-3}	3.8×10^{-3}	4.6×10^{-3}	3.1×10^{-3}	1.1×10^{-3}	2.8×10^{-3}
Norway	1.6×10^1	4.4×10^1	2.8×10^1	7.7×10^0	1.4×10^1	1.1×10^1	2.6×10^0	1.3×10^1
Oman	2.1×10^0	2.2×10^0	1.8×10^0	1.8×10^0	1.9×10^0	1.3×10^0	4.0×10^{-1}	1.1×10^0
Pakistan	2.5×10^2	1.4×10^2	9.6×10^1	7.8×10^1	9.4×10^1	5.7×10^1	3.0×10^1	5.9×10^1
Palau	4.4×10^{-3}	2.9×10^{-3}	2.1×10^{-3}	2.0×10^{-3}	2.3×10^{-3}	1.7×10^{-3}	4.5×10^{-4}	2.1×10^{-3}
Panama	6.3×10^0	2.4×10^0	1.4×10^0	8.2×10^{-1}	1.4×10^0	9.7×10^{-1}	5.4×10^{-1}	9.9×10^{-1}
Papua New Guinea	3.1×10^1	1.1×10^1	6.0×10^0	2.9×10^0	5.6×10^0	3.9×10^0	2.5×10^0	3.7×10^0
Paraguay	3.3×10^1	2.0×10^1	7.8×10^0	1.2×10^1	1.1×10^1	2.7×10^1	1.5×10^1	7.8×10^0
Peru	4.3×10^1	1.8×10^1	1.1×10^1	7.3×10^0	1.1×10^1	9.4×10^0	5.0×10^0	7.3×10^0
Philippines	7.2×10^1	2.9×10^1	1.8×10^1	1.1×10^1	1.7×10^1	1.2×10^1	6.3×10^0	1.3×10^1
Pitcairn Islands	2.2×10^{-6}	1.8×10^{-6}	1.3×10^{-6}	1.4×10^{-6}	1.5×10^{-6}	1.3×10^{-6}	3.0×10^{-7}	2.2×10^{-6}
Poland	1.2×10^2	1.7×10^2	2.4×10^2	3.6×10^1	4.1×10^1	2.7×10^1	3.0×10^1	5.9×10^1
Portugal	5.1×10^0	4.1×10^0	3.2×10^0	3.1×10^0	3.3×10^0	2.3×10^0	8.3×10^{-1}	2.1×10^0
Puerto Rico	9.1×10^{-1}	5.1×10^{-1}	3.7×10^{-1}	2.8×10^{-1}	3.4×10^{-1}	2.4×10^{-1}	9.0×10^{-2}	2.3×10^{-1}
Qatar	6.2×10^{-2}	6.7×10^{-2}	1.8×10^{-1}	4.3×10^{-2}	6.6×10^{-2}	1.4×10^{-1}	5.2×10^{-2}	1.6×10^{-1}
Reunion	8.0×10^{-2}	6.3×10^{-2}	5.0×10^{-2}	4.5×10^{-2}	5.3×10^{-2}	4.4×10^{-2}	6.8×10^{-3}	7.2×10^{-2}
Romania	2.5×10^1	1.8×10^1	1.5×10^1	9.2×10^0	1.1×10^1	8.5×10^0	3.2×10^0	1.1×10^1
Russia	2.1×10^2	5.1×10^2	4.0×10^2	1.0×10^2	1.6×10^2	1.4×10^2	6.3×10^1	1.3×10^2
Rwanda	5.3×10^1	1.9×10^1	1.0×10^1	4.7×10^0	9.3×10^0	6.0×10^0	3.9×10^0	6.2×10^0

(continued)

Table A.2 (continued)

Country	BaA	CHR	BbF	BkF	BaP	IcdP	DahA	BghiP
Samoa	4.0×10^{-1}	1.5×10^{-1}	8.4×10^{-2}	4.4×10^{-2}	7.9×10^{-2}	5.2×10^{-2}	3.0×10^{-2}	5.5×10^{-2}
San Marino	2.0×10^{-2}	1.5×10^{-2}	1.1×10^{-2}	1.2×10^{-2}	1.2×10^{-2}	9.4×10^{-3}	2.6×10^{-3}	1.2×10^{-2}
Sao Tome and Principe	6.7×10^0	2.3×10^0	1.3×10^0	5.7×10^{-1}	1.2×10^0	7.4×10^{-1}	4.9×10^{-1}	7.5×10^{-1}
Saudi Arabia	4.6×10^0	3.7×10^0	3.1×10^0	1.9×10^0	2.1×10^0	1.7×10^0	1.3×10^0	3.1×10^0
Senegal	1.2×10^1	4.9×10^0	2.5×10^0	1.7×10^0	2.6×10^0	2.7×10^0	1.6×10^0	1.8×10^0
Serbia and Montenegro	2.7×10^1	2.6×10^1	3.3×10^1	4.8×10^0	6.1×10^0	4.9×10^0	5.1×10^0	9.8×10^0
Seychelles	2.0×10^{-2}	1.9×10^{-2}	1.6×10^{-2}	1.6×10^{-2}	1.7×10^{-2}	1.2×10^{-2}	2.8×10^{-3}	1.1×10^{-2}
Sierra Leone	3.2×10^1	1.2×10^1	6.2×10^0	3.6×10^0	6.0×10^0	5.7×10^0	3.4×10^0	4.0×10^0
Singapore	8.6×10^{-2}	4.8×10^{-2}	7.6×10^{-2}	3.4×10^{-2}	4.6×10^{-2}	4.4×10^{-2}	3.2×10^{-2}	5.8×10^{-2}
Slovakia	6.3×10^0	8.8×10^0	1.2×10^1	2.1×10^0	2.8×10^0	2.4×10^0	1.5×10^0	4.8×10^0
Slovenia	3.5×10^0	2.4×10^0	2.0×10^0	9.8×10^{-1}	1.2×10^0	1.0×10^0	4.2×10^{-1}	1.4×10^0
Solomon Islands	7.0×10^{-1}	2.5×10^{-1}	1.4×10^{-1}	7.0×10^{-2}	1.3×10^{-1}	8.6×10^{-2}	5.2×10^{-2}	8.7×10^{-2}
Somalia	6.4×10^1	2.3×10^1	1.3×10^1	5.9×10^0	1.2×10^1	7.5×10^0	4.7×10^0	7.8×10^0
South Africa	1.8×10^2	1.8×10^2	2.4×10^2	4.3×10^1	5.2×10^1	4.2×10^1	3.6×10^1	7.4×10^1
South Georgia and the South Sandwich Islands	0.0×10^0	0.0×10^0	0.0×10^0	0.0×10^0	0.0×10^0	0.0×10^0	0.0×10^0	0.0×10^0
Spain	2.5×10^1	3.5×10^1	2.7×10^1	1.6×10^1	1.9×10^1	1.3×10^1	4.4×10^0	1.3×10^1
Sri Lanka	3.8×10^1	1.8×10^1	1.1×10^1	8.9×10^0	1.3×10^1	7.6×10^0	3.6×10^0	6.9×10^0
St. Helena	1.2×10^{-4}	9.9×10^{-5}	7.1×10^{-5}	8.4×10^{-5}	8.6×10^{-5}	7.1×10^{-5}	1.9×10^{-5}	1.3×10^{-4}
St. Kitts and Nevis	1.3×10^{-2}	9.2×10^{-3}	7.0×10^{-3}	6.4×10^{-3}	7.6×10^{-3}	6.0×10^{-3}	1.2×10^{-3}	8.8×10^{-3}
St. Lucia	4.4×10^{-2}	3.1×10^{-2}	2.3×10^{-2}	2.2×10^{-2}	2.5×10^{-2}	2.0×10^{-2}	4.6×10^{-3}	2.9×10^{-2}
St. Pierre and Miquelon	5.7×10^{-4}	4.4×10^{-4}	3.6×10^{-4}	2.8×10^{-4}	3.7×10^{-4}	3.1×10^{-4}	3.7×10^{-5}	4.8×10^{-4}
St. Vincent and the Grenadines	3.2×10^{-2}	2.2×10^{-2}	1.6×10^{-2}	1.5×10^{-2}	1.6×10^{-2}	1.3×10^{-2}	3.5×10^{-3}	1.9×10^{-2}
Sudan	9.5×10^1	4.2×10^1	2.0×10^1	1.8×10^1	2.3×10^1	3.6×10^1	2.0×10^1	1.6×10^1

(continued)

Table A.2 (continued)

Country	BaA	CHR	BbF	BkF	BaP	IcdP	DahA	BghiP
Suriname	3.5×10^{-1}	1.7×10^{-1}	1.1×10^{-1}	8.8×10^{-2}	1.1×10^{-1}	1.1×10^{-1}	5.1×10^{-2}	1.1×10^{-1}
Swaziland	5.8×10^0	2.2×10^0	1.2×10^0	6.7×10^{-1}	1.1×10^0	9.1×10^{-1}	5.4×10^{-1}	7.7×10^{-1}
Sweden	1.2×10^1	9.6×10^0	6.1×10^0	2.4×10^0	4.0×10^0	2.6×10^0	1.3×10^0	3.0×10^0
Switzerland	5.2×10^0	2.9×10^0	2.5×10^0	1.0×10^0	1.4×10^0	8.5×10^{-1}	6.2×10^{-1}	1.2×10^0
Syria	4.4×10^0	4.0×10^0	3.2×10^0	2.0×10^0	1.8×10^0	1.1×10^0	1.4×10^0	2.8×10^0
Tajikistan	4.3×10^0	7.8×10^0	1.1×10^1	1.4×10^0	1.5×10^0	2.2×10^0	1.4×10^0	5.0×10^0
United Republic of Tanzania	1.4×10^2	6.1×10^1	3.4×10^1	2.7×10^1	3.6×10^1	3.7×10^1	1.9×10^1	2.2×10^1
Thailand	8.6×10^1	4.0×10^1	2.4×10^1	1.8×10^1	2.4×10^1	2.8×10^1	1.5×10^1	1.9×10^1
Timor Leste	1.6×10^1	6.1×10^0	3.5×10^0	2.1×10^0	3.5×10^0	2.2×10^0	1.2×10^0	2.1×10^0
Togo	1.6×10^1	6.0×10^0	3.2×10^0	1.7×10^0	3.0×10^0	2.5×10^0	1.5×10^0	2.0×10^0
Tokelau	4.6×10^{-5}	3.7×10^{-5}	2.7×10^{-5}	3.0×10^{-5}	3.2×10^{-5}	2.7×10^{-5}	6.3×10^{-6}	4.6×10^{-5}
Tonga	2.4×10^{-1}	8.7×10^{-2}	4.9×10^{-2}	2.5×10^{-2}	4.6×10^{-2}	3.0×10^{-2}	1.8×10^{-2}	3.1×10^{-2}
Trinidad and Tobago	3.6×10^{-1}	2.5×10^{-1}	2.3×10^{-1}	1.7×10^{-1}	1.7×10^{-1}	2.1×10^{-1}	9.7×10^{-2}	2.2×10^{-1}
Tunisia	1.4×10^1	6.6×10^0	4.3×10^0	3.2×10^0	4.2×10^0	2.9×10^0	1.3×10^0	2.9×10^0
Turkey	1.2×10^2	1.5×10^2	1.9×10^2	4.3×10^1	4.8×10^1	3.2×10^1	2.9×10^1	5.7×10^1
Turkmenistan	2.8×10^0	3.3×10^0	3.5×10^0	8.9×10^{-1}	7.5×10^{-1}	4.3×10^{-1}	8.7×10^{-1}	1.6×10^0
Turks and Caicos Islands	2.8×10^{-3}	2.1×10^{-3}	1.8×10^{-3}	1.3×10^{-3}	1.8×10^{-3}	1.5×10^{-3}	1.7×10^{-4}	2.3×10^{-3}
Tuvalu	4.2×10^{-4}	3.4×10^{-4}	2.5×10^{-4}	2.8×10^{-4}	3.0×10^{-4}	2.5×10^{-4}	5.7×10^{-5}	4.3×10^{-4}
Uganda	2.1×10^2	7.6×10^1	4.1×10^1	2.0×10^1	3.8×10^1	2.7×10^1	1.7×10^1	2.5×10^1
Ukraine	4.0×10^1	4.6×10^1	5.6×10^1	1.4×10^1	1.8×10^1	1.1×10^1	8.5×10^0	2.1×10^1
United Arab Emirates	1.7×10^0	7.7×10^0	9.1×10^0	2.6×10^0	2.9×10^0	5.8×10^0	8.4×10^{-1}	1.0×10^1
United Kingdom	1.3×10^1	1.6×10^1	2.1×10^1	5.1×10^0	6.1×10^0	4.5×10^0	3.4×10^0	8.6×10^0
United States	2.3×10^2	1.4×10^2	1.1×10^2	4.4×10^1	5.8×10^1	5.4×10^1	3.6×10^1	5.2×10^1
Uruguay	7.3×10^0	3.0×10^0	2.0×10^0	9.2×10^{-1}	1.5×10^0	9.3×10^{-1}	7.2×10^{-1}	1.2×10^0

(continued)

Table A.2 (continued)

Country	BaA	CHR	BbF	BkF	BaP	IcdP	DahA	BghiP
Uzbekistan	1.1×10^1	1.5×10^1	1.8×10^1	3.4×10^0	2.9×10^0	1.8×10^0	3.7×10^0	5.9×10^0
Vanuatu	5.1×10^{-1}	1.8×10^{-1}	1.0×10^{-1}	4.9×10^{-2}	9.3×10^{-2}	6.2×10^{-2}	3.9×10^{-2}	6.3×10^{-2}
Venezuela	1.1×10^1	1.2×10^1	1.0×10^1	5.8×10^0	6.1×10^0	1.2×10^1	4.3×10^0	1.2×10^1
Vietnam	2.7×10^2	1.8×10^2	1.8×10^2	7.6×10^1	1.0×10^2	6.5×10^1	3.6×10^1	6.9×10^1
Wallis and Futuna	5.4×10^{-4}	4.4×10^{-4}	3.3×10^{-4}	3.4×10^{-4}	3.8×10^{-4}	3.1×10^{-4}	6.3×10^{-5}	5.3×10^{-4}
Western Sahara	0.0×10^0	0.0×10^0	0.0×10^0	0.0×10^0	0.0×10^0	0.0×10^0	0.0×10^0	0.0×10^0
Yemen	1.3×10^4	9.6×10^3	8.3×10^3	3.4×10^3	4.7×10^3	4.1×10^3	2.5×10^3	3.7×10^3
Zambia	1.1×10^1	5.5×10^0	3.6×10^0	1.5×10^0	2.0×10^0	1.1×10^0	1.5×10^0	2.1×10^0
Zimbabwe	2.0×10^0	1.6×10^0	1.3×10^0	8.5×10^{-1}	9.0×10^{-1}	9.7×10^{-1}	4.9×10^{-1}	7.9×10^{-1}

The results here are source-aggregated for the base year of 2007 only